The role of adaptive and innate immune cells in patients with colorectal cancer

Jitwadee Inthagard

BSc., MSc. (Medical Technology)

This thesis is submitted to the University of Glasgow
in fulfilment of the requirements for the
Degree of Doctor of Philosophy

Institute of Cancer Sciences
Collage of Medical and Veterinary Life Sciences
University of Glasgow

December 2021

Summary

The aim of this study was to fully understand the differing immune landscapes within colorectal cancer (CRC) patients' tumours, how these affected histological subtypes and response to immunotherapy as well as assessing their underlying genetic backgrounds.

The first part assessed IHC staining for the full patient cohort to obtain baseline results of the association between immune cells infiltration and patients' survival. Then immune landscapes were developed from a combination of T-lymphocytes and myeloid cells to mimic different immune statuses within the tumour. The results found that high level of T-lymphocytes infiltration was associated with improved patients' survival independent of myeloid cells infiltration within both tumour cell nests and tumour stroma. Whereas high level of myeloid cells infiltration was associated with decreased patient's survival only when T-lymphocytes where low.

The association between immune cells infiltration and CRC phenotypic subtyping was then assessed to understand if there is a different immune cell composition specific to each phenotypic subtype which could be used as prognostic biomarkers or as targets for immunotherapy. This showed that each subtype had a separate immune landscape, with the immune subtype being associated with lymphoid cells, and the stromal subtype with myeloid cells.

The second part involved genomics and transcriptomics analysis to obtain potentially mutated and differentially expressed genes specific to each immune landscape which might be used as biomarkers. The genomics analysis showed that *TP53* mutation was the most significantly mutated gene which showed a high mutation frequency in patients with high myeloid cells in their tumour stroma, especially when combined with high levels of $CD80^+$ M1-like macrophages. In addition, at the protein level, p53 protein expression showed significant correlation with *TP53* mutations, and high *TP53* mutations were associated with high p53 expression, which significantly improved patients' survival. As *TP53* mutation showed a higher frequency in patients with high levels of $CD80^+$ M1-like macrophages infiltration within their tumour stroma, *TP53* mutations and its effects on p53 expression might be one of the factors to influence myeloid cells infiltration into stroma.

Similarly, transcriptomics analysis found different pattern of gene expressions for each immune landscape. The results suggested that expression of significantly differentially expressed genes might be influenced by high myeloid cell infiltration independent of which other cell types are present in the tumour microenvironment. The most significantly differentially expressed genes were again linked to the *TP53* network at a protein-protein interaction level, further strengthening the link between the TP53 network and immune response in CRC. Interestingly, when assessing the

correlation between *TP53* mutation and differentially expressed genes, it was found that the REGs gene family, *REG1A*, *REG3A*, and *REG3G*, were downregulated in patients with *TP53* mutations. As *REG*s genes are proposed to play a role in promoting colon tissues tumorigenesis this would fit with previous research. However, one limitation of this study was its small sample size. Therefore, validation in a larger cohort is needed to confirm these findings.

The final part was to assess the efficacy of three anti-PD-1/anti-PD-L1 checkpoint inhibitors individually and in combination on a 3-D CRC tumour spheroids model co-cultured with different immune cell types. This model was designed to co-culture CRC tumour spheroids with non-adherent lymphocytes and macrophages, either individually or in combination. The model was developed by assessing the optimum cell density, media, and inhibitor concentrations. However, the result showed no difference in tumour spheroid viability for any immune checkpoint inhibitor at either 48 or 96 hours for any of the co-culture combinations. This suggests that further optimisation of the model is needed to be a useful tool for immunotherapy research.

In conclusion, the results show that differing immune landscapes can stratify CRC patient prognosis. Furthermore, these immune landscapes vary between histological phenotypic subtypes and are linked to mutant p53 expression. With further research, these immune landscapes may be a useful tool to assess and stratify patients for treatment with immunotherapy.

Table of Content

List of Tables

Chapter 4

Chapter 5

Chapter 6

List of Figures

Chapter 4

Chapter 5

Chapter 6

Chapter 7

Acknowledgements

There are many important supporters involved during a long road of studying. First of all, I would like to express my sincere gratitude to my supervisor Dr. Antonia Roseweir for the invaluable guidance, encouraging, motivation, enthusiasm, and understanding throughout my study. I could not explain more but you are genius and always impressed me from your scientific thought and vision. I've learnt so much from you. Thank you very much for understanding and everything.

The next important supporters I would like to express my sincere thank are my organization, Princess of Naradhiwas University, and the scholarship supporter, Ministry of Sciences and Technology, for the opportunity for PhD study. This is one of a meaningful chapter in my life. Also thank you very much to the officers in London and in Thailand who has assisted and solved the problems during my study.

I would like to thank my second supervisor Professor Joanne Edwards for the guidance and comments throughout the project to make everything stay on track and keep high quality results.

I would also like to thank everyone in the Edward's Lab group for assisting, especially Dr. Jean Quinn for cell culture technique and WB running, Dr. Kathryn Pennel for cutting slides for me and many other things during lab time, Liam Hayman for teaching me how to do mutational analysis, you are superb!

Another person I would like to thank are Mr. Allan McVie, and Ms. Sharon Burns, thank you very much for demonstrating me how to use confocal microscopes and other equipment, that made my life easier. Thanks again Allan and Sharon.

Also, thank you so much to everyone I have contacted at any time at WWCRC for their friendliness.

I would like to thank Ms. Clair Orange and Dr. Jennifer Hey for cutting patient slides and scanning IHC staining slides. To Dr. Aula Ammar, you were trying so hard to scan cell pellets staining for me, it is a precious picture for my study, also some advice for macrophages culture and study designs, thank you Aula!

I would like to thank you very much to Mr. Colin Nixon for cutting cell pellets slides and some advice for making blocks from cell pellets, I appreciate so much.

For transcriptomics analysis, I would like to thank you very much to Mr. John Cole for the superb bioinformatics training courses, I have learnt so many things.

I would like to thank very much Dr. Seth Coffelt's lab for kindly providing the macrophage cell line that was critical for my lab work.

To my friends and colleagues in Thailand, thank you very much for your support and consultant throughout my study. You are always with me when I need, that means a lot to me.

An important person I would like to express my sincere gratitude and would never forget is Dr. Hester Van Wyk for all supports through my tough time from illness during pandemic, I appreciate so much. You prove my belief and attitude for having positive thinking, treating others good, and pass the good things forward. Thank you so much for everything, your soup tasted so good! Also, thank you so much to Kathryn and Liam for buying me foods when I was ill!

For the most important person in my life, my parents and sister, thank you so much for their support and endless love for me, unconditional love, understanding, and always by my side in everything I do. Thank you so much to everyone in our family, uncles, aunt, cousins for taking care of my parents while I was away from home for four and a half years. Thank you very much for your support.

Finally, for everyone I couldn't mentioned you here, but you know I appreciate so much for your support in any aspect and I wouldn't be here without you all!

List of publications and presentations

Publications relating to this thesis:

Al-Badran SS, Grant L, Campo MV, **Inthagard J**, Pennel K, Quinn J, Konanahalli P, Hayman L, Horgan PG, McMillan DC, Roxburgh CS, Roseweir A, Park JH, Edwards J. Relationship between immune checkpoint proteins, tumour microenvironment characteristics, and prognosis in primary operable colorectal cancer. J Pathol Clin Res. 2021 Mar;7(2):121-134. doi: 10.1002/cjp2.193. Epub 2020 Dec 18. PMID: 33338327; PMCID: PMC7869939.

Inthagard J, Edwards J, Roseweir AK. Immunotherapy: enhancing the efficacy of this promising therapeutic in multiple cancers. Clin Sci (Lond). 2019 Jan 18;133(2):181-193. doi: 10.1042/CS20181003. PMID: 30659159.

Roseweir, A. K. , Powell, A. G.M.T., Horstman, S. L., **Inthagard, J.**, Park, J. A. , McMillan, D. C. , Horgan, P. G. and Edwards, J. (2019) Src family kinases, HCK and FGR, associate with local inflammation and tumour progression in colorectal cancer. *Cellular Signalling*, 56, pp. 15-22. (doi: 10.1016/j.cellsig.2019.01.007)(PMID:30684564)

Poster presentations:

The prognostic impact of adaptive and innate immune landscapes in patients with stage I-III colorectal cancer. **Jitwadee Inthagard**, Donald C McMillan, Joanne Edwards, and Antonia Roseweir. AACR special conference 2019 on Tumor Immunology and Immunotherapy – Boston, MA, USA

The impact of T-lymphocyte subsets, macrophages, and neutrophils infiltrate in stage I-III colorectal cancer. **Jitwadee Inthagard**, Joanne Edwards, Antonia Roseweir. British Association of Cancer Research Tumour Microenvironment conference 2019 – Nottingham, UK

The relationship between the immune landscape and phenotypic subtypes in patients with colorectal cancer. **Jitwadee Inthagard**, Joanne Edwards, and Antonia Roseweir, British Association of Cancer Research Student Conference 2018 – London, UK

Author's Declaration

"I declare that this thesis is the results of my own work, except were referenced from others work and this thesis or any part of work has not been submitted for any degree or diploma at University of Glasgow or any other institution."

Jitwadee Inthagard
December 2021

Abbreviations

A

ACG = American Collage of Gastroenterology

APC = Antigen presenting cell

ASCO = American Society of Clinical Oncology

B

BRAF = v-raf murine sarcoma viral oncogene homolog B1

BSA = Bovine serum albumin

C

CAFs = Cancer-associated fibroblasts

CAR = Chimeric antigen receptor

CCL2 = C-C motif chemokine ligand 2

CD = Cluster of differentiation

cHL = Classical Hodgkin lymphoma

CI = Confidence Interval

CIMP = CpG Island Methylator Phenotype

CIN = Chromosomal Instability

CMS = The Consensus Molecular Subtype

CR = Complete response rate

CRC = Colorectal cancer

CRCSC = CRC Subtyping Consortium

CRIS = Colorectal Cancer Intrinsic Subtype

CRP = C-reactive protein

CSS = Cancer specific survival

CTLA-4 = Cytotoxic T-lymphocyte antigen 4

D

DCC = Deleted in colorectal cancer

DCR = Disease control rate

DE = Differential expression

DEL = Deletion

DFS = Disease-free survival

DEG = Differential expressed gene

DNA = Deoxyribonucleic acid

DSS = Disease-specific survival

DTT = Dithiothreitol

E

EDTA = Ethylene diamine tetra acetic acid

EGF = Epidermal growth factor

EGFR = Endothelial growth factor receptor

EMT = Epithelial-to-mesenchymal transition

ERBB = Erb-B2 receptor tyrosine kinase

F

FBS = Foetal bovine serum

FDR = False discovery rate

FFPE = Formalin-fixed paraffin-embedded

FoxP3 = Forkhead box protein 3

G

GMS = Glasgow microenvironment score

Gp100 = Glycoprotein 100

GPS = Glasgow prognostic score

H

H&E = Haematoxylin and Eosin

HGF = Hepatocyte Growth Factor

HLA = Human leucocyte antigen

HPV = Human papilloma virus

HR = Hazard ratio

HRP = Horse-radish peroxidase

I

IBD = Inflammatory bowel disease

ICCC = Intra-class correlation coefficient

ICIs = Immune checkpoint inhibitors

IGF = Insulin-like growth factor 1

IHC = Immunohistochemistry

IL = Interleukin

INS = Insertion

K

Ki67 = Marker of proliferation 67

KM = Klintrup-Makinen

KRAS = Kirsten rat sarcoma virus

L

LDH = Lactate dehydrogenase

M

mCRC = Metastatic colorectal cancer

MDSCs = Myeloid-derived suppressor cells

mGPS = Modified Glasgow Prognostic Score

miRNA = microRNA

MLH1 = MutL homolog 1

MMR = Mismatch Repair

MSH2 = MutS homolog 2

MSH6 = MutS homolog 6

MSI = Microsatellite instability

MSS = Microsatellite stable

mUCC = Metastatic urothelial carcinoma

MYC = MYC protooncogene

N

NK = Natural killer

NLR = Neutrophil-to-lymphocyte ratio

NSCLC = Non-small-cell lung cancer

O

ORA = Over-representative analysis

ORR = Overall response rate

OS = Overall survival

P

PAGE = Polyacrylamide gel electrophoresis

PBS = Phosphate buffer saline

PCA = Principal component analysis

PD-1 = Program cell death protein 1

PD-L1 = Program cell death ligand 1

PD-L2 = Program cell death ligand 2

PDX = Patient derived xenograft

PMS2 = Postmeiotic segregation increased 2

PPIs = Protein-protein interactions

R

REMARK = Reporting Recommendations for Tumour Marker Prognostic Studies

RFS = Recurrence-free survival

RNA = Ribonucleic acid

RR = Recurrence risk

S

SNP = Single nucleotide polymorphism

SNV = Single nucleotide variant

T

TAMs = Tumour-associated macrophages

TANs = Tumour-associated neutrophils

TBST = Tris-buffered saline with 0.1% Tween® 20

TGF-β = Transforming growth factor beta

TILs = Tumour infiltrating lymphocytes

TMAs = Tissue microarrays

TME = Tumour microenvironment

TNF-α = Tumour necrosis factor α

TNM = T (Tumour), N (Lymph Node), M (Metastasis)

TP53 = Tumour protein 53

Tregs = Regulatory T-lymphocytes

TSP = Tumour stroma percentage

U

UICC = The Union for International Cancer Control

ULA = Ultra-low attachment

V

VEGF = Vascular endothelial growth factor

W

WGS = Whole genome sequencing

WST-1 = Water-soluble tetrazolium salt 1

WNT = Wingless-related integration site

Chapter 1 Introduction

1.1 Colorectal cancer incidence

Colorectal cancer (CRC) includes any cancer of the colon or rectum. The Global Cancer Statistics (GLOBOCAN) estimated new cancer cases were around 18.1 million in 2018, of which, CRC exhibited a 6.1% incidence rate after lung cancer (11.6%), and prostate cancer (7.1%). In terms of mortality, CRC caused a 9.2% mortality rate, after lung cancer (18.4%) (Bray et al., 2018). In 2020, the GLOBOCAN estimated 19.3 million new cancer cases worldwide, of which CRC represented 10% of new cases after breast cancer (11.7%), and lung cancer (11.4%). For mortality rate, lung cancer was the leading cause of cancer death (18%), followed by CRC (9.4%) (Sung et al., 2021). From the estimation for this 2 years period, overall, new cancer cases increased every year worldwide. For CRC, the incidence was increased from 6.1% to 10%, and mortality rate from 9.2% to 9.4%. Even though CRC deaths were only slightly increased, the high increase in new cases needs close monitoring, as the cases were still high even with screening tests implemented worldwide.

1.2 CRC screening

Generally, most people diagnosed with CRC are aged 60 or above. However, CRC incidence rises in individuals from age 50 onwards (Bretthauer (2011). Recently, the incidence of CRC cases in patients with age less than 40 years have been rising in Europe and other regions including Asia, New Zealand, and United States (Campos et al., 2017; Vuik et al., 2019). A similar trend is also seen in developing countries (Zahir et al., 2014). These indicate that CRC has become a substantial burden worldwide. However, early detection to remove precancerous lesions could lead to successful treatment of CRC and lessen this burden (Cardoso et al., 2021). Therefore, CRC screening in individuals with average-risk including young adult is crucial for future management of CRC.

Recently, the American College of Gastroenterology (ACG) clinical guidelines for CRC screening has been launched. They strongly recommend CRC screening in individuals with average-risk aged between 50 and 75 years to decrease the incidence of advanced adenoma and mortality. In addition, the screening in individuals with average-risk aged 40 and 49 years is a conditional recommendation (Shaukat et al., 2021). In Europe, a study by Cardoso et. al. from over 3 million patients between 2000-2016, found that countries which had long-standing screening programme that included faecal tests and colonoscopy decreased CRC incidence substantially (Cardoso et al., 2021). Whereas in countries that implemented screening during the study period, countries that reported a high screening coverage and uptake, showed an initial increased followed by a substantial decreased. Conversely, in countries where no large-scale screening programme was implemented, an elevate CRC incidence continued. Taken together, this suggests that implementing screening programme in individuals from age 40 years could reduce CRC incidence worldwide by allowing earlier stage

detection of tumours; however, this still not universally agreed. In Scotland, bowel screening is conducted from age 50-74, whereas in England and Northern Ireland screening occurs from 60-74 years suggesting that implementing screening at 40 years is still a way off in the UK (Hirst et al., 2018; Koo et al., 2017; Schreuders et al., 2015).

1.3 Stage and grade of CRC

CRC staging and grading systems are widely used and have consisted of three systems, TNM classification, tumour grading, and Dukes staging. As Dukes' staging used a similar method to TNM staging, this system is now no longer in use and has been replaced by TNM stage because of its more detailed specification. TNM stage is the most reliable prognostic indicator in patients with CRC and treatment decision are based on this classification. Patient's 5-year survival rates, in England has been reported as 90% for stage 1, 80% for stage 2, 70% for stage 3, and 10% for stage 4 (Broggio, 2019) **(Table 1.2)**. Apart from TNM staging, other histopathological features reported at diagnosis, are associated with prognosis and can influence treatment, including venous invasion, tumour perforation/serosal involvement, and tumour budding.

1.3.1 TNM classification

The TNM classification of malignant tumours is the most commonly used staging system internationally for CRC. TNM is a system that defines cancer stage to provide a patient's prognosis. T (tumour) describes how deep the tumour has invaded into the bowel lining. N (Lymph node) describes the involvement of regional lymph nodes or lymph nodes near the colon and rectum. M (Metastasis) describes the spread of cancer into other parts of the body (ASCO.org., 2021a) (**Table 1.1**). The stage of cancer is then defined by combining T, N, and M classifications (**Table 1.2**). TNM is now maintained by the Union for International Cancer Control (UICC) for consensus as a global standard to classify cancer progression and spread (UICC, 2021).

Table 1.1 - TNM stage definition and description for T-, N-, M-stage (table adapted from (ASCO.org., 2021a).

TNM staging		Description
T (Tumor)	TX	The primary tumour cannot be evaluated.
	T0 (T plus zero)	There is no evidence of cancer in the colon or rectum.
	Tis	Refers to carcinoma in situ (also called cancer in situ). Cancer cells are found only in the epithelium or lamina propria, which are the top layers lining the inside of the colon or rectum.
	T1	The tumour has grown into the submucosa, which is the layer of tissue underneath the mucosa or lining of the colon.
	T2	The tumour has grown into the muscularis propria, a deeper, thick layer of muscle that contracts to force along the contents of the intestines.
	T3	The tumour has grown through the muscularis propria and into the subserosa, which is a thin layer of connective tissue beneath the outer layer of some parts of the large intestine, or it has grown into tissues surrounding the colon or rectum.
	T4a	The tumour has grown into the surface of the visceral peritoneum, which means it has grown through all layers of the colon.
	T4b	The tumour has grown into or has attached to other organs or structures.
N (Node)	NX	The regional lymph nodes cannot be evaluated.
	N0 (N plus zero)	There is no spread to regional lymph nodes.
	N1a	There are tumour cells found in 1 regional lymph node.
	N1b	There are tumour cells found in 2 or 3 regional lymph nodes.
	N1c	There are nodules made up of tumour cells found in the structures near the colon that do not appear to be lymph nodes.
	N2a	There are tumour cells found in 4 to 6 regional lymph nodes.
	N2b	There are tumour cells found in 7 or more regional lymph nodes.
M (Metastasis)	M0	The disease has not spread to a distant part of the body.
	M1a	The cancer has spread to 1 other part of the body beyond the colon or rectum.
	M1b	The cancer has spread to more than 1 part of the body other than the colon or rectum.
	M1c	The cancer has spread to the peritoneal surface.

Table 1.2 - The description of cancer staging by combining TNM Classifications (table adapted from (ASCO.ORG., 2021A; BROGGIO, 2019)

Stage	Description	TNM	5-year survival rate
Stage 0	cancer cells are only on mucosa or inner lining of colon or rectum (cancer in situ)		
Stage I	cancer has grown through mucosa and has invaded muscular layer of colon or rectum, but not spread into nearby tissue or lymph nodes	-T1 or T2, N0, M0	90%
Stage IIA	cancer has grown through the wall of colon or rectum but not spread to nearby tissue or lymph nodes	-T3, N0, M0	80%
Stage IIB	cancer has grown through the layers of the muscle to the lining of the abdomen called the visceral peritoneum, but not spread to the nearby lymph nodes or elsewhere	-T4a, N0, M0	
Stage IIC	tumour has spread through the wall of colon or rectum and has grown into nearby structures, but nit spread to nearby lymph nodes or elsewhere	-T4b, N0, M0	
Stage IIIA	Cancer has grown through the inner lining or into muscular layers of intestine and spread to 1-3 lymph nodes or to nodule of tumour cells in tissue around colon and rectum, but not spread to other parts of the body	-T1 or T2, N1 or N1c, M0 -T1, N2a, M0	70%
Stage IIIB	Cancer has grown through the bowel wall or to surrounding organs and into 1-3 lymph nodes or to a nodule of tumour in tissues around colon and rectum, but not spread to other parts of the body	-T3 or T4a, N1 or N1c, M0 -T2 or T3, N2a, M0 -T1 or T2, N2b, M0	
Stage IIIC	cancer has spread to 4 or more lymph nodes, but not to other distant parts of the body	-T4a, N2a, M0 -T3 or T4a, N2b, M0 -T4b, N1 or N2, M0	
Stage IVA	cancer has spread to a single distant part of the body, i.e., liver or lung	-any T, any N, M1a	10%
Stage IVB	cancer has spread to more than 1 part of the body	-any T, any N, M1b	
Stage IVC	Cancer has spread to the peritoneum; it may also spread to other sites or organs	-any T, any N, M1c	

1.3.2 Tumour grading

Grading system is also used to describe how much cancer cells look like normal healthy cells under a microscope. If cancerous tissue looks like normal healthy tissue it is termed "well differentiated" or a "low-grade tumour". Whereas if cancerous tissue looks incredibly different from normal healthy tissue is termed "poorly differentiated" or a "high-grade tumour" (ASCO.org., 2021a) (**Table 1.3**).

Table 1.3 - Tumour grading description (table adapted from (ASCO.ORG., 2021A)

Grade	Description
GX	The tumour grade cannot be identified.
G1	The cells are more like healthy cells, termed well differentiated.
G2	The cells are somewhat like healthy cells, termed moderately differentiated.
G3	The cells look less like healthy cells, termed poorly differentiated.
G4	The cells barely look like healthy cells, termed undifferentiated.

1.4 CRC metastasis

Metastasis is the process of tumour cells that migrate and spread to other distant organs. In CRC, metastasis mainly spreads to liver and lung than to other distant organs. Metastatic CRC (mCRC) patients that present with metastatic disease at the time of diagnosed is around 20% and metastasis develops after surgery in around 30%-50% (Palaghia et al., 2015). Current mCRC treatment cannot successfully eliminate all tumour cells, therefore, mCRC patients have only a short period of survival once diagnosed.

1.5 Current CRC treatment regimens

CRC treatment is considered and assessed by a multidisciplinary team and is assessed using the TNM stage of cancer (stage 0 – stage IV) and the location of other organs invaded during metastasis. Currently, CRC treatment consists of many diverse therapies including surgery, radiotherapy, chemotherapy, and targeted therapies (ASCO.org., 2021b; Brenner et al., 2014).

1.5.1 Surgery

Surgery is the gold standard CRC colon cancer treatment to remove the area containing the tumour cells and surrounding environment including lymph nodes. Whereas for rectal cancer, total mesorectal excision is the gold standard technique. Surgical decisions are first determined by the

tumour's localisation and the blood vessel supplies. In the past, open surgery was the regular method used. However, another alternative method has been developed called laparoscopic resection. It has been shown that the laparoscopic approach can achieve the same results as the open surgery but can benefit patients in many aspects including decreasing the need for a blood transfusion, faster recovery, earlier discharge, reduced postoperative complication and lower infection rate. Therefore, this method is now become commonly used in clinical setting. Recently, robotic surgery has also been utilized for CRC surgery. Robotic surgery does have advantages for use as a method for CRC surgery. However, the disadvantage of this method are the high cost and the lack of extensive validation (Park & Baik, 2016).

1.5.2 Neoadjuvant radiotherapy

Normally, neoadjuvant radiotherapy, is used before surgery to reduce the rate of positive margins, especially in patients with margin threatening disease.

1.5.3 Adjuvant chemotherapy

Adjuvant chemotherapy is routinely used and recommended to treat all patients with stage III colon cancer and high-risk stage II colon cancer after surgery. High-risk stage II disease is defined as having either T4 tumours, perforation, perineural invasion, lymphovascular invasion, poor differentiation, positive margin, or obstruction (Babcock et al., 2018). Oxaliplatin-based treatment for six months has been the main choice for many years but can cause neurotoxic side effects. Fluorouracil (5FU) regimens such as FOLFOX, which is oxaliplatin combined with 5FU, and CAPOX, which is oxaliplatin combined with capecitabine, have been shown to decrease recurrence rates and increase survival rates. Recently, the SCOT clinical trial, an international phase III randomised non-inferiority trial compared 3 months and 6 months chemotherapy utilising either FOLFOX or CAPOX in Stage III/ high risk Stage II CRC patients. The results showed that 3 months treatment was not inferior to 6 months treatment for patients receiving CAPOX; however, patients receiving FOLFOX responded better to 6 months of treatment (Ascopubs.org, 2018). This suggests that 3 months of CAPOX would be a suitable choice for CRC patients that may reduce neurotoxic side effects.

1.5.4 Treatment for metastatic CRC

In metastatic colorectal cancer, adjuvant chemotherapy is commonly used; the main regimens are 5-FU, capecitabine, oxaliplatin, irinotecan. Leucovorin (LV), which is a biomodulation of 5-FU, has been shown to increase the activity with improvement of patient survival rates. Combined chemotherapy regimens have also been proposed, such as FOLFOX (oxaliplatin+5-FU+LV) followed by FOLFIRI (irinotecan+5-FU+LV). Besides first- and second-line chemotherapy, other

kinds of treatment have been developed for metastatic disease. One is novel targeted therapies, for example antibodies such as bevacizumab which act against angiogenesis via the VEGF receptor or panitumumab and cetuximab which inhibit the endothelial growth factor receptor (EGFR) (Mitchell, 2013; Palaghia et al., 2015). These targeted therapies can also be used in combination with chemotherapy (Palaghia et al., 2015). For example, a combination treatment including the chemotherapeutic drug regimen, CAPOX, combined with monoclonal antibodies against VEGF or EGFR, has been proposed. (Cartwright, 2012; Edwards et al., 2012; Palaghia et al., 2015).

1.6 Genomic instability and development of CRC

One of the issues with treating CRC is the heterogeneous nature of the tumours, which is in part due to the range of genetic instability found in these tumours. Tumorigenesis is known as a multistep process which is initiated and progresses due to underlying molecular events including both genetics and epigenetics alterations (Feinberg et al., 2006). CRC is one of the most well characterised cancer types in terms of genetic alterations, with the disease developing over time due to the sequential accumulation of genetic and epigenetic aberrations in genes that resulting in transformation of normal epithelium cells into cancer cells (Fearon & Vogelstein, 1990) (**Figure 1.1**).

CRC tumorigenesis has been explored at both the genetic and epigenetic level, resulting in it becoming an obvious model to utilised for studying cancer development and progression (Fearon & Vogelstein, 1990; Wong et al., 2007; Worthley et al., 2007). CRC has been extensively studied for tumorigenesis focussing on genetic alterations (Armaghany et al., 2012) and the underlying pathways (Chung, 2000). From cumulative finding over time, at least three genomic instability pathways are involved in CRC development mechanisms from adenoma to carcinoma includes chromosomal instability (CIN), microsatellite instability (MSI) pathways, and CpG Island Methylator Phenotype (CIMP) (Colussi et al., 2013).

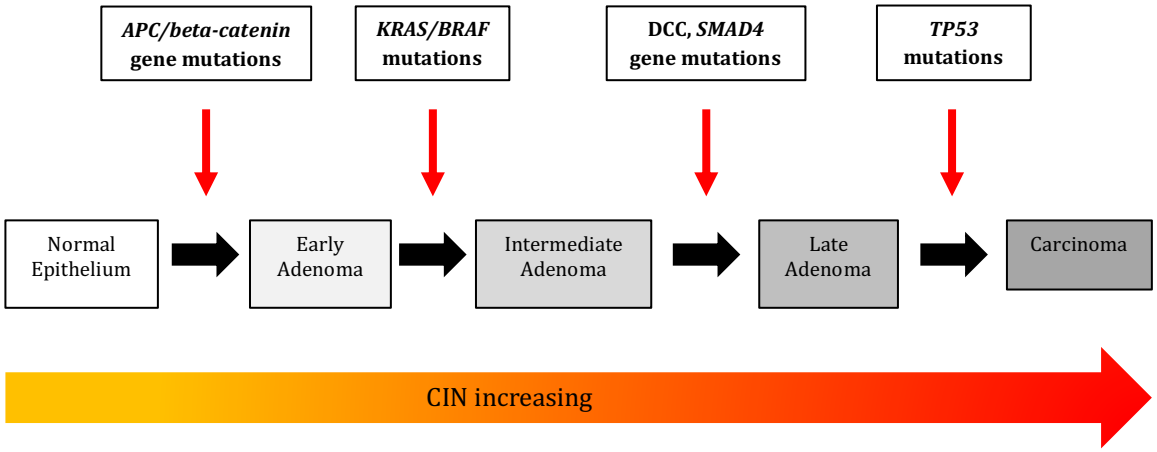

Figure 1.1 - Adenoma-carcinoma sequences model (Fearon & Vogelstein, 1990). In the accumulated of sequential genes mutation from multistep process of CRC formation, *APC* or *Beta-catenin* genes mutations is an early event acquired to transform normal epithelium into early adenoma. Subsequent *KRAS* or *BRAF* mutations then trigger the progression into intermediate adenoma, following by further DCC and *SMAD4* genes mutation reaching late adenoma. Mutations in *TP53* tumour suppressor gene along with increasing genomic instability, CIN finally transform late adenoma to carcinoma and metastasis.

1.6.1 Chromosomal Instability pathway

Chromosomal instability (CIN) refers to the gain or loss of whole or large portions of chromosomes resulting in loss of function of genes. In CRC, CIN is characterized by a major accumulation of oncogenes including *KRAS* (proto-oncogene K-*ras*), and *BRAF* (B-raf protooncogene serine/threonine kinase). As well as mutations in tumour suppressor genes, *APC* (Adenomatous polyposis coli), tumour protein p53 (*TP53*, tumour suppressor transcription factor 53)*, and SMAD4* genes. CIN is present in 70-85% of CRC tumours (Ewing et al., 2014; Nguyen & Duong, 2018).

Normally in CRC, the top three mutated genes are *APC*, *KRAS*, and *TP53*. *APC* is the most important tumour suppressor gene, around 75% of CRC cases have mutation in this gene. It is also usually the first mutation to occur, making it a common driver mutation of CRC (Tariq & Ghias, 2016). *KRAS,* is another important gene, mutated *KRAS* found around 35-42% of CRC cases. KRAS is also important for treatment decisions, as patients with a KRAS mutation are insensitive to EGFR monoclonal antibody targeted therapies. Finally, *TP53*, impairment is present in around 50-75% in CRC cases and is usually the mutation that drives the tumour towards full carcinogenesis (Worthley & Leggett, 2010).

1.6.2 Microsatellite Instability pathway

Microsatellite instability (MSI) is another crucial genetic variation in CRC development, which occurs in 15% of CRC patients (Armaghany et al., 2012; Park, Powell, et al., 2016; Ryan et al., 2017). Microsatellites are repetitive DNA sequences consisting of mononucleotide or dinucleotide

repeats, usually one to five base pairs, found throughout the entire genome. This repetitive nature causes replication errors (Nguyen & Duong, 2018). Tumorigenesis derived from MSI status normally results from inactivation of DNA mismatch repair (MMR) genes through somatic mutation or aberrant methylation. It is widely reported that MSI is associated with post-replication DNA MMR deficiency of *MLH1*, *MSH2*, *MSH6*, and *PMS2* (Ewing et al., 2014). In most cases, MMR deficiency is due to somatic inactivation of the *MLH1* gene via promoter hypermethylation (Singh et al., 2021). MMR can be further divided into three types based on MSI status: MSI-High, MSI-Low, and MSI Stable (MSS) (Boland & Goel, 2010). However, MSI only occurs in a small proportion of patients, whereas MSS tumours usually develop via the CIN pathway making it the more dominant form of genomic instability in CRC (de la Chapelle & Hampel, 2010; Gupta et al., 2018; Markowitz & Bertagnolli, 2009).

1.6.3 CpG island methylator phenotype pathway

CpG island methylator phenotype (CIMP) or aberrant DNA methylation is another important pathway in CRC, with $CIMP^{+}$ cancer presenting in 20-30% of CRC patients. DNA hypermethylation at CpG islands of tumour suppressor gene promoters lead to gene silencing, which is the main mechanism for loss of MMR function (Ewing et al., 2014; Nguyen & Duong, 2018). This pathway is characterised by various criteria, for example, Shen et al., subtyped CRC into 3 subgroups, CIMP1, CIMP2, and CIMP negative via various genetic correlation with *BRAF*, *KRAS*, and *TP53*. CIMP1 had high levels of *BRAF* mutations and was often MSI-High. Whereas, CIMP2 has high *KRAS* mutations and low *BRAF* or *TP53* mutations (Shen & Waterland, 2007; Singh et al., 2021).

1.7 CRC molecular subtyping

Tumour staging relies on TNM classification; however, it is recognized that patients with same stage of disease develop different clinical outcomes. Furthermore, although TNM system is the best and most widely used predictor of long-term outcome in CRC; it does not predict patients' post-operative consequences. Therefore, novel prognostic classifications of CRC are needed. Molecular subtyping based on gene expression and genomic instability has widely studied in multiple research groups for this purpose. However, this resulted in multiple subtyping methods from different groups utilising a wide variety of different data processing methods, patient cohorts, samples preparation methods, and analysis workflows. This was due to the absence of gold standard analysis for subtyping in CRC. Therefore, in 2015, these groups came together to form the CRC Subtyping Consortium (CRCSC), with the aim of looking for consensus between the different subtyping methods developed to establish a definitive subtyping method for CRC (Guinney, Dienstmann, Wang, de Reynies,

Schlicker, Soneson, Marisa, Roepman, Nyamundanda, Angelino, Bot, Morris, Simon, Gerster, Fessler, Melo, et al., 2015).

1.7.1 The Consensus Molecular Subtypes

The CRCSC assessed the core subtype patterns from gene expression data of over 3000 patients from six independent research groups to create four robust and internationally validated classification called the consensus molecular subtypes (CMSs): CMS1-CMS4 (Guinney, Dienstmann, Wang, de Reynies, Schlicker, Soneson, Marisa, Roepman, Nyamundanda, Angelino, Bot, Morris, Simon, Gerster, Fessler, De Sousa, et al., 2015). CMS1 (MS1 immune, 14%) was characterised by hypermutation, MSI-High, strong immune activation, and showed good prognosis. CMS2 (canonical, 37%) was marked by WNT and MYC signalling activation. CMS3 (metabolic, 13%) was marked by evidence of metabolic dysregulation. CMS4 (mesenchymal, 23%) was marked by high level of transforming growth factor (TGF) beta activation, stromal invasion, and high density of stromal cells (CAFs), and had the worst prognosis (**Table 1.5**) (Buikhuisen et al., 2020; Fessler & Medema, 2016; Guinney, Dienstmann, Wang, de Reynies, Schlicker, Soneson, Marisa, Roepman, Nyamundanda, Angelino, Bot, Morris, Simon, Gerster, Fessler, De Sousa, et al., 2015. This classification system is the most robust and internationally utilised CRC classification system used for research.

Table 1.4 - The Consensus molecular subtypes of CRC (adapted from Buikhuisen et al., 2020; Fessler & Medema, 2016; Guinney, et al., 2015)

	CMS1 (MSI immune)	CMS2 (Canonical)	CMS3 (Metabolic)	CMS4 (Mesenchymal)
Percent of total cancer	14%	37%	13%	23%
Molecular characteristics	*BRAF* mutations Hypermutation MSI-High	*TP53* mutation CIN-High	*KRAS* mutations CIN-intermediate CIMP-Low	CIN-High
Pathways	JAK-STAT High	WNT High MYC High SRC High	Metabolic dysregulation	EMT High TGF-beta High
Microenvironment	Strong immune infiltration and activation			Stromal invasion High density of stromal cells (CAFs)
Prognosis	Good prognosis Poor prognosis after recurrence	Intermediate	Intermediate	Poor prognosis

1.7.2 CRC intrinsic subtypes

Another molecular subtyping system, the cancer-intrinsic subtypes (CRIS) was developed in 2017. This system was developed in patient-derived xenografts (PDXs) to assess human-specific expression profiling of CRC PDXs to determine cancer-cell intrinsic transcriptional features (Isella et al., 2017). The rationale was to specifically look at characteristics of the human cancer cells, to remove any dominating features of stromal cells within the tumour. From this method they produced five CRIS groups with distinct molecular, functional, and phenotypic characteristics. CRIS-A presented as mucinous, glycolytic, MSI enriched or *KRAS* mutant. CRIS-B was enriched for TGF-beta activity, high in epithelial-mesenchymal transition and presented with poor prognosis. CRIS-C had elevated EGFR signalling and sensitivity to EGFR inhibitors. Whereas CRIS-D had increased WNT activation, and overexpression of the *IGF2* gene. CRIS-E had a Paneth cell-like phenotype with *TP53* mutations. Furthermore, CRIS subtypes can categorize primary and metastatic CRCs independently (**Table 1.6**).

Table 1.5 - CRC intrinsic subtypes (CRISs) (table modified from (Buikhuisen et al., 2020; Singh et al., 2021)

	CRIS-A	CRIS-B	CRIS-C	CRIS-D	CRIS-E
Phenotype	Mucinous Glycolytic				Paneth cell-like phenotype
Molecular features	MSI-High CIMP-High $BRAF^{V600E}$ MSS CIN-Low CIMP-Low $KRAS^{mut}$		CIN-High $TP53^{mut}$ MYC Amplified	CIN-High -IGF2 gene overexpression and amplification	CIN-High $KRAS^{mut}$ $TP53^{mut}$
Pathways	Glycolysis Inflammation MSI-like Mucinous	EMT High TGF-beta High	EGFR High ERBB3 High	IGFR High FGFR High WNT High $Lgr5^{+}$-like	WNT High

CMSs and CRISs classification systems utilized transcriptional signatures which could potentially be implemented in a clinical setting to better assess patients' prognosis. However, the ability to employ these methods in pre-treatment biopsies, which would be most beneficial, was still

unconfirmed. Therefore, Alderdice et al. validated these systems in biopsies in 2018. They performed a comprehensive assessment of CRC signatures of CMSs and CRISs utilizing tumour sampling methodologies currently implemented in clinical and translational research including laser-capture micro-dissected CRC tissue, publicly available rectal cancer biopsy data sets from eight sources, serial biopsies from AXEBeam trial, NCT00828672, multi-regional biopsies from colon tumours, and pre-treatment biopsies from the COPERNICUS phase II rectal cancer trial (NCT01263171). The results were compared to results from CRC resection and found that CRIS classification provided significantly better classification than CMS for subtyping CRC primary tumour biopsies (Alderdice et al., 2018).

Although these two molecular subtyping methods are successfully validated CRC subtypes and widely implemented internationally for research, they both methods utilise transcriptomics approaches which have high costs associated and specialist equipment needed to analyse the gene expression data sets. Therefore, these have not yet been transferred to clinical practice, suggesting a cheaper clinically translatable method is still required.

1.8 Tumour microenvironment (TME)

One important feature of all these subtyping methods, it's that they consider the TME as an important part of the neoplastic process. Once cancer has developed, not only malignant cells are found within the tumour, but also non-transformed cells located around the malignant cells that form the tumour microenvironment. Non-malignant cells infiltrate into the tumour area including immune cells and stromal cells. Among the infiltrating cells in TME, immune cells play a crucial role either in killing the tumour cells or creating a microenvironment filled with chemokine, cytokines, and growth factors promoting tumour progression. Therefore, TME can be a tumour promoting environment or tumour suppressive environment depending on the role/make-up of the immune cells (Ahmad et al., 2014; Church & Galon, 2015; Dougan & Dougan, 2017; Pitt et al., 2016) (**Figure 1.2**). Other cells found in TME include cancer-associated fibroblasts (CAFs), adipocytes, vascular endothelial cells, pericytes, and lymphatic endothelial cells. These cells also play an important role in TME and can promote or suppress tumour progression. Among these cells, CAFs are well recognized as playing a significant role in carcinogenesis.

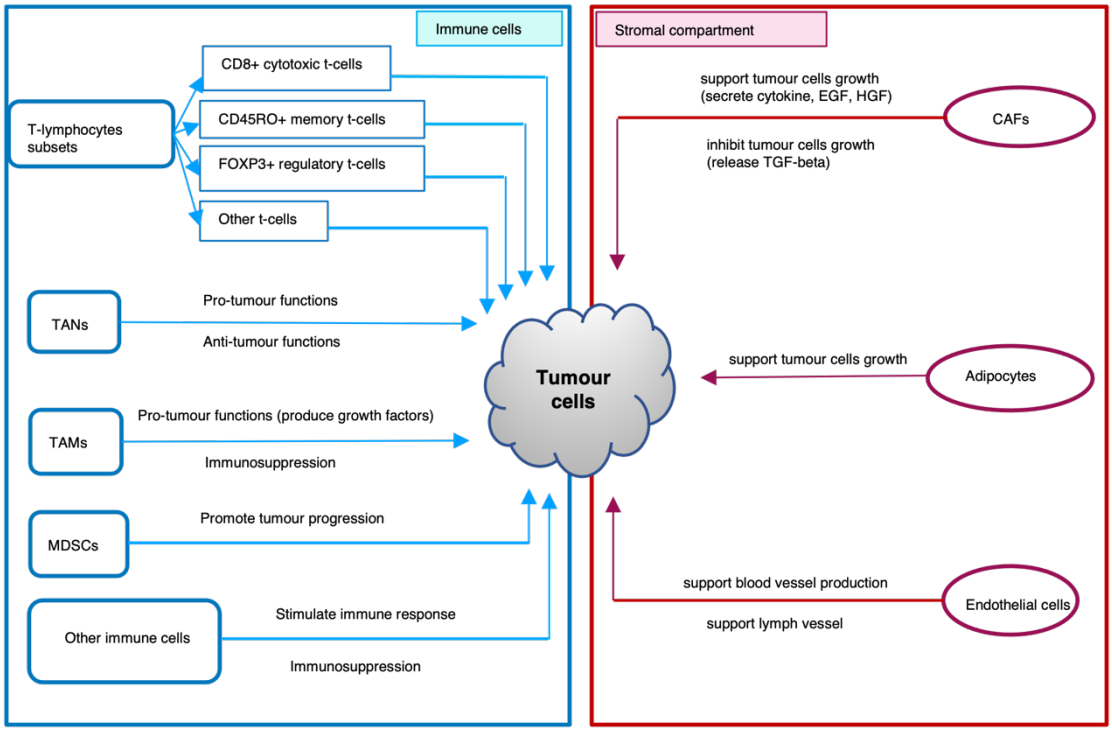

Figure 1.2 - Immune cells and stromal compartment in tumour microenvironment (TME). TME consist of two parts, stromal compartment, and immune cells infiltration. The important cells in stromal compartment such as CAFs, adipocytes, endothelial cells. Each cell type can support tumour growth and/or inhibit tumour growth. Immune cells infiltration such as T-lymphocytes subsets, TANs, TAMs, MDSCs, and other immune cells which can function as pro-tumorigenic and/or anti-tumorigenic. CAFs – cancer-associated fibroblasts, TANs – tumour-associated neutrophils, TAMs – tumour-associated macrophages, MDSCs – myeloid-derived suppressor cells

1.8.1 Stromal cells in the TME

As cancer cells grow, develop, and progress they need many factors including oxygen and nutrients, from the surrounding TME, tissues, and vessels. Stromal cells within the TME provide many of these essential factors. Stromal cells communicate with each other by complex networks (chemokines, cytokines, inflammatory enzymes, and growth factors) (Korneev et al., 2017) and can directly influence the cancer cells to promote tumour suppression or tumour-progression depending upon the overall make-up of the TME (Balkwill et al., 2012; Hanahan & Coussens, 2012). The stromal cells present within the TME are mainly CAFs and adipocytes.

In CRC, CAFs are the main component and play various roles in CRC metastasis, prognosis, and driven drug resistance. Adipocytes also have a role in CRC progression and survival. The infiltration of stromal cells into the TME could be used to determine the progression of disease and patient outcome using the TSP, and high stromal infiltrate was found to be associated with poor patient prognosis. This could be because high stroma may inhibit immune infiltration into tumour area due to the factors they secrete.

1.8.1.1 Cancer-associated fibroblasts (CAFs)

CAFs are the major type of stromal cells within the TME and are recognized to play an essential role in carcinogenesis, tumour progression, and invasion by directly communicating with both the cancer cells and other stromal cells through chemokine production. CAFs secrete regulatory factors into the TME that support many tumour actions such as tumour growth and metastasis; therefore, CAFs act as a support for tumour cells. CAFs are differentiated from various progenitor cells including mesenchymal stem cells, epithelial cells, endothelial cells, and pericytes; and further develop into a heterogeneous cell population with distinct roles (Shiga et al., 2015). CAFs secrete cytokines, epidermal growth factors (EGF) and hepatocyte growth factors (HGF) to induce tumour growth and survival. These proteins secrete by CAFs can act as cancer cell enhancers to promote tumour migration, invasion, and metastasis (Tao et al., 2017). As well as their role in tumour promotion, CAFs can also have a tumour-suppressive role by releasing TGF-β in the early stages of carcinogenesis to lower tumour initiation. Their role then switches in later stages to promote tumour development (Ishii et al., 2016). Thus, CAFs can act as both tumour promoting and tumour suppressive depending on stage, potentially due to the immune cells within the tumour and are therefore potential drug targets for cancer therapy in advanced disease; however, CAFs have been implicated in promoting cancer cells resistance to therapy (Tao et al., 2017).

In CRC, CAFs have been identified as having a variety of roles and play a major role in promoting CRC metastasis as studied by Potdar and Chaudhary et al. They formed primary cultures of CAFs from CRC patients with metastasis and performed cellular characterization by histological staining and assessed the molecular characterization of the metastasis promoting genes. The result showed that CAFs preserve their phenotype and maintain proliferation but also found the expression of genes associated with cancer stem cells and genes that play a role in resistance to chemotherapeutic drugs (Potdar & Chaudhary, 2017). There is now a rising role for CAFs in driving drug resistance in CRC, which may explain their association with poor prognosis (Garvey et al., 2017).

1.8.1.2 Adipocytes

Previously, adipocytes were recognized as a main source of energy storage and their role in cancer was not well understood. Recently, adipocytes have been proposed as the main source of endocrine cells that secrete hormones, cytokines, growth factors, and adipokines. Cytokines produced from adipocytes include TNF-α, IL-6, CCL2, and IL-1β to recruit inflammatory cells to infiltrate adipose tissue and create a low-grade inflammation. This type of chronic inflammation leads to metabolic deregulations that end up causing obesity, which is related to cancer development and poor prognosis. It is known that chronic inflammation is a risk factor for CRC development and tumour progression. Adipose tissue consists not only of adipocytes but also contains other cells including

lymphocytes, macrophage, pericytes, endothelial cells, and adipocyte progenitor cells. It works in many ways to regulate tumour development, for example, through adipokines, cytokines, or miRNA. Recently, miRNA has been proposed as one of the key factors associated with development of many diseases including cancer (Correa et al., 2017).

In CRC, adipocytes and other loose connective tissue are parts of mesentery, which is the envelope of colon. Adipocyte's accumulation and distribution in the submucosal compartment has been reported, and this is thought to be a cause of inflammatory bowel disease. A molecular pathological epidemiology study has shown that obesity associated with molecular alterations promotes CRC development. However, the relationship between TME-associated adipocytes and the induction of epigenetic modifications has not been reported (Tabuso et al., 2017). Recently, adipocytes isolated from CRC patient's adipose tissue has been studied. The result showed that adipocytes play a role in cellular metabolism that could modulate and support both tumour growth and survival. Therefore, adipocytes not only provide energy to cells in TME but also have a role in regulating tumour cell growth and survival and could be a good target for CRC therapeutics (Wen et al., 2017).

1.8.2 Immune cells in TME

Generally, tumour tissue is infiltrated with inflammatory cells, which is the normal reaction of the host immune response reacting to the foreign tumour cells. The immune cells consist of cells in the lymphoid lineage and myeloid lineage. Lymphoid lineage cells are mostly T-lymphocytes, B-lymphocytes, and natural killer (NK) cells. Myeloid lineage cells are TAMs, MDSCs, TANs, and mast cells (Balkwill et al., 2012).

It is now known that many cancer types are preceded by chronic inflammation due to mucosal epithelial cells or microorganism colonisation, for example, hepatocellular carcinoma arising from hepatitis B and hepatitis C virus, cervical cancer arising from human papilloma virus (HPV), or gastric cancer arising from *Helicobacter pylori* (Moss & Blaser, 2005). The chronic inflammatory response in wound healing and in cancer is therefore similar; however, tumours can co-opt this wound healing response to promote maintenance and growth (Dvorak, 2015).

In early-stage tumours, immune cells participate in preventing tumour progression by detecting tumour cells and destroy them, however, these cells can be hijacked by the tumour to perform another role promoting cancer development, by dampening the lymphoid immune response and promoting the myeloid immune cells, which have been shown to be crucial for tumour progression (Edmondson et al.; Grivennikov & Karin, 2010).

1.8.3 Immune cells in CRC

In CRC carcinogenesis, a major risk of colon cancer development is inflammation occurring in bowel or inflammatory bowel disease (IBD), which is responsible for 10% to 15% of colon cancer deaths (Dyson & Rutter, 2012; Terzic et al., 2010). IBD is more likely to progress to colon cancer in younger patients than sporadic CRC. The higher risk of CRC associated with IBD is potentially due to genetic factors (Kim & Chang, 2014). Although a connection between inflammation and cancer is also indicated. However, the mechanism behind how IBD can initiate CRC and the role of chronic inflammation is still a highly active area of research.

Recently, Mariani et al. examined the crucial inflammatory pathways involved in the initial step of CRC developments including tissue injury, chemical agents, and continuing inflammation of large bowel (Mariani et al., 2014). These can all lead to chronic inflammation hyper-stimulating cells of immune system and their related proteins within the systemic inflammatory response to promote a central mechanism for CRC development for example changes in cell proliferation, DNA damage, and apoptosis. This systemic inflammatory response is predominantly due to innate immune cells. This may be why an increase in the systemic inflammatory response has been shown to associate with a poor prognosis for patients.

Systemic inflammatory response could be measured by using C-reactive protein (CRP); which has been reported as an independent prognostic value in CRC. McMillan et al. has presented that elevated CRP concentrations in the circulation and decreased albumin concentration has the same relationship in different tumours and could be used as a prognostic score (McMillan, 2013). This systemic inflammation-based prognostic score was termed the Glasgow Prognostic Score (GPS) and the GPS was then further modified (mGPS) by removing the score for decreased albumin without elevated CRP (**Table 1.9**). Today, the GPS/mGPS is clearly validated and could be used in a patient's routine risk assessment and as therapeutic target for future research. However, mGPS is not the only score to assess the systemic inflammatory response, the neutrophil to lymphocyte ration (NLR) and Lymphocytes to macrophage ration (LMR) are among a host of novel scores being developed for this purpose.

Table 1.6 - mGPS systemic inflammation score (adapted from McMillan, 2013)

Biochemical characteristics	Score
CRP < 10 mg/L + any albumin	0
CRP > 10 mg/L + albumin > 3.5 g/dL	1
CRP > 10 mg/L + albumin < 3.5 g/dL	2

In contrast, a local immune response is crucial for preventing tumour progression. The local inflammatory response in CRC patients has been evaluated and the result indicated that when there is a strong immune cell infiltrate at tumour sites patients live longer (Richards et al., 2014); therefore, local inflammation could be the significant indicators of CRC prognosis. Local inflammatory response in CRC could be utilised as a prognostic score; for example, the Klintrup-Makinen (KM) grade, which uses an H&E slide, looking at general inflammation at the invasive margin; the Galon's Immunoscore, which uses an immunohistochemistry (IHC)-based score grading lymphocytes infiltration at both invasive margin and central tumour. Local inflammation in early-stage CRC can strongly recruit many T-cell subtypes including CD8+ cytotoxic T-cells, CD45RO+ memory T-cells, and FOXP3+ Tregs, which are crucial for a good patient prognosis due to their role in eliminating tumour cells. However, in later stages, tumour cells can evade the host immune response and escape from immunity, or the system can be hijacked by tumour cells to utilise TAMs and MDSC to promote its growth.

1.8.3.1 Lymphocytes

One of the most important inflammatory cells found infiltrating cancer cell nests are T-lymphocyte known as tumour infiltrating lymphocytes (TILs). Yoshitaka et al., (1998) analysed the localisation of $CD8^+$ T-lymphocytes (cytotoxic T-lymphocyte) in CRC patients. The results showed that $CD8^+$ T-lymphocytes localised in three different areas: within cancer cell nest, in the stroma, and at the invasive margin. The role of $CD8^+$ T-lymphocytes was analysed by performing CD8 and Ki-67 immunohistochemistry. The result indicated that $CD8^+$ T-lymphocytes were mainly present in highly proliferative cancer cells nests, and this associated with increased patient survival. Therefore, $CD8^+$ T-lymphocytes has been used as a useful prognostic factor for patient's better survival. Furthermore, the local inflammatory response has been assessed by analysing T-lymphocytes subtypes including $CD3^+$, $CD8^+$, $CD45RO^+$, $FoxP3^+$ and their relationship with host characteristics in CRC patients (Richards et al., 2014). The result found that a strong lymphocyte infiltration was associated with improved cancer-specific survival. Strong $CD3^+$ T-lymphocytes at the invasive margin or $CD8^+$ cells within cancer cell nests were the best predictors of improved survival. These two studies both suggest that $CD8^+$ T-lymphocytes present in CRC cell nest are a strong predictor of patient survival. Interestingly, a study by Hagland et al. about the location and density of $CD3^+$ and $CD8^+$ T-lymphocytes in pre-surgical blood and at the intra-tumoral site in CRC patients showed that $CD3^+$ and $CD8^+$ T-lymphocytes numbers in the circulation significantly correlate with $CD3^+$ and $CD8^+$ numbers at invasive margin and centre of the tumour (Hagland et al., 2017). Therefore, circulating T-lymphocytes in the blood could be used as liquid biopsy to determine patient's immune status to assist clinical decision making since blood samples collection is easier than tumour tissue biopsy.

Regulatory T-lymphocytes (Tregs) play an important role in homeostasis of the immune response by inhibiting self-antigens defence mechanisms and non-self-antigens response. Moreover, Tregs are also involved in controlling many mechanisms of immune system i.e. inflammation, infection, autoimmunity (Sakaguchi et al., 2008). Normally, Tregs, express $CD4^+CD25^+$ and were later found to also express Forkhead box protein 3 (FoxP3), regulatory transcription factor, which can be used as markers to identify the cells (Hori et al., 2003). The clinical impact of Tregs has studied by determining the expression of FoxP3 and CD8 cells (Zeestraten et al., 2013). The result showed that $FoxP3^+$ cells were present in tumour stroma and tumour epithelium separately; and this result related to clinical outcome. They found that high level $FoxP3^+$ cells in tumour epithelium related to down regulation of HLA Class I expression, which resulted in low host immune cells recognition leading to a decrease in tumour cells elimination. They also showed that the $CD8^+/Foxp3^+$ cell ratio significantly correlated with improved patient's survival. These studies suggest that T-cells subsets, $CD8^+$, $CD45RO^+$, $Foxp3^+$ could be good prognostic markers for patient survival.

1.8.3.2 Myeloid-derived suppressor cells (MDSCs)

MDSCs is the immature myeloid cells present in most cancer patients. Their main role is to inhibit innate and adaptive immunity and prevent the immune system from eradicating transformed cells including cancer cells. MDSCs and Tregs have been designated as the main negative regulation mediators of the immune response within TME, leading to a poor prognosis and increased tumour progression. In short, MDSCs are a heterogeneous population of myeloid cells, which have ability to suppress T-lymphocytes responses. Commonly, MDSCs express $CD33^+$ and $CD11b^+$ markers, but have no expression of mature cell markers. Many studies have indicated that MDSCs are present at high levels in peripheral blood and TME and exhibited tumour-specific immunosuppressive effects to promote tumour progression. MDSCs has also been shown to be a major factor that can reduce the efficacy of current cancer immunotherapy treatment by suppressing the cells activated (Toor et al., 2016). Toor et al., (2016) showed a significant increase of myeloid cells in CRC patient's peripheral blood and tumour tissue compared to healthy donors suggesting these cells are contributing to tumour progression and inhibiting MDSCs may be a potential target for immunotherapy in CRC in combination with current regimens (Toor et al., 2016).

1.8.3.3 Tumour-associated macrophages (TAMs)

In the CRC TME, macrophages are the most abundant immune cell populations (Wang et al., 2021; Yahaya et al., 2019). Many studies have proposed that TAMs engaged pro-tumour functions, and that TAMs infiltration correlates with tumour progression, growth, aggression, and prognosis. In contrast, some studies suggested that TAMs in CRC express an anti-tumour activity and improve patient's survival. This may be explained as macrophages are divided into two subtypes; M1-like macrophages promote response to Th1 lymphocytes, have microbicidal, and tumoricidal effects, and

secrete tumour necrosis factor-α (TNF-α), IL-1, and IL-12 to supress tumour growth; whereas M2-like macrophages stimulate response to Th2 and Tregs, and promote tissue remodelling, immune tolerance, and tumour progression.

1.8.3.4 Tumour-associated neutrophils (TANs)

It is known that neutrophils are the most abundance granulocytes which play a role in the first line of the host defence mechanism to pathogens. In cancer biology, TANs (Liu et al.) play a crucial role and make up the significant part of inflammatory cell infiltrate. However, the role of TANs within the CRC TME was investigated by Rao et al. by assessing CD66b, which is specific to neutrophil granulocytes ($CD66b^+$ cells), and their associations with clinicopathological factors. The results showed that TANs increase within the TME, and this independently associated with CRC malignancy and low survival rate in CRC patients (Rao et al., 2012). This suggest that, like macrophages, TANs can be both anti- and pro-tumorigenic and this may be due to different subtypes as seen in macrophages. However, the occurrence and significance of TAN in CRC patients is still the subject of controversy. Governa et al. have studied the association of $CD8^+$ T-lymphocytes and TANs (Governa et al., 2017). The study proposed that there is interplay between $CD8^+$ T-lymphocytes and TANs, which can improve CRC survival. Recently, Berry et al. has counted TANs levels in CRC patients with stage II disease to determine whether TAN levels could have a role in prognosis (Berry et al., 2017). The results showed that patients with high TANs lived three times longer than those with low TANs and that woman survived longer than men. However, TANs level has no association with stage III/IV patients. In addition, Wikberg et al. has elucidated the prognostic role of TANs infiltration in CRC by assessing the relationship to other immune cells including T-lymphocytes and macrophages (Wikberg et al., 2017). The result found that TANs infiltration, whether correlated to other immune cells infiltration or not, had prognostic value itself. The author concluded that even low TANs infiltration at the tumour front could represent an independent prognostic factor for poor prognosis in CRC early stages. Therefore, $CD66b^+$ TANs within the TME can have dual roles and more detailed investigation is needed to unravel this fully.

1.9 Histological classification

Histological classification is a conventional clinical prediction of tumour in patients normally performed by evaluating histopathological characteristics in tissue samples i.e., the size of tumour, histological grading, proteins and genetic markers expression, malignant transformation, proliferation, venous invasion, tumour perforation/serosal involvement, margin involvement, vascularization, and tumour budding (Loughrey, 2020; Loughrey, 2018). It is a cheap method currently used in most clinical laboratories, making it highly translatable to clinical practice.

Therefore, could histological classification be used to subtype patients by considering the tumour and the components of the TME.

1.9.1 Immunoscore

Most conventional classifications, such as TNM, focus only on tumour cells and do not consider the local immune response involved. However, the impact of local immune system has been recognized as providing a role in the regulation of tumour progression. Therefore, a classification based on immune cells infiltrate into tumour was proposed in 2012 called 'Immunoscore' which has been validated and widely used to predict patient's prognosis (Galon et al., 2012).

The Immunoscore is based on the measurement of t-cells populations infiltration in tumour by utilizing immunohistochemistry (IHC) techniques. Immunoscore (I) categorizes by lymphocyte populations, $CD3^+/CD45RO^+$, $CD3^+/CD8^+$ or $CD45RO^+/CD8^+$, at the centre of the tumour (CT) and at the invasive margin (IM) (**Figure 1.2**). From the two large cohorts evaluated using CD8 and CD45RO, the Immunoscore was scored from I0 (if low densities of both cells in both locations) - I4 (if high densities of both cells at both locations). Of which, only 4.8% of patients were I4 but had high survival rate (86.2%), whereas 72% of patients with I0 or I1 and had only a 27.5% survival rate (Galon et al., 2012). Later, a standardized consensus found that Immunoscore was a strong prognostic factor for DFS, DSS, and OS including in early-stage CRC superior to conventional TNM classification (Galon et al., 2014). Therefore, if Immunoscore was introduced into a clinical setting it could classify patient prognosis and potentially predict patients likely to respond and benefit from immunotherapy (Galon & Lanzi, 2020).

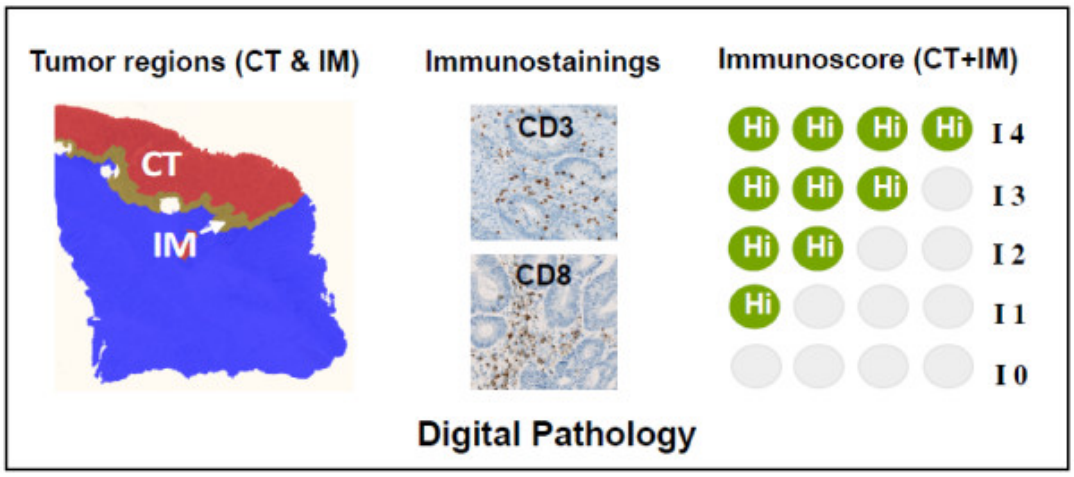

Figure 1.3 - Immunoscore classification (Galon et al, 2012). Immunoscore assessing the CD3 and CD8 infiltration at center of tumour and at invasive margin based on immunostaining and characterizded into I0 - I4 from infiltration level.

1.9.2 Glasgow Microenvironment Score

Glasgow Microenvironment Score (GMS) is another histological subtyping method that has been developed for CRC classification. GMS is a tumour microenvironment-based prognostic score based on assessment of inflammatory cells infiltrate and tumour stroma in primary operable CRC patients (Park et al., 2015). For this method, inflammatory cells infiltrate, and tumour stroma infiltration were assessed based on the Klintrup-Makinen (KM) grade and tumour stroma percentage (TSP), respectively. The KM grade measures inflammatory cell infiltrate at the invasive front of tumour using H&E-stained sections. The sections are subjectively graded into four-point scale (0-3), and then classified into low-grade (scale 0-1, no or mild increase of inflammatory cells) or high-grade (2-3, inflammatory cells forming a prominent band or florid cup-like infiltrate). TSP measures the stromal proportion within an H&E section by assessing the percentage of stromal cells within the visible field excluding areas of necrosis and are then graded into low TSP (<=50%) and high TSP (>=50%) (Park et al., 2015).

GMS stratified patients into three prognostic groups; strong KM (GMS=0), weak KM/low TSP (GMS=1), and weak KM/high TSP (GMS=2) (**Table 1.7**), which presented a significant difference in 5 years survival rate from 89%, 75%, and 51%, respectively (Park et al., 2015). GMS has subsequently been validated in two cohorts: TNM I-III CRC validation cohort and TNM II-III CRC adjuvant chemotherapy cohort (TransSCOT). Disease-free survival (DFS) and recurrence-free survival (RFS) were the primary endpoint for both cohorts and adjuvant chemotherapy interaction as exploratory endpoint for the TransSCOT cohort. The result showed that GMS is independently associated with DFS and RFS in both cohorts. In addition, GMS0 significantly associated with improved DFS in patients receiving FOLFOX when compared to CAPOX chemotherapy (Alexander et al., 2021).

Table 1.7 - GMS classification **(**adapted from Park et al, 2015)

	GMS 0	**GMS 1**	**GMS 2**
Intra-tumor immune infiltrate (KM grade; 0-1/2-3)	High	Low	Low
Stromal invasion (TSP; ≤50%/>50%)	Any	Low	High

1.9.3 Phenotypic subtypes

Recently, Roseweir et al. has proposed histological phenotypic subtypes based on CRC phenotypic features related to the CMS subtypes. They utilised the three features most differentially associated with each CMS group; immune infiltrate measured by the KM grade, proliferation rate measured using Ki67 immunohistochemistry and stromal invasion measured by TSP, to propose a simple phenotypic subtyping method with four groups: immune, canonical, latent, and stromal (**Table 1.8**). The effect of the phenotypic subtypes on DFS and recurrence risk (RR) was assessed as the primary outcome in three independent stage I-III CRC cohorts; the result found significant associations with both DFS and RR in all three cohorts. Of these, immune presented with a good prognosis, canonical and latent having intermediate prognosis, while stromal showed the worst prognosis (Roseweir et al., 2020). Similar to GMS, the exploratory outcome within the TranSCOT cohort was associations with chemotherapy. The results, showed that immune subtype patients responded better to FOLFOX compared to CAPOX chemotherapy, confirming the results of the GMS study. From the results, phenotypic subtypes or GMS could be used in routine clinical pathology for CRC patient's prognosis and to predict response to chemotherapy.

Table 1.8 - Phenotypic subtype classification (adapted from Roseweir et al, 2020)

	Immune	Canonical	Latent	Stromal
Intra-tumor immune infiltrate (KM grade; 0-1/2-3)	High	Low	Low	Low
Stromal invasion (TSP; ≤50%/>50%)	Any	Low	Low	High
Proliferation rate (Ki67; ≤30%/>30%)	Any	High	Low	Any

1.10 Targeting immune cells for CRC treatment

Recently, immunotherapy based on immune system modulation has been proposed as an alternative CRC treatment to increase the effect of T-lymphocytes, to increase the immune response. Of this, immune system negative regulators, known as immune checkpoints, play a crucial role to limit the anti-tumour immune response and are an important immunotherapeutic target (Passardi et al., 2017).

1.10.1 Immunotherapy in cancer

Cancer therapy is mainly focussed on surgery, chemotherapy, radiotherapy, and endocrine therapy (Urruticoechea et al., 2010). However, these strategies frequently reach a refractory period leading to treatment failure and the patient developing disease recurrence (Housman et al., 2014; Raguz & Yague, 2008). One solution may be to focus on enhancing the patient's own immune system to attack the tumour; as once cancer is initiated, it can progress because of tumour cells escaping from the immune system. Tumour cells can escape the immune response in variety ways in order to survive and further progress without being attacked by immune cells (Ahmad et al., 2004). Additionally, tumour cells can prevent immune cell actions, with the support of multiple cell types to create an immunosuppressive microenvironment (R J Seager, 2017). Therefore, tumour escape from immunologic control is confirmed as one of the hallmarks of cancer (Hanahan & Weinberg, 2011).

The immune responses recognise tumour cells and eradicate them by multiple processes involving cooperation of both the innate and adaptive arms (Blair & Cook, 2008; Shanker & Marincola, 2011). This process involves both positive and negative regulators. Positive regulators enhance anti-tumour activity, whereas negative regulators inhibit this killing process and enhance tumour growth instead. Therefore, immunotherapy that targets the immune response negative regulators to enhance the anti-tumour responses could be a promising alternative treatment strategy and may be a powerful tool to treat cancer.

Immunotherapy is now a main focus for many cancer types; it works by restoring the patient's immune responses to eliminate tumour cells (Farkona S, 2016; Stanley J. Oiseth, 2017a). It can be classified as active or passive by assessing the mechanism by which the therapy activates an immune response (Galluzzi et al., 2014). Active immunotherapy includes preventive and therapeutic vaccines, immunomodulatory monoclonal antibodies, i.e., immune checkpoint inhibitors, and immunostimulatory cytokines, that stimulate the host's adaptive immune response in situ. Passive immunotherapy focuses on activating the host's immune response in vitro and transfers it back to the host known as adoptive cell transfer or cell-based therapy, i.e., chimeric antigen receptor (CAR-T) cell therapy. Immune checkpoint inhibitors have been a major focus of immunotherapy research.

1.10.2 Immune checkpoints

Active immunotherapy targets the host's immune response to induce activation and restore anti-tumour function. Immune checkpoints are negative regulators of the immune system and play a crucial role in limiting anti-tumour immune responses. In the normal anti-cancer immune response, antigens on the surface of tumour cells bind to checkpoint proteins on the surface of T-lymphocytes leading to decreased T-lymphocytes function. This controls the anti-tumour response and avoids T-

lymphocytes exhaustion; however, the tumour can hijack this mechanism to suppress anti-tumour functions and promotes tumour progression. Therefore, these immune checkpoints are important immunotherapeutic targets, with checkpoint blockade inhibiting this immune system modulation resulting in increased effector T-lymphocytes that can coordinate an anti-tumour response (Passardi et al., 2017). Immune checkpoint inhibitors are the most widely studied active immunotherapy in cancer research leading to some having been approved for clinical use (Dine et al., 2017). Two types of co-inhibitory proteins that are widely studied are programmed cell death protein 1 (PD-1) and cytotoxic T-lymphocyte antigen 4 (CTLA-4) (**Figure 1.4**).

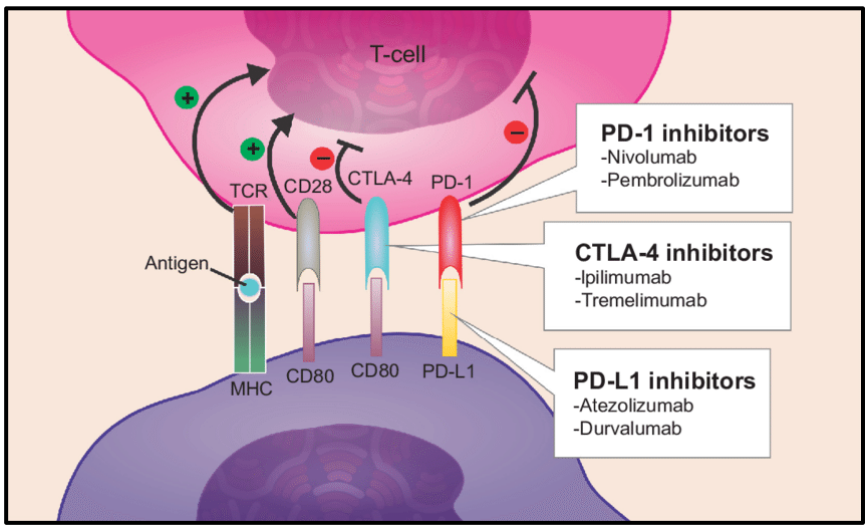

Figure 1.4 - Immune checkpoints and inhibitors ; Showing checkpoint proteins : PD-1, PD-L1, and CTLA-4 and their inhibitors ; PD-1 inhibitors : Nivolumab and Pembrolizumab, CTLA-4 inhibitors : Ipilimumab, Tremelimumab, PD-L1 inhibitors : Atezolizumab, Durvalumab (RA de Mello, 2016).

1.10.2.1 PD-1 and PD-L1

PD-1 (program cell death-1), known as CD279, is a type I transmembrane protein, a member of the CD28 family which is expressed on activated and exhausted T- and B-lymphocyte. PD-1 is expressed during the effector phase in peripheral tissue and is upregulated in many tumours. It binds to specific ligands, called PD-L1 (program cell death ligand-1) and PD-L2 (program cell death ligand-2), on tumour cells.

PD-L1 is expressed on various types of solid tumours, but is not expressed in normal epithelial tissue, where PD-L2 is the dominant form. When PD-1 binds to PD-L1 there is decreased cytokine production and inhibition of T-lymphocytes proliferation and function within peripheral tissues and tumours. This plays a key role in negative immune cell regulation resulting in tumour immunity balancing and attenuation of the T-lymphocyte response within the tumour microenvironment (Robert et al., 2015; Singh et al., 2015).

1.10.2.2 CTLA-4

Cytotoxic T-lymphocyte antigen-4 (CTLA-4), also known as CD152, is a CD28 homolog membrane glycoprotein on T-lymphocyte, found during the priming phase in lymph nodes. CTLA-4 interacts with specific protein (B7) on tumour and antigen presenting cells (APC) to produce co-inhibitory signals to decrease T-lymphocyte anti-tumour responses (Buchbinder & Desai, 2016). This was the first pathway for immune checkpoint regulation that was proposed in 1996 by Leach et al. (Leach D, 1996).

1.10.3 Immune checkpoints inhibitors

Immune checkpoint interactions can be blocked with anti-PD-1/anti-PD-L1/anti-CTLA-4 antibodies leading to immune cell re-activation and a coordinated anti-tumour response of T-lymphocytes. Currently, three anti-PD-1 immune checkpoint inhibitors, pembrolizumab, nivolumab, and cemiplimab are approved for use within the clinical setting. Three anti-PD-L1 antibodies were also approved: atezolizumab, durvalumab, and avelumab. Ipilimumab is the only anti-CTLA-4 approved for clinical use.

1.10.3.1 Anti-PD-1 therapy

Pembrolizumab has been studied in multiple solid tumours and showed anti-tumour activity in clinical trials. As a result, in 2014, it was approved to treat advanced melanoma based on a phase III studied comparing pembrolizumab and the anti-CTLA-4, ipilimumab; pembrolizumab demonstrated prolong overall survival and less toxicity than ipilimumab (Schachter et al., 2017). In 2015, pembrolizumab was further approved to treat advanced non-small-cell lung cancer (NSCLC) based on the result that it showed anti-tumour activity with manageable side-effects (Garon E, 2015). In 2016, pembrolizumab was approved for recurrent or metastatic head and neck squamous cell carcinoma patients (Seiwert et al., 2015). A study by Seiwert et al. showed that pembrolizumab has efficacy over standard therapy by cetuximab. However, the latest phase III trial by Merck and Co., showed that this drug did not result in improved overall survival as previously observed (Cohen et al., 2015). This finding did not affect the previous approval but does show variability in results for this cancer type and suggests that a predictive biomarker is needed to select responsive patients.

Pembrolizumab has been approved for multiple types of cancer including classical Hodgkin Lymphoma (cHL), metastatic urothelial carcinoma (mUCC), gastric cancer or gastroesophageal junction (GEJ) adenocarcinoma, and CRC. In cHL, pembrolizumab was approved based on the study that treated both adults and pediatric patients with resistance to current therapy. The result showed a 69% overall response rate with 11.1 months (Moskowitz et al., 2016). In advanced mUCC, it was approved based on the study the phase II trial that compared pembrolizumab to chemotherapy. Pembrolizumab showed a median overall survival of 10.3 months, whereas chemotherapy only

showed a median survival of 7.4 months (Bajorin et al., 2015). In the same year, pembrolizumab was also approved for non-resectable or MSI-High/mismatch-repair deficient (dMMR) solid tumours including CRC (D.T. Le et al., 2015) (Diaz et al., 2017; Le et al., 2016; Seiwert et al., 2015). This was the first approval based on the specific biomarkers regardless of the origin of tumour.

In gastric cancer or GEJ adenocarcinoma, pembrolizumab was approved based on the phase II (Fuchs et al., 2018). From the 143 patients, the result showed 13.3% objective response rate and response duration of 2.8-19.4 months. MSI-H was observed in 7 patients showing a 57% objective response rate and response duration from 5.3-14.1 months suggesting MSI status could predict response to pembrolizumab as seen in other cancers. Recently, pembrolizumab was further approved for treatment of recurrent or metastatic cervical cancer for patients who express PD-L1 on tumour cells (Chung et al., 2018). In the same month, it was further approved to treat resistant primary mediating large B-cell lymphoma (PMBCL) in adults and pediatrics and showed a 45% response rate (Michot et al., 2016). However, 26% of patients did develop serious adverse effects suggesting further work is still needed in the cancer type.

Nivolumab, a second PD-1 inhibitor, has also been investigated in several tumours and shown anti-tumour activity. In 2014, it was approved for metastatic melanoma treatment (Long et al., 2015; Raedler, 2015), and in 2015, nivolumab was further approved for metastatic NSCLC after a study demonstrated improved overall survival compered to docetaxel therapy (Kazandjian et al., 2016). Nivolumab was also approved for use in advanced metastatic renal cell carcinoma (RCC) as it showed improved overall survival over everolimus (Afinitor) (Motzer et al., 2015). In 2016, nivolumab was approved for recurrent or metastatic head and neck squamous cell carcinoma (HNSCC) after a study showed longer overall survival when compared to chemotherapy (Ferris et al., 2016).

Recently, in September 2018, cemiplimab (REGN2810) is approved to treat patients with metastatic cutaneous squamous cell carcinoma (CSCC) or locally advanced CSCC who are not candidates for curative surgery or curative radiation (Papadopoulos et al., 2018). There are also many other anti-PD-1 antibodies, for example, pidilizumab (a humanized anti-PD-1), AMP-224, MEDI0680, PDR001, CT-001, in clinical trials for several tumour types (Alsaab et al., 2017).

1.10.3.2 Anti-PD-L1 therapy

PD-L1 inhibitors have also been approved for use in solid tumours. Atezolizumab was approved for advanced bladder cancer (Jean H. Hoffman-Censits 2016) and metastatic NSCLC in 2016 (Fehrenbacher et al., 2016; Rittmeyer et al., 2017). In 2017, avelumab was approved for merkel cell cancer, an aggressive skin cancer, and urothelial carcinoma. In merkel cell cancer, avelumab was the

first targeted therapy approved for this disease, the phase II trial studied avelumab in stage IV chemotherapy refractory disease via an international multicenter trial across North America, Europe, Asia, and Australia (Kaufman et al., 2016). The result showed a 31% response rate and 10.4 months response duration. In urothelial carcinoma, a study in metastatic urothelial carcinoma patients showed 11.4 weeks median response rate. However, almost all patients developed adverse events (Patel et al., 2016). Overall, PD-1 and PD-L1 inhibitors have shown good response rates across a variety of cancers but further work is needed to enhance their efficacy and decrease toxicity. In addition, durvalumab is approved for advanced or metastatic urothelial carcinoma in 2017 and NSCLC in 2018 (Scott J. Antonia, 2017; Thomas Powles, 2017).

1.10.3.3 Anti-CTLA-4 therapy

The main CTLA-4 inhibitor studied to date is ipilimumab, a monoclonal antibody that was the first checkpoint inhibitor the FDA-approved for advanced melanoma in 2014. It was shown to increase T-lymphocyte proliferation and restore the anti-tumour immune response (Pardoll, 2012). Based on the phase III clinical study in unresectable stage III or IV melanoma that divided patients into 3 treatment groups, ipilimumab plus glycoprotein 100 (gp100) peptide vaccine, ipilimumab alone, and gp100 alone. The result showed that ipilimumab significantly improved patients overall survival compared to the gp100 alone or the combination (Hodi et al., 2010). Ipilimumab has now also been approved for use in renal cell carcinoma in combination with nivolumab (Hammers et al., 2015).

Tremilimumab, an IgG2 monoclonal antibody, is another anti-CTLA-4 that showed satisfactory result in phase I/II studies in advance melanoma (Comin-Anduix et al., 2016). However, when test in a phase III trial compared with chemotherapy, tremilimumb induced toxicity and showed no survival benefit over chemotherapy (Ribas et al., 2013). Therefore, tremilimumab was not approved, but further clinical trials are now ongoing to study this drug in combinations with current therapies and to assess potential biomarkers to predict treatment response.

1.10.4 Immune checkpoint inhibitors in CRC

Although checkpoint inhibitors have exhibited successful results in other tumours, in CRC, the results for immunotherapy are not as favorable. Initial studies showed some promising results in metastatic CRC patients with MSI-High tumours, but not in MSS patients, which only represents a small proportion of metastatic patients. Therefore, pembrolizumab and nivolumab are only FDA-approved for this small group of patients with metastatic MSI-High CRC, suggesting that other strategies are required for these inhibitors to be translated to a wider range of CRC tumours.

To address this, immune checkpoint inhibitors are now being trialed in combination with chemotherapy, radiotherapy, and other agents that might block factors that suppress the immune response or agents that directly stimulate the immune response, to prime for immunotherapy use (Boland & Ma, 2017). However, there is still a problem with resistance to checkpoint inhibitor due to various factors including signaling pathways which inhibit the anti-tumour activity of immune cells (Jenkins et al., 2018). Now, monotherapy or combination therapy to enhance the drug efficacy and reduce this resistance rate in CRC is being considered in parallel to examining new therapeutic targets.

Therefore, a combination of pembrolizumab with azacytidine chemotherapy was performed in MSS metastatic CRC. The results observed an enhancement of pembrolizumab anti-tumour activity when combined with this chemotherapy in MSS metastatic CRC. The trial is now in phase II with a cohort of 31 MSS metastatic CRC patients receiving 200 mg pembrolizumab every 3 weeks and 100 mg azacytidine daily. However, the results showed a low response rate (3%), and the median overall survival was only 6.2 months. Ten patients did, however, developed rapid stabilization of tumour progression but treatment-related adverse events occurred in 63% of patients (Lee et al., 2017). Therefore, pembrolizumab plus azacytidine showed a low anti-tumour activity for MSS metastatic CRC, however, disease stabilization in some patients may suggest that biomarkers are needed to predict those patients that will achieve disease stabilization and those that will develop toxicity.

Similarly, a combination of nivolumab and ipilimumab was preliminary studied and showed potential efficacy in the same cohort. The result from 27 patients showed a 41% objective response rate with 78% disease control rate. Tumour related adverse events occurred in 37% of patients but there was no death due to this therapy (Lonardi et al., 2017). The phase II trial study for 13.4 months presented 55% overall response rate (ORR) and 80% for disease control rate (DCR) for >= 12 weeks with 76% showed progression-free survival (PFS) rate at 9 months and 71% at 12 months, overall survival (OS) rate was 87% and 85% respectively. The adverse events occurred in 32% of patients which were manageable (Overman et al., 2018). For long-term follow-up for 25.4 months for 119 patients which 76% had two or more lines of prior therapy, presented 58% ORR and 81% DCR with complete response (CR) rate increased from 3% to 6% within the duration of 13.4 months to 25.4 months. Progression-free survival at 24 months were 60% and OS were 74% with treatment related adverse events grade 3-4 occurred in 31% of patients were manageable (Overman et al., 2019). Recently, Nivolumab received US FDA approval for mCRC with MSI-H/dMMR treatment as single or in combination with ipilimumab following treatment with fluoropyrimidine, oxaliplatin, and irinotecan based on the previous trial, CheckMate 142. The results presented 29.0 months median follow-up period, the ORR was 69% and DCR was 84%, with 13% complete response rate. Median

progression-free survival at 24 months was 74% and median OS was 79%. The adverse events grade 3-4 occurred in 22% of patients (Lenz et al., 2021). Therefore, based on the promising results, Nivolumab plus low-dose ipilimumab presented a robust and clinical benefit which rewarded as a first-line treatment for MSI-High/dMMR metastatic CRC (mCRC). This trial now warranted for randomized studies for next step.

As the PD-L1 inhibitor, atezolizumab, has shown only a partial response in CRC Phase I studies, currently, studies of atezolizumab combined with the vascular endothelial growth factor (VEGF) inhibitor bevacizumab, or atezolizumab plus bevacizumab and FOLFOX in metastatic CRC are looking promising (Bendell et al., 2015). Both studies showed significant anti-tumour effects. Many other anti-PD-L1 compounds are also in ongoing studies for combination therapy i.e., durvalumab and avelumab. Recently, the WNT/β-catenin signaling pathway has been reported to block anti-tumour activity of tumour-infiltrating lymphocytes and enhance resistance to anti-PD-1/PD-L1. In addition, immune evasion was further promoted by STAT3 signaling; BBI608 is an inhibitor that blocks STAT3 and down-regulate WNT/β-catenin signaling. Therefore, combination of pembrolizumab plus BBI608 is currently undergoing assessment for efficacy and safety in a multicenter phase I/II trial (Shinozaki et al., 2018). These results suggest that for CRC the way forward for immunotherapy is combination with other drugs to prime the immune landscape. Developing predictive biomarkers for treatment response and toxicity may further enhance the efficacy of these drugs.

1.10.5 Enhancing the efficacy of current immunotherapy

Although immunotherapy has shown satisfactory results in multiple types of cancer, many patients show no response, for example, in MSS CRC. Therefore, strategies that enhance the efficacy of immunotherapy are now the focus of many studies. Some approaches to enhance the efficacy of immunotherapy include performing immune checkpoints combination therapy to increase treatment yield, evaluating biomarkers for treatment responses to observe treatment effectiveness, assessing biomarkers for treatment toxicities to reduce treatment failure, and investigating new potential targets.

Immunotherapy may have shown disappointing results in some tumours because of the genetic variability or differing strengths of the host immune response within each patient. Therefore, specific biomarkers or clinical features that could be used to predict response to treatment are likely to be key improving the effectiveness of immunotherapy in these patients. This is already suggested with MMR status or MSI being used as a predictive marker for pembrolizumab and nivolumab in a variety of cancers. Another potential biomarker candidate for immune checkpoint therapies includes

immunological biomarkers, such as intratumoral expressed PD-L1. However, a study from Aguiar et al. showed that PD-L1 negative tumours still respond to checkpoint inhibitor drugs (Aguiar et al., 2016). Suggesting that intratumorally expressed PD-L1 might not be an effective marker for PD-1/PD-L1 inhibitor. Recently, PD-L2 expression was also found to be an independent prognostic factor that may also predict the effectiveness of anti-PD-1 therapy (Hopkins et al., 2017; Yearley et al., 2017).

Biomarkers related to clinical responses to anti-PD-1, anti-PD-L1, and anti-CTLA-4 checkpoint inhibitors therapies are currently being studied in both patient's tumour tissue and blood samples (Hopkins et al., 2017; Manson et al., 2016). In tumour tissues, many biomarkers have been studied, for example, TILs, PD-L1 expression, and mutational load. TILs present in the intratumoral site have been shown to be associated with improved clinical benefit for anti-CTLA-4 therapy in advanced melanoma (Hamid et al., 2011). Also, PD-L1 expression has been shown to associate with improved clinical benefit from anti-PD-1/anti-PD-L1 therapy in multiple cancer types including advanced melanoma and breast cancer (Baptista et al., 2016; Kefford et al., 2014). Furthermore, mutational load has been performed in both anti-CTLA-4 and anti-PD-1 therapy. In melanoma, it was shown that high mutational load related to improved efficacy for anti-CTLA4 therapy (Van Allen et al., 2015); whereas in NSCLC high mutational load was associated with better efficacy for anti-PD-1 therapy (Rizvi et al., 2015). From these studies, it suggests that assessing treatment responses using various predictive biomarkers may benefit immunotherapy outcomes.

In blood samples, several biomarkers have been studied including circulating leukocytes (lymphocytes, neutrophils, eosinophils, and monocytes), MDSCs level, and lactate dehydrogenase (LDH) level (Le et al.). For anti-CTLA-4, high lymphocytes level during treatment related to better overall survival on this therapy (Delyon et al., 2013). Furthermore, the neutrophil-to-lymphocyte ratio (NLR) declined during on-going treatment, and this showed association with a higher survival rate (Di Giacomo et al., 2013). In contrast, high serum LDH level prior to treatment with anti-CTLA-4 therapy was associated with resistance to treatment (Kelderman et al., 2014). Although wide varieties of biomarkers have been investigated in multiple cancers, validation is now required before translation into clinical setting can be achieved. Therefore, choosing suitable in vitro models may be key to unlocking the best biomarker to enhance efficacy prior to use in clinical trials.

1.11 Current *in vitro* models to study the tumour and TME

In vitro or cell culture models have been utilised in cancer research in multiple aspects such as drug discovery, stem cell study, cell-cell interactions, mainly utilising 2D models over the past century along with *in vivo* animal models (Jensen & Teng, 2020). However, 2D models lack the complexity of tumour characteristics and the TME, whereas co-culture 3D models mimic several aspects of tumour physiology and the TME (Han et al., 2021; Vis et al., 2020). Although animal models can mimic the tumour complexity of multicellular components, however, there are limitations including the cost of animal models and the difficulties of therapeutic translation to human because of species differences (Reidy et al., 2021). 3D multicellular tumour models, tumour spheroids and tumour organoids are becoming promising tools as they are a better representative of *in vivo* solid tumour than 2D monolayer models (Fitzgerald et al., 2020). Furthermore, 3D models are thought to be superior in terms of monitoring drug effects as they represent an *in vivo*-like human tissue better and should be employed alongside animal models (Goers et al., 2014).

In CRC, there is rising implementation of tumour spheroids from human cell lines as study models for potential drug screening by many research groups. However, human cell lines model still lack of the complexity of original tumour heterogeneity. Therefore, patient-derived organoid tumour models could be the better model. Therefore, 3D spheroid models and, patient-derived tumour organoid models, are a promising approach in various types of studies including co-culture of cancer cells with other cells in TME such as immune cells, and fibroblast mimicking *in vivo* status for multiple tumour types including CRC (Bauleth-Ramos et al., 2020; Franchi-Mendes et al., 2021; Koh et al., 2019; Venter & Niesler, 2018).

Recently, patient-derived xenografts (PDXs) have been reviewed as the most suitable model for CRC pre-clinical studies (Rizzo et al., 2021). PDXs based on the implantation of patients' tumour tissue into mouse host with immunodeficiency is now widely reported ranging from primary tumour to metastatic tumours. This model has been confirmed by many studies as having high concordance with primary tumour in histopathological and molecular features which could maintain genetic stability over several passages (Rizzo et al., 2021). However, this model needs high level of laboratory facilities and well-trained personnel to perform experiments.

1.12 Aims of thesis

The primary aim of thesis is to investigate the immune landscape of patients with stage I-III CRC by assessing the association of individual immune cell types and different immune landscapes on CRC prognosis.

The secondary aims are:

1. to investigate the immune landscape of each phenotypic subtype in stage I-III CRC patients to assess the association of individual immune cell types specific to each phenotypic subtype

2. to assess transcriptomics and mutational profiles between differing immune cell landscapes in patients with CRC to assess potential novel biomarkers for each and to confirm the most significantly dysregulated genes at a protein level with IHC in our patient cohort tissue

3. to assess the effect of immune checkpoint inhibitors (ICIs) targeting PD-1/PD-L1, in CRC cell lines co-cultured with different immune cell lines modelling the differing immune landscapes developed in the patient sample (adaptive, innate, and mixed populations) to assess if efficacy is different between each immune landscape.

Chapter 2 Materials & Methods

2.1 Tissue Studies

2.1.1 Patients' cohort

2.1.1.1 Scottish Discovery Cohort

Patients (n=1009) who underwent resection for potentially curable stage I-III CRC at the Glasgow Royal infirmary, Western Infirmary and Stobhill Hospitals (Glasgow, UK) between 1997 and 2006 and were contained within two previously constructed tissue microarrays (TMAs) and full sections were utilised. TMAs consisted of four 0.6 mm cores per patient, and full clinical and pathological data was available for the cohort. Patients that had died within 30 days of surgery were excluded. Ethical approval was obtained from the West of Scotland Research Ethics Committee.

2.1.1.2 Norwegian Validation Cohort

Patients (n=299) who underwent resection for potentially curable stage II-III CRC at Southern Hospital Trust, Norway between 2000 and 2017 with full section tissue available were utilised. Full clinical and pathological data was available for the cohort. Patients who died within 30 days of surgery were excluded. Local institutional ethics was obtained for this study.

2.1.2 Clinical characteristics

Tumours were staged using the fifth edition of the AJCC/UICC-TNM staging system as was appropriate at the time of resection for the Discovery cohort. For the validation cohort, the fifth TNM edition was used until January 2009, seventh edition until August 2018 and eight edition afterwards (James D.B., 2017). The presence of venous invasion was assessed using elastica staining. Following surgery, patients with stage III or high-risk stage II disease and without significant co-morbid disease precluding adjuvant treatment were considered for 5-fluorouracil-based chemotherapy. Other clinical factors were obtained from patient records and pathology reports. Tumour microenvironment and systemic inflammatory response measures were already available for both cohorts. Patients were followed up for at least 10 years and date and cause of death confirmed using electronic case records. Cancer-specific survival (CSS) was measured from date of surgery until date of death from CRC. Overall survival (OS) was measured from date of surgery until date of death from any cause.

The presence of tumour necrosis and TSP were assessed as previously described (Richards et al., 2012a). Briefly, utilising an H&E slide, tumour necrosis assessed tumour cells degradation presenting with an amorphous coagulum and mixing with nuclear derbies and was graded on a four-point scale, which later classified into low and high for this study (Pollheimer et al., 2010; Richards et al., 2012b). Utilising an H&E slide of the deepest point of invasion, TSP measured the stromal proportion by assessing the percentage of stromal cells within the visible field excluding areas of necrosis and was graded into low TSP (<=50%) and high TSP (>=50%) (Park et al., 2015). MMR

status was assessed as previously described (Park et al., 2015). Briefly, TMA slides were stained for MLH1, MSH6, MSH2, and PMS2 protein expression by automated immunohistochemical (IHC) staining. Analysis of the protein expression was performed using UK NEQAS scoring guidelines. The expression was reported as MMR proficient if strong nuclear staining was seen in tumour cells along with positive immune cell staining, or MMR deficient if the intensity of staining was weak/patchy or negative within tumour cells with positive immune cells staining. Ki67 proliferation index was previously established for both cohorts by staining for Ki67 protein expression via IHC, and then defining cell staining as low (<30%) or high (>30%) positivity. The general local inflammatory cell infiltrate was assessed using the KM grade as previously described (Richards et al., 2014). Briefly, utilising an H&E from the deepest point of invasion, immune cells at the invasive margin were assessed and a score of 0-1 (no increase or mild/patchy increase in inflammatory cells) was graded as weak and a score of 2-3 (prominent inflammatory reaction forming a band at the invasive margin, or florid cup-like infiltrate at the invasive edge with destruction of cancer cell islands) was graded as strong. Systemic inflammation was assessed using serum CRP and albumin that were recorded prospectively and measured within 30 days prior to surgery. The pre-operative systemic inflammatory response was defined using the mGPS. The mGPS was calculated as previously described (Park, Watt, et al., 2016). Briefly, patients with CRP ≤10mg/L were allocated a score of 0, patients with CRP >10mg/L a score of 1, and patients with CRP >10mg/L and albumin <35g/L were allocated a score of 2.

2.1.3 Immune cells markers

Immunohistochemistry of markers for lymphoid and myeloid cells lineages and subpopulations were performed on TMAs and full sections slides (**Table 2.1**).

Table 2.1 - T-lymphocytes subpopulations and myeloid cells markers

Immune cells	Markers
Pan-T-lymphocytes	CD3
Cytotoxic T-lymphocytes	CD8
Regulatory T-lymphocytes	FoxP3
Pan-macrophages	CD68
M1-like macrophages	CD80
M2-like macrophages	CD163
Granulocytes	CD66b

2.1.4 Antibody specificity

Specificity for new antibodies was performed to check for positive and negative result by using specific tissue types (**Table 2.2**). Specificity for anti-CD3, anti-CD8, anti-FoxP3 was previously performed (Richards et al., 2014).

Table 2.2 - Antibody specificity testing for positive and negative controls

Antibody	Positive control tissue	Negative control tissue
CD68	Liver	Breast
CD80	Liver	Breast
CD163	Liver	Breast
CD66b	Colon	Prostate

2.1.5 Immunohistochemistry (IHC)

Slides were dewaxed in histoclear, then rehydrated through graded alcohols. Antigen retrieval was performed in buffer for each marker; Tris-EDTA buffer or citrate buffer under pressure for 5 mins. Peroxidases were blocked in 3% H_2O_2 for 10 mins then non-specific binding blocked with 1.5% horse serum (Vector Laboratories), 5% goat serum, or 10% casein. Primary antibody was added and incubated at RT for 60 mins or overnight at 4°C utilising anti-CD3 (1:500, Thermo Fisher), anti-CD8 (1:100, DAKO), anti-FoxP3 (1:400, Abcam), anti-CD68 (1:100, Abcam), anti-CD80 (1:750, Abcam), anti-CD163 (1:1500, Abcam), and anti-CD66b (1:400, Novus Biosciences). Envision (DAKO) or ImPRESS (Vector Laboratories) secondary antibody was added for 30 mins then slides washed with TBS. Slides were visualised using ImPACT DAB (Vector Laboratories) then counterstained with haematoxylin and dehydrated through graded alcohols and histoclear. Coverslips were mounted with distrene, plasticizer, xylene (DPX) (**Table 2.3**).

Table 2.3 - Antibodies, IHC conditions and product details

Primary antibody	Code/sources	Retrieval	Blocking	Primary antibody condition	Secondary antibody
CD3	RM-9107-S/ Thermo Fisher	EDTA pH8, microwave, 8 mins	5% goat serum	1/500 @ 4°C, O.N.	Anti-mouse/rabbit, @RT, 30 mins
CD8	Clone C8/144B, M7103/DAKO	EDTA pH8, microwave, 8 mins	5% goat serum	1/100@4°C, O.N.	Anti-mouse/rabbit, @RT, 30 mins
FoxP3	ab215206/ Abcam	EDTA pH8, microwave, 8 mins	1.5% horse serum	1/200@RT, 30 mins	Anti-mouse/rabbit, @RT, 30 mins
CD68	Ab125212/Abcam	EDTA pH8, microwave, 8 mins	10% casein	1/200@RT, 30 mins	Anti-mouse/rabbit, @RT, 30 mins
CD80	ab254579/Abcam	EDTA pH9, microwave, 8 mins	10% casein	1/1500@4°C, O.N.	Anti-mouse/rabbit, @RT, 30 mins
CD163	ab182422/Abcam	EDTA pH9, microwave, 8 mins	10% casein	1/750@4°C, O.N.	Anti-mouse/rabbit, @RT, 30 mins
CD66b	G10F5, NB100-77808/Novus Biosciences	EDTA pH8, microwave, 8 mins	10% casein	1/400@RT, 30 mins	Anti-mouse/rabbit, @RT, 30 mins

2.1.6 IHC scoring method

Stained slides were initially scanned onto Slidepath Digital Image Hub, version 4.0.1 (Leica Biosystems, UK) using a Hamamatsu NanoZoomer at x20 magnification (Welwyn Garden City, UK), they were then transferred over to NDP viewer image analysis software (Hamamatsu Photonics). For TMA cores, positive cells were manually counted within the tumour cell nests and tumour stromal area within the centre of tumour separately (**Figure 2.1**). The final score was calculated as the average of the four cores for each patient. For full sections, three different areas were randomly selected and applied the same size as TMA cores. Positive cells were counted within tumour nest and tumour stroma separately as performed on TMA slides. The final score was calculated as the average of three areas for each patient. Assessment of all markers was performed by myself blinded to clinical data at x20 magnification (total magnification x400). To ensure reproducibility, 10% of cores were co-scored by a co-investigator (Antonia Roseweir).

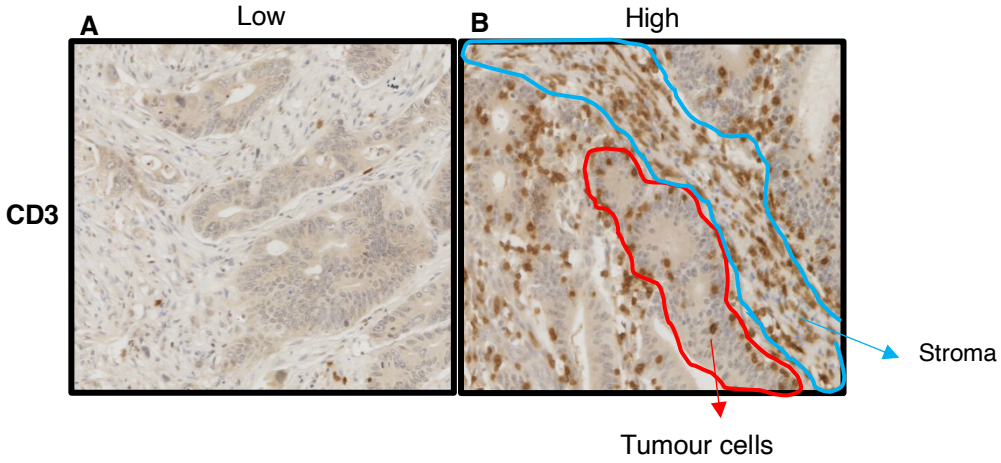

Figure 2.1 – Example of low and high infiltration in tumour cell nests and tumour stroma. Images showing **A.** low infiltration, **B.** high infiltration. Picture **B** shows representative counting areas, for tumour cells (area within red line) and for tumour stroma (area within blue line). The pictures were taken at 20X magnification.

2.1.7 Statistics analysis

The average scores from the four cores were divided into weak and strong infiltrate using maximal rank stats analysis on Bioconductor R Studio version 4.0.5 (2021-03-31) based on CSS from Scottish cohort to define the optimal cut-off values displayed as number of positive cells per 0.6 mm^2. These cut-off values in tumour cells nest were 16.25 for CD3, 7.5 for CD8, 2 for FoxP3, 0.75 for CD68, 1.67 for CD80, 4.33 for CD163, and 1.67 for CD66b. The cut-off values in tumour stroma were 166.75 for CD3, 13.67 for CD8, 33.75 for FoxP3, 53 for CD68, 8.67 for CD80, 10.33 for CD163, and 0.5 for CD66b. All statistical analysis was performed using SPSS version 27. The relationship between immune markers and CSS was examined using Kaplan-Meier log-rank analysis. Hazard ratios (HR) and 95% confidence intervals (CI) were evaluated using univariate cox regression survival analysis. The relationship between clinicopathological characteristics and immune markers was examined using Chi-square analysis. Multivariate cox regression survival analysis utilising a backward conditional model was used to evaluate prognostic independence compared to common clinical factors. Statistical significance was set at $p<0.05$ and conformed to the REMARK criteria.

2.1.8 Colocalization of myeloid lineage markers

Myeloid cells markers for M1-like macrophages and M2-like macrophages were performed to see the colocalization between pan-macrophages marker CD68 and CD80 for M1-like macrophages, and CD68 and CD163 for M2-like macrophages by dual immunofluorescent assay. Briefly, slides were baked at 60°C for 10 mins and cooled down for 10 mins. Rehydration of slides was performed using same protocol as IHC, before blocking with 2% FCS in PBS for 20 mins. Dual primary antibodies were diluted in 2% FCS, anti-CD68 (1:200) + anti-CD80 (1:1500), anti-CD68 (1:200) + anti-CD163

(1:750), then added to slides and incubated at 4°C, overnight. The following steps were performed in the dark; secondary antibodies were prepared using Alexa Fluor 488 goat anti-rabbit IgG in 2% FCS at 1:500 for (green colour, Life Technologies™), or Alexa Fluor 568 goat anti-rabbit IgG (red, Life Technologies™). Slides were incubated with secondary antibody for 1 hour, RT in the dark. Slides were mounted with Vectashield mountant (included DAPI), then coverslip added and sealed with nail varnish. Image capture was performed on a confocal microscope (LSM780) and image processing was performed using Zeiss ZEN blue software.

2.2 In vitro studies

2.2.1 Cell lines

In vitro studies to assess effects of immune checkpoint inhibitors on tumour cell lines co-culture with immune cell lines utilised HT29 human colon tumour cell line, Jurkat E6-1 (ATCC®TIB-152™) human lymphocytes cell line, and RAW264.7 (ATCC®TIB71™) murine macrophages cell line. All cell lines were tested for Mycoplasma contamination and stocked before starting experiments.

2.2.2 Raising cells from liquid nitrogen

Cell lines were removed from liquid nitrogen and defrosted then resuspended in 10 mL medium. Cells were then centrifuged at 1200 rpm for 3 mins, then medium removed, and pellet re-suspended in 10 mL fresh medium in a T75 flask. Flasks were incubated at 37°C, 5% CO2 for 24 hours, then cells checked under a microscope for monolayer forming to assess cell line attachment and clumping for suspension cell lines. Medium was changed every 2 days until cells reached 80% confluency.

2.2.3 Passaging cell lines

Cells were split every 3-4 days when 80% confluent. Briefly, cells were washed with DPBS (Gibco), then 0.005% trypsin in DPBS added (1.5 ml for T25 flask and 3 ml for T75 flask). Flasks were transferred to incubator, 37°C with 5% CO_2, for up to 5 mins for HT29, and up to 20 mins for RAW264.7 macrophages. Once detached, media was added to stop reaction (3.5 ml for T25 and 5 ml for T75 flask). Cells were then centrifuged at 1200 rpm for 3 mins to remove trypsin and resuspend in appropriate media in a new flask at a passage ratio of 1:5. For Jurkat E6-1 lymphocytes, cells were centrifuged at 1200 g, for 3 mins, wash with DPBS, and resuspend in completed RPMI1640, at a passage ratio of 1:5.

2.2.4 Cell lines cryopreservation

Cell lines were stocked after testing for mycoplasma, and before starting experiments, by following normal culture process until cell pellets obtained. Pellets were then re-suspended in 70% media: 20%

FBS: 10% DMSO, counted cells, and 1 mL aliquoted into cryopreservation tube. Cells were stored at -80°C, and later transfer to liquid nitrogen for long term storage.

2.2.5 HT29 spheroid formation

HT29 colon cell line spheroid formation was performed in ultralow-attachment (ULA) 96-well U bottom plates (Nunclon Sphera, Thermofisher) at seeding density gradient of 10^3 - 10^4 cells per well (Scepter™ Sensors- 60 µm cell counter) to identify the optimal spheroid size needed for further experiments.

2.2.6 Immunoblotting for PD-L1 expression on HT29 cells

2.2.6.1 Protein extraction

HT29 colon cell line was seeded in a T75 flask until 80% confluent. Protein extraction was performed by washing with ice-cold PBS, then adding lysis buffer (4X Laemlli sample buffer - Tris-HCL 252 mM, $Na_2P_2O^7$ 8 mM, EDTA 20 mM, glycerol 40%(v/v), SDS 8%, bromophenol blue 0.028%) to a final 1X concentration supplemented by 0.08 g DTT. Cells were scraped down and aspirated 4-5 times with needle to sheer cells. Aspirated sample was transferred to a fresh Eppendorf tube and stored at -20C.

2.2.6.2 SDS-PAGE

Samples were denatured by heating at 95°C for 5 mins. SDS-PAGE was performed using 4-20% Mini-Protein® TGX™ Precast Gels (Bio-Rad) and 1x Tris/Glycine/SDS Buffer (Bio-Rad). Precision Plus Protein™ Dual Xtra standard (Bio-Rad) was used as standard protein ladder. Gels were run at 120V for 90 mins (PowerPac™ Basic, Bio-RAD).

2.2.6.3 Immunoblotting

Proteins were transferred to nitrocellulose membrane (Immobilon®-P transfer membrane) by 1x transfer buffer (Bio-Rad), running at 300mA for 90 mins. For protein visualization, membrane with transferred protein were blocked with 4% BSA in TBST for 60 mins. Incubated with primary antibody (anti-PD-L1 1:1000 in 0.4% BSA in TBST) in cold room overnight. Membranes were then washed with TBST 3x10 mins, and incubated with secondary antibody (anti-rabbit IgG, HRP-linked Antibody, Cell Signalling) plus anti-ladder for 60 mins at RT with shaking. Membranes were then washed with TBST 3x10 mins and incubated with ECL blotting substrate for 5 mins. Protein visualization and image processing were performed by using SynGene GeneSys software.

2.2.7 Cell Pellets

To assess the expression of PD-1 on Jurkat E6-1 cells, cell pellets were prepared from this cell line with PD-1 DNA plasmid transfection used as a positive control. To assess PD-L1 and macrophage markers on RAW264.7 cells, cell pellets were prepared.

2.2.7.1 PD-1 DNA plasmid transfection

DNA plasmid transfection was set up by using Lipofectamine 2000 (Invitrogen). According to company protocol, in a 6-well plate. Briefly, at day 1, Jurkat cells were seeded at $1x10^6$ cells/well in 2 mL completed RPMI1640 media, and incubated at 37°C, 5% CO_2 for 6-8 hours. Then cells were centrifuged at 200g for 5 mins, and resuspend in 2 mL Opti-MEM media, then plated in a 6-well plate and incubate at 37°C, 5% CO_2 overnight. At day 2, DNA plasmid (2 µg/plate) and Lipofectamine 2000 were prepared in Opti-MEM, and incubated for 20-30 mins at RT. These were then combined at a 1:1 ratio, mixed gently, and incubated for 20-30 mins at RT. Then 500 µL was added to each well dropwise at various area, and mixed gently by rocking, then incubated for 6-8 hours at 37°C, 5% CO_2. Next media was changed to complete RPMI1640, and plate incubated for 48 hours at 37°C, 5% CO_2. Cells were then harvested for cell pellet formation for further IHC staining.

2.2.7.2 Cell pellet preparation

Cell pellets of Jurkat E6-1 or RAW 264.7 cell lines were prepared from non-transfected or transfected cells. Cells were centrifuged at 1200 rpm for 5 mins to form pellets, then supernatant discarded. Pellets were resuspended in 1 mL DPBS and transferred to 1.5 mL Eppendorf tube, before centrifugation at 2500 rpm for 3 mins. Supernatant was discarded and pellets were resuspended in 1 mL 4% formaldehyde in PBS for 15 mins. Suspension was centrifuged at 2500 rpm for 3 mins to remove excess, and supernatant was discarded. 1 mL PBS was added to wash away formalin, then was drained by placing Eppendorf tube upside down on tissue paper. 1% agarose in PBS was then added to cell pellets, ensuring agarose gets underneath pellet before setting at 4°C overnight. To make blocks for cell pellets, a needle was used to gently remove agarose coated pellet and place pellet in specimen cassette with lid. The pellet was dehydrated through a series of alcohols (50%, 75%, 99%, 99%) for 15 mins each, followed by histoclear, 2x15 mins. Cassette was placed into wax and left for 60 mins. The pellet was removed and placed in centre of mould, filled with little wax, and placed on cold block for a few seconds. A plastic cassette was then placed on top of the mould and filled right up to the top with wax and placed on the cool block until set. The block was then removed from mould. Blocks were then cut using a microtome at 0.4um thickness and sections placed on glass slides and baked at 50°C for 1 hour before being used for IHC staining.

2.2.7.3 IHC for PD-1 on Jurkat E6-1 cell pellets

Cell pellets slides from non-transfected and transfected positive control Jurkat E6-1 were processed for PD-1 staining. Briefly, slides were dewaxed in histoclear, then rehydrated through graded alcohols. Antigen retrieval was performed in citrate buffer pH 6.0 under pressure for 5 mins. Peroxidases were blocked in 3% H_2O_2 for 20 mins then non-specific binding blocked with 1.5% horse serum. Primary antibody was added and incubate overnight at 4°C utilising anti-CD163 (1:100, Thermo Fisher). ImPRESS (Vector Laboratories) secondary antibody was added for 30 mins then slides washed with TBS. Slides were visualised using ImPACT DAB (Vector Laboratories) then counterstained with haematoxylin and dehydrated through graded alcohols and histoclear. Coverslips were mounted with distrene, plasticizer, xylene (DPX) (**Table 2.4**).

Table 2.4 - IHC conditions of PD-1 antibody and product details

Primary antibody	Code/sources	Retrieval	Blocking	Primary antibody condition	Secondary antibody
PD-1	HPA035981, Thermo Fisher	Citrate pH6, microwave, 8 mins	1.5% horse serum	1:100@4°C, O.N.	Anti-mouse/rabbit, @RT, 30 mins

2.2.7.4 IHC for PD-L1 and macrophage markers on RAW264.7 cell pellets

RAW264.7 murine macrophages cell pellets were tested for PD-L1 expression and M2-like macrophages expression by utilizing CD163 marker. PD-L1 expression was performed by Mr. Colin Nixon, histology unit, Beatson Cancer Research Institute. For CD163 expression, slides were dewaxed in histoclear, then rehydrated through graded alcohols. Antigen retrieval was performed in Tris-EDTA buffer pH 9.0 under pressure for 5 mins. Peroxidases were blocked in 3% H_2O_2 for 20 mins then non-specific binding blocked with 10% casein. Primary antibody was added and incubate overnight at 4°C utilising anti-CD163 (1:750, Abcam). ImPRESS (Vector Laboratories) secondary antibody was added for 30 mins then slides washed with TBS. Slides were visualised using ImPACT DAB (Vector Laboratories) then counterstained with haematoxylin and dehydrated through graded alcohols and histoclear. Coverslips were mounted with distrene, plasticizer, xylene (DPX) (**Table 2.5**).

Table 2.5 - IHC condition of CD163 antibody and product details

Primary antibody	Code/sources	Retrieval	Blocking	Primary antibody condition	Secondary antibody
CD163	ab182422/Abcam	EDTA pH9, microwave, 8 mins	10% casein	1/750@4°C, O.N.	Anti-mouse/rabbit, @RT, 30 mins

2.2.8 Anti-PD1/anti-PD-L1 drugs concentration optimization

The effect of anti-PD1 (pembrolizumab (SellectChem, A2005), nivolumab (SellectChem, A2002)) and anti-PD-L1 (atezolizumab (SellectChem, A2004)) immunotherapies were tested by varying inhibitor concentrations from 1-10 µg/mL, and testing on HT29 spheroids, Jurkat E6.1 and RAW264.7 cell lines individually using cell viability to identify the optimal concentration which does not affect the cell viability of each cell line when cultured alone.

2.2.9 Cell viability

The current studies were utilized three cell viability assays for different conditions.

2.2.9.1 WST-1 assay

Single cell line HT29 and Jurkat E6-1 viability testing after treatment with inhibitors was performed by WST-1 assay (Abcam). The assay is based on tetrazolium salt cleavage to formazan by cellular mitochondrial dehydrogenase. Viable cells show higher activity by formation of formazan dye. Briefly, cells were seeded at 2500 cells/well with 200 µL media in a 96-well plate, and incubated in at 37°C, 5% CO_2 until 80% confluent, then treated with 1-10ug pembrolizumab, or nivolumab or atezolizumab for 24-48 hours. Then 10 µL of WST-1 reagent was added to each well and incubated for 2 hours. The plate was analysed using luminescence after shaking for 30 seconds and reading at 450 nm (TECAN Infinite M200 PRO).

2.2.9.2 CellTiter-Glo® Luminescent cell viability assay

Assessment of single cell line RAW264.7 murine macrophages treated with inhibitors was performed by CellTiter-Glo® Luminescent cell viability assay (Promega, Cat. #G7570). The assay determining viable cell numbers based on quantification of ATP presenting in culture, which represent metabolically active cells. Briefly, RAW264.7 were seeded at 2500 cells/well in 200 µL DMEM media in 96 well plate and incubated in 37°C with 5% CO_2 until 80% confluent, then treated with 1-10ug pembrolizumab, or nivolumab or atezolizumab for 24-48 hours. Reagent buffers were thawed and equilibrated at RT before use, then transferred to substrate bottle and mix thoroughly. Cells were

also left to equilibrate at RT for 30 minutes. Next 100 µL medium was removed and replacing with 100 µL buffer per well and mixed vigorously by pipetting 10 times to lyse cells. Lysate was then transferred to white opaque plate (Flat bottom, white, CellStar®) and incubated at RT for 10 minutes to stabilize luminescent signal. Luminescent signal was then read after activated for 5 minutes before detecting luminescence signal (GLOMAX, Multi, Promega).

2.2.9.3 CellTiter-Glo®3D Cell Viability Assay

HT29 spheroids viability were tested with CellTiter-Glo®3D Cell Viability Assay (Promega, Cat. #G9681). The assay determines viable cell numbers in 3D cell culture based on ATP present, which represent metabolically active cells. Briefly, HT29 cells were seeded at 2500 cells/well in a 96-well plate and treated with 1-10ug pembrolizumab, or nivolumab or atezolizumab for 24-48 hours. Reagents were thawed overnight and equilibrated at RT for 20 mins prior to use. Cells were also left to equilibrate at RT for 30 minutes. Next 100 µL medium was removed and replacing with 100 µL buffer per well and mixed vigorously by pipetting 10 times to lyse cells. Lysates were then transferred to white opaque plate (Flat bottom, white, CellStar®)) and incubated at RT for 25 minutes to stabilize luminescent signal. Luminescent signal was read after PMT activated for 5 minutes before detecting luminescence signal (GLOMAX, Multi, Promega).

2.2.10 Co-cultures

2.2.10.1 Co-culturing of HT29 and immune cells

Co-culturing of HT29 spheroids and immune cells, either Jurkat E6-1 lymphocytes and/or RAW264.7 macrophages. The optimal HT29 seeding density for optimal spheroids size was identified from section 2.2.5, which was 2500 cells/well were plated on day 0 in ultra-low attachment plates and incubated at 37C for 24 hours to allow spheroid formation. After 24 hours, 2500 immune cells/well in suspension were then added to the HT-29 spheroids and incubated at 37C for 24 hours to allow infiltration. Inhibitors were then added as discussed below.

2.2.10.2 Media preparations for co-culture studies

For co-culturing of HT29 tumour cells spheroids with immune cells; Jurkat E6-1 lymphocytes, RAW264.7 macrophages or both; different media combinations were tested to assess optimal growth. The following media was tested: complete McCoy's 5A (1X) + GlutaMax™-I (Modified Medium; FBS 10%); complete RPMI1640 (1X) (HEPES 10 mM, Sodium pyruvate 1 mM, FBS 10%), and complete DMEM (1X) + GlutaMAX™-I (FBS 10%, Penicillin/Streptomycin 1%). Complete McCoy's 5A (1X) + GlutaMax™-I was chosen as the optimal media for all combinations.

2.2.10.3 Immune cells infiltration into HT29 spheroids

Before testing for effects of immune checkpoint inhibitors on HT29 spheroids co-culture with immune cells, the infiltration of immune cells into tumour cell spheroids were checked by labelling immune cells, Jurkat E6-1 lymphocytes or RAW264.7 macrophages with Cell Tracker^{TM} Green CMFDA Dye (Thermo Fisher, Cat.#C2925) and infiltration observed under confocal microscope. Briefly, according to the protocol from manufacturer, reconstitute reagent was reconstituted with DMSO, and diluted to working concentration with serum-free media. Jurkat E6-1 or RAW264.7 cells from a T75 flask were pelleted then resuspend in serum-free media, and working reagent added to reach final concentration of 1-10 μM per well, then incubate for 45 minutes at 37C, 5% CO2. Cells were centrifuge to remove cell tracker solution, then resuspend in complete medium (McCoy's 5A + 10%FBS). Labelled immune cells were added to HT29 spheroids plates and incubate for 24 hours. Infiltration was assessed by observing green dye in 96 well plate by confocal microscopy (LSM780).

2.2.10.4 Immune checkpoint inhibitors treatments for co-cultures

Checkpoint inhibitors were assessed using co-cultures of HT29 spheroids and Jurkat E6-1, HT29 spheroids and RAW264.7, or triple-culturing of HT29 spheroids with Jurkat E6-1 and RAW264.7 cells. Briefly, HT29 cells were seeded at 2500 cells/well in ULA 96-well plates. After 24 hours, 2500 cells/well of Jurkat E6-1, RAW264.7, or a mixed population of Jurkat E6-1 (1250 cells/well) and RAW264.7 macrophages (1250 cells/well) were seeded with the HT29 spheroid. Checkpoint inhibitors, Pembrolizumab, Nivolumab or Atezolizumab were added 24 hours later at a concentration of 1ug. Cell viability was then assessed at 48 and 96 hours using the CellTiter Glo® 3D Cell Viability assay as described above.

2.2.11 Statistical Analysis

All cell work were performed in triplicate. Multiple comparison of raw data from the three experiments were tested for significant difference by ANOVA. Raw data was then converted to fold-change using 48hrs HT29 spheroid in media alone as the standard factor. Statistical significance changes of pairwise data from all conditions of treated and un-treated results were performed by Student's paired t-test. All analysis was performed in Microsoft Excel (version 16.59, Microsoft Corporation) and statistical significance was set at p-value < 0.05. The error bars were calculated from standard deviations.

2.3 Genomics

Whole genome mutational profiling was performed on a subset of patients from the Scottish cohort (n=252). DNA was previously extracted from FFPE sections by NHS molecular diagnostics, Dundee and stored at -80ºC. DNA quality and concentration were determined using the Qubit assay (ThermoFisher, Massachusetts, USA). Samples with a DNA concentration of >10ng/µL were included in the study. Sequencing was outsourced and performed by Dr Susie Cooke and the Glasgow Precision Oncology Laboratory (GPOL) using a custom in-house designed panel of 151 cancer-associated genes. Statistical analysis was performed relative to tumour immune landscaping groups using Bioconductor: Maftools packages version 2.6.05 within R studio version 4.0.5. The data were first summarized to identify variants per sample. Fisher's exact tests were performed to identified any significantly different mutations across groups and results were visualised in forest plots and co-bar plots.

2.4 Transcriptomics

Whole transcriptome RNA-Seq was performed on a subset of patients from the Scottish cohort (n=100). To utilise available FFPE full section tissue, novel RNA-Seq technique, TempO-Seq was employed (Biospyder Technologies, Carlsbad, CA, USA). This was performed by BioClavis Glasgow using the following method. TempO-Seq gene expression profiling was performed according to manufacturer's directions. Briefly, whole sections (~100 mm2 x 0.5 µm) were excised from FFPE slides of CRC resection samples and placed into wells of a PCR plate. TempO-Seq Lysis Buffer was added, and the sample was overlaid with mineral oil. After deparaffinization by heating, the tissue was lysed using TempO-Seq Protease mix. The lysate was then combined with a mixture of detector oligonucleotides (DOs), designed as pairs that anneal adjacent to one another on the target RNAs. After a hybridization step, unbound DOs were degraded in an enzymatic step, and the bound DOs were ligated into a complete probe sequence. The ligated probes were amplified in a PCR step, purified, and combined in an indexed multiplex library which was sequencing using an Illumina instrument (Illumina, CA, United States) to count the relative amount of each target DO pair representing each gene's expression level.

Data analysis was done using R studio version 4.0.5. RNA-sequencing raw data normalization and differential gene expression (DGE) were performed by using DESeq2 packages version 1.30.1 for the full 22,000 gene transcriptome. Analysis was performed for each tumour immune landscape groups (Both Low, Lymphoid, Myeloid, Both Strong) compared to all other patients. Volcano plots and MA plots were generated to visualise DEGs by displaying mean expression levels, log 2-fold changes, and adjusted *p*-value. The significance was set at adjusted *p*-value < 0.05 with log 2-fold

changes > 1 for significant up-regulated genes; while adjusted *p*-value < 0.05 with log 2-fold changes < 1 was set for significant down-regulated genes. PCA plot was performed to explore the sample-to-sample distance relationship. The hierarchical clustering of gene expressions was presented by heatmap clustering. Gene network analysis was plotted by Cluster Profiler package in R-studio. Protein-protein interactions (PPIs) was generated by STRING online tool.

2.5 IHC for P53 protein expression

From mutational analysis, the most significant genes were selected for IHC analysis to assess their expression at a protein level. P53 expression was selected for IHC analysis as it is a common tumour suppressor in CRC and important for cancer development. This protein was previously stained within the laboratory.

2.5.1 p53 scoring method

Scoring was performed by a single observer blinded to the clinical data (Charis Fraser). To ensure consistency, 10% of each was co-scored by a second observer (Antonia Roseweir). Tumour cell expression was assessed using the weighted Histoscore method. p53 expression was scored for nuclear staining. The weighted Histoscore was calculated as follows: (% of unstained tumour cells x 0) + (% of weakly stained tumour cells x 1) + (% of moderately stained tumour cells x 2) + (% of strongly stained tumour cells x 3) and given a range from 0 to 300. All cores were scored separately, and an average score was taken for each patient.

2.5.2 Statistics Analysis

Scores were divided into low and high expression using maximal rank stats analysis on R based on CSS from Scottish cohort to define the optimal cut-off values. All statistical analysis was performed using SPSS version 27. The relationship between P53 expressions and CSS was examined using Kaplan-Meier log-rank analysis. Hazard ratios (HR) and 95% confidence intervals (CI) were evaluated using univariate cox regression survival analysis. The relationship between clinicopathological characteristics and p53 expressions were examined using Chi-square analysis. Multivariate cox regression survival analysis utilising a backward conditional model was used to evaluate prognostic independence compared to common clinical factors. Statistical significance was set at $p<0.05$ and conformed to the REMARK criteria.

Chapter 3 Adaptive and innate immune cells associations with survival and clinical outcomes in CRC patients

3.1 Background

CRC is associated with a systemic inflammatory response and a local immune cell infiltration. It is thought that patient's survival depends on an effective immune response within the tumour and its microenvironment to fight tumour progression. The tumour microenvironment is infiltrated by a mix of lymphoid and myeloid lineage cells which function as anti-tumorigenic or pro-tumorigenic depending on the cell types presented. Strong T-lymphocytes ($CD3^+$) infiltration alone has been proposed to improve prognosis in multiple cancers (Braha et al., 2016). Cytotoxic T-lymphocytes ($CD8^+$) are recognised as a good prognostic factor when present within the primary tumour in several cancer types including CRC (Gao et al., 2007; Ohtani, 2007). Regulatory T-lymphocytes ($FoxP3^+$) are well recognised as an inhibitor of cytotoxic T-lymphocytes function that maintains stability of the local immune response which showed poor prognosis in other solid tumours such as breast cancer, however, in CRC showed positive effects on survival (Hu et al., 2017; Ling et al., 2014; Vlad et al., 2015).

TAMs and TANs are the most abundance myeloid cells in tumour microenvironment (Liu et al.), which are known as driving pro-tumorigenic effects (Kim & Bae, 2016). However, the role of myeloid cells present in the tumour microenvironment is still controversial between enhancing tumour progression and improving patient's survival (Elliott et al., 2017; Powell & Huttenlocher, 2016). The interplay between lymphoid and myeloid lineage is key to these effects. The interaction of regulatory T-lymphocytes and macrophages has been studied and suggested that TAMs could be one of the factors that modulate regulatory T-lymphocyte function leading to poorer prognosis in CRC (Waniczek et al., 2017). Therefore, the interaction between T-lymphocytes and myeloid cells is being recognised as an important factor in cancer progression, which affects treatment outcome and patient's survival.

For that reason, apart from T-lymphocytes, understanding the role of myeloid cells, and the interplay between the two is important to distinguish their role in tumour progression which might be able to benefit patient's prognosis and therapeutic targets for immunotherapy. Therefore, this study aimed to investigate T-lymphocytes and myeloid cells in patients with stage I-III CRC to assess the effect of individual immune cell types and combinations of lymphoid and myeloid lineages on prognosis.

3.2 Methods

Full sections and TMAs slide from stage I-III CRC patient samples of Scottish cohort and stage II-III CRC patient samples of Norwegian cohort were stained by utilising IHC technique. The positive cells were scored in tumour cell nests and tumour stroma. The final score for each marker was the average from three randomly selected areas in full sections, and four cores per patient on TMAs. The agreement between two independent scorers were assessed by intra-class correlation coefficient (ICCC), scatter plot and Bland-Altman plot. Then the cut-off value for each marker were generated by Bioconductor R studio using the maximal log-rank method. The analysis was performed in SPSS for immune cells markers in terms of the infiltration levels in each stage of disease, survival effects utilising CSS, and OS, associations with clinical, tumour microenvironment, and systemic characteristics, and lastly univariate, and multivariate survival analysis. The combination of T-lymphocytes and myeloid lineages were also performed and analysed in the same manner.

3.3 Scottish discovery cohort's patient's characteristics

The current study was performed firstly in a Scottish discovery cohort. The basic patient's characteristics includes age, sex, tumour site, stages, and survival status. From 930 patients with stage I-III CRC, patients with a valid score for any marker were included in the analysis (**Figure 3.1**). Briefly, 306 (33%) were aged less than 65 years and 493 (53%) were male. 377 (41%) patients had right-sided colon cancer, 308 (33%) patients had left-sided colon cancer, and 238 (26%) had rectal cancer. 125 (13%) patients had stage I disease, 448 (48%) had stage II disease, with 357 (38%) stage III patients. The median follows up for patients was 7.5 years (range 2 months -17 years) with 279 (30%) cancer-related deaths and 296 (32%) non-cancer related deaths (**Table 3.1**).

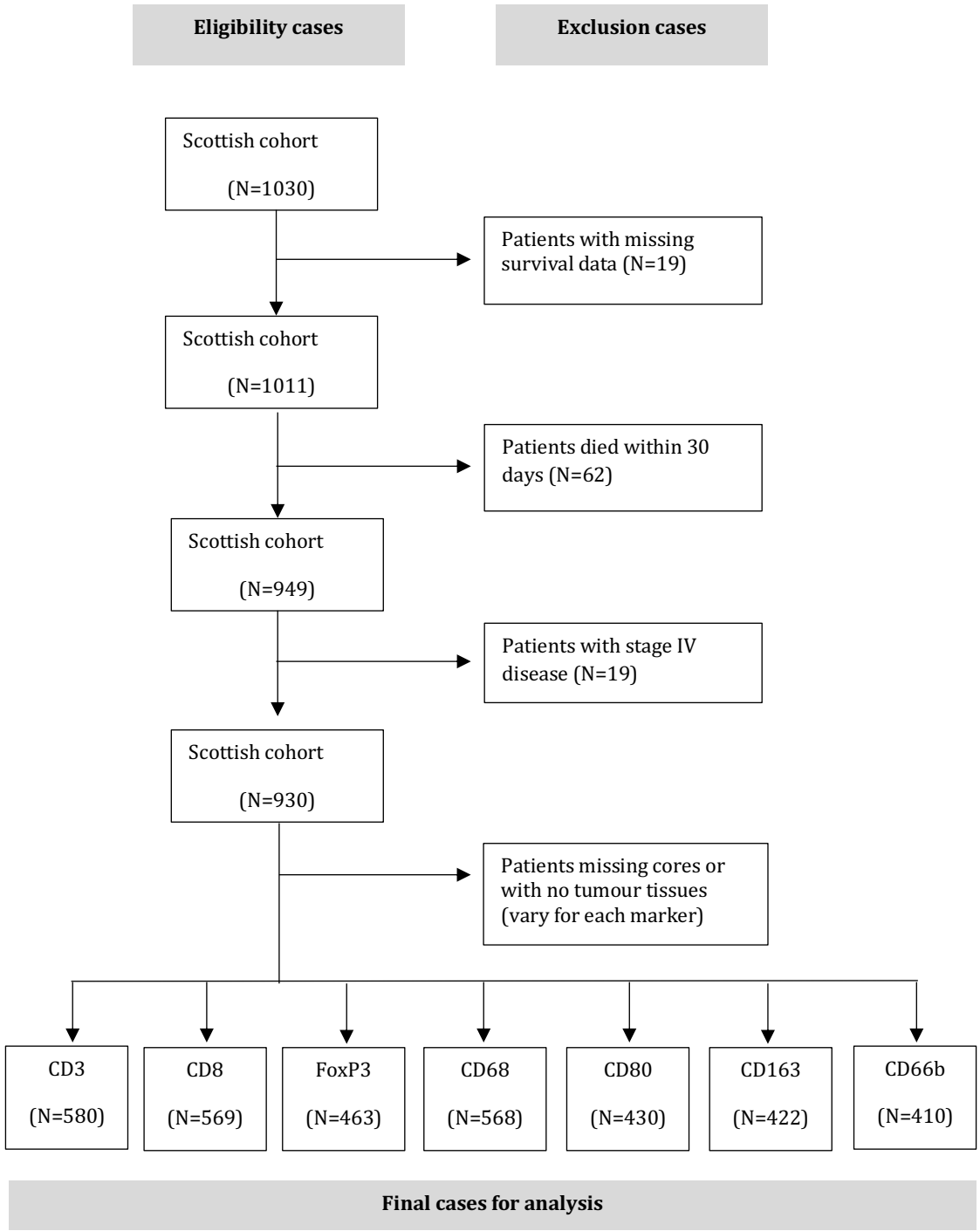

Figure 3.1 - Consort diagram of Scottish cohort patients eligible for analysis. Showing patient samples were available in the study with excluding criteria by missing survival data, died within 30 days, stage IV disease, missing cores, or no tumour tissues.

Table 3.1 - CRC patient's characteristics of Scottish discovery cohort (n=930)

Characteristics	Scottish discovery cohort
	Number of patients (%)
Age	
<65	306 (33)
>65	624 (67)
Sex	
Female	437 (47)
Male	493 (53)
Tumour site	
Colon – Right	377 (41)
Colon - Left	308 (33)
Rectum	238 (26)
Stage	
I	125 (13)
II	448 (48)
III	357 (38)
Survival	
Alive	355 (38)
Cancer death	279 (30)
Non-cancer death	296 (32)

3.4 CD68/CD80/CD163 macrophage markers expression

As this study selected CD68 for pan-macrophages marker, CD80 for M1-like macrophages, and CD163 for M2-like macrophages separately for IHC staining and, the markers were never applied in the lab before. Therefore, double-immunofluorescence staining for CD68/CD80 M1-like and CD68/CD163 M2-like were performed from the same CRC patients to confirm macrophage markers expression. The results indicated that positive $CD68^{+}/CD80^{+}$ for M1-like macrophages (**Figure 3.2 A1-A4**) and positive $CD68^{+}/CD163^{+}$ for M2-like macrophages (**Figure 3.2 A2-D2**).

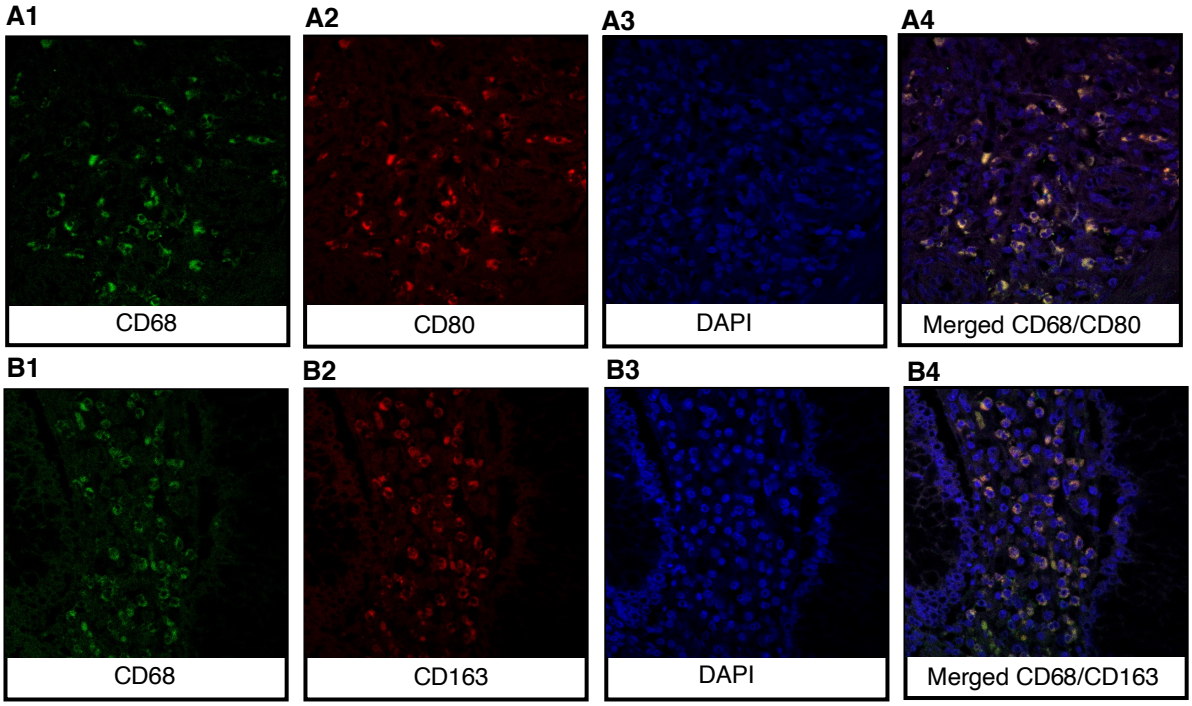

Figure 3.2 - Expression of $CD68^+/CD80^+$ and $CD68^+/CD163^+$ macrophage markers in tumour cells and tumour stroma by double-immunofluorescence staining. A1. CD68, **A2**. CD80, **A3.** DAPI, **A4**. merged $CD68^+/CD80^+$, **B1**. CD68, **B2**. CD163, **B3**. DAPI, **B4**. merged $CD68^+/CD163^+$. Green colour represented $CD68^+$, Red colour represented $CD80^+/CD163^+$. Nuclei was stained by DAPI (blue). The pictures were presented at 20x magnification.

3.5 T-lymphocytes and myeloid cells expression

The expression of T-lymphocytes markers; $CD3^+$, $CD8^+$, $FoxP3^+$, and myeloid cells markers; $CD68^+$, $CD80^+$, $CD163^+$, $CD66b^+$ were performed by IHC. Positive cells were assessed from tumour cell nests and tumour stroma area separately (**Figure 3.3**).

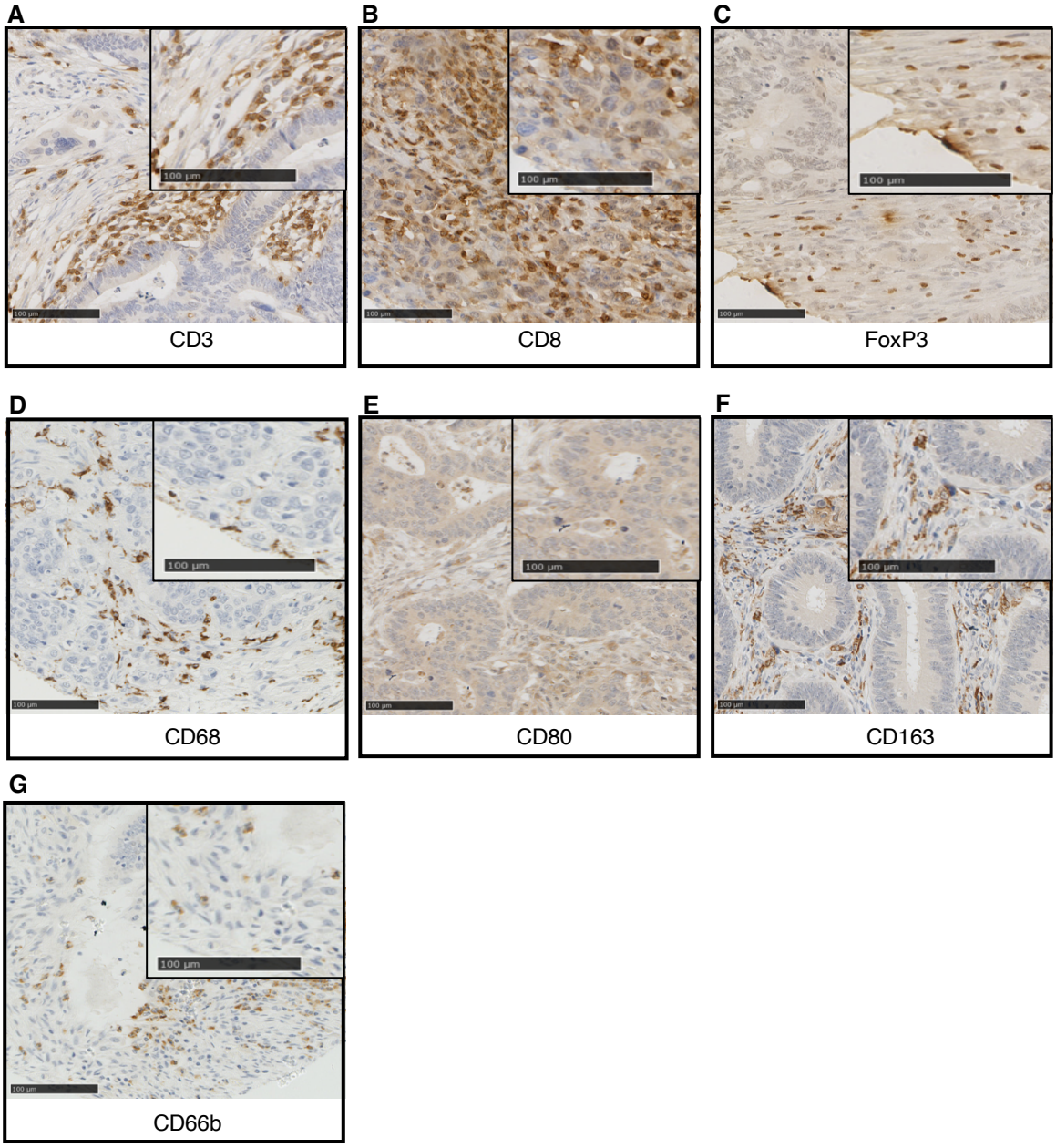

Figure 3.3 - The expression of T-lymphocytes and myeloid cells markers in tumour cells and stromal areas by IHC staining. **A**. $CD3^+$, **B**. $CD8^+$, **C**. $FoxP3^+$, **D**. $CD68^+$, **E**. $CD80^+$, **F**. $CD163^+$, **G**. $CD66b^+$. The pictures were presented at 20x magnification.

3.6 ICCC of myeloid cells markers on Scottish discovery cohort (full sections)

For the current study, full sections were staining for myeloid cell markers for part of the cohort (CD68, CD80, CD163, and CD66b). The scoring of all markers was performed by J.I. and 10% were double scored by Antonia Roseweir. The agreement of co-scoring for all markers were performed by using ICCC, Bland-Altman plots, and scatter plots. For Bland-Altman plots, the solid line represented mean of scores, and the dash lines represented upper and lower levels of 95% confidence intervals (**Figure 3.4 – 3.7**).

3.6.1 CD68

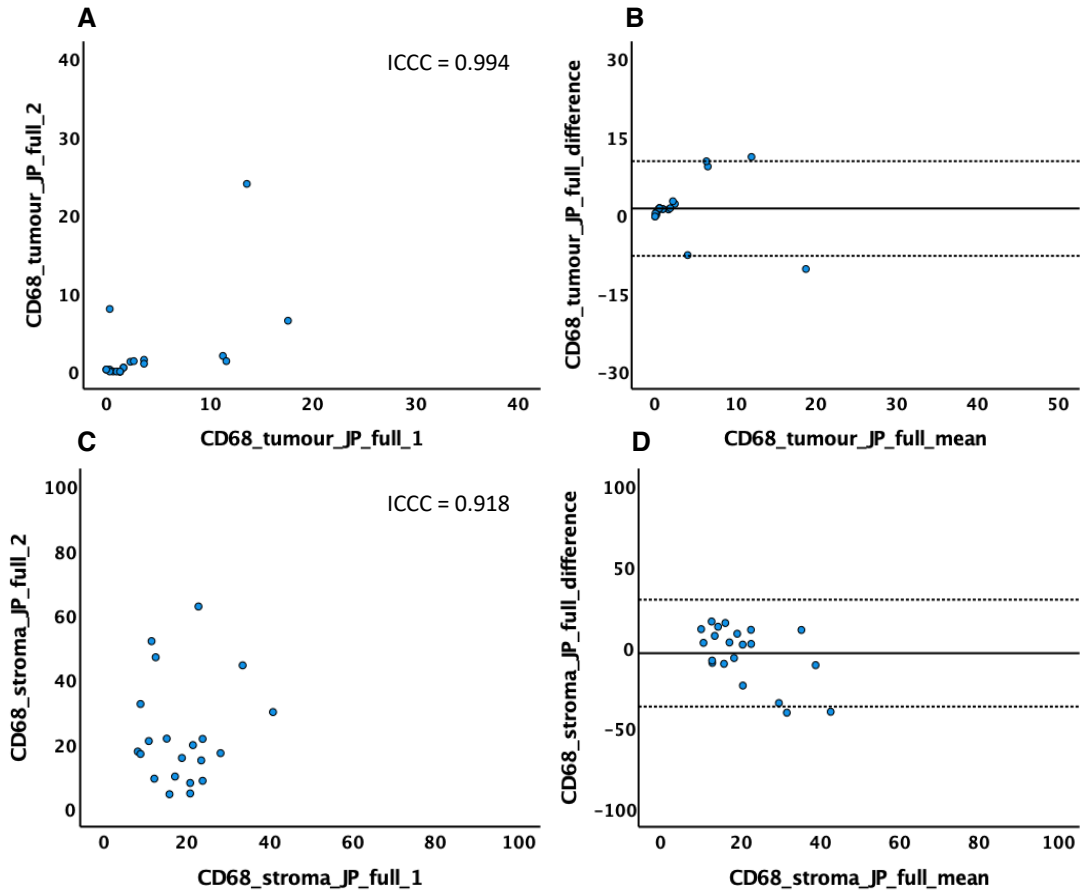

Figure 3.4 - ICCC, scatter plot, Bland-Altman plot of CD68^{+} in tumour cell nests and tumour stroma in stage I-III CRC Scottish cohort full sections; A, B. tumour cell nests, **C**, **D**. tumour stroma

3.6.2 CD80

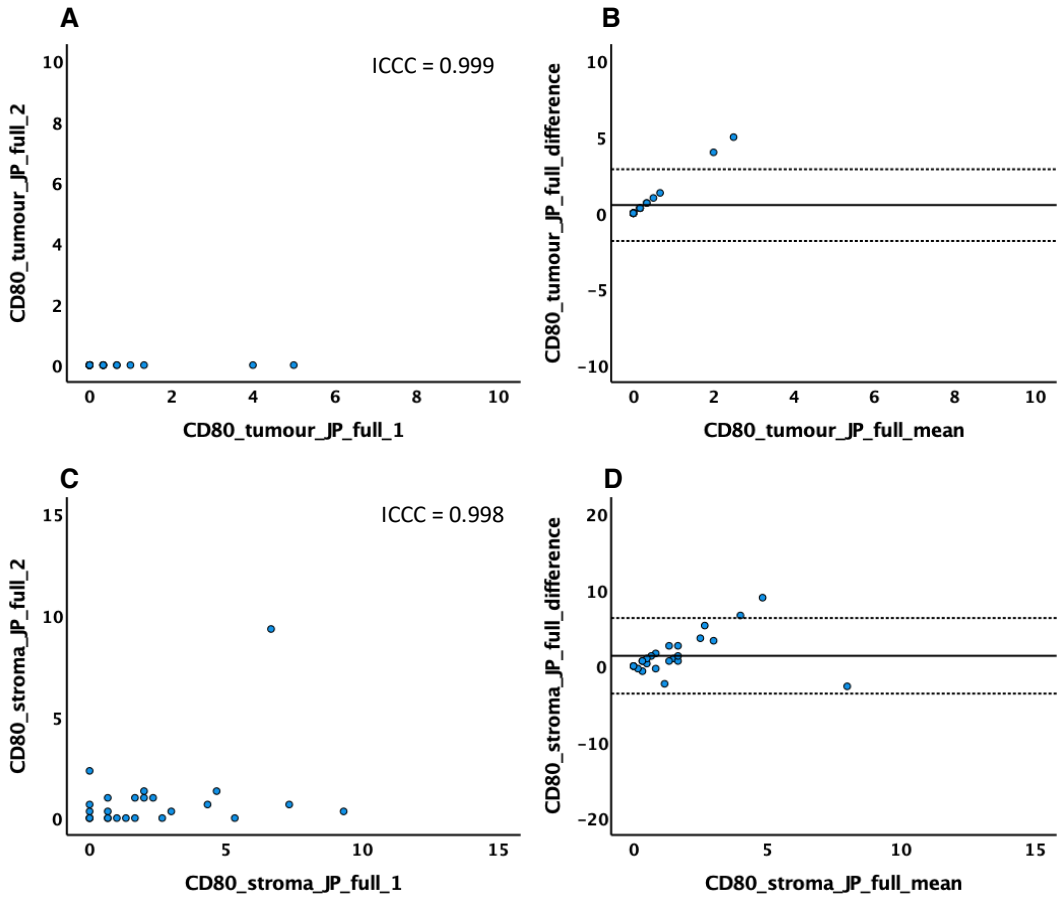

Figure 3.5 - ICCC, scatter plot, Bland-Altman plot of CD80$^+$ in tumour cell nests and tumour stroma in stage I-III CRC Scottish cohort full sections; A, **B**. tumour cell nests, **C**, **D**. tumour stroma

3.6.3 CD163

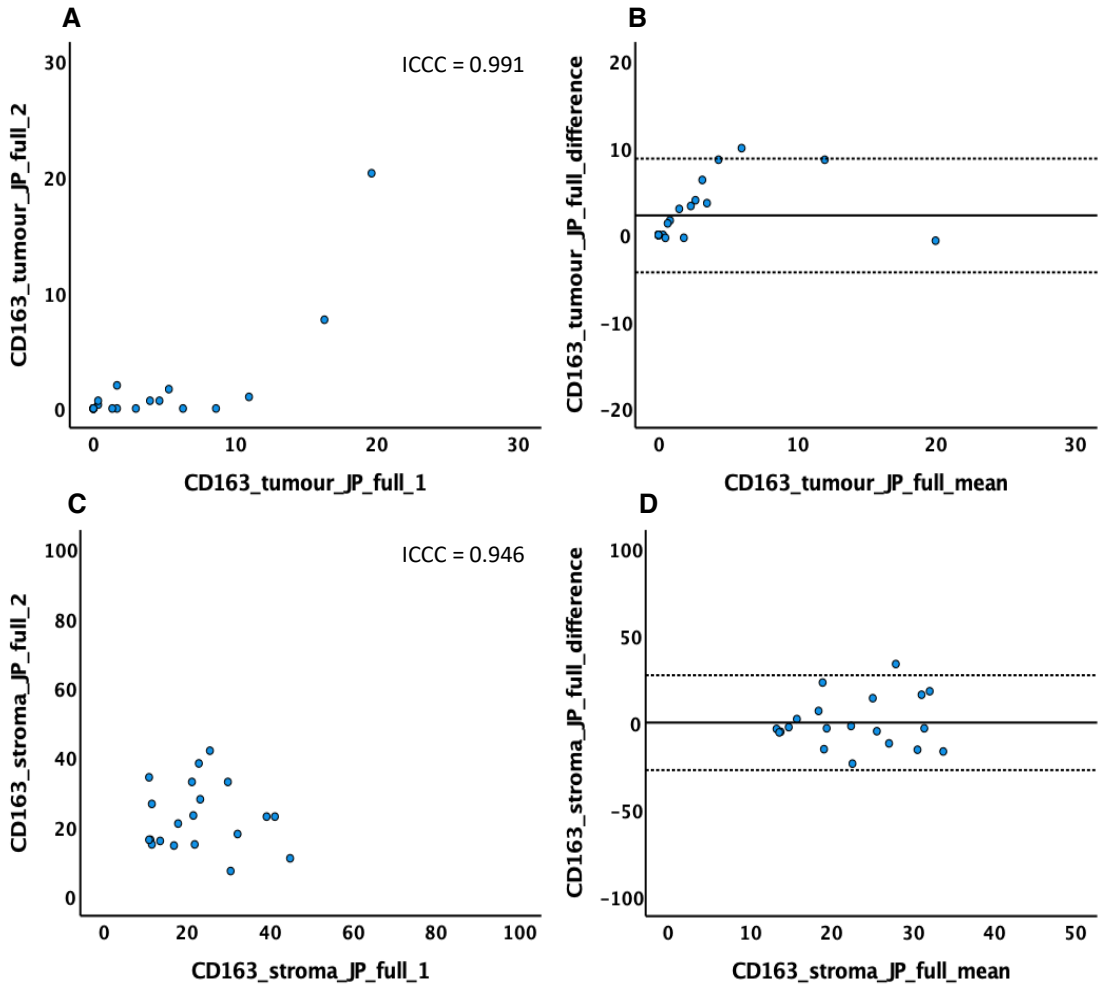

Figure 3.6 - ICCC, scatter plot, Bland-Altman plot of CD163$^+$ in tumour cell nests and tumour stroma in stage I-III CRC Scottish cohort full sections; A, **B**. tumour cell nests, **C**, **D**. tumour stroma

3.6.4 CD66b

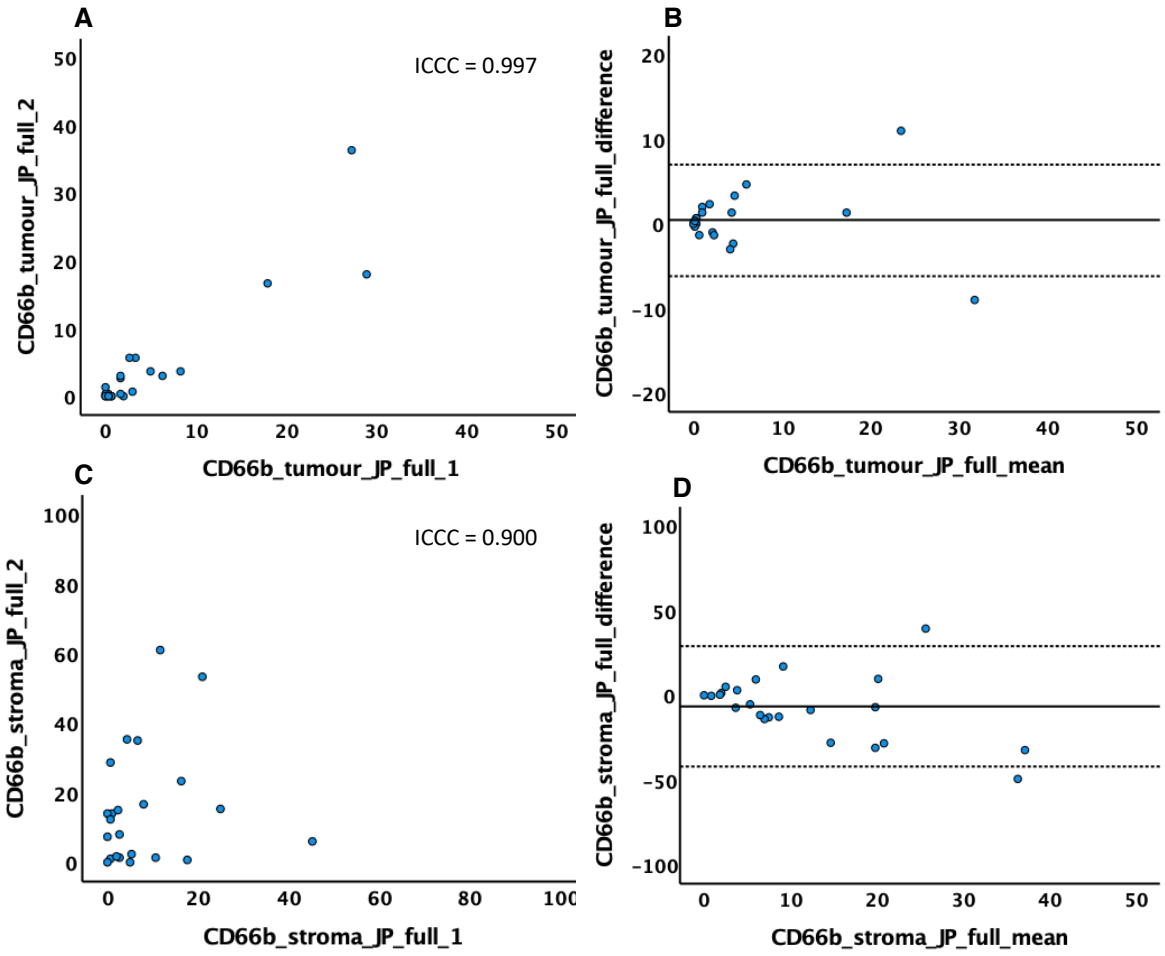

Figure 3.7 - ICCC, scatter plot, Bland-Altman plot of CD66b$^+$ in tumour cell nests and tumour stroma in stage I-IIICRC Scottish cohort full sections; A, **B**. tumour cell nests, **C**, **D**. tumour stroma

3.7 Correlation between full sections and TMA slides

As immune cells markers were initially performed on full sections which was time consuming, it was decided to compare full section scoring to TMA scores to assess if TMAs could be utilised for the rest of the cohort and other markers. Therefore, $CD68^+$ scoring was compared between full sections and a TMA containing the same patients. These results showed significant positive correlation for both in tumour cell nests (r=0.418, p<0.001) and in tumour stroma (r=0.227, p=0.011) (**Figure 3.7**). Therefore, TMAs where utilised for the remainder of the cohort and markers.

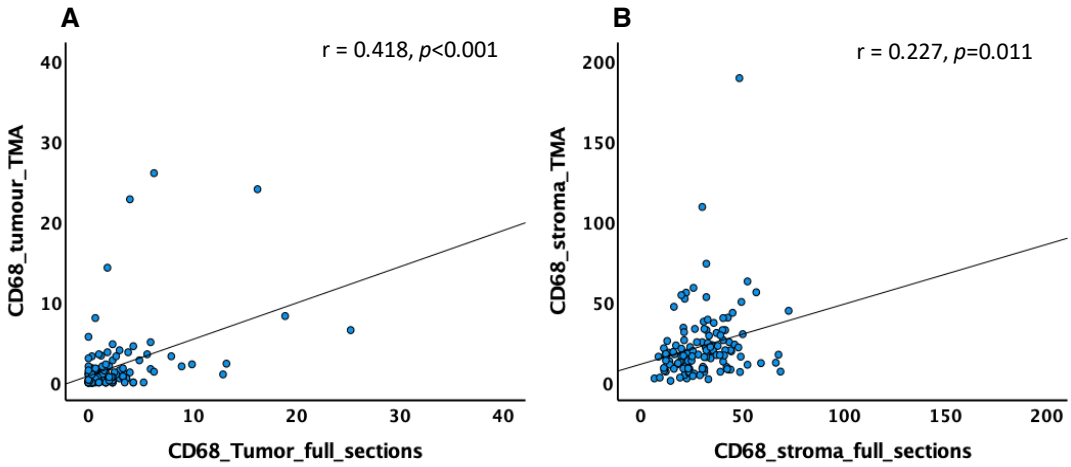

Figure 3.8 - Correlation between $CD68^+$ scoring in full sections and TMA slides in stage I-III CRC Scottish cohort (n=131). **A**. $CD68^+$ in tumour cell nests, **B**. $CD68^+$ in tumour stroma

3.8 ICCC and cut off values of T-cells and myeloid cells TMAs

TMA slides were stained for T-lymphocytes and myeloid cells markers. The agreement between the two independent scorers was analysed utilising ICCC, Bland-Altman plots, and scatter plots. The cut off values of all markers were then generated by using maximally selected rank statistics on R Studio based on patient's CSS categorised into high and low values. For Bland-Altman plots, the solid line represented mean of scoring, and the dash lines represented upper and lower levels of 95% confidence intervals (**Figure 3.9 – 3.22**).

3.8.1 CD3_tumour

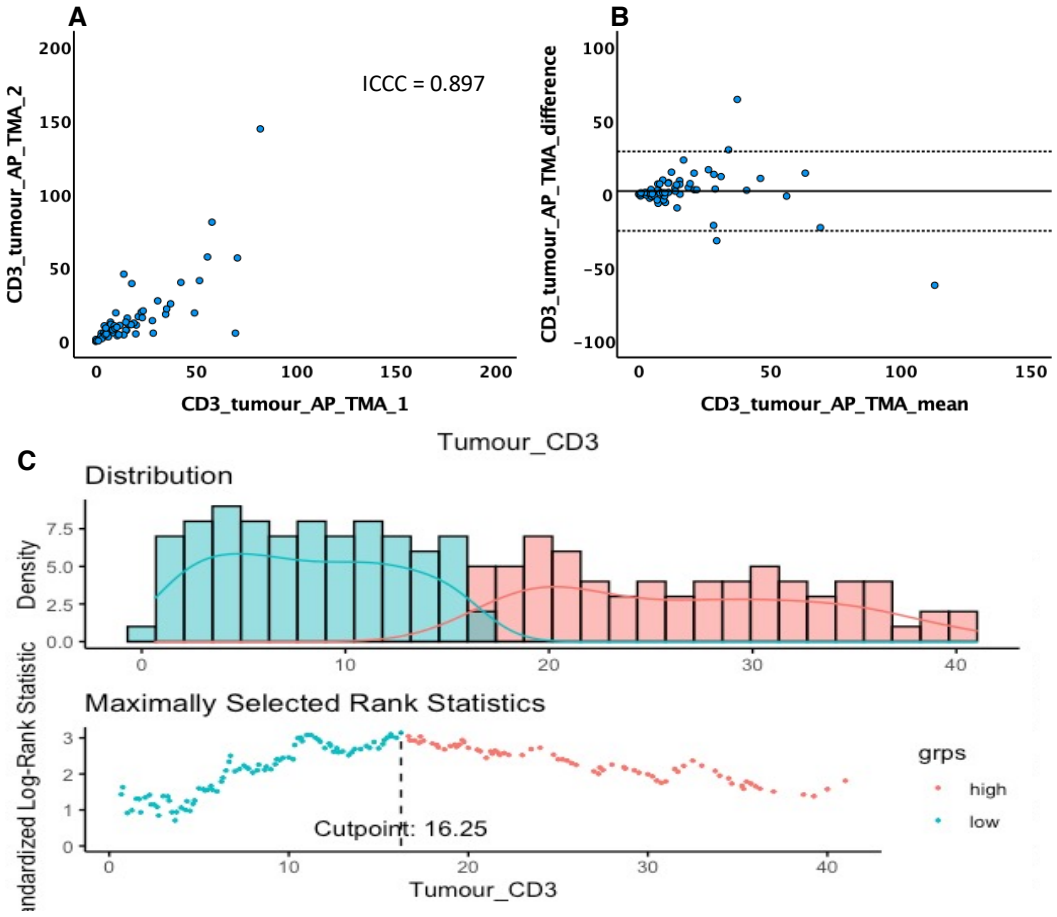

Figure 3.9 - ICCC, scatter plot, Bland-Altman plot of CD3$^+$ in tumour cell nests in stage I-III CRC Scottish cohort TMA. A. ICCC 0.897 and scatter plot, **B**. Bland-Altman plot with upper and lower 95% confidence intervals, **C**. cut-off value 16.25

3.8.2 CD3_stroma

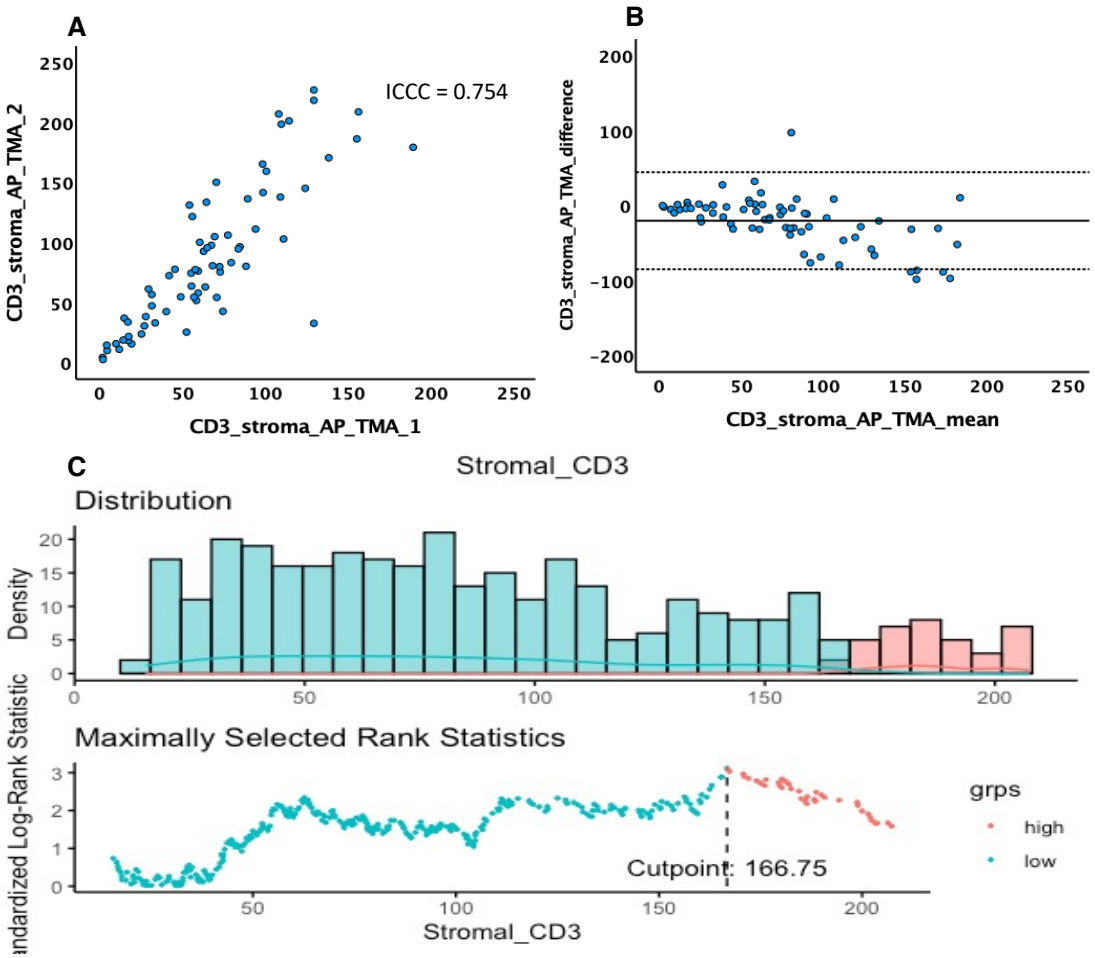

Figure 3.10 - ICCC, scatter plot, Bland-Altman plot of CD3$^+$ in tumour stroma of stage I-III CRC Scottish cohort TMAs. **A**. ICCC 0.754 and scatter plot, **B**. Bland-Altman plot with upper and lower 95% confidence intervals, **C**. cut-off value 166.75

3.8.3 CD8_tumour

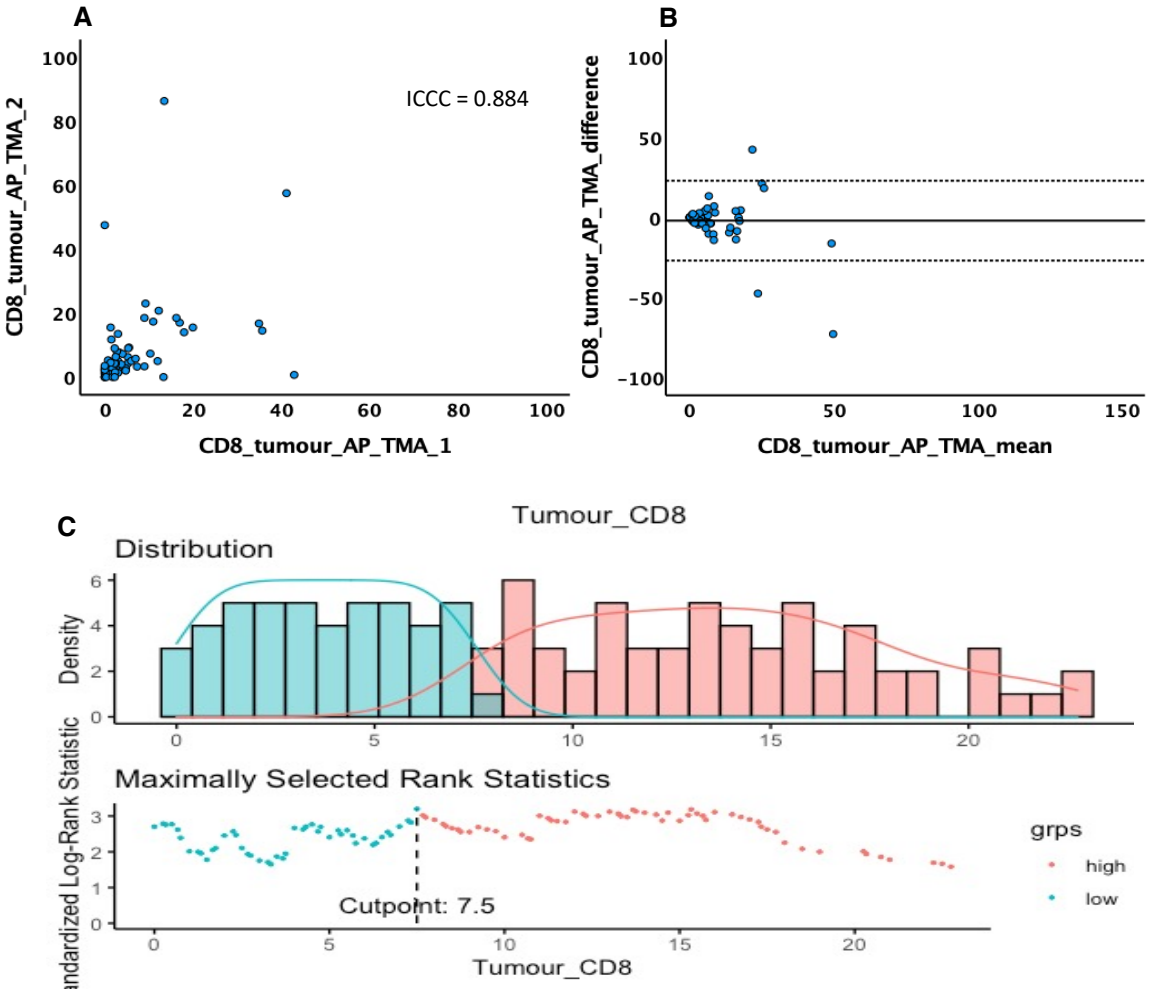

Figure 3.11 - ICCC, scatter plot, Bland-Altman plot of CD8$^+$ in tumour cell nests of stage I-III CRC Scottish cohort TMAs. **A**. ICCC 0.884 and scatter plot, **B**. Bland-Altman plot with upper and lower 95% confidence intervals, **C**. cut-off value 7.5

3.8.4 CD8_stroma

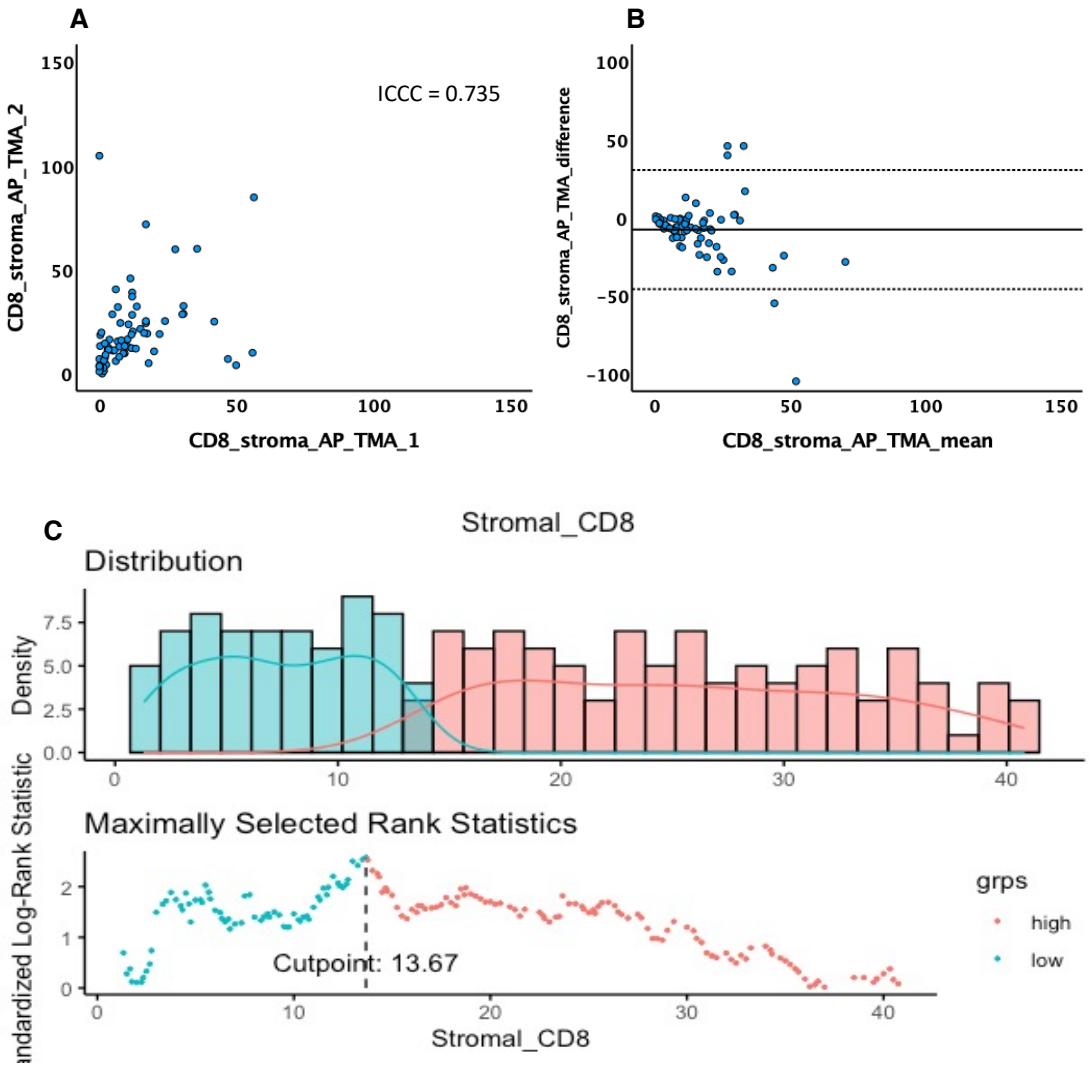

Figure 3.12 - ICCC, scatter plot, Bland-Altman plot of CD8$^+$ in tumour stroma of stage I-III CRC Scottish cohort TMAs. **A**. ICCC 0.735 and scatter plot, **B**. Bland-Altman plot with upper and lower 95% confidence intervals, **C**. cut-off value 13.67

3.8.5 FoxP3_tumour

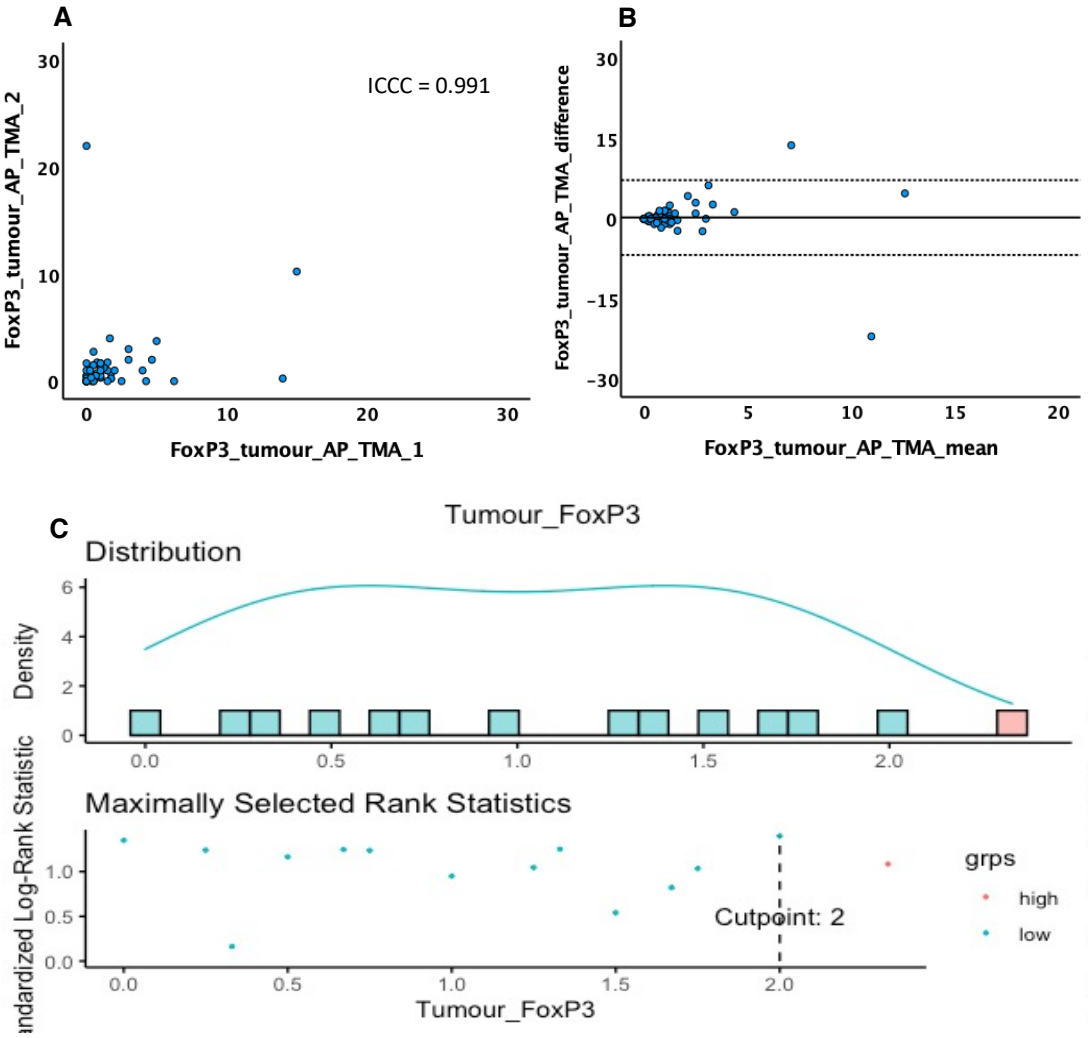

Figure 3.13 - ICCC, scatter plot, Bland-Altman plot of FoxP3^{+} in tumour cell nests of stage I-III CRC Scottish cohort TMAs. A. ICCC 0.991 and scatter plot, **B.** Bland-Altman plot with upper and lower 95% confidence intervals, **C**. cut-off value 2

3.8.6 FoxP3_stroma

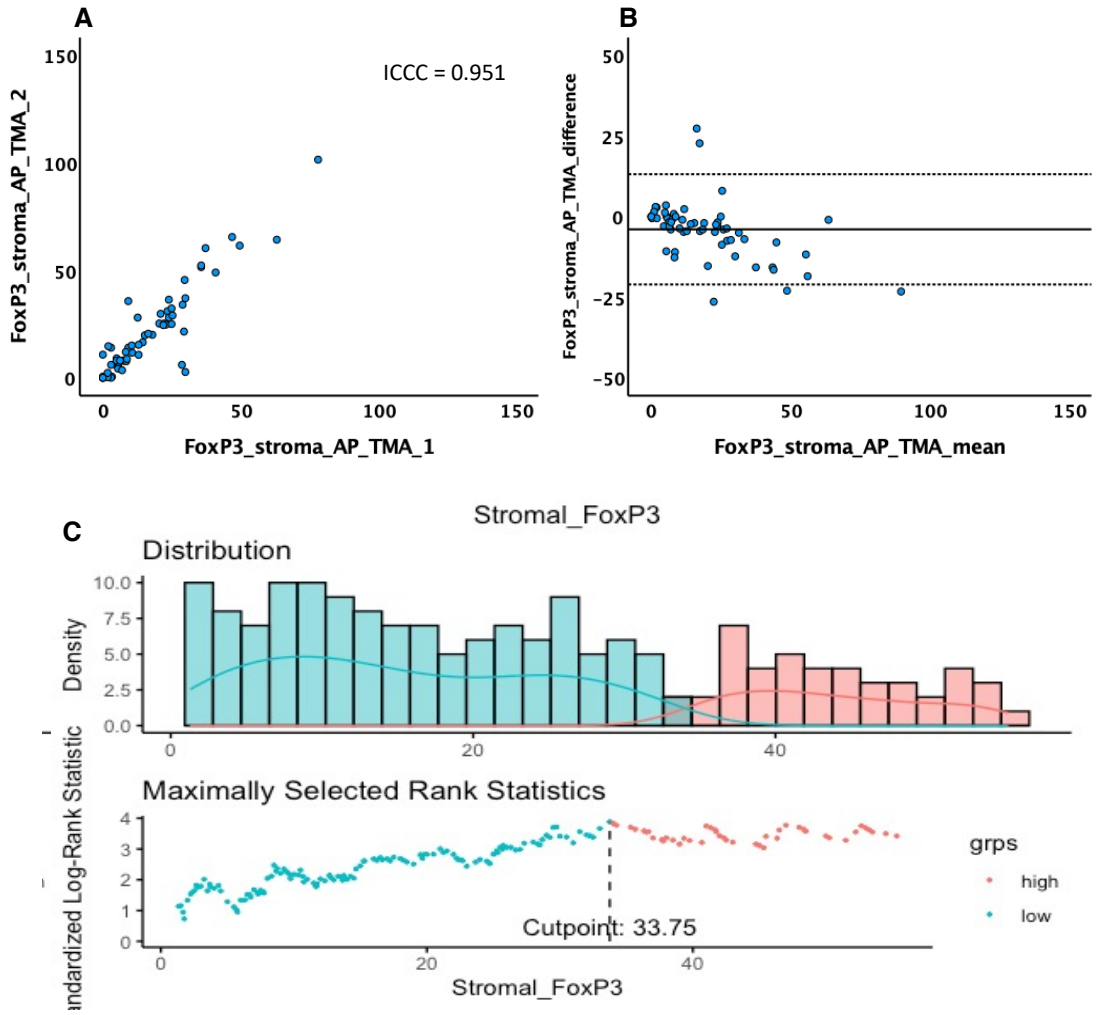

Figure 3.14 - ICCC, scatter plot, Bland-Altman plot of FoxP3$^+$ in tumour stroma of stage I-III CRC Scottish cohort TMAs. **A**. ICCC 0.951 and scatter plot, **B**. Bland-Altman plot with upper and lower 95% confidence intervals, **C**. cut-off value 33.75

3.8.7 CD68_tumour

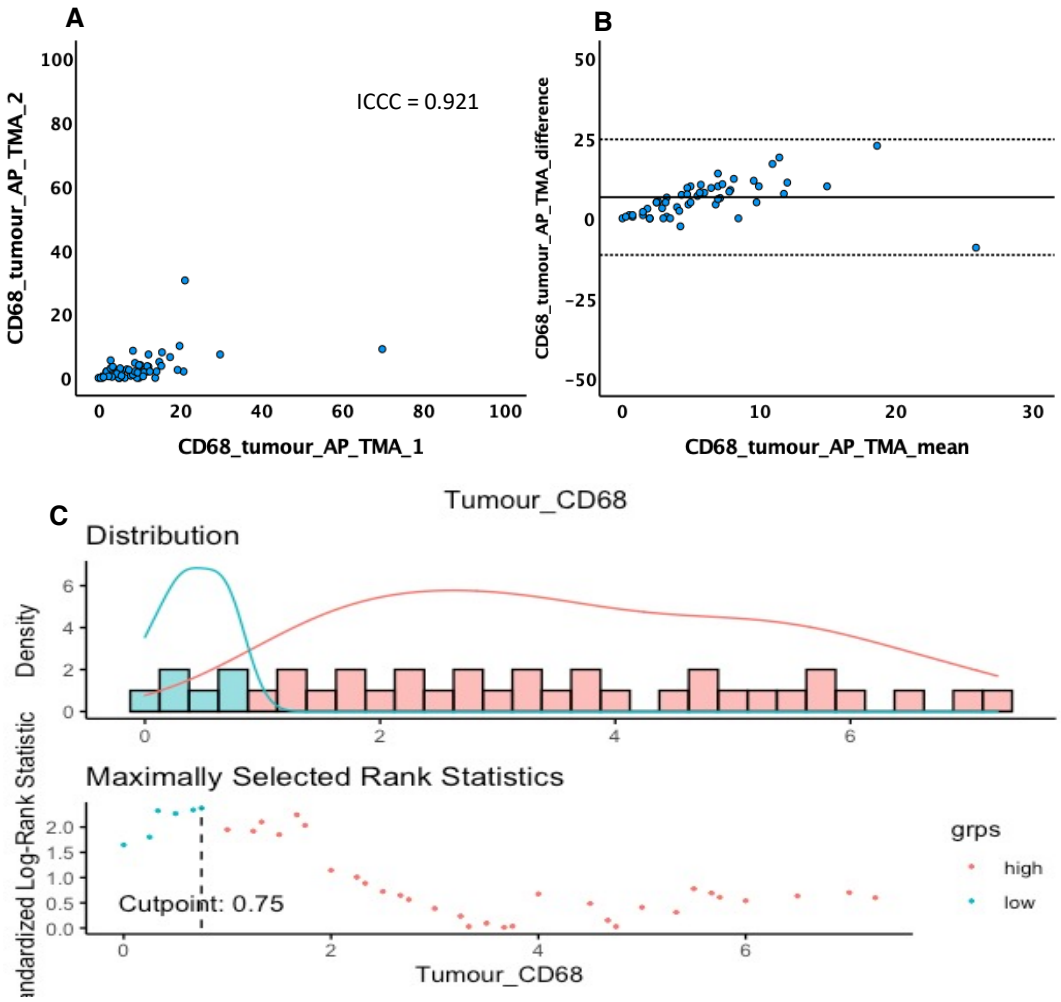

Figure 3.15 - ICCC, scatter plot, Bland-Altman plot of CD68$^+$ in tumour cell nests of stage I-III CRC Scottish cohort TMAs. A. ICCC 0.921 and scatter plot, **B**. Bland-Altman plot with upper and lower 95% confidence intervals, **C.** cut-off value 0.75

3.8.8 CD68_stroma

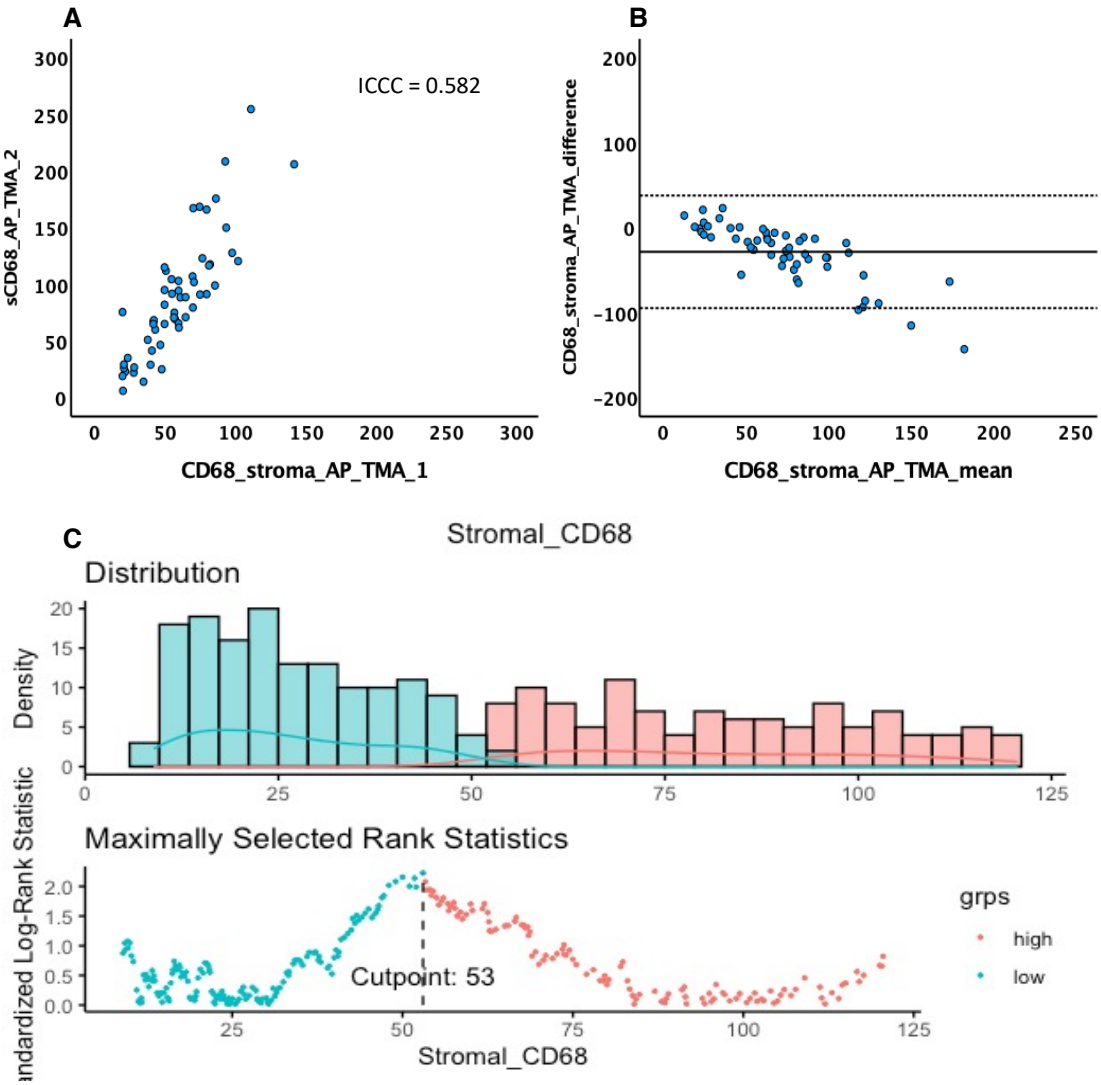

Figure 3.16 - ICCC, scatter plot, Bland-Altman plot of CD68$^+$ in tumour stroma of stage I-III CRC Scottish cohort TMAs. A. ICCC 0.582 and scatter plot, **B.** Bland-Altman plot with upper and lower 95% confidence intervals, **C.** cut-off value 53

3.8.9 CD80_tumour

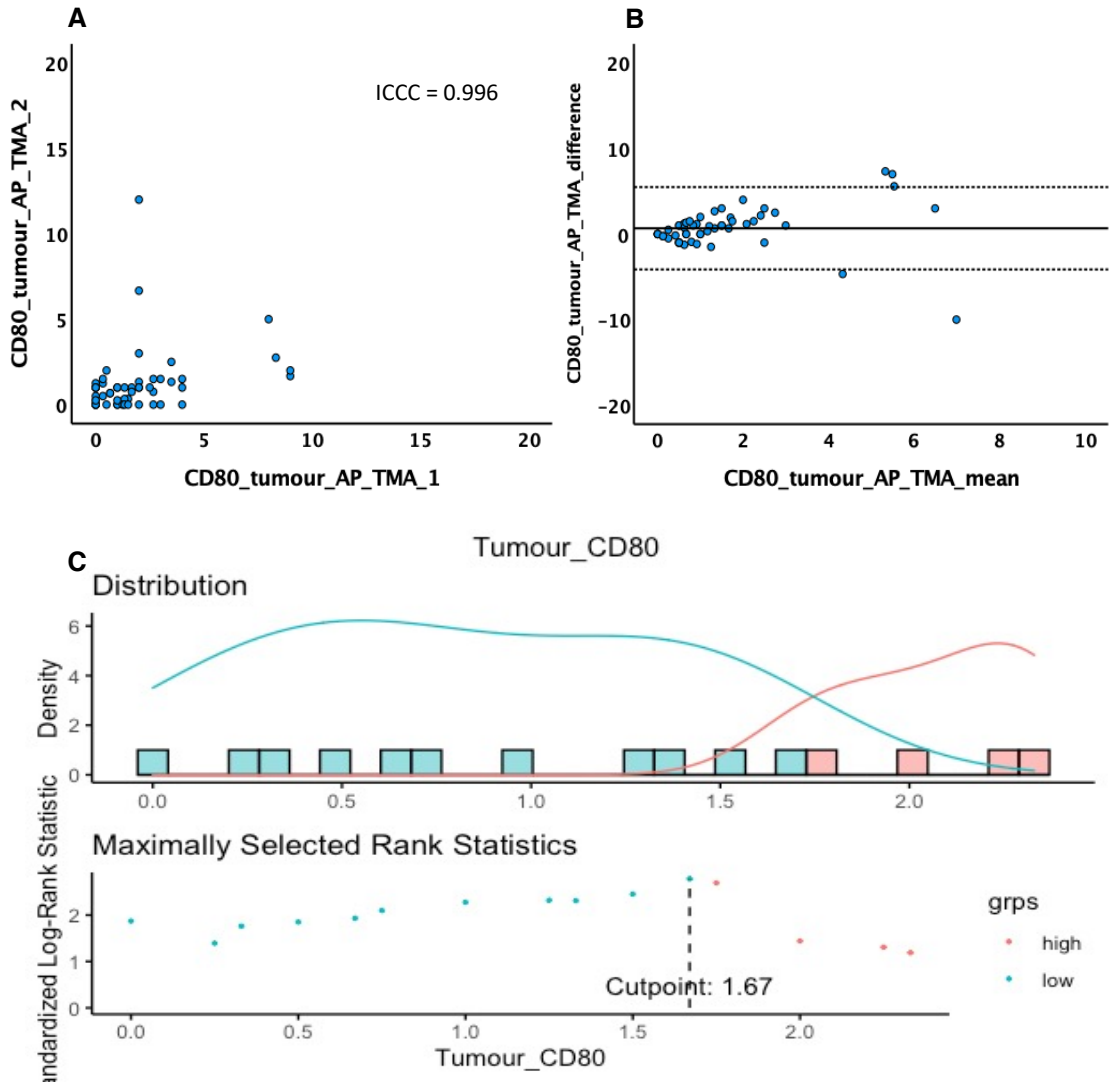

Figure 3.17 - ICCC, scatter plot, Bland-Altman plot of CD80$^+$ in tumour cell nests of stage I-III CRC Scottish cohort TMAs. A. ICCC 0.996 and scatter plot, **B.** Bland-Altman plot with upper and lower 95% confidence intervals, **C.** cut-off value 1.67

3.8.10 CD80_stroma

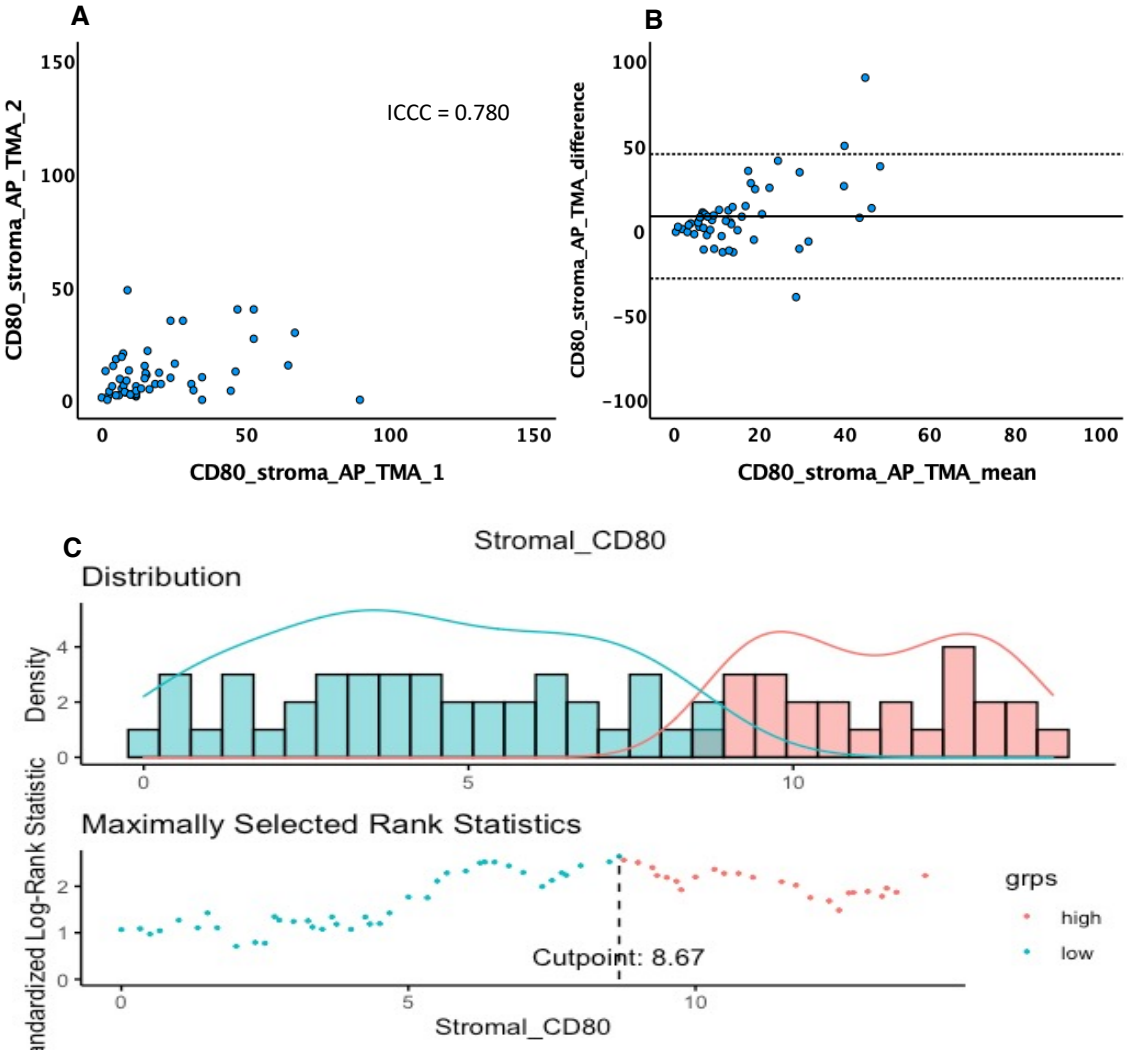

Figure 3.18 - ICCC, scatter plot, Bland-Altman plot of CD80^{+} in tumour stroma of stage I-III CRC Scottish cohort TMAs. A. ICCC 0.780 and scatter plot, **B.** Bland-Altman plot with upper and lower 95% confidence intervals, **C.** cut-off value 8.67

3.8.11 CD163_tumour

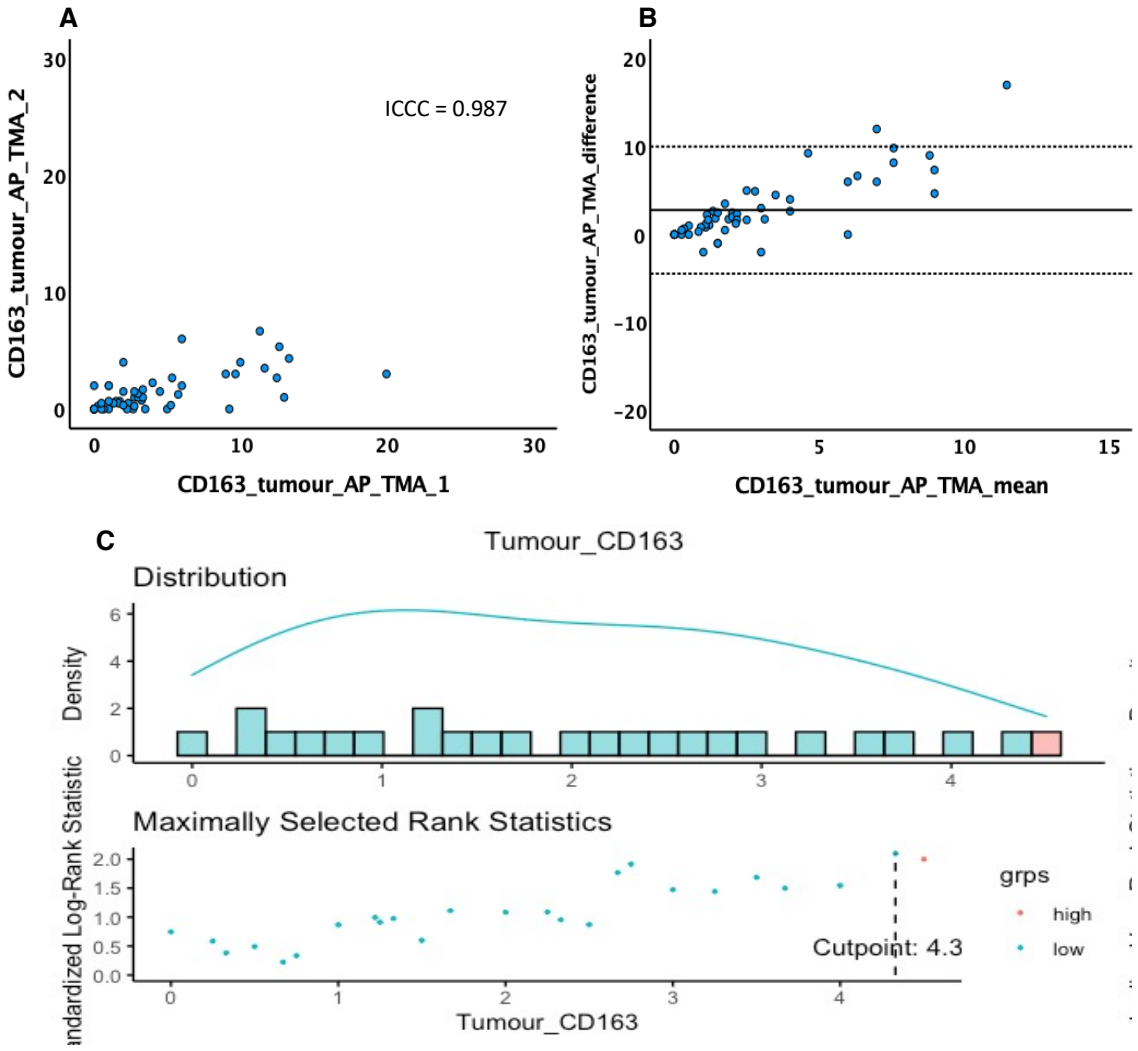

Figure 3.19 - ICCC, scatter plot, Bland-Altman plot of CD163^{+} in tumour cell nests of stage I-III CRC Scottish cohort TMAs. A. ICCC 0.987 and scatter plot, **B.** Bland-Altman plot with upper and lower 95% confidence intervals, **C.** cut-off value 4.3

3.8.12 CD163_stroma

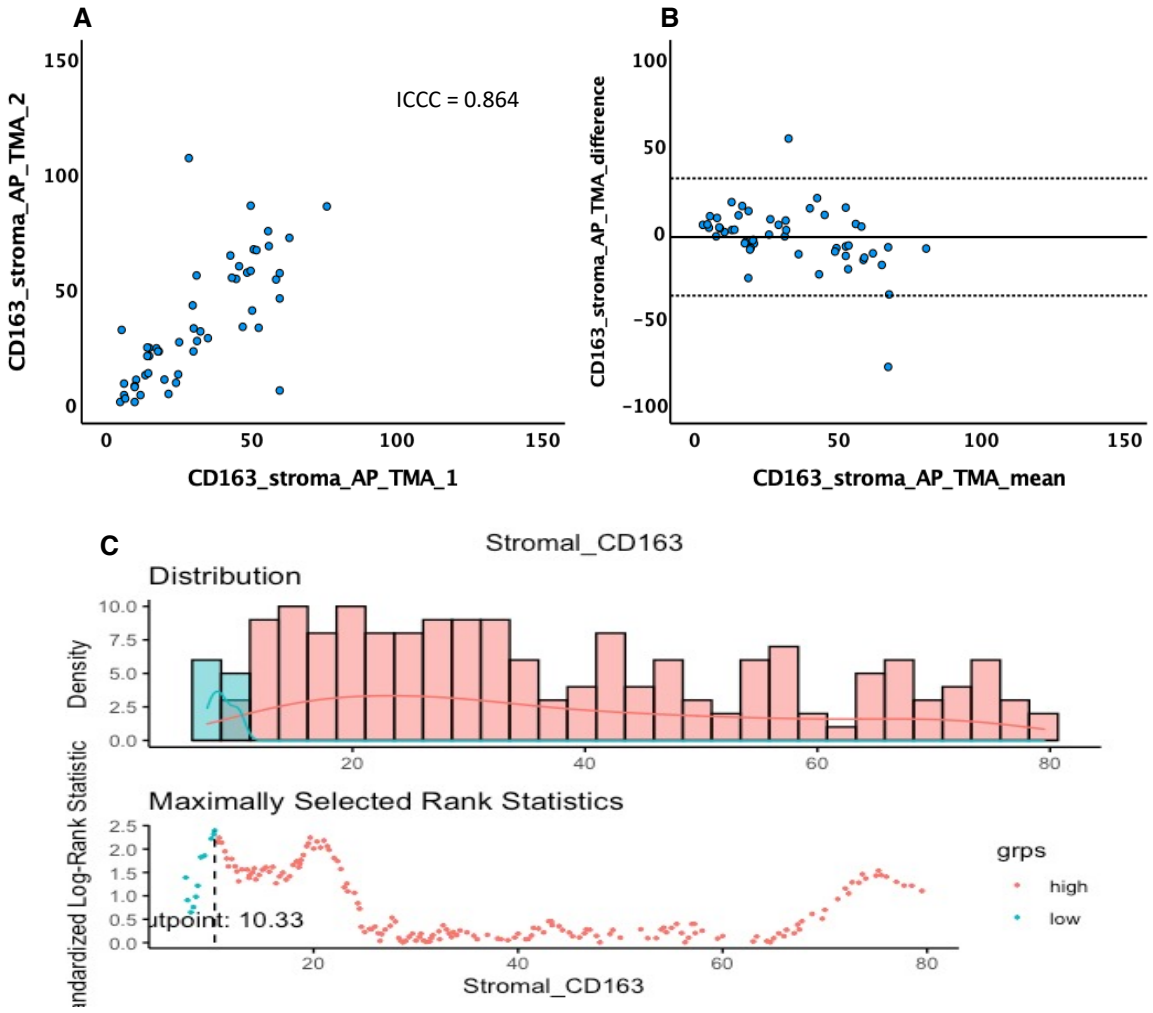

Figure 3.20 - ICCC, scatter plot, Bland-Altman plot of CD163^{+} in tumour stroma of stage I-III CRC Scottish cohort TMAs. A. ICCC 0.864 and scatter plot, **B.** Bland-Altman plot with upper and lower 95% confidence intervals, **C.** cut-off value 10.33

3.8.13 CD66b_tumour

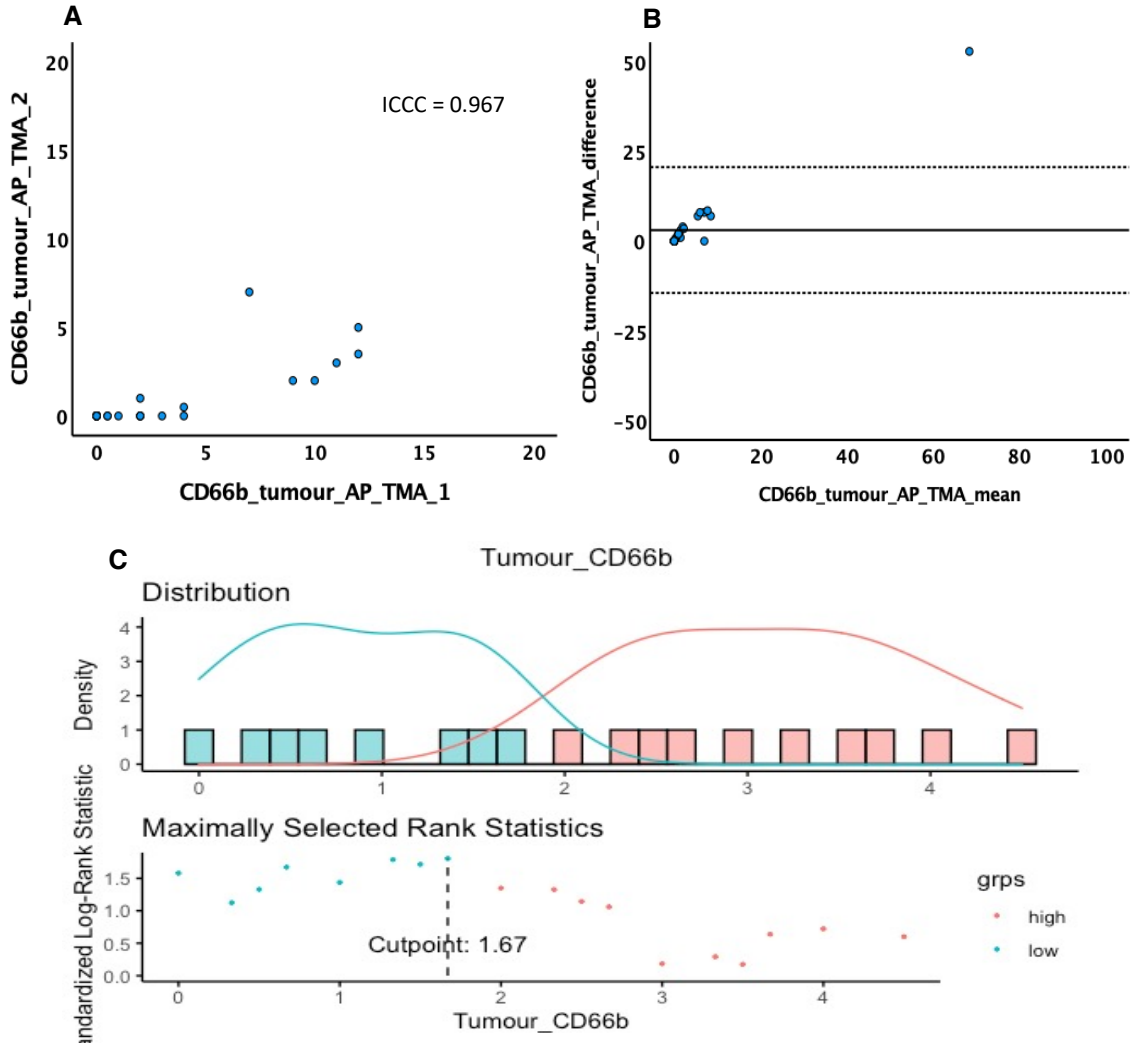

Figure 3.21 - ICCC, scatter plot, Bland-Altman plot of CD66b$^+$ in tumour cell nests of stage I-III CRC Scottish cohort TMAs. A. ICCC 0.967 and scatter plot, **B.** Bland-Altman plot with upper and lower 95% confidence intervals, **C.** cut-off value 1.67

3.8.14 CD66b_stroma

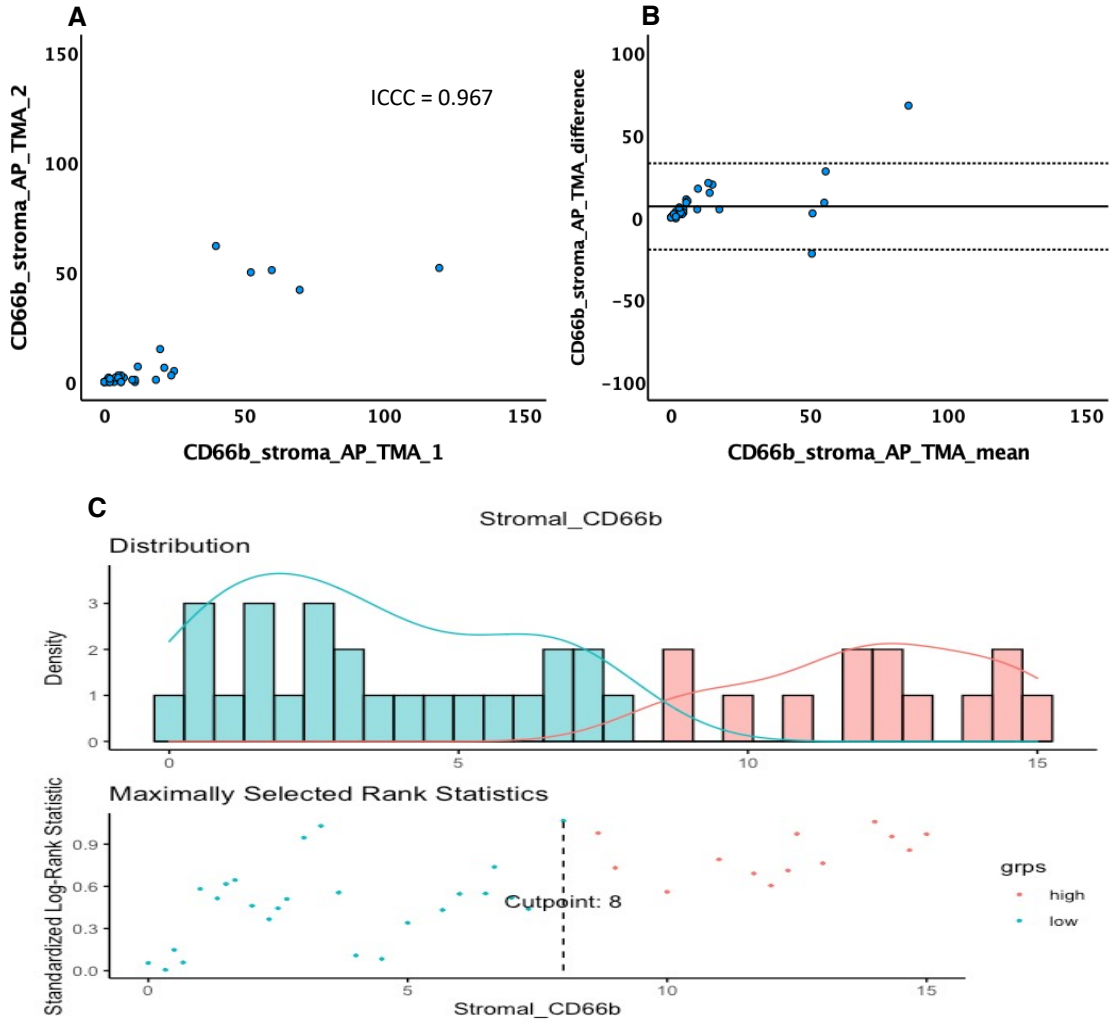

Figure 3.22 - ICCC, scatter plot, Bland-Altman plot of CD66b$^+$ in tumour stroma of stage I-III CRC Scottish cohort TMAs. A. ICCC 0.967 and scatter plot, **B.** Bland-Altman plot with upper and lower 95% confidence intervals, **C.** cut-off value 8

3.9 Immune cells infiltration level in stages I-III CRC patients

To define the differences of immune cells infiltration at each stage of disease, the levels of T-lymphocytes and myeloid cells in stage I-III were assessed in tumour cell nests and tumour stroma.

3.9.1 Levels of immune cells in tumour cell nests

In tumour cell nests, the infiltration of all T-lymphocytes presented highest in stage I and gradually decreased when the disease reached stage II and III, respectively. Numbers of CD3$^+$ in stage I was

significantly higher than stage II (p=0.006), and stage III (p=0.026). Similarly, numbers of $CD8^+$ in stage I was significantly higher than stage II (p=0.009), and stage III (p<0.001), while in stage II was significantly greater than stage III (p=0.012). However, $FoxP3^+$ cells presented no significant changes between all stages (**Figure 3.23, A-C**). As for myeloid cells, macrophages, and granulocytes, infiltrations were at much lower levels in all stages. Among them, only $CD80^+$ M1-like macrophages was statistically significance (p=0.030); however, the numbers of infiltration are very small to observe the differences between stages (**Figure 3.23, D-G**).

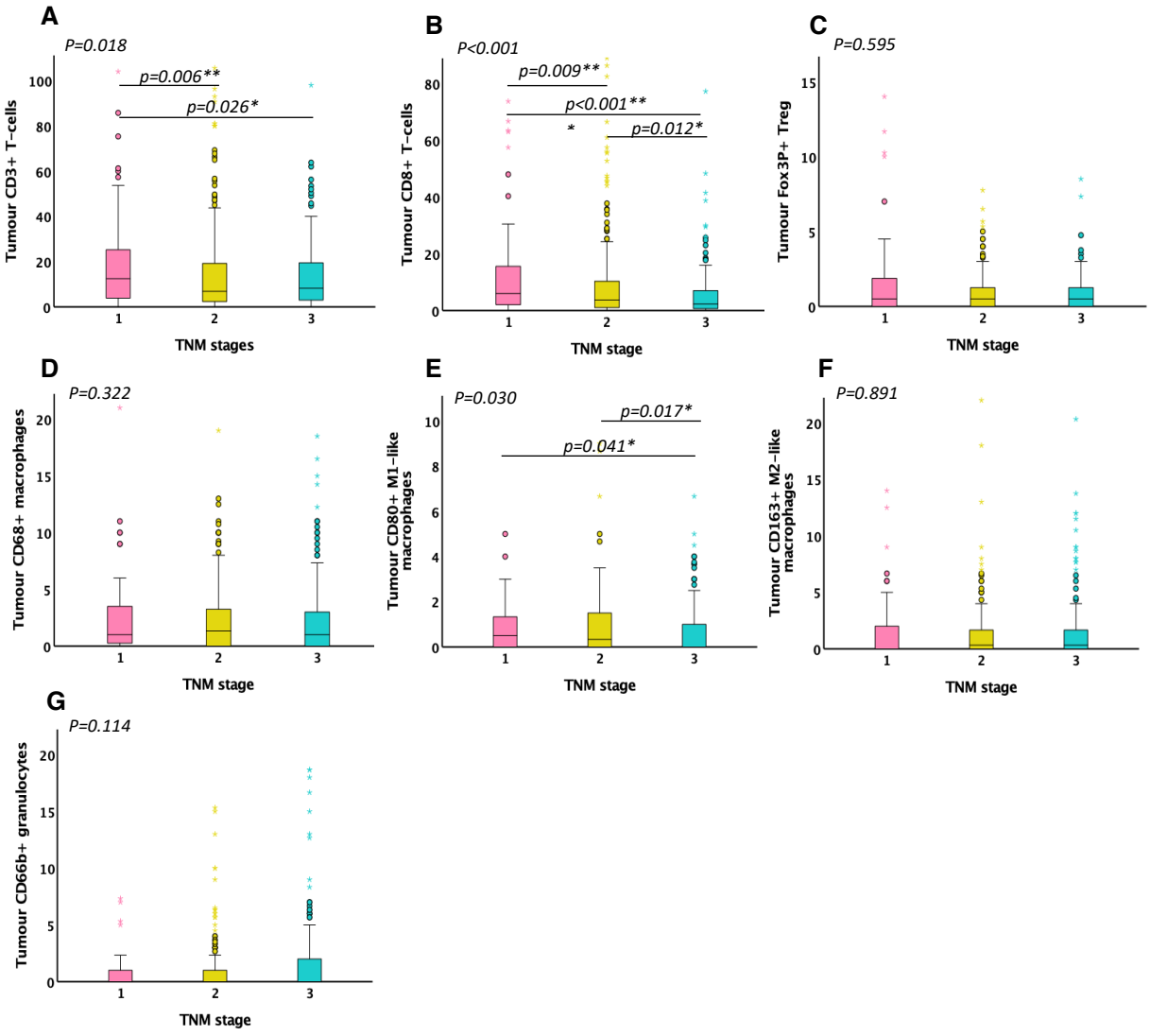

Figure 3.23 - T-lymphocytes and myeloid cells infiltration level in tumour cell nests in stage I-III CRC Scottish cohort. A. $CD3^+$, **B.** $CD8^+$, **C.** $FoxP3^+$, **D.** $CD68^+$, **E.** $CD80^+$, **F.** $CD163^+$, **G.** $CD66b^+$. The colour represented; pink=stage I, yellow=stage II, and blue=stage III, *p<0.05, **p<0.01, ***p<0.001

3.9.2 Levels of immune cells in tumour stroma

As for levels in tumour stroma, in general, the levels of all markers were elevated compared to tumour cell nests. However, $CD3^+$ and $CD8^+$ T-lymphocytes levels presented no significant differences between stages, which $CD3^+$ reached maximum levels in stage I and gradually decreased in stage II and III, whereas $CD8^+$ cytotoxic T-lymphocytes reached maximum in stage II. $FoxP3^+$ was significant difference in stage I and II (p=0.009), and stage I and III (p=0.002), which was decreased in stage II and III when compared to stage I, and slightly decreased from stage II compared to stage III (**Figure 3.24, A-C**). Myeloid cells, $CD68^+$ macrophage was significantly high in stage I than stage III (p=0.006). Similarly, $CD80^+$ M1-like macrophage significantly elevated in stage I than stage III (p=0.006), however, no significance was observed for $CD163^+$ M2-like macrophage. Whereas $CD66b^+$ granulocytes presented gradually increase from stage I and reach maximum in stage III, however, these changes did not reach significance (**Figure 3.24, D-G**).

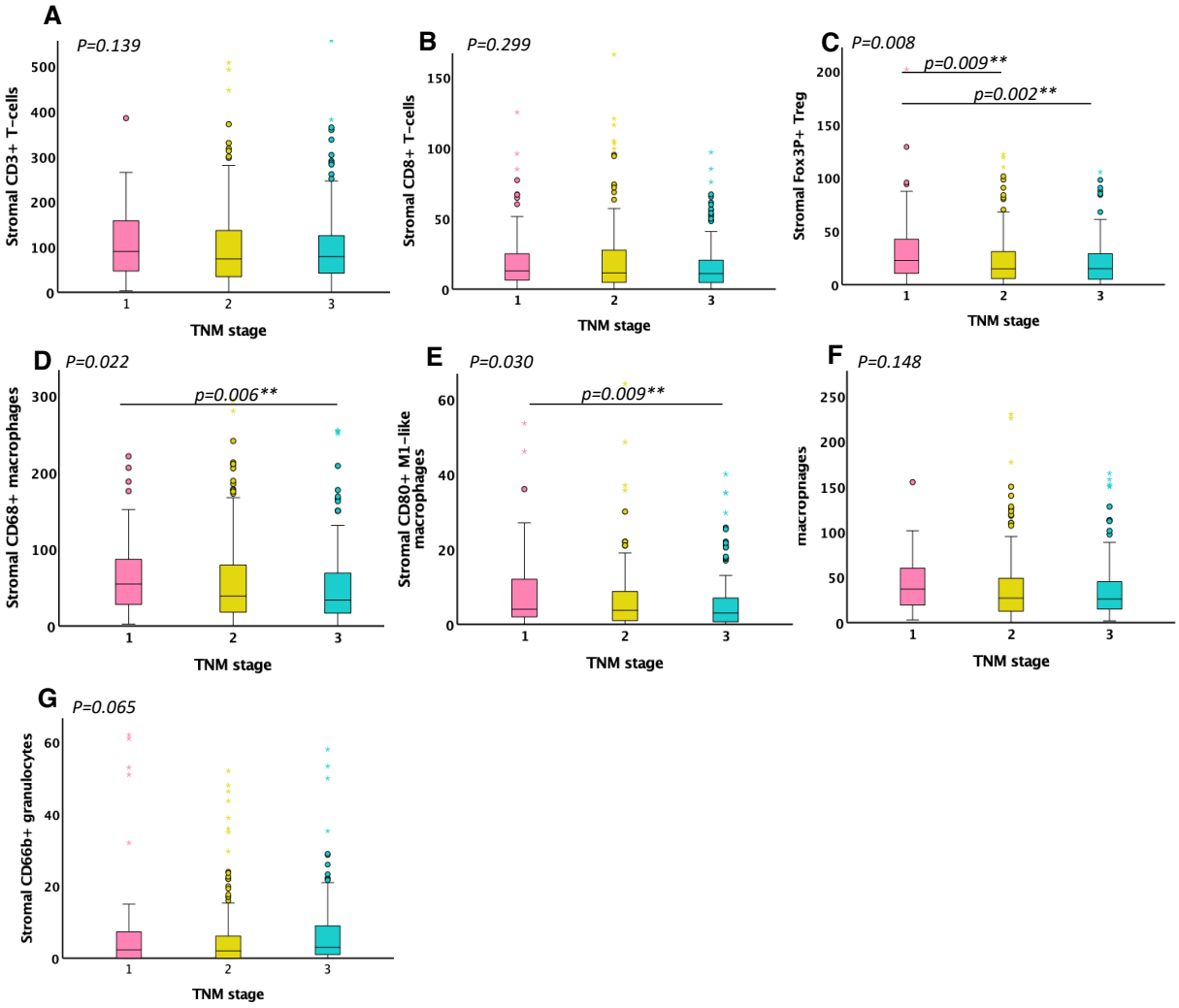

Figure 3.24 - T-lymphocytes and myeloid cells infiltration level in tumour stroma in stage I-III CRC Scottish cohort. A. $CD3^+$, **B.** $CD8^+$, **C.** $FoxP3^+$, **D.** $CD68^+$, **E.** $CD80^+$, **F.** $CD163^+$, **G.** $CD66b^+$. The colour represented; pink=stage I, yellow=stage II, and blue=stage III, *p<0.05, **p<0.01, ***p<0.001

3.10 Scottish discovery cohort survival analysis

The Scottish discovery cohort was analysed in tumour cell nest and tumour stroma separately to assess the effects of infiltration levels of T-lymphocytes and myeloid cells on patients' survival, focussing on CSS, and OS.

3.10.1 T-lymphocytes infiltration and patient's survival

3.10.1.1 T-lymphocytes in tumour cell nests

In tumour cells nest, high $CD3^+$ was significantly associated with improved CSS (HR 0.55, 95% CI 0.37-0.80, *p*=0.002, **Figure 3.25, A**) with 10-year survival stratified from 79% (high) to 63% (low). Similarly, high $CD8^+$ was associated with improved CSS (HR 0.54, 95% CI 0.37-0.80, *p*=0.002, **Figure 3.25, C**) with 10-year survival stratified from 77% (high) to 63% (low) (**Table 3.2**). No associations were seen with FoxP3 for any survival measure or OS with any marker.

Table 3.2 - Relationship between T-lymphocytes in tumour cell nest, tumour stroma, and CSS and OS (% survival at 10 years) in stage I-III CRC Scottish cohort (n=930)

	N (%)	CSS (SE)	P	OS (SE)	P
Tumour cell nest					
$CD3^+$ (n=580)			**0.002**		0.399
Low	398 (69)	63 (3)		30 (3)	
High	182 (31)	79 (3)		33 (4)	
$CD8^+$ (n=569)			**0.002**		0.143
Low	391 (69)	63 (3)		29 (3)	
High	178 (31)	77 (4)		34 (4)	
$FoxP3^+$ (n=463)			0.153		0.320
Absent	407 (88)	68 (3)		32 (3)	
Present	56 (12)	77 (9)		23 (7)	
Tumour stroma					
CD3+ (n=581)			**0.002**		0.473
Low	482 (83)	65 (3)		31 (2)	
High	99 (17)	81 (5)		30 (6)	
CD8+ (n=568)			**0.010**		0.624
Low	316 (56)	62 (3)		29 (3)	
High	252 (44)	74 (3)		32 (3)	
FoxP3+ (n=462)			**<0.001**		**0.020**
Absent	357 (77)	64 (3)		28 (3)	
Present	105 (23)	83 (5)		39 (5)	

CSS = Cancer-specific survival, OS = Overall survival, SE = Standard error

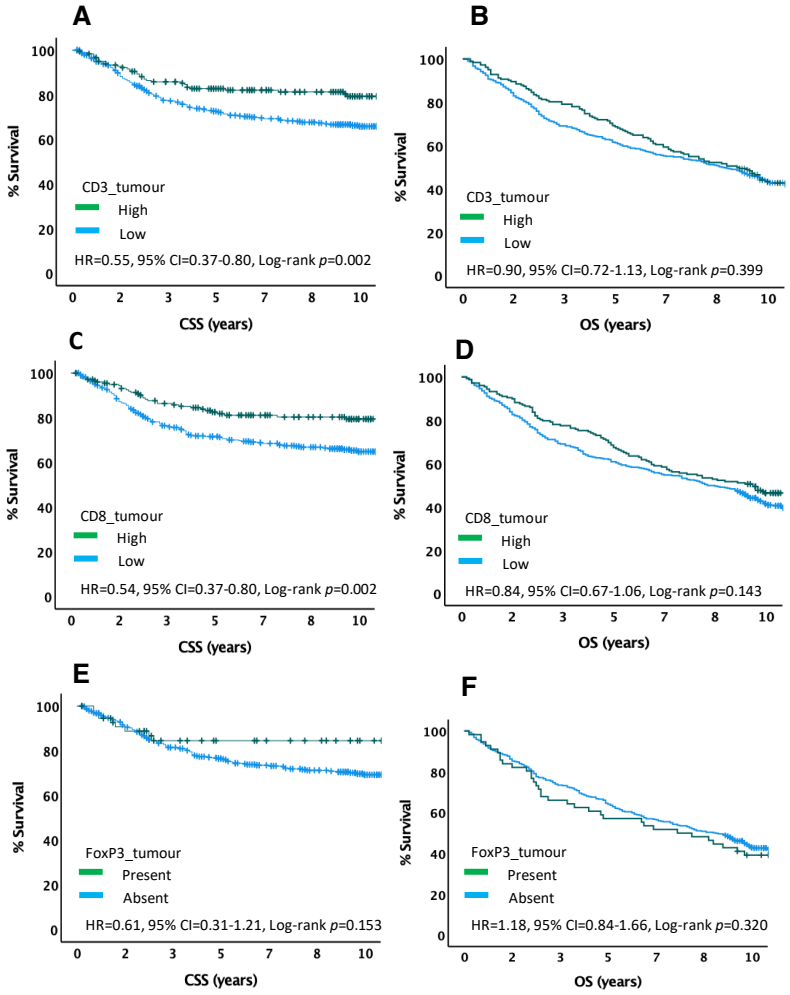

Figure 3.25 - KM plots of T-lymphocytes in tumour cell nests and CSS, OS in stage I-III CRC Scottish cohort (n=930); A. $CD3^+$ CSS (p=0.002), **B.** $CD3^+$ OS (p=0.399), **C.** $CD8^+$ CSS (p=0.002), **D.** $CD8^+$ OS (p=0.143), **E.** $FoxP3^+$ CSS (p=0.153), **F.** $FoxP3^+$ OS (p=0.320)

3.10.1.2 T-lymphocytes in tumour stroma

In tumour stroma, high $CD3^+$ was significantly associated with improved CSS (HR 0.45, 95% CI 0.26-0.76, p=0.002, **Figure 3.26, A**) with10-year survival stratified from 81% (high) to 65% (low). Similarly, high $CD8^+$ was associated with improved CSS (HR 0.65, 95% CI 0.47-0.90, p=0.010, **Figure 3.26, C**) with 10-year survival stratified from 74% (high) to 56% (low). High $FoxP3^+$ was associated with associated with improved CSS (HR 0.35, 95% CI 0.19-0.62, p<0.001, **Figure 3.26, E**) with 10-year survival stratified from 83% (high) to 64% (low); and associated with improved OS (HR 0.71, 95% CI 0.53-0.95, p=0.020, **Figure 3.26, F**) with 10-year survival stratified from 39% (present) to 28% (absent). No associations were seen with $CD3^+$ and $CD8^+$ for OS (**Table 3.2**).

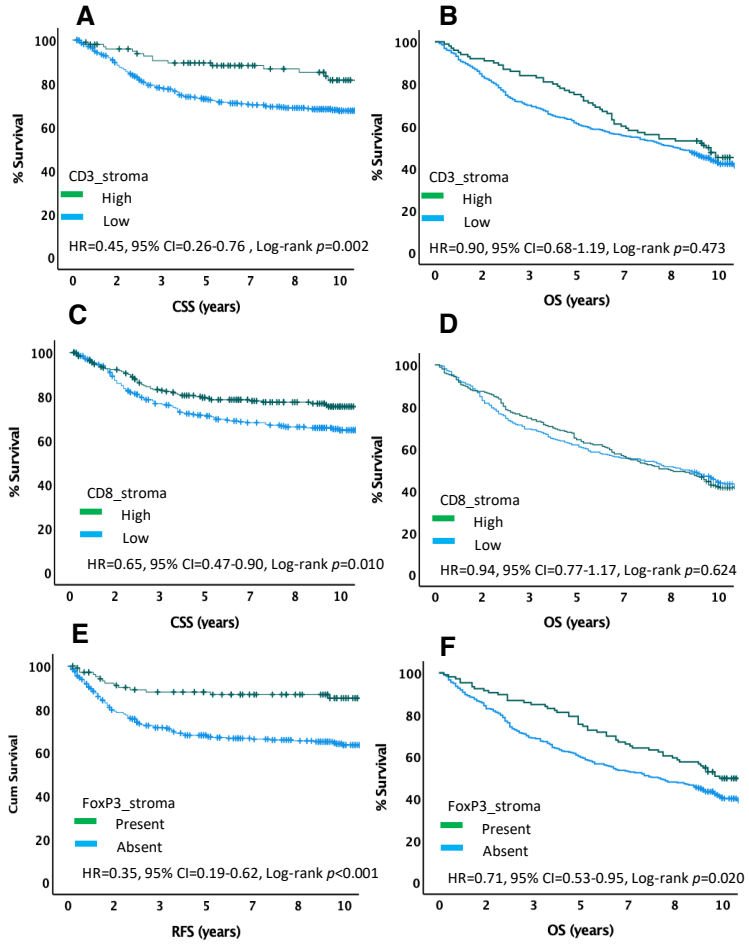

Figure 3.26 - KM plots of T-lymphocytes in tumour stroma and CSS, OS in stage I-III CRC Scottish cohort (n=930); A. $CD3^+$ CSS (p=0.002), **B.** $CD3^+$ OS (p=0.473), **C.** $CD8^+$ CSS (p=0.010), **D.** $CD8^+$ OS (p=0.624), **E.** $FoxP3^+$ CSS (p<0.001), **F.** $FoxP3^+$ OS (p=0.020)

3.10.2 Myeloid cells infiltration and patient's survival

3.10.2.1 Myeloid cells in tumour and CSS, OS

In tumour cell nests, high $CD68^+$ was associated with improved CSS (HR 0.70, 95% CI 0.52-0.94, p=0.017, **Figure 3.27, A**) with 10-year survival stratified from 68% (high) to 54% (low). High $CD80^+$ was associated with improved CSS (HR 0.47, 95% CI 0.27-0.83, p=0.007, **Figure 3.27, C**) with 10-year survival stratified from 78% (high) to 59% (low). Whereas high $CD66b^+$ was significantly associated with decreased CSS (HR 1.58, 95% CI 1.08-2.31, p=0.004, **Figure 3.27, G**) with 10-year survival stratified from 52% (high) to 71% (low). None of them were significant for OS (**Table 3.3**).

Table 3.3 - Relationship between myeloid cells in tumour cell nests, tumour stroma, and CSS, and OS (% survival at 10 years) in stage I-III CRC Scottish cohort (n=930)

Tumour cell nest					
	N (%)	**CSS (SE)**	**P**	**OS (SE)**	**P**
CD68+ (n=568)			**0.017**		0.181
Low	248 (44)	54 (4)		26 (3)	
High	320 (56)	68 (3)		31 (3)	
CD80+ (n=430)			**0.007**		0.077
Low	358 (83)	59 (3)		24 (3)	
High	72 (17)	78 (5)		35 (7)	
CD163+ (n=422)			0.080		0.121
Low	375 (89)	60 (3)		27 (3)	
High	47 (11)	77 (6)		39 (9)	
CD66b+ (n=410)			**0.004**		0.120
Low	315 (77)	71 (3)		30 (3)	
High	95 (23)	52 (7)		24 (6)	
Tumour stroma					
CD68+ (n=309)			**0.024**		**0.045**
Low	107 (35)	65 (3)		31 (3)	
High	202 (65)	57 (4)		25 (4)	
CD80+ (n=297)			**0.009**		0.118
Low	198 (67)	58 (3)		24 (3)	
High	99 (33)	74 (5)		33 (6)	
CD163+ (n=293)			**0.022**		0.404
Low	49 (17)	71 (8)		24 (7)	
High	244 (83)	60 (3)		30 (3)	
CD66b+ (n=278)			0.054		0.134
Low	236 (85)	69 (3)		30 (3)	
High	42 (15)	57 (7)		25 (6)	

CSS = Cancer-specific survival, OS = Overall survival, SE = Standard error

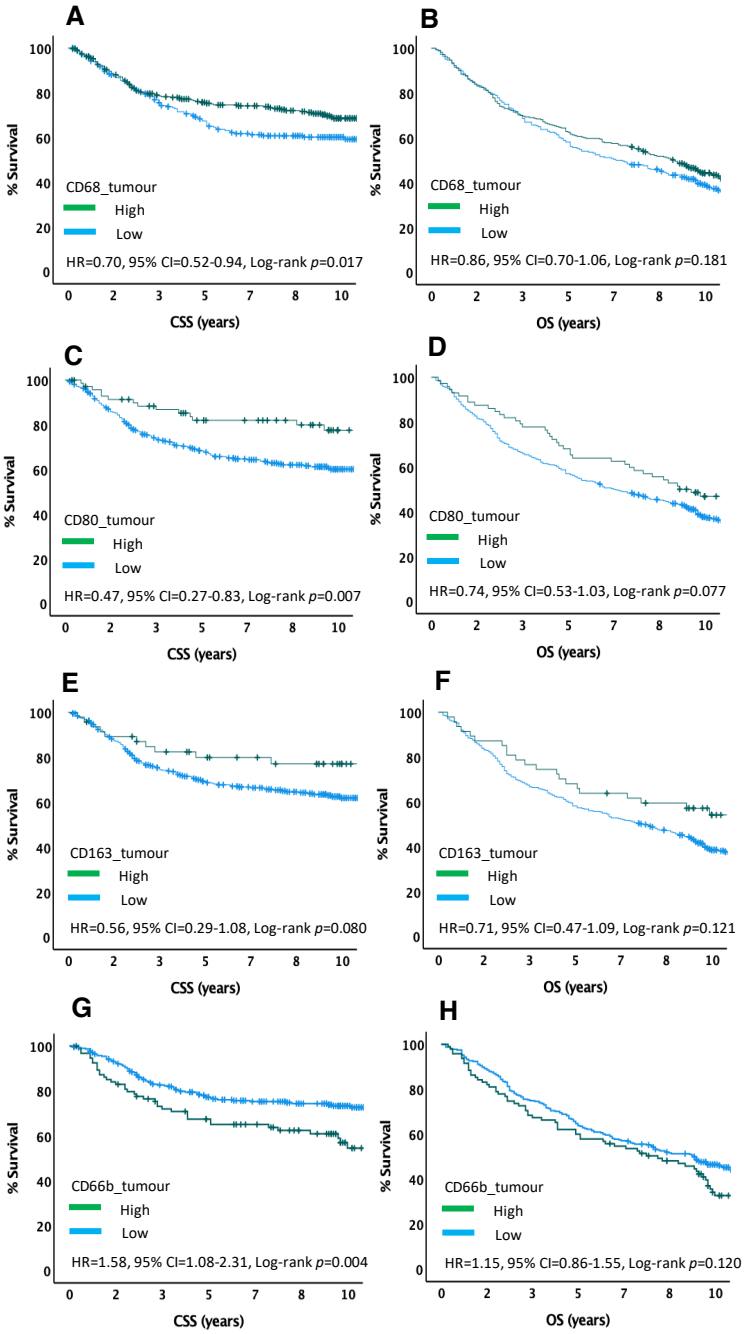

Figure 3.27 - KM plots of myeloid cells in tumour cell nests and CSS, OS in stage I-III CRC Scottish cohort (n=930); A. $CD68^+$ CSS (p=0.017), **B.** $CD68^+$ OS (p=0.181), **C.** $CD80^+$ CSS (p=0.007), **D.** $CD80^+$ OS (p=0.077), **E.** $CD163^+$ CSS (p=0.080), **F.** $CD163^+$ OS (p=0.121), **G.** $CD66b^+$ CSS (p=0.004), **H.** $CD66b^+$ OS (p=0.120)

3.10.2.2 Myeloid cells in tumour stroma and CSS, OS

In tumour stroma, high $CD68^+$ was significantly associated with decreased CSS (HR 1.39, 95% CI 1.04-1.86, p=0.024, **Figure 3.28, A**) with 10-year survival stratified from 57% (high) to 65% (low); and was associated with decreased OS (HR 1.23, 95% CI 1.00-1.52, p=0.045, **Figure 3.28, B**) with 10-year survival stratified from 25% (high) to 31% (low). High $CD80^+$ was significantly associated with improved CSS (HR 0.55, 95% CI 0.35-0.87, p=0.009, **Figure 3.28, C**) with 10-year survival stratified from 74% (high) to 58% (low). High $CD163^+$ was significantly associated with decreased CSS (HR 1.84, 95% CI 1.08-3.16, p=0.022, **Figure 3.28, E**) with 10-year survival stratified from 60% (high) to 71% (low) (**Table 3.3**). No associations were seen with $CD66b^+$ for any survival measure.

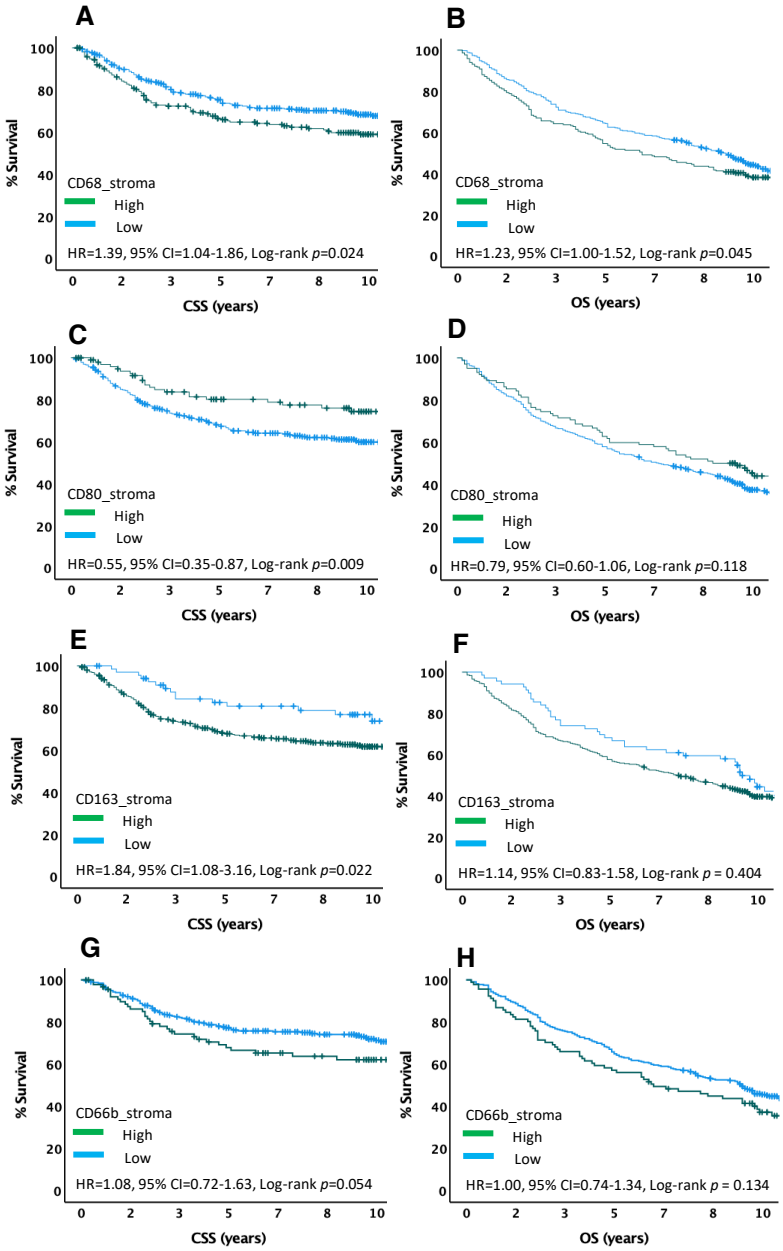

Figure 3.28 - KM plots of myeloid cells in tumour stroma and CSS, OS in stage I-III CRC Scottish cohort (n=930); A. $CD68^+$ CSS (p=0.024), **B.** $CD68^+$ OS (p=0.045), **C.** $CD80^+$ CSS (p=0.009), **D.** $CD80^+$ OS (p=0.118), **E.** $CD163^+$ CSS (p=0.022), **F.** $CD163^+$ OS (p=0.404), **G.** $CD66b^+$ CSS (p=0.054), **H.** $CD66b^+$ OS (p=0.134)

3.10.3 Association between T-lymphocytes infiltration and clinical, TME, and systemic characteristics

Next associations with clinicopathological factors were assessed for each marker focussing on factors relating to clinical, tumour microenvironment and systemic inflammatory features. Analysis was conducted using Chi-squared test.

3.10.3.1 T-lymphocytes in tumour cell nests

In tumour cell nests, the associations between T-lymphocytes and clinical factors were assessed. High $CD3^+$ associated with lower disease stage (p=0.019), low TSP (p=0.008), a strong KM grade (p=0.008), and an immune phenotypic subtypes (p=0.007). High $CD8^+$ was associated with right-sided colon (p=0.017), lower disease stage (p<0.001), poorer differentiation (p=0.014), no peritoneal involvement (p=0.021), deficient MMR status (p<0.001), high proliferation (p=0.001), low tumour budding (p=0.005), a strong KM grade (p<0.001), and an immune phenotypic subtype (p<0.001). Whereas the presence of $FoxP3^+$ associated with right-sided colon (p<0.001), poorer differentiation (p<0.001), deficient MMR status (p=0.004), high proliferation (p=0.002), low TSP (p=0.025), a strong KM grade (p=0.040), and immune or canonical phenotypic subtypes (p<0.001). There is no association with systemic characteristics (**Table 3.4**).

Table 3.4 - Association between T-lymphocytes in tumour cell nest and clinical, TME, and systemic characteristics in stage I-III CRC Scottish cohort (N=930)

	Tumour cell nests								
	CD3+			CD8+			FoxP3+		
	Low (n=398)	High (n=182)	*P*	Low (n=385)	High (n=175)	*P*	Absent (n=401)	Present (n=56)	*P*
Clinical Characteristics									
Age (n=580)			0.256			0.177			0.490
<65	121 (30)	47 (26)		118 (30)	44 (25)		112 (28)	13 (23)	
>65	277 (70)	135 (74)		273 (70)	134 (75)		295 (72)	43 (77)	
Sex (n=580)			0.648			0.399			0.877
Female	194 (49)	85 (47)		185 (47)	91 (51)		199 (49)	28 (50)	
Male	204 (51)	97 (53)		206 (53)	87 (49)		208 (51)	28 (50)	
Tumour site (n=576)			0.051			**0.017**			**<0.001**
Colon – Right	154 (39)	89 (49)		150 (38)	89 (50)		162 (40)	35 (63)	
Colon - Left	154 (39)	54 (30)		153 (39)	50 (28)		165 (41)	9 (16)	
Rectum	86 (22)	39 (21)		85 (22)	38 (22)		76 (19)	12 (21)	
Stage (n=580)			**0.019**			**<0.001**			0.050
I	54 (14)	42 (23)		52 (13)	43 (24)		64 (16)	16 (29)	
II	199 (50)	79 (43)		182 (47)	90 (51)		196 (48)	26 (46)	
III	145 (36)	61 (34)		157 (40)	45 (25)		147 (36)	14 (25)	
Differentiation (n=580)			0.061			**0.014**			**<0.001**
Mod/well	364 (92)	157 (86)		359 (92)	151 (85)		373 (92)	41 (73)	
Poor	34 (8)	25 (14)		32 (8)	27 (15)		34 (8)	15 (27)	
Vascular invasion (n=580)			0.384			0.074			0.545
Absent	270 (68)	130 (71)		261 (67)	132 (74)		282 (69)	41 (73)	
Present	128 (32)	52 (29)		130 (33)	46 (26)		125 (31)	15 (27)	
Peritoneal involvement (n=580)			0.637			**0.021**			0.111
No	290 (73)	136 (75)		274 (70)	141 (79)		295 (73)	46 (82)	
Yes	108 (27)	46 (25)		117 (30)	37 (21)		112 (27)	10 (18)	
Mismatch Repair Status (n=578)			0.630			**<0.001**			**0.004**
Competent	329 (83)	147 (81)		341 (87)	126 (71)		344 (85)	38 (68)	
Deficient	68 (17)	34 (19)		49 (13)	51 (29)		63 (15)	18 (32)	
Proliferation (n=579)			0.063			**0.001**			**0.002**
Low	156 (39)	57 (31)		164 (42)	49 (28)		155 (38)	10 (18)	
High	241 (61)	125 (69)		227 (58)	129 (72)		252 (62)	46 (82)	
Tumour Necrosis (n=567)			0.113			0.231			0.336
Low	252 (65)	102 (58)		235 (61)	115 (67)		250 (63)	38 (69)	
High	138 (35)	75 (42)		149 (39)	58 (33)		150 (37)	17 (31)	
Tumour Microenvironment Characteristics									
Tumour budding (n=536)			0.168			**0.005**			0.205
Low	271 (74)	134 (79)		260 (72)	136 (83)		280 (75)	42 (84)	
High	96 (26)	35 (21)		102 (28)	28 (17)		96 (25)	9 (16)	
Tumour stroma percentage (n=579)			**0.008**			0.354			**0.025**
Low	290 (73)	151 (83)		296 (76)	141 (79)		304 (75)	49 (88)	
High	107 (27)	31 (17)		95 (24)	37 (21)		103 (25)	7 (12)	
Klintrup-Makinen grade (n=567)			**0.008**			**<0.001**			**0.040**
Weak	280 (72)	107 (60)		290 (76)	91 (53)		275 (69)	30 (55)	
Strong	110 (28)	70 (40)		94 (24)	82 (47)		125 (31)	25 (45)	
Phenotypic subtypes (n=570)			**0.007**			**<0.001**			**<0.001**
Immune	110 (28)	72 (40)		94 (24)	84 (48)		126 (31)	25 (45)	
Canonical	134 (34)	59 (33)		137 (36)	53 (30)		128 (32)	26 (46)	
Latent	69 (18)	30 (17)		82 (21)	18 (10)		72 (18)	4 (7)	
Stromal	77 (20)	19 (10)		72 (19)	20 (12)		75 (19)	1 (2)	
Systemic Characteristics									
Serum CRP (n=425)			0.665			0.941			0.633
Normal	162 (56)	74 (54)		160 (55)	68 (54)		165 (57)	21 (53)	
High	126 (44)	63 (46)		132 (45)	57 (46)		127 (43)	19 (47)	
Serum Albumin (n=467)			0.548			0.819			0.638
Normal	242 (76)	116 (78)		240 (77)	109 (76)		242 (76)	34 (79)	
Low	77 (24)	32 (22)		73 (23)	35 (24)		77 (24)	9 (21)	
mGPS (n=429)			0.847			0.438			0.869
0	163 (56)	76 (54)		163 (55)	68 (53)		167 (57)	21 (53)	
1	69 (24)	37 (26)		77 (26)	29 (23)		71 (24)	11 (27)	
2	57 (20)	27 (20)		54 (18)	30 (24)		57 (19)	8 (20)	

3.10.3.2 T-lymphocytes in tumour stroma

In stroma, the association between stromal T-lymphocytes and clinical characteristics were assessed. High $CD3^+$ was associated with strong KM grade ($p<0.001$), and an immune subtype ($p=0.001$). High $CD8^+$ was associated with no peritoneal involvement ($p=0.004$), deficient mismatch repair status ($p=0.018$), strong KM grade ($p<0.001$), immune subtype ($p<0.001$), low serum albumin ($p=0.002$), and high mGPS ($p=0.006$). Whereas the presence of $FoxP3^+$ was associated with lower disease stage ($p=0.046$), moderate/well differentiation ($p=0.016$), absent vascular invasion ($p=0.048$), no peritoneal involvement ($p=0.002$), low tumour budding ($p=0.018$), a strong KM grade ($p=0.001$), an immune subtype ($p=0.012$), normal serum CRP ($p=0.025$), normal serum albumin ($p=0.030$), and a low mGPS ($p=0.037$) (**Table 3.5**).

Table 3.5 - Associations between T-lymphocytes in tumour stroma and clinical, TME, and systemic characteristics in stage I-III CRC Scottish cohort (n=930)

	Tumour stroma								
	CD3+			CD8+			FoxP3+		
	Low (n=482)	High (n=100)	*P*	Low (n=317)	High (n=252)	*P*	Absent (n=357)	Present (n=106)	*P*
Clinical Characteristics									
Age (n=582)			0.323			0.744			0.185
<65	144 (30)	25 (25)		92 (29)	70 (28)		91 (26)	34 (32)	
>65	338 (70)	75 (75)		225 (71)	182 (72)		266 (74)	72 (68)	
Sex (n=582)			0.845			0.897			0.503
Female	231 (48)	49 (49)		153 (48)	123 (49)		172 (48)	55 (52)	
Male	251 (52)	51 (51)		164 (52)	129 (51)		185 (52)	51 (48)	
Tumour site (n=578)			0.769			0.698			0.523
Colon – Right	199 (42)	45 (46)		128 (41)	111 (44)		154 (43)	43 (41)	
Colon - Left	174 (36)	34 (34)		115 (37)	88 (35)		137 (39)	37 (36)	
Rectum	106 (22)	20 (20)		71 (23)	52 (21)		64 (18)	24 (23)	
Stage (n=582)			0.170			0.588			**0.046**
I	74 (15)	22 (22)		50 (16)	45 (18)		54 (15)	26 (25)	
II	231 (48)	49 (49)		149 (47)	123 (49)		171 (48)	51 (48)	
III	177 (37)	29 (36)		118 (37)	84 (33)		132 (37)	29 (27)	
Differentiation (n=582)			0.675			0.754			**0.016**
Mod/well	432 (90)	91 (91)		283 (89)	227 (90)		313 (88)	101 (95)	
Poor	50 (10)	9 (9)		34 (11)	25 (10)		44 (12)	5 (5)	
Vascular invasion (n=582)			0.645			0.277			**0.048**
Absent	331 (69)	71 (71)		213 (67)	180 (71)		241 (68)	82 (77)	
Present	151 (31)	29 (29)		104 (33)	72 (29)		116 (32)	24 (23)	
Peritoneal involvement (n=582)			0.153			**0.004**			**0.002**
No	348 (72)	79 (79)		216 (68)	199 (79)		251 (70)	90 (85)	
Yes	134 (28)	21 (21)		101 (32)	53 (21)		106 (30)	16 (15)	
Mismatch Repair Status (n=580)			0.333			**0.018**			0.095
Competent	399 (83)	79 (79)		271 (86)	196 (78)		289 (81)	93 (88)	
Deficient	81 (17)	21 (21)		45 (14)	55 (22)		68 (19)	13 (12)	
Proliferation (n=581)			0.675			0.954			0.069
Low	179 (37)	35 (35)		119 (38)	94 (37)		135 (38)	30 (28)	
High	302 (63)	65 (65)		198 (62)	158 (63)		222 (62)	76 (72)	
Tumour Necrosis (n=569)			0.258			0.831			0.781
Low	298 (63)	56 (57)		196 (63)	154 (62)		224 (64)	64 (62)	
High	173 (37)	42 (43)		114 (37)	93 (38)		128 (36)	39 (38)	
Tumour Microenvironment Characteristics									
Tumour budding (n=538)			0.559			0.278			**0.018**
Low	336 (75)	71 (78)		213 (73)	183 (78)		238 (73)	84 (84)	
High	111 (25)	20 (22)		77 (27)	53 (22)		89 (27)	16 (16)	
Tumour stroma percentage (n=581)			0.280			0.488			0.568
Low	371 (77)	72 (72)		240 (76)	197 (78)		270 (76)	83 (78)	
High	110 (23)	28 (28)		77 (24)	55 (22)		87 (24)	23 (22)	
Klintrup-Makinen grade (n=569)			**<0.001**			**<0.001**			**0.001**
Weak	337 (72)	50 (51)		238 (77)	143 (58)		250 (71)	55 (53)	
Strong	134 (28)	48 (49)		72 (23)	104 (42)		102 (29)	48 (47)	
Phenotypic subtypes (n=572)			**0.001**			**<0.001**			**0.012**
Immune	135 (29)	49 (49)		73 (23)	105 (42)		103 (29)	48 (47)	
Canonical	172 (36)	21 (21)		119 (38)	71 (29)		127 (36)	27 (26)	
Latent	84 (18)	15 (15)		59 (19)	41 (17)		61 (17)	15 (15)	
Stromal	82 (17)	14 (14)		61 (20)	31 (12)		63 (18)	13 (12)	
Systemic Characteristics									
Serum CRP (n=427)			0.559			0.282			**0.025**
Normal	199 (56)	37 (52)		135 (57)	93 (52)		135 (53)	51 (67)	
High	157 (44)	34 (48)		102 (43)	87 (48)		121 (47)	25 (33)	
Serum Albumin (n=469)			0.561			**0.002**			**0.030**
Normal	295 (76)	64 (79)		211 (82)	138 (69)		204 (74)	72 (85)	
Low	93 (24)	17 (21)		47 (18)	61 (31)		73 (26)	13 (15)	
mGPS (n=431)			0.695			**0.006**			**0.037**
0	201 (56)	38 (52)		135 (57)	96 (53)		137 (53)	51 (66)	
1	86 (24)	21 (29)		68 (29)	38 (20)		64 (25)	18 (23)	
2	71 (20)	14 (19)		35 (14)	49 (27)		57 (22)	8 (11)	

3.10.4 Association between myeloid cells infiltration and clinical, TME, and systemic characteristics

3.10.4.1 Myeloid cells in tumour cell nests

In tumour cell nests, the associations between innate immune cells and clinical characteristics were assessed. High $CD68^+$ was associated with deficient mismatch repair status ($p<0.001$), high proliferation ($p<0.001$), and low tumour budding ($p=0.006$). High $CD80^+$ was associated with stage II disease ($p=0.017$), and high proliferation ($p=0.048$). High $CD163^+$ was associated with poor differentiation ($p=0.010$), no peritoneal involvement ($p=0.030$), high proliferation ($p=0.009$), low tumour budding ($p=0.045$), and an immune or canonical phenotypic subtype ($p=0.006$). High $CD66b^+$ was associated with poor differentiation ($p=0.010$), vascular invasion ($p=0.009$), low proliferation ($p=0.017$), and normal serum albumin ($p=0.032$) (**Table 3.6**).

Table 3.6 - Association between myeloid cells in tumour cell nest and clinical, TME, and systemic characteristics in stage I-III CRC Scottish cohort (n=930)

	Tumour cell nests											
	CD68+			CD80+			CD163+			CD66b+		
	Low (n=248)	High (n=320)	*P*	Low (n=358)	High (n=72)	*P*	Low (n=375)	High (n=47)	*P*	Low (n=315)	High (n=95)	*P*
Clinical Characteristics												
Age (n=410)			0.611			0.757			0.341			0.038
<65	88 (36)	107 (33)		111 (31)	21 (29)		121 (32)	12 (26)		90 (29)	38 (40)	
>65	160 (64)	213 (67)		247 (69)	51 (71)		254 (68)	35 (74)		225 (71)	57 (60)	
Sex (n=410)			0.371			0.860			0.399			0.810
Female	110 (44)	154 (48)		165 (46)	34 (47)		175 (47)	25 (53)		147 (47)	43 (45)	
Male	138 (56)	166 (52)		193 (54)	38 (53)		200 (53)	22 (47)		168 (53)	52 (55)	
Tumour site (n=408)			0.088			0.293			0.053			0.075
Colon – Right	89 (36)	142 (45)		137 (38)	29 (40)		138 (37)	26 (56)		115 (37)	47 (49)	
Colon - Left	86 (35)	89 (28)		109 (31)	27 (38)		124 (33)	10 (21)		111 (36)	29 (31)	
Rectum	72 (29)	86 (27)		109 (31)	16 (22)		110 (30)	11 (23)		87 (27)	19 (20)	
Stage (n=410)			0.273			**0.017**			0.418			0.162
I	29 (12)	42 (13)		45 (13)	9 (13)		44 (12)	8 (17)		47 (15)	10 (11)	
II	111 (45)	160 (50)		158 (44)	44 (61)		177 (47)	18 (38)		155 (49)	41 (43)	
III	108 (44)	118 (37)		155 (43)	19 (26)		154 (41)	21 (45)		113 (36)	44 (46)	
Differentiation (n=410)			0.052			0.272			**0.010**			**0.010**
Mod/well	228 (92)	278 (87)		320 (89)	61 (85)		339 (90)	36 (77)		287 (91)	77 (81)	
Poor	20 (8)	42 (13)		38 (11)	11 (15)		36 (10)	11 (23)		28 (9)	18 (19)	
Vascular invasion (n=410)			0.114			0.992			0.713			**0.009**
Absent	170 (69)	199 (62)		219 (61)	44 (61)		229 (61)	30 (64)		219 (70)	52 (55)	
Present	78 (31)	121 (38)		139 (39)	28 (39)		146 (39)	17 (36)		96 (30)	43 (45)	
Peritoneal involvement (n=410)			0.168			0.215			**0.030**			0.268
No	169 (68)	235 (73)		260 (73)	47 (65)		266 (71)	40 (85)		237 (75)	66 (70)	
Yes	79 (32)	85 (27)		98 (27)	25 (35)		109 (29)	7 (15)		78 (25)	29 (30)	
Mismatch Repair Status (n=402)			**<0.001**			0.299			0.659			0.171
Competent	211 (90)	244 (78)		283 (82)	55 (76)		301 (83)	36 (80)		256 (83)	70 (76)	
Deficient	24 (10)	70 (22)		63 (18)	17 (24)		63 (17)	9 (20)		54 (17)	22 (24)	
Proliferation (n=405)			**<0.001**			**0.048**			**0.009**			**0.017**
Low	162 (66)	160 (51)		197 (56)	31 (43)		212 (57)	17 (37)		144 (46)	56 (60)	
High	82 (34)	156 (49)		156 (44)	41 (57)		159 (43)	29 (63)		168 (54)	37 (40)	
Tumour Necrosis (n=402)			0.553			0.114			0.899			0.808
Low	156 (63)	190 (61)		218 (62)	51 (72)		239 (65)	30 (64)		197 (64)	58 (62)	
High	91 (37)	123 (39)		133 (38)	20 (28)		130 (35)	17 (36)		112 (36)	35 (38)	
Tumour Microenvironment Characteristics												
Tumour budding (n=382)			**0.006**			0.140			**0.045**			0.086
Low	146 (63)	220 (74)		229 (69)	52 (78)		242 (69)	35 (83)		216 (74)	59 (65)	
High	85 (37)	76 (26)		104 (31)	15 (22)		108 (31)	7 (17)		75 (26)	32 (35)	
Tumour stroma percentage (n=397)			0.240			0.582			0.228			0.238
Low	163 (69)	226 (73)		245 (70)	53 (74)		258 (71)	37 (78)		231 (75)	63 (72)	
High	74 (31)	82 (27)		103 (30)	19 (26)		108 (29)	10 (22)		75 (25)	28 (28)	
Klintrup-Makinen grade (n=402)			0.112			0.286			0.154			0.434
Weak	177 (71)	205 (65)		246 (70)	45 (63)		259 (70)	28 (60)		216 (70)	61 (66)	
Strong	71 (29)	110 (35)		106 (30)	26 (37)		19 (40)	19 (40)		93 (30)	32 (34)	
Phenotypic subtypes (n=392)			0.057			0.139			**0.006**			0.614
Immune	71 (30)	110 (36)		106 (31)	26 (37)		111 (31)	19 (40)		93 (31)	33 (37)	
Canonical	45 (19)	76 (25)		78 (22)	22 (31)		78 (21)	17 (36)		90 (30)	21 (24)	
Latent	64 (27)	66 (21)		86 (25)	11 (15)		95 (26)	4 (9)		63 (21)	18 (20)	
Stromal	57 (24)	55 (18)		76 (22)	12 (17)		80 (22)	7 (15)		57 (19)	17 (19)	
Systemic Characteristics												
Serum CRP (n=329)			0.337			0.733			0.725			0.476
Normal	126 (58)	134 (53)		154 (56)	28 (54)		162 (56)	20 (59)		129 (53)	48 (57)	
High	92 (42)	117 (47)		119 (44)	24 (46)		129 (44)	14 (41)		116 (47)	36 (43)	
Serum Albumin (n=350)			0.993			0.053			0.114			**0.032**
Normal	179 (80)	212 (80)		236 (82)	41 (71)		250 (82)	27 (71)		203 (77)	75 (87)	
Low	44 (20)	52 (20)		51 (18)	17 (29)		54 (18)	11 (29)		61 (23)	11 (13)	
mGPS (n=332)			0.643			0.350			0.224			0.165
0	127 (58)	135 (54)		156 (57)	28 (54)		164 (56)	20 (59)		130 (52)	44 (57)	
1	60 (27)	74 (30)		77 (28)	12 (23)		85 (29)	6 (18)		70 (28)	27 (32)	
2	32 (15)	42 (16)		41 (15)	12 (23)		43 (15)	8 (23)		48 (19)	9 (11)	

3.10.4.2 Myeloid cells in tumour stroma

In tumour stroma, the association between stromal innate immune cells and clinical characteristics were assessed. High $CD68^+$ was associated with lower age (p=0.001), lower disease stage (p=0.031), high proliferation (p<0.001), low tumour necrosis (p=0.034), low serum albumin (p=0.001), and a high mGPS (p<0.001). High $CD80^+$ was associated with lower disease stage (p=0.015). High $CD163^+$ was associated with low serum albumin (p=0.002), and a high mGPS (p=0.003). High $CD66b^+$ was associated with low proliferation (p=0.001), high tumour budding (p<0.001), high tumour stroma percentage (p=0.013), a strong KM grade (p=0.027), and an immune or stromal subtype (p=0.003) (**Table 3.7**).

Table 3.7 - Association between myeloid cells in tumour stroma and clinical, TME, and systemic characteristics in stage I-III CRC Scottish cohort (n=930)

	Tumour stroma											
		CD68+			CD80+			CD163+			CD66b+	
	Low (n=350)	High (n=218)	*P*	Low (n=327)	High (n=102)	*P*	Low (n=69)	High (n=246)	*P*	Low (n=319)	High (n=91)	*P*
Clinical Characteristics												
Age (n=410)			**0.001**			0.649			0.234			0.156
<65	138 (39)	57 (26)		98 (30)	33 (32)		26 (38)	107 (30)		94 (30)	34 (37)	
>65	212 (61)	161 (74)		229 (70)	69 (68)		43 (62)	246 (70)		225 (70)	57 (63)	
Sex (n=410)			0.149			0.662			0.853			0.925
Female	171 (49)	93 (43)		149 (46)	49 (48)		32 (46)	168 (48)		149 (47)	42 (46)	
Male	179 (51)	125 (57)		178 (54)	53 (52)		37 (54)	185 (52)		170 (53)	49 (54)	
Tumour site (n=408)			0.275			0.120			0.299			0.461
Colon – Right	139 (40)	92 (43)		127 (39)	39 (38)		28 (41)	136 (39)		125 (39)	37 (40)	
Colon - Left	104 (30)	71 (3)		96 (30)	40 (39)		26 (38)	108 (31)		114 (36)	27 (30)	
Rectum	106 (30)	52 (24)		101 (31)	23 (23)		15 (22)	106 (30)		78 (25)	27 (30)	
Stage (n=410)			**0.031**			**0.015**			0.112			0.128
I	34 (10)	37 (17)		34 (10)	20 (20)		4 (6)	48 (13)		45 (14)	12 (13)	
II	168 (48)	103 (47)		151 (46)	51 (50)		37 (54)	158 (45)		160 (50)	36 (40)	
III	148 (42)	78 (36)		142 (43)	31 (30)		28 (41)	147 (42)		114 (36)	43 (47)	
Differentiation (n=410)			0.955			0.816			0.896			0.937
Mod/well	312 (89)	194 (89)		289 (88)	91 (89)		61 (88)	314 (89)		283 (89)	81 (89)	
Poor	38 (11)	24 (11)		38 (12)	11 (11)		8 (12)	39 (11)		36 (11)	10 (11)	
Vascular invasion (n=410)			0.248			0.181			0.243			0.181
Absent	221 (63)	148 (68)		194 (59)	68 (67)		38 (55)	221 (55)		217 (68)	55 (60)	
Present	129 (37)	70 (32)		133 (41)	34 (33)		31 (45)	132 (37)		102 (32)	36 (40)	
Peritoneal involvement			0.696			0.850			0.762			0.793
(n=410)	251 (72)	153 (70)		234 (72)	72 (71)		49 (71)	257 (73)		234 (73)	68 (75)	
No	99 (28)	65 (30)		93 (28)	30 (29)		20 (29)	96 (27)		85 (27)	23 (25)	
Yes												
Mismatch Repair Status			0.247			0.478			0.522			0.348
(n=402)	281 (84)	174 (81)		258 (82)	80 (78)		57 (85)	280 (82)		250 (80)	76 (84)	
Competent	52 (16)	42 (19)		58 (18)	22 (22)		10 (15)	62 (28)		62 (20)	14 (16)	
Deficient												
Proliferation (n=405)			**<0.001**			0.193			0.074			**0.001**
Low	221 (64)	101 (47)		179 (55)	49 (48)		44 (65)	185 (53)		141 (45)	59 (65)	
High	123 (36)	115 (53)		144 (45)	53 (52)		24 (35)	164 (47)		173 (55)	32 (35)	
Tumour Necrosis (n=402)			**0.034**			0.590			0.473			0.809
Low	202 (58)	144 (67)		203 (63)	66 (66)		42 (61)	227 (65)		199 (63)	57 (65)	
High	144 (42)	70 (33)		119 (37)	34 (34)		27 (39)	120 (35)		115 (37)	31 (35)	
Tumour Microenvironment Characteristics												
Tumour budding (n=382)			0.400			0.129			0.105			**<0.001**
Low	220 (68)	146 (72)		207 (68)	74 (76)		49 (79)	228 (69)		226 (77)	50 (57)	
High	103 (32)	58 (28)		96 (32)	23 (24)		13 (21)	102 (31)		68 (23)	38 (43)	
Tumour stroma percentage			0.539			0.682			0.734			**0.013**
(n=396)	238 (72)	151 (70)		224 (70)	74 (73)		49 (73)	246 (71)		240 (77)	53 (63)	
Low	91 (27)	65 (30)		94 (30)	28 (27)		18 (27)	100 (29)		72 (23)	31 (37)	
High												
Klintrup-Makinen grade			0.602			0.157			0.666			**0.027**
(n=402)	234 (67)	148 (69)		228 (71)	63 (63)		49 (71)	238 (68)		225 (72)	52 (59)	
Weak	115 (33)	66 (31)		95 (29)	37 (37)		20 (29)	110 (32)		89 (28)	36 (41)	
Strong												
Phenotypic subtypes (n=391)			0.057			0.635			0.080			**0.002**
Immune	115 (35)	66 (31)		95 (30)	37 (36)		20 (29)	110 (32)		89 (29)	37 (44)	
Canonical	62 (19)	59 (27)		76 (24)	24 (24)		10 (15)	85 (25)		99 (32)	12 (14)	
Latent	87 (26)	43 (20)		76 (24)	21 (21)		24 (35)	75 (22)		65 (21)	15 (18)	
Stromal	65 (20)	47 (22)		69 (22)	19 (19)		14 (21)	73 (21)		54 (18)	20 (24)	
Systemic Characteristics												
Serum CRP (n=329)			0.571			0.392			0.263			0.992
Normal	174 (55)	86 (57)		151 (57)	30 (51)		31 (63)	151 (55)		135 (54)	42 (54)	
High	145 (45)	64 (43)		114 (43)	29 (49)		18 (37)	125 (45)		116 (46)	36 (46)	
Serum Albumin (n=350)			**0.001**			0.560			**0.002**			0.303
Normal	277 (85)	114 (72)		223 (80)	53 (83)		51 (94)	226 (79)		217 (81)	61 (75)	
Low	51 (15)	45 (28)		57 (20)	11 (17)		3 (6)	62 (21)		52 (19)	20 (25)	
mGPS (n=332)			**<0.001**			0.608			**0.003**			0.439
0	176 (55)	86 (57)		153 (58)	30 (51)		32 (64)	152 (55)		136 (54)	42 (53)	
1	107 (33)	27 (18)		70 (26)	19 (32)		17 (34)	74 (27)		77 (30)	20 (25)	
2	37 (12)	37 (15)		43 (16)	10 (17)		1 (2)	50 (18)		40 (16)	17 (22)	

3.10.5 Immune cells landscapes (CD3/CD68/CD66b) and patient survival

As myeloid cells have been reported having pro-tumorigenic and anti-tumorigenic effect, to elucidate the influences of myeloid cells and T-lymphocytes in CRC patients. T-lymphocytes marker ($CD3^+$) and myeloid cell markers ($CD68^+$, $CD66b^+$) were combined and divided into four categories 1) both low, 2) myeloid high, 3) T-cell high, and 4) both high, and analysed as grouping in tumour cells called tumour immune landscape and in stroma called stromal immune landscape (**Table 3.8**). When assessing effects on patient's survival, the tumour immune landscape did not significantly associate with patient's survival. Whereas, the stromal immune landscape was significantly associated with improved CSS, (HR 0.81, CI 0.64-1.03, p=0.005, **Figure 3.29, B**) with 10-year survival stratified from 44% (T-cell high), 27% (myeloid high), 26% (both high and both low).

Table 3.8 - Relationship between tumour and stromal immune landscapes and CSS, and OS (% survival at 10 years) in stage I-III CRC Scottish cohort (n=257)

Immune landscapes (CD3/CD68/CD66b)					
	N (%)	**CSS (SE)**	**P**	**OS (SE)**	**P**
Tumour immune landscape (n=246)			0.067		0.939
Both low	31 (13)	74 (9)		21 (9)	
Myeloid high	131 (53)	58 (5)		27 (5)	
T-cell high	8 (3)	58 (19)		38 (17)	
Both high	76 (31)	79 (5)		29 (6)	
Stromal immune landscape (n=257)			**0.005**		0.311
Both low	35 (14)	72 (9)		26 (9)	
Myeloid high	167 (65)	56 (4)		27 (4)	
T-cell high	10 (4)	85 (14)		44 (21)	
Both high	45 (17)	81 (7)		26 (8)	

CSS = Cancer-specific survival, OS = Overall survival, SE = Standard error

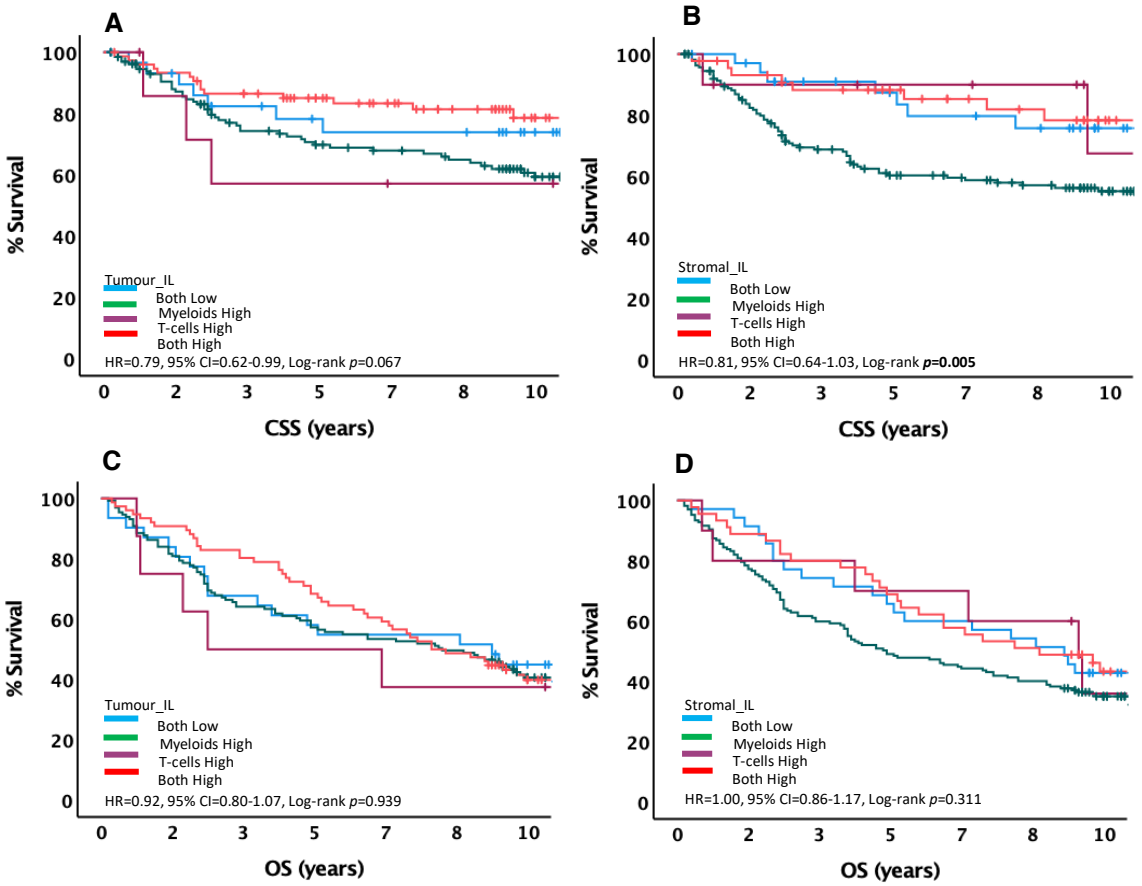

Figure 3.29 - KM plots of tumour and stromal immune landscapes and CSS, OS in stage I-III CRC Scottish cohort; **A.** Tumour_IL CSS (p=0.067), **B.** Stromal_IL CSS (p=0.005), **C.** Tumour_IL OS (p=0.939), **D.** Stromal_IL OS (p=0.311)

3.10.6 Association between immune landscapes and clinical, TME, and systemic characteristics

For tumour immune landscape, the myeloid high group associated with lower age (p=0.031), and an increased mGPS (p=0.040). However, the both high group associated with low tumour stroma percentage (p=0.002). Whereas for the stromal immune landscape, the myeloid high group associated with weak KM grade (p=0.035), however, the both high group associated with an immune phenotypic subtype (p=0.046) (**Table 3.9.**).

Table 3.9 - Association between immune landscapes and clinical, TME, and systemic characteristics in stage I-III CRC Scottish cohort (n=930)

	Tumour immune landscape					Stromal immune landscape				
	Both low (n=31)	**Myeloid high (n=131)**	**T-cell high (n=8)**	**Both high (n=76)**	***P***	**Both low (n=35)**	**Myeloid high (n=164)**	**T-cell high (n=10)**	**Both high (n=45)**	***P***
Clinical Characteristics										
Age (n=246)					**0.031**					0.637
<65	7 (23)	48 (37)	1 (13)	15 (20)		12 (34)	45 (27)	2 (20)	10 (22)	
>65	24 (77)	83 (63)	7 (87)	61 (80)		23 (66)	122 (73)	8 (80)	35 (78)	
Sex (n=246)					0.809					0.396
Female	13 (42)	65 (50)	3 (38)	37 (49)		20 (57)	74 (44)	6 (60)	19 (42)	
Male	18 (58)	66 (50)	5 (62)	39 (51)		15 (43)	93 (56)	4 (40)	26 (58)	
Tumour site (n=243)					0.567					0.178
Colon – Right	9 (29)	61 (48)	4 (50)	36 (47)		16 (46)	70 (42)	6 (60)	17 (38)	
Colon - Left	13 (42)	41 (32)	2 (25)	21 (28)		8 (23)	59 (36)	4 (40)	15 (33)	
Rectum	9 (29)	26 (20)	2 (25)	19 (25)		11 (31)	36 (22)	0 (0)	13 (29)	
Stage (n=246)					0.318					0.091
I	5 (16)	15 (12)	2 (25)	19 (25)		4 (11)	25 (15)	1 (10)	12 (27)	
II	16 (52)	66 (50)	4 (50)	32 (42)		19 (54)	77 (46)	8 (80)	15 (33)	
III	10 (32)	50 (38)	2 (25)	25 (33)		12 (35)	65 (39)	1 (10)	18 (40)	
Differentiation (n=246)					0.856					0.767
Mod/well	29 (94)	116 (89)	7 (88)	68 (90)		29 (83)	149 (89)	9 (90)	39 (87)	
Poor	2 (6)	15 (11)	1 (12)	8 (10)		6 (17)	18 (11)	1 (10)	6 (13)	
Vascular invasion (n=246)					0.616					0.769
Absent	19 (61)	82 (63)	5 (63)	54 (71)		21 (60)	114 (68)	6 (60)	29 (64)	
Present	12 (39)	49 (37)	3 (37)	22 (29)		14 (40)	53 (32)	4 (40)	16 (36)	
Peritoneal involvement (n=246)					0.430					0.077
No	23 (74)	95 (72)	4 (50)	59 (78)		28 (80)	111 (67)	5 (50)	36 (80)	
Yes	8 (26)	36 (28)	4 (50)	17 (22)		7 (20)	56 (33)	5 (50)	9 (20)	
Mismatch Repair Status (n=246)					0.223					0.577
Competent	28 (90)	99 (76)	7 (88)	62 (82)		28 (80)	141 (84)	8 (80)	34 (76)	
Deficient	3 (10)	32 (24)	1 (12)	14 (18)		7 (20)	26 (16)	2 (20)	11 (24)	
Proliferation (n=246)					0.459					0.153
Low	14 (45)	59 (45)	3 (38)	26 (34)		10 (29)	80 (48)	4 (40)	17 (38)	
High	17 (55)	72 (55)	5 (62)	50 (66)		25 (71)	87 (52)	6 (60)	28 (62)	
Tumour Necrosis (n=241)					0.151					0.382
Low	17 (55)	87 (67)	7 (88)	42 (58)		19 (54)	112 (69)	6 (60)	27 (61)	
High	14 (45)	42 (33)	1 (12)	31 (42)		16 (46)	51 (31)	4 (30)	17 (39)	
Tumour Microenvironment Characteristics										
Tumour budding (n=230)					0.097					0.142
Low	21 (72)	88 (71)	5 (62)	59 (86)		27 (82)	106 (67)	6 (67)	34 (81)	
High	8 (28)	36 (29)	3 (28)	10 (14)		6 (18)	52 (33)	3 (33)	8 (19)	
Tumour stroma percentage (n=246)					**0.002**					0.735
Low	20 (65)	84 (64)	5 (62)	66 (87)		26 (74)	116 (70)	6 (60)	29 (64)	
High	11 (35)	47 (36)	3 (38)	10 (13)		9 (26)	51 (30)	4 (40)	16 (36)	
Klintrup-Makinen grade (n=241)					0.150					**0.035**
Weak	23 (74)	97 (75)	5 (63)	44 (60)		26 (74)	122 (75)	5 (50)	24 (55)	
Strong	8 (26)	32 (25)	3 (37)	29 (40)		9 (26)	41 (25)	5 (50)	20 (45)	
Phenotypic subtypes (n=243)					0.083					**0.046**
Immune	8 (26)	32 (25)	3 3 (38)	30 (40)		9 (25)	41 (25)	5 (50)	21 (47)	
Canonical	10 (32)	37 (29)	2 2 (25)	23 (31)		16 (46)	47 (29)	1 (10)	12 (27)	
Latent	4 (13)	27 (21)	1 1 (12)	16 (21)		3 (9)	36 (22)	2 (20)	5 (11)	
Stromal	9 (29)	33 (25)	2 2 (25)	6 (8)		7 (20)	40 (24)	2 (20)	7 (16)	
Systemic Characteristics										
Serum CRP (n=161)					0.264					0.526
Normal	11 (69)	45 (53)	2 (29)	32 (60)		12 (63)	62 (54)	3 (33)	15 (56)	
High	5 (31)	40 (47)	5 (71)	21 (40)		7 (37)	52 (46)	6 (67)	12 (44)	
Serum Albumin (n=178)					0.081					0.299
Normal	16 (80)	68 (72)	3 (43)	47 (84)		20 (87)	82 (70)	8 (80)	24 (75)	
Low	4 (20)	27 (28)	4 (57)	9 (16)		3 (13)	36 (30)	2 (20)	8 (25)	
mGPS (n=162)					**0.040**					0.444
0	12 (71)	46 (54)	2 (29)	32 (60)		13 (65)	62 (55)	3 (33)	15 (54)	
1	4 (23)	16 (19)	1 (14)	15 (28)		5 (25)	22 (19)	4 (44)	7 (25)	
2	1 (6)	23 (27)	4 (27)	6 (12)		2 (10)	30 (26)	2 (23)	6 (21)	

3.10.7 Multivariate analysis

As CSS had the most significant impact on patient's survival, multivariate analysis was performed for CSS to evaluate the relationship between t-lymphocyte markers, myeloid cell markers, clinical characteristics, and tumour microenvironment characteristics. For CSS, tumour stage (HR 2.84, CI 1.24-6.48, p=0.013), peritoneal involvement (HR 4.17, CI 1.58-11.02, p=0.004), tumour budding (HR 6.35, CI 2.29-17.57, p<0.001), tumour stroma percentage (HR 0.04, CI 0.005-0.42, p=0.007), KM grade (HR 32.52, CI 1.57-672.47, p=0.024), phenotypic subtypes (HR 9.65, CI 2.25-41.36, p=0.002), $CD3^+$ tumour (HR 0.23, CI 0.06-0.93, p=0.039), and $CD163^+$ stroma (HR 13.47, CI 2.68-67.56, p=0.002) were independent prognostic factors (**Table 3.10**).

Table 3.10 - Univariate and multivariate analysis of immune cells, clinicopathological and inflammatory characteristics, and CSS in stage I-III CRC Scottish cohort (n=279)

	Univariate HR (95% CI)	*P*	Multivariate HR (95% CI)	*P*
Clinical characteristics				
Age (<65/>65) (n=279)	1.04 (0.81-1.34)	0.714	-	-
Sex (female/male)	1.15 (0.90-1.45)	0.243	-	-
Tumour site (left/right/rectum)	1.02 (0.88-1.18)	0.770	-	-
Stage (1/2/3)	2.43 (1.98-2.97)	**<0.001**	2.84 (1.24-6.48)	**0.013**
Differentiation (low grade/high grade)	1.97 (1.41-2.73)	**<0.001**	0.48 (0.07-3.17)	0.453
Vascular Invasion (absent/present)	2.07 (1.63-2.62)	**<0.001**	2.55 (0.77-8.35)	0.122
Peritoneal Involvement (no/yes)	2.59 (2.04-3.28)	**<0.001**	4.17 (1.58-11.02)	**0.004**
Mismatch repair status (Competent/Deficient)	0.77 (0.55-1.09)	0.148	-	-
Proliferation index (low/high)	0.64 (0.50-0.81)	**<0.001**	0.94 (0.23-3.75)	0.931
Tumour necrosis (Low/High)	1.24 (0.8-1.58)	0.071	-	-
Tumour Microenvironment Characteristics				
Tumour budding (low/high)	6.43 (4.97-8.31)	**<0.001**	6.35 (2.29-17.57)	**<0.001**
Tumour stroma percentage (low/high)	1.96 (1.53-2.52)	**<0.001**	0.04 (0.005-0.42)	**0.007**
Klintrup-Makinen Grade (weak/strong)	0.39 (0.29-0.54)	**<0.001**	32.52 (1.57-672.47)	**0.024**
Phenotypic subtypes (Immune/Canonical/Latent/Stromal)	1.50 (1.34-1.67)	**<0.001**	9.65 (2.25-41.36)	**0.002**
Immune cell markers				
CD3 tumour (Low/High)	0.55 (0.37-0.80)	**0.002**	0.23 (0.06-0.93)	**0.039**
CD3 stroma (Low/High)	0.45 (0.26-0.76)	**0.003**	0.90 (0.12-6.67)	0.924
CD8 tumour (Low/High)	0.54 (0.37-0.80)	**0.002**	3.12 (0.95-10.22)	0.060
CD8 stroma (Low/High)	0.65 (0.47-0.90)	**0.011**	0.46 (0.15-1.34)	0.155
FoxP3 tumour (Low/High)	0.61 (0.31-1.21)	0.158	-	-
FoxP3 stroma (Low/High)	0.35 (0.19-0.62)	**<0.001**	0.25 (0.06-1.07)	0.062
CD68 tumour (Low/High)	0.70 (0.52-0.94)	**0.018**	0.66 (0.27-1.62)	0.375
CD68 stroma (Low/High)	1.39 (1.04-1.86)	**0.025**	1.13 (0.27-4.68)	0.859
CD80 tumour (Low/High)	0.47 (0.27-0.83)	**0.009**	0.31 (0.08-1.24)	0.100
CD80 stroma (Low/High)	0.55 (0.35-0.87)	**0.010**	1.50 (0.49-4.60)	0.472
CD163 tumour (Low/High)	0.56 (0.29-1.08)	0.084	-	-
CD163 stroma (Low/High)	1.84 (1.08-3.16)	**0.025**	13.47 (2.68-67.56)	**0.002**
CD66b tumour (Low/High)	1.74 (1.18-2.57)	**0.005**	0.82 (0.21-3.13)	0.779
CD66b stroma (Low/High)	1.48 (0.99-2.23)	0.056	-	-

HR = Hazard Ratio, CI = Confidence Intervals

3.11 Norwegian Validation Cohort

To validate the findings in the Scottish cohort, a cohort of stage II/III CRC patients from Norwegian were utilised. Firstly, IHC for T-lymphocytes (CD3, CD8), and myeloid cells (CD68, CD66b) were performed in full sections. Three randomly selected areas of 0.6 mm^2 were scored for positive cells to be representative of TMA cores in tumour cell nests and tumour stroma separately by two independent scorers. All markers were scored by myself and 10% of each marker were scored by Antonia Roseweir to check for the consistency. The cut-off values determined from the Scottish cohort were applied to the Norwegian cohort; survival and Chi-squared analysis were performed in comparison to Scottish findings.

3.11.1 Patient's characteristics

294 patients with stage II-III CRC and a valid score for all markers were included in the analysis (**Figure 3.29**). Briefly, 62 (21%) were aged less than 65 years and 155 (53%) were male. 177 (60%) patients had right-sided colon cancer, 31 (10%) patients had left-sided colon cancer, and 86 (30%) had rectal cancer. 186 (63%) had stage II disease, with 108 (37%) stage III patients. The median follows up for patients was 6 years (range 2 months -14.25 years) with 33 (11%) cancer-related deaths and 75 (26%) non-cancer related deaths (**Table 3.11**). The two cohorts were assessed for the difference by utilizing Chi-square test, the result presented no significant differences for basic patient's characteristics (**Table 3.11**).

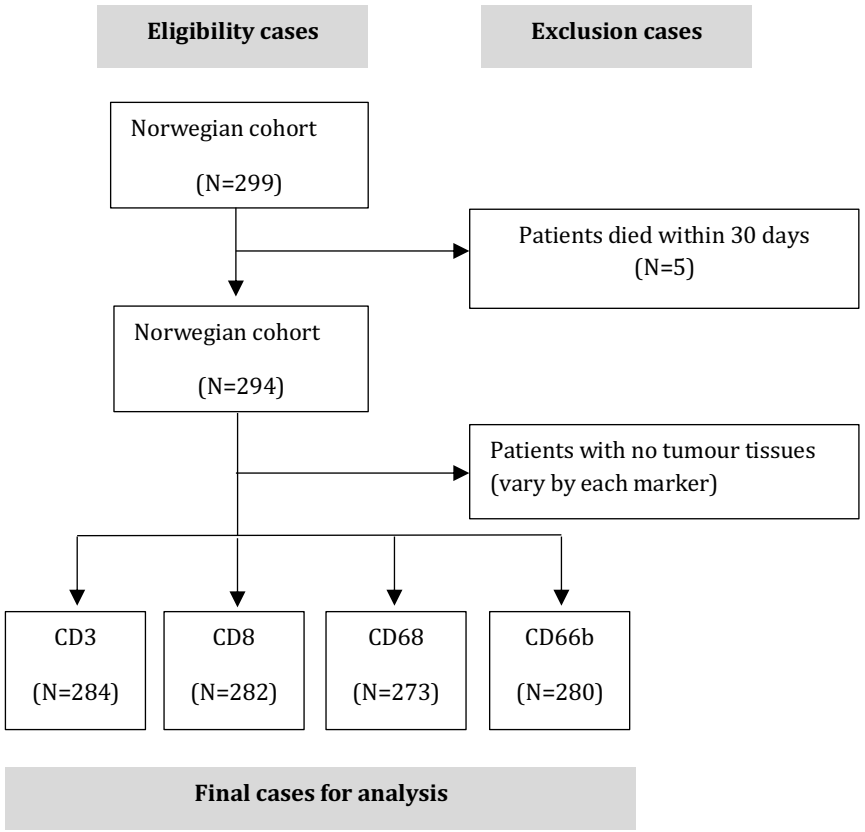

Figure 3.30 - Consort diagram of Norwegian cohort eligible for analysis; Patients available in the study were excluded by died within 30 days and no tumour tissues.

Table 3.11 - CRC patient's characteristics of Scottish discovery cohort (n=930) and Norwegian validation cohort (n=294)

Characteristics	Scottish discovery cohort	Norwegian validation cohort	*p*-value
	Number of patients (%)	Number of patients (%)	
Age			0.701
<65	306 (33)	62 (21)	
>65	624 (67)	232 (79)	
Sex			0.105
Female	437 (47)	139 (47)	
Male	493 (53)	155 (53)	
Tumour site			0.697
Colon – Right	377 (41)	177 (60)	
Colon - Left	308 (33)	31 (10)	
Rectum	238 (26)	86 (30)	
Stage			0.299
I	125 (13)	-	
II	448 (48)	186 (63)	
III	357 (38)	108 (37)	
Survival			0.282
Alive	355 (38)	186 (63)	
Cancer death	279 (30)	33 (11)	
Non-cancer death	296 (32)	75 (26)	

3.11.2 ICCC of scoring (full sections)

Firstly, inter-observer agreement was determined using ICCC, Bland Altman and scatter plots for the four markers (**Figure 3.31 – 3.34**).

3.11.2.1 CD3

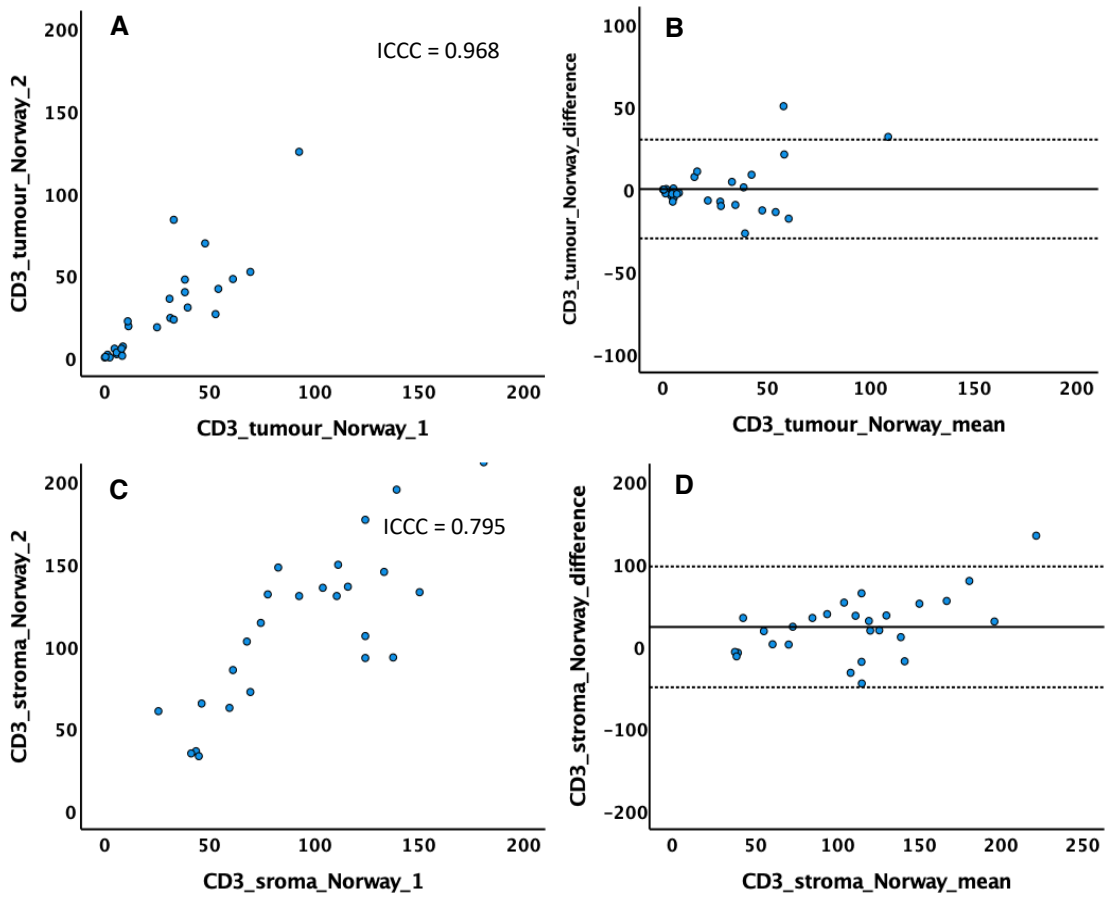

Figure 3.31 - ICCC, scatter plot, Bland-Altman plot of $CD3^+$ in tumour cell nests and tumour stroma in stage II-III CRC Norwegian cohort full sections; **A, B.** tumour cell nests, **C, D.** tumour stroma

3.11.2.2 CD8

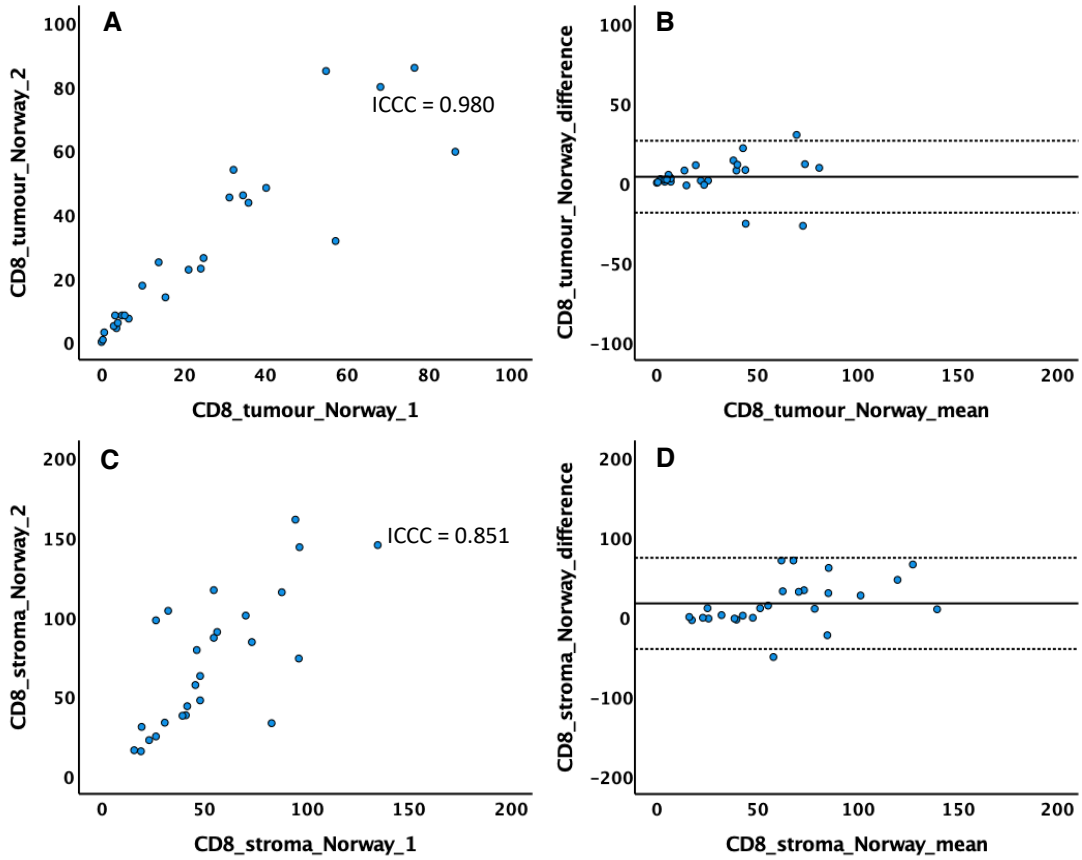

Figure 3.32 - ICCC, scatter plot, Bland-Altman plot of CD8$^+$ in tumour cell nests and tumour stroma in stage II-III CRC Norwegian cohort full sections; **A, B.** tumour cell nests, **C, D.** tumour stroma

3.11.2.3 CD68

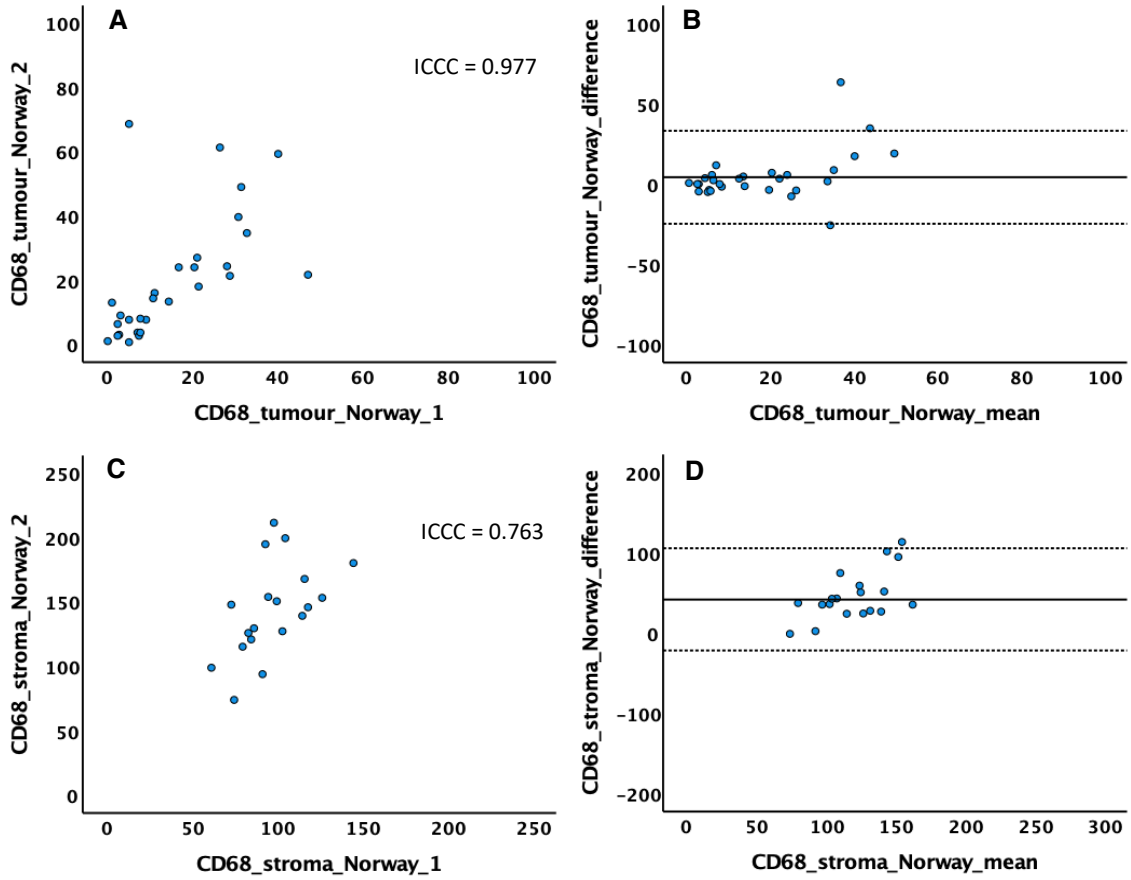

Figure 3.33 - ICCC, scatter plot, Bland-Altman plot of CD68$^+$ in tumour cell nests and tumour stroma in stage II-III CRC Norwegian cohort full sections; **A, B**. tumour cell nests, **C, D.** tumour stroma

3.11.2.4 CD66b

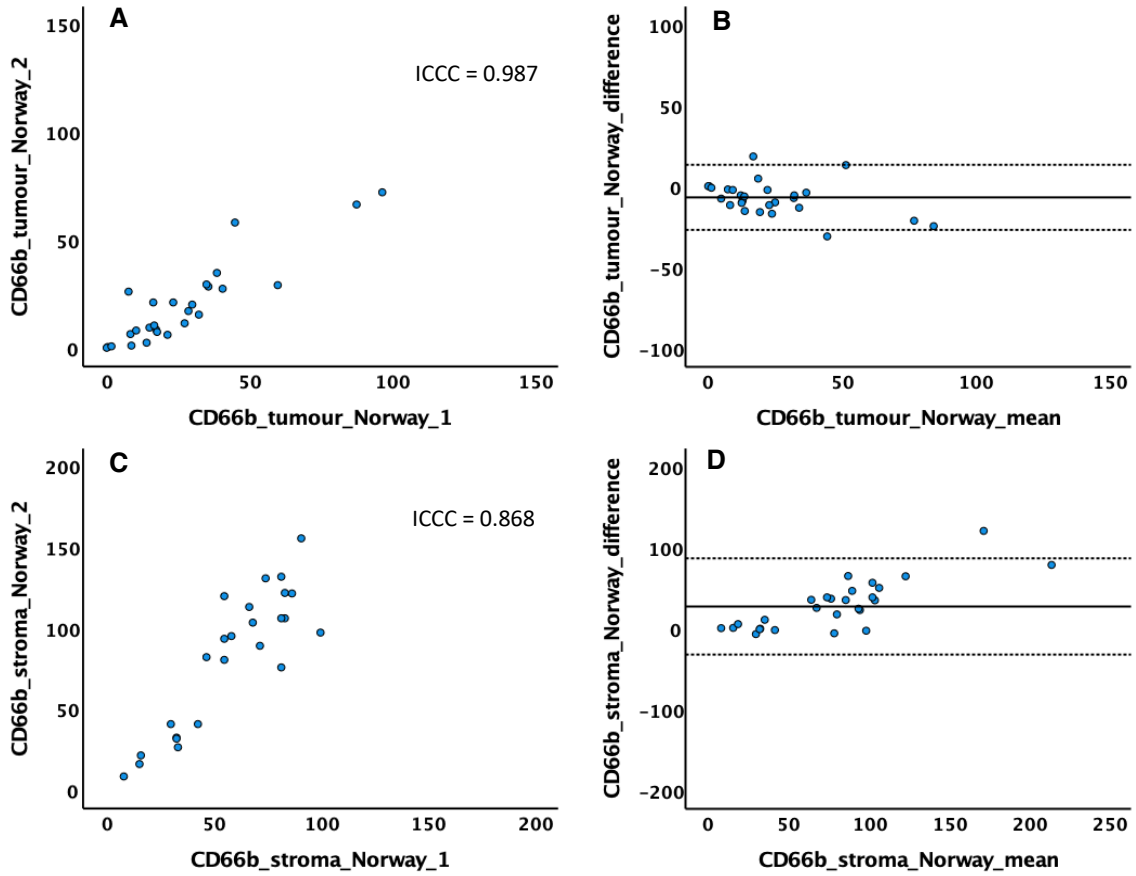

Figure 3.34 - ICCC, scatter plot, Bland-Altman plot of CD66b$^+$ in tumour cell nests and tumour stroma in stage II-III CRC Norwegian cohort full sections; **A, B.** tumour cell nests, **C, D.** tumour stroma

3.11.3 Immune cell levels in Scottish and Norwegian cohorts

The current study aimed to investigate in the influence of T-lymphocytes and myeloid cells in CRC patients with stage I-III in Scottish cohort as a discovery cohort and stage II-III in Norwegian as a validation cohort. As the two cohorts presented non significance differences in basic patient's characteristics. The levels of T-lymphocytes and myeloid cells infiltrated in tumour cell nest and tumour stroma were assessed and compared between them. All T-lymphocytes and myeloid cells in Norwegian validation cohort were significantly higher when compared to Scottish discovery cohort in both tumour cell nest and tumour stroma (**Figure 3.35**).

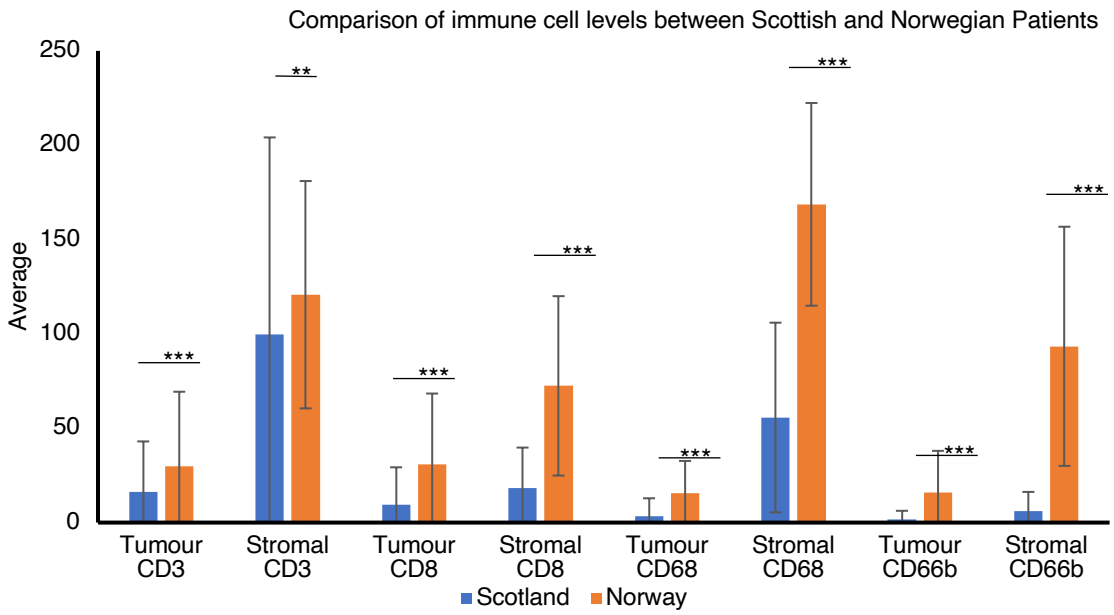

Figure 3.35 - Comparison of T-lymphocytes and myeloid cell levels between Scottish discovery cohort (n=930) and Norwegian validation cohort (n=284); *p<0.05, **p<0.01, ***p<0.001

3.11.4 T-lymphocytes infiltration and patient's survival

3.11.4.1 T-lymphocytes in tumour cell nests

The relationship between T-lymphocytes infiltration in tumour cells nests were high $CD3^+$ was associated with improved CSS (HR 0.38, 95% CI 0.18-0.80, p=0.009, **Figure 3.36, A**) with 10-year survival stratified from 92% (high) to 79% (low). Furthermore, high $CD8^+$ was associated with improved CSS (HR 0.28, 95% CI 0.13-0.59, p<0.001, **Figure 3.36, C**) with 10-year survival stratified from 92% (high) to 75% (low); and improved OS (HR 0.66, 95% CI 0.45-0.98, p=0.041, **Figure 3.36, D**) with 10-year survival stratified from 92% (high) to 75% (low) was associated with improved survival (**Table 3.12**).

Table 3.12 - Relationship between T-lymphocytes and myeloid cells in tumour cell nest and tumour stroma CSS, and OS (% survival at 10 years) in stage II-III CRC of Norwegian cohort (n=284)

	N (%)	CSS (SE)	P	OS (SE)	P
Tumour cell nest					
$CD3^+$ (n=284)			**0.009**		0.055
Low	139 (49)	79 (5)		79 (5)	
High	145 (51)	92 (2)		92 (2)	
$CD8^+$ (n=282)			**<0.001**		**0.041**
Low	103 (37)	75 (5)		75 (5)	
High	179 (63)	92 (2)		92 (2)	
Tumour stroma					
$CD3^+$ (n=284)			**0.032**		**0.005**
Low	229 (81)	83 (3)		39 (6)	
High	55 (19)	96 (3)		64 (10)	
$CD8^+$ (n=282)			0.668		0.276
Low	15 (5)	70 (19)		47 (15)	
High	267 (95)	82 (2)		44 (6)	

CSS = Cancer-specific survival, OS = Overall survival, SE = Standard error

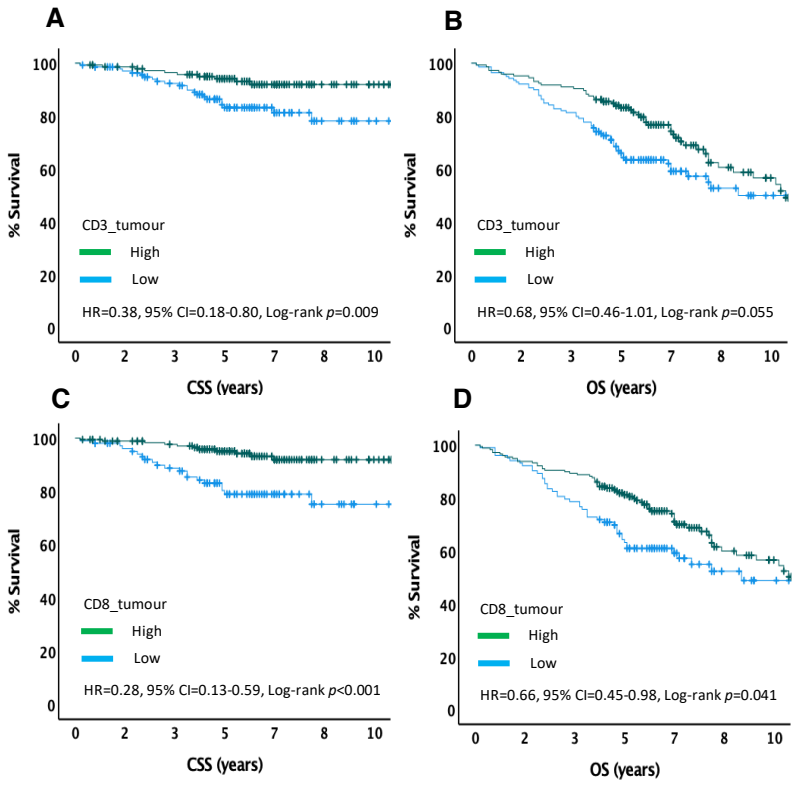

Figure 3.36 - KM plots of T-lymphocytes in tumour cell nests and CSS, OS (% survival at 10 years) in stage II-III CRC Norwegian cohort (n=284); **A**. $CD3^+$ CSS (p=0.009), **B**. $CD3^+$ OS (p=0.055), **C**. $CD8^+$ CSS (p<0.001), **D**. $CD8^+$ OS (p=0.041)

3.11.4.2 T-lymphocytes in tumour stroma

In tumour stroma, high $CD3^+$ was significantly associated with improved CSS (HR 0.23, 95% CI 0.05-0.99, p=0.032, **Figure 3.37, A**) with 10-year CSS stratified from 96% (high) to 83% (low); improved OS (HR 0.42, 95% CI 0.22-0.79, p=0.005, **Figure 3.37, B**) with 10-year CSS stratified from 64% (high) to 39% (low) (**Table 3.12**).

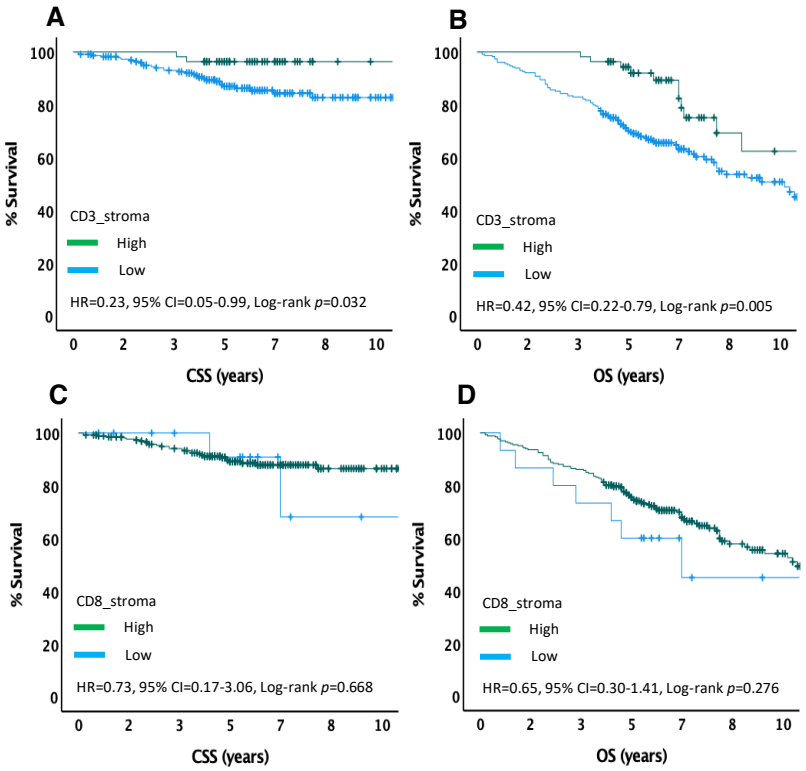

Figure 3.37 - KM plots of T-lymphocytes in tumour stroma and CSS, OS (% survival at 10 years) in stage II-III CRC Norwegian cohort (n=284); **A**. $CD3^+$ CSS (p=0.032), **B**. $CD3^+$ OS (p=0.005), **C**. $CD8^+$ CSS (p=0.668), **D**. $CD8^+$ OS (p=0.276)

3.11.5 Myeloid cells infiltration and patient's survival

3.11.5.1 Myeloid cells in tumour cell nests

The relationship between myeloid cells infiltration in tumour cells nests and CSS, and OS were assessed, no significant was observed (**Table 3.13, Figure 3.38**).

Table 3.13 - Relationship between myeloid cells in tumour cell nest and tumour stroma and CSS, and OS (% survival at 10 years) in stage II-III CRC of Norwegian cohort (n=284)

	N (%)	CSS (SE)	P	OS (SE)	P
Tumour cell nest					
CD68+ (n=273)			0.285		0.923
Low	16 (6)	80 (10)		80 (10)	
High	257 (94)	87 (3)		87 (3)	
CD66b+ (n=280)			0.652		0.932
Low	46 (16)	79 (8)		79 (8)	
High	234 (84)	87 (2)		87 (2)	
Tumour stroma					
CD68+ (n=273)			-		-
Low	1 (1)	-		-	
High	272 (99)	87 (2)		43 (6)	
CD66b+ (n=279)			0.633		0.987
Low	14 (5)	91 (9)		49 (17)	
High	265 (95)	86 (3)		42 (6)	

CSS = Cancer-specific survival, OS = Overall survival, SE = Standard error

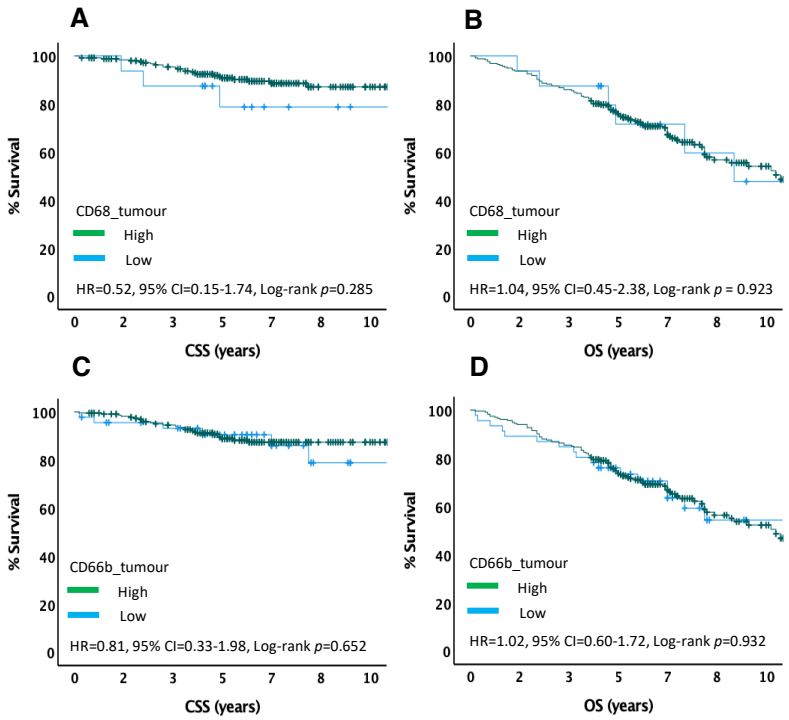

Figure 3.38 - KM plots of myeloid cells in tumour cell nests and CSS, OS (% survival at 10 years) in stage II-III CRC Norwegian cohort (n=284). A. CD68+ CSS (*p*=0.285), **B.** CD68+ OS (*p*=0.923), **C.** CD66b+ CSS (*p*=0.652), **D.** CD66b+ OS (*p*=0.932)

3.11.5.2 Myeloid cells in tumour stroma

In tumour stroma, due to lack of patients with low CD68$^+$, therefore, the statistically significant cannot be calculated. For CD66b$^+$, no significant was observed (**Figure 3.39**, **Table 3.13**).

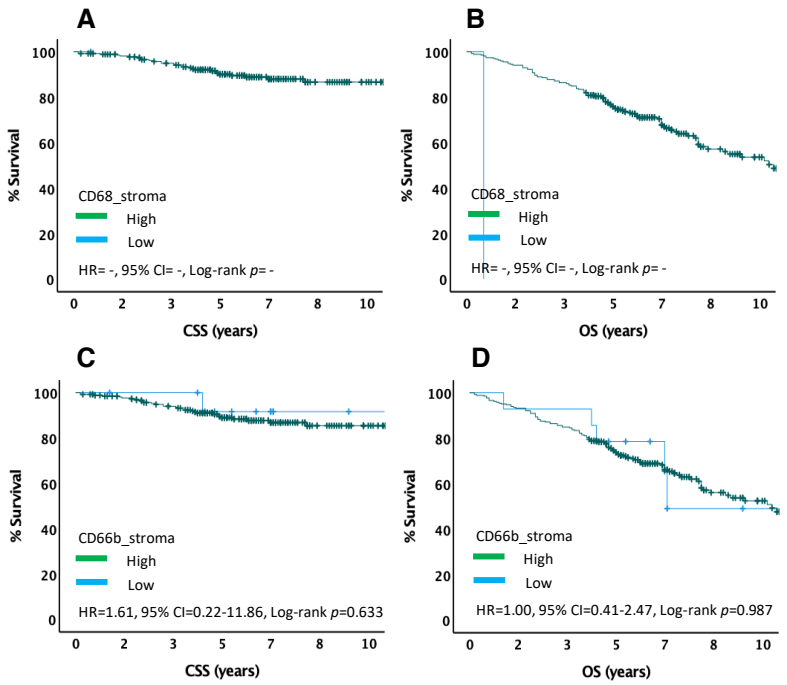

Figure 3.39 - KM plots of myeloid cells in tumour stroma and CSS, OS in patients with stage II-III CRC Norwegian cohort (n=284); A. CD68$^+$ CSS (p=0.932), **B.** CD68$^+$ OS (p<0.001), **C.** CD66b$^+$ CSS (p=0.633), **D.** CD66b$^+$ OS (p=0.987)

3.11.6 Associations between T-lymphocytes, myeloid cells and clinical, TME, and systemic characteristics

3.11.6.1 T-lymphocytes and myeloid cells in tumour cell nests

In tumour cell nests, high CD3$^+$ associated with no adjuvant therapy (p=0.003), stage II disease (p=0.002), absent vascular invasion (p=0.023), low tumour stroma percentage (p=0.001), a strong KM grade (p=0.025), and an immune phenotypic subtype (p=0.003). High CD8$^+$ associated with right-sided colon (p=0.007), no adjuvant therapy (p=0.009), stage II disease (p<0.001), and lower tumour stroma percentage (p<0.001). High CD68$^+$ associated with male (p=0.022), and right-sided colon (p=0.024). There is no significant association with CD66b$^+$ (**Table 3.14**).

Table 3.14 - Association between T-lymphocytes and myeloid cells in tumour cell nest and clinical, TME, systemic characteristics in stage II-III CRC Norwegian cohort (n=284)

	Tumour cell nest											
		CD3+			CD8+			CD68+			CD66b+	
	Low (n=139)	High (n=145)	*P*	Low (n=103)	High (n=179)	*P*	Low (n=16)	High (n=257)	*P*	Low (n=235)	High (n=176)	*P*
Clinical Characteristics												
Age (n=284)			0.535			0.354			0.710			0.734
<65	32 (23)	29 (20)		25 (24)	35 (20)		4 (25)	54 (21)		9 (20)	51 (22)	
>65	107 (77)	116 (80)		78 (76)	144 (80)		12 (75)	203 (79)		37 (80)	183 (78)	
Sex (n=284)			0.647			0.611			**0.022**			0.703
Female	68 (49)	67 (46)		51 (50)	83 (46)		12 (75)	118 (46)		21 (46)	114 (49)	
Male	71 (51)	78 (54)		52 (50)	96 (54)		4 (25)	139 (54)		25 (54)	120 (51)	
Tumour site (n=284)			0.080			**0.007**			**0.024**			0.295
Colon – Right	74 (53)	96 (66)		49 (48)	119 (67)		5 (31)	160 (62)		23 (50)	146 (63)	
Colon - Left	17 (12)	14 (10)		16 (15)	15 (8)		5 (31)	26 (10)		6 (13)	24 (10)	
Rectum	48 (35)	35 (24)		38 (37)	45 (25)		6 (38)	71 (28)		17 (37)	64 (27)	
Adjuvant therapy (n=284)			**0.003**			**0.009**			0.945			0.330
No	99 (71)	124 (86)		74 (72)	152 (85)		13 (81)	207 (81)		39 (85)	184 (79)	
Yes	40 (29)	21 (14)		29 (28)	27 (15)		3 (19)	50 (19)		7 (15)	50 (21)	
Stage (n=284)			**0.002**			**<0.001**			0.210			0.323
II	75 (54)	104 (72)		51 (50)	128 (72)		8 (50)	169 (66)		32 (70)	145 (62)	
III	64 (46)	41 (28)		52 (50)	51 (28)		8 (50)	88 (34)		14 (30)	89 (38)	
Vascular invasion (n=284)			**0.023**			0.083			0.146			0.347
Absent	111(87)	117 (94)		76 (85)	151 (93)		15 (94)	208 (91)		38 (88)	187 (92)	
Present	17 (13)	7 (6)		13 (15)	11 (7)		1 (6)	20 (9)		5 (12)	17 (8)	
Proliferation (n=55)			0.854			0.325			0.556			0.398
Low	1 (4)	1 (3)		2 (9)	1 (3)		0 (0)	3 (6)		0 (0)	3 (6)	
High	23 (96)	30 (97)		20 (91)	33 (97)		3 (100)	49 (94)		6 (100)	46 (94)	
Tumour Microenvironment Characteristics												
Tumour stroma percentage			**0.001**			**<0.001**			0.104			0.989
(n=284)	63 (45)	95 (66)		43 (42)	115 (64)		6 (38)	150 (58)		26 (57)	132 (56)	
Low	76 (55)	50 (34)		60 (58)	64 (36)		10 (62)	107 (42)		20 (43)	102 (44)	
High												
Klintrup-Makinen grade (n=284)			**0.025**			0.352			0.142			0.172
Weak	128 (92)	121 (83)		93 (90)	155 (87)		12 (75)	228 (89)		43 (94)	203 (87)	
Strong	11 (8)	24 (17)		10 (10)	24 (13)		4 (25)	29 (11)		3 (6)	31 (13)	
Phenotypic subtypes (n=175)			**0.003**			0.114			0.204			0.439
Immune	11 (12)	24 (28)		10 (14)	24 (24)		4 (33)	29 (19)		3 (12)	31 (21)	
Canonical	7 (8)	15 (17)		7 (10)	15 (15)		0 (0)	23 (15)		2 (8)	20 (14)	
Latent	0 (0)	1 (1)		0 (0)	1 (1)		0 (0)	1 (1)		0 (0)	1 (1)	
Stromal	70 (80)	47 (54)		55 (76)	60 (60)		8 (67)	100 (65)		20 (80)	94 (64)	
Systemic Characteristics												
Serum CRP (n=284)			0.227			0.478			0.114			0.867
Normal	103 (74)	98 (68)		76 (74)	125 (70)		14 (88)	181 (70)		33 (72)	165 (71)	
High	36 (26)	47 (32)		27 (26)	54 (30)		2 (12)	76 (30)		13 (28)	69 (29)	
Serum Albumin (n=263)			0.569			0.219			0.478			0.543
Normal	15 (12)	19 (14)		15 (16)	18 (11)		1 (7)	32 (13)		7 (16)	27 (12)	
Low	113 (88)	116 (86)		79 (84)	151 (89)		13 (93)	210 (87)		37 (84)	190 (88)	
mGPS (n=264)			0.544			0.357			0.245			0.780
0	94 (73)	91 (68)		68 (73)	117 (69)		12 (86)	170 (70)		31 (71)	152 (70)	
1	28 (22)	33 (24)		18 (19)	43 (25)		2 (14)	55 (23)		9 (20)	51 (23)	
2	7 (5)	11 (8)		8 (8)	9 (6)		0 (0)	17 (7)		4 (9)	14 (7)	

3.11.6.2 T-lymphocytes and myeloid cells in tumour stroma

In tumour stroma, high $CD3^+$ associated with low tumour stroma percentage (p=0.010), a strong KM grade (p=0.008), and immune phenotypic subtype (p=0.002). High $CD8^+$ associated with strong KM grade (p=0.046) and normal serum albumin (p=0.042). High $CD68^+$ associated with normal serum albumin (p=0.042) (**Table 3.15**).

Table 3.15 - Association between T-lymphocytes and myeloid cells in tumour stroma and clinical, TME, and systemic characteristics in stage II-III CRC Norwegian cohort (n=284)

	Tumour stroma											
	CD3+			CD8+			CD68+			CD66b+		
	Low (n=229)	High (n=55)	*P*	Low (n=15)	High (n=267)	*P*	Low (n=1)	High (n=272)	*P*	Low (n=14)	High (n=265)	*P*
Clinical Characteristics												
Age (n=284)			0.946			0.610			0.489			0.994
<65	49 (21)	12 (22)		4 (27)	56 (21)		0 (0)	58 (21)		3 (21)	57 (22)	
>65	180 (79)	43 (78)		11 (73)	211 (79)		1 (100)	214 (79)		11 (79)	208 (78)	
Sex (n=284)			0.965			0.946			0.255			0.670
Female	109 (48)	26 (47)		7 (47)	127 (47)		0 (0)	130 (48)		6 (43)	129 (49)	
Male	120 (52)	29 (53)		8 (53)	140 (53)		1 (100)	142 (52)		8 (57)	136 (51)	
Tumour site (n=284)			0.777			0.475			0.604			0.886
Colon – Right	135 (59)	35 (64)		9 (60)	159 (60)		1 (100)	164 (60)		9 (64)	159 (60)	
Colon - Left	25 (11)	6 (11)		3 (20)	28 (10)		0 (0)	31 (12)		1 (7)	29 (11)	
Rectum	69 (30)	14 (25)		3 (20)	80 (30)		0 (0)	77 (28)		4 (29)	77 (29)	
Adjuvant therapy (n=284)			0.667			0.512			0.511			0.542
No	181 (79)	42 (76)		11 (73)	215 (81)		1 (100)	219 (81)		12 (86)	210 (79)	
Yes	48 (21)	13 (24)		4 (27)	52 (19)		0 (0)	53 (19)		2 (14)	55 (21)	
Stage (n=284)			0.677			0.775			0.148			0.306
II	143 (62)	36 (66)		9 (60)	170 (64)		0 (0)	177 (65)		7 (50)	169 (64)	
III	86 (38)	19 (34)		6 (40)	97 (36)		1 (100)	95 (35)		7 (50)	96 (36)	
Vascular invasion (n=284)			0.980			0.328			0.817			0.827
Absent	184 (91)	44 (90)		11 (79)	216 (91)		1 (100)	222 (91)		12 (92)	212 (91)	
Present	19 (9)	5 (10)		3 (21)	21 (9)		0 (0)	21 (9)		1 (8)	21 (9)	
Proliferation (n=55)			0.273			0.218			-			0.495
Low	2 (5)	0 (0)		1 (20)	2 (4)		-	3 (6)		0 (0)	3 (6)	
High	39 (95)	14 (100)		4 (80)	49 (96)		-	52 (94)		4 (100)	48 (94)	
Tumour Microenvironment Characteristics												
Tumour stroma percentage (n=284)			**0.010**			0.749			0.192			0.946
Low	119 (52)	39 (71)		9 (60)	149 (56)		0 (0)	156 (57)		8 (57)	149 (56)	
High	110 (48)	16 (29)		6 (40)	118 (44)		1 (100)	116 (43)		6 (43)	116 (44)	
Klintrup-Makinen grade (n=284)			**0.008**			**0.046**			0.611			0.553
Weak	207 (90)	42 (76)		15 (100)	233 (87)		1 (100)	239 (88)		13 (93)	233 (88)	
Strong	22 (10)	13 (24)		0 (0)	34 (13)		0 (0)	33 (12)		1 (7)	32 (12)	
Phenotypic subtypes (n=175)			**0.002**			0.242			0.837			0.938
Immune	22 (16)	13 (37)		0 (0)	34 (21)		0 (0)	33 (20)		1 (12)	32 (20)	
Canonical	14 (10)	8 (23)		2 (25)	20 (12)		0 (0)	23 (14)		1 (12)	21 (13)	
Latent	1 (1)	0 (0)		0 (0)	1 (1)		0 (0)	1 (1)		0 (0)	1 (1)	
Stromal	103 (73)	14 (40)		6 (75)	109 (66)		1 (100)	107 (65)		6 (76)	108 (66)	
Systemic characteristics												
Serum CRP (n=284)			0.169			0.855			0.113			0.945
Normal	158 (69)	43 (78)		11 (73)	190 (71)		0 (0)	195 (71)		10 (71)	187 (71)	
High	71 (31)	12 (22)		4 (27)	77 (29)		1 (100)	77 (29)		4 (29)	78 (29)	
Serum Albumin (n=263)			0.446			**0.042**			**0.042**			0.486
Normal	29 (14)	5 (10)		0 (0)	33 (13)		1 (100)	32 (13)		1 (7)	33 (13)	
Low	183 (86)	46 (90)		15 (100)	215 (87)		0 (0)	223 (87)		13 (93)	213 (87)	
mGPS (n=264)			0.450			0.351			0.065			0.337
0	146 (69)	39 (76)		11 (73)	174 (70)		0 (0)	182 (71)		10 (71)	172 (70)	
1	51 (24)	10 (20)		4 (27)	57 (23)		0 (0)	57 (22)		4 (29)	56 (23)	
2	16 (7)	2 (4)		0 (0)	17 (7)		1 (100)	16 (7)		0 (0)	18 (7)	

3.11.7 Immune cells landscapes (CD3/CD68/CD66b) and patient's survival

The associations of immune landscapes and patient's survival were assessed next. For tumour immune landscape, no associations with any survival measure were noted. Whereas stromal immune landscape displayed that the both high group was significantly associated with improved CSS and OS. For CSS indicated that both high group had the best survival (HR 0.50, 95% CI 0.24-1.03, *p*=0.043, **Figure 3.39, B**). For OS, the both high group had the best survival, (HR 0.69, 95% CI 0.51-0.93, *p*=0.006**, Figure 3.39, D**) (**Table 3.16**).

Table 3.16 - Relationship between tumour and stromal immune landscapes and CSS, and OS (% survival at 10 years) in stage II-III CRC Norwegian cohort (n=284)

Immune landscapes (CD3/CD68/CD66b)					
	N (%)	**CSS (SE)**	**P**	**OS (SE)**	**P**
Tumour immune landscape (n=272)			0.143		0.218
Both low	1 (0.5)	100 (0)		100 (0)	
Myeloid high	129 (47)	79 (5)		79 (5)	
T-cells high	1 (0.5)	100 (0)		100 (0)	
Both high	141 (52)	92 (3)		92 (3)	
Stromal immune landscape (n=278)			**0.043**		**0.006**
Both low	-	-		-	
Myeloid high	224 (81)	83 (3)		39 (6)	
T-cells high	-	-		-	
Both high	54 (19)	96 (3)		60 (10)	

CSS = Cancer-specific survival, OS = Overall survival, SE = Standard error

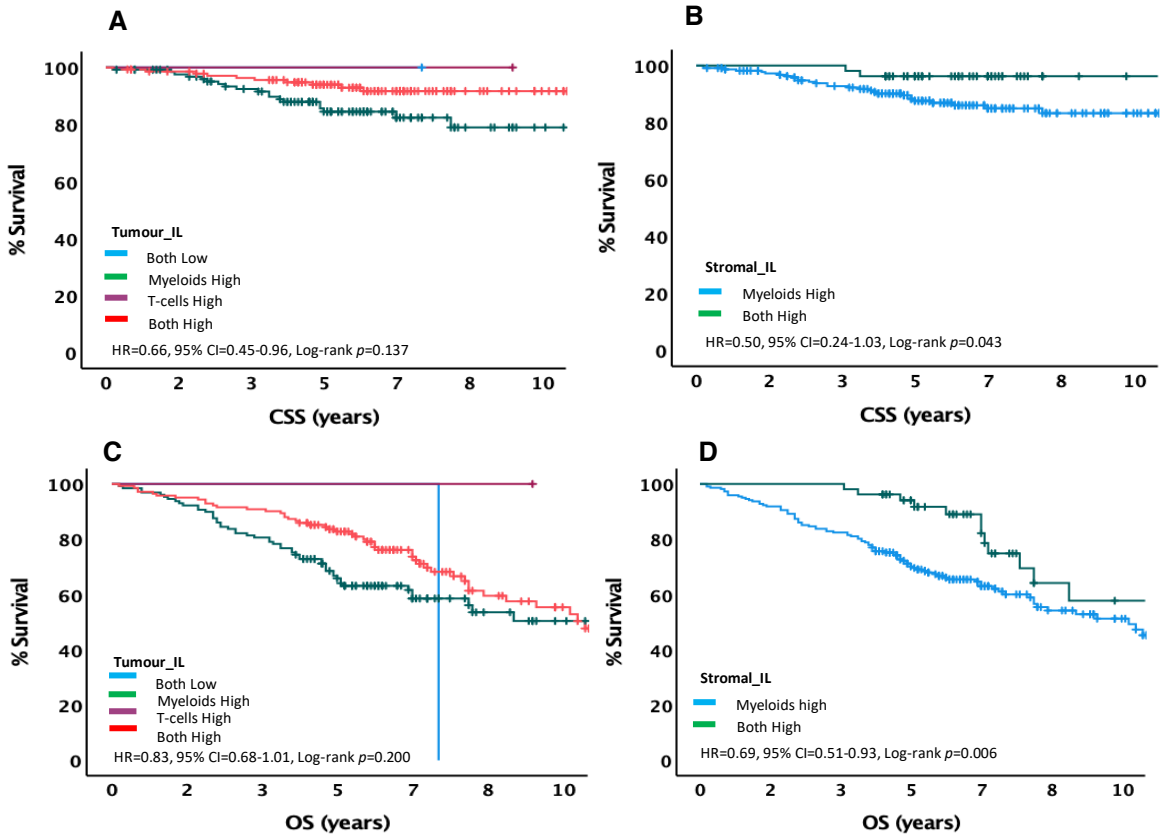

Figure 3.40 - KM plots of tumour and stromal immune landscapes and CSS, OS (% survival at 10 years) in stage II-III CRC Norwegian cohort (n=284); A. Tumour_IL CSS (*p*=0.137), **B.** Stromal_IL CSS (*p*=0.043), **C**. Tumour_IL OS (*p*=0.200), **D.** Stromal_IL OS (*p*=0.006)

3.11.8 Associations between immune landscapes and clinical, TME, systemic characteristics

For tumour immune landscape, the myeloid high associated with increased adjuvant therapy (*p*=0.022), lower stage (*p*=0.004), high tumour stomal percentage (*p*=0.010), and a stromal phenotypic subtype (*p*=0.025)**.** The both high group associated with stage II disease (*p*=0.008), low tumour stroma percentage (*p*=0.004) and an immune phenotypic subtype (*p*=0.025). For stromal immune landscape, myeloid high group associated with high tumour stroma percentage (*p*=0.010), a weak KM grade (*p*=0.008), and a stromal phenotypic subtype (*p*=0.002) (**Table 3.17)**. Whereas, the both high group associated with a low tumour stroma percentage (*p*=0.010), a strong KM grade (*p*=0.008), and an immune phenotypic subtype (*p*=0.002)

Table 3.17 - Association between immune cell landscapes in tumour cell nest and stroma and clinical, TME, and systemic characteristics in stage II-III CRC Norwegian cohort (n=284)

	Tumour immune landscape					Stromal immune landscape				
	Both low (n=1)	**Myeloid high (n=129)**	**T-cell high (n=1)**	**Both high (n=141)**	***P***	**Both low (n=0)**	**Myeloid high (n=224)**	**T-cell high (n=0)**	**Both high (n=54)**	***P***
Clinical Characteristics										
Age (n=272)					0.700					0.785
<65	0 (0)	30 (23)	0 (0)	28 (20)		-	46 (21)	-	12 (22)	
>65	1 (100)	99 (77)	1 (100)	113 (80)			178 (79)		42 (78)	
Sex (n=272)					0.376					0.913
Female	1 (100)	62 (48)	1 (100)	65 (46)		-	106 (47)	-	26 (48)	
Male	0 (0)	67 (52)	0 (0)	76 (54)			118 (53)		28 (52)	
Tumour site (n=272)					0.068					0.867
Colon – Right	0 (0)	72 (56)	0 (0)	93 (66)		-	133 (59)	-	34 (63)	
Colon - Left	1 (100)	16 (12)	1 (100)	13 (9)			25 (11)		6 (11)	
Rectum	0 (0)	41 (32)	0 (0)	35 (25)			66 (30)		14 (26)	
Adjuvant therapy (n=272)					**0.022**					0.620
No	1 (100)	93 (72)	1 (100)	122 (87)		-	181 (81)	-	42 (78)	
Yes	0 (0)	36 (28)	0 (0)	19 (13)			43 (19)		12 (22)	
Stage (n=272)					**0.008**					0.845
II	0 (0)	71 (55)	1 (100)	102 (73)		-	142 (63)	-	35 (65)	
III	1 (100)	58 (45)	0 (0)	39 (27)			82 (37)		19 (35)	
Vascular invasion (n=272)					0.159					0.959
Absent	1 (100)	104 (87)	1 (100)	113 (94)		-	181 (91)	-	43 (90)	
Present	0 (0)	16 (13)	0 (0)	7 (6)			18 (9)		5 (10)	
Proliferation (n=53)					0.938					0.177
Low	-	1 (5)	0 (0)	1 (3)		-	3 (7)	-	0 (0)	
High	-	21 (95)	1 (100)	29 (93)			38 (93)		14 (100)	
Tumour Microenvironment Characteristics										
Tumour stroma percentage (n=272)					**0.004**					**0.010**
Low	1 (100)	61 (47)	0 (0)	94 (67)		-	119 (53)	-	39 (72)	
High	0 (0)	68 (53)	1 (100)	47 (33)			105 (47)		15 (28)	
Klintrup-Makinen grade (n=272)					0.114					**0.008**
Weak	1 (100)	119 (92)	1 (100)	117 (83)		-	202 (90)	-	41 (76)	
Strong	0 (0)	10 (8)	0 (0)	24 (17)			22 (10)		13 (24)	
Phenotypic subtypes (n=165)					**0.025**					**0.002**
Immune	-	10 (12)	0 (0)	24 (29)		-	22 (16)	-	13 (38)	
Canonical	-	7 (9)	0 (0)	15 (18)			14 (10)		8 (24)	
Latent	-	0 (0)	0 (0)	1 (1)			1 (1)		0 (0)	
Stromal	-	63 (79)	1 (100)	44 (52)			98 (73)		13 (38)	
Systemic Characteristics										
Serum CRP (n=578)					0.445					0.182
Normal	1 (100)	95 (74)	1 (100)	95 (67)		-	154 (69)	-	42 (78)	
High	0 (0)	34 (26)	0 (0)	46 (33)			70 (31)		12 (22)	
Serum Albumin (n=609)					0.784					0.446
Normal	0 (0)	14 (12)	0 (0)	19 (15)		-	29 (14)	-	5 (10)	
Low	1 (100)	108 (88)	1 (100)	112 (85)			179 (86)		45 (90)	
mGPS (n=581)					0.806	-				0.465
0	1 (100)	89 (73)	1 (100)	88 (67)		-	142 (68)	-	38 (76)	
1	0 (0)	27 (22)	0 (0)	32 (24)			50 (24)		10 (20)	
2	0 (0)	6 (5)	0 (0)	11 (9)			16 (8)		2 (4)	

3.11.9 Multivariate analysis

Multivariate analysed was then performed to evaluate the independence of prognostic factors when comparing T-lymphocyte markers, myeloid cell markers, clinical characteristics, and CSS. For clinical and tumour microenvironment characteristics, patient's age (HR 8.01, 95% CI 1.88-34.62, *p*=0.005), tumour stage (HR 3.19, 95% CI 1.50-6.77, *p*=0.002), and tumour stroma percentage (HR 2.41, 95% CI 1.11-5.23, *p*=0.026) were independent prognostic factors. For immune cells, $CD8^+$ tumour (HR 0.28, 95% CI 0.11-0.68, *p*=0.005) was an independent prognostic factor (**Table 3.18**).

Table 3.18 - Univariate and multivariate analysis for clinical, TME, immune cell markers, and CSS (% survival at 10 years) in stage II-III CRC of Norwegian cohort (n=284)

	Univariate HR (95% CI)	***P***	**Multivariate HR (95% CI)**	***P***
Clinical Characteristics				
Age (<65/>65)	5.05 (1.20-21.13)	**0.026**	8.01 (1.88-34.62)	**0.005**
Sex (female/male)	1.15 (0.58-2.28)	0.688	-	-
Tumour site (right/left/rectum)	0.71 (0.46-1.09)	0.127	-	-
Adjuvant therapy (no/yes)	1.05 (0.47-2.34)	0.890	-	-
Stage (2/3)	2.58 (1.29-5.15)	**0.007**	3.19 (1.50-6.77)	**0.002**
Vascular invasion (no/yes)	1.71 (0.59-4.93)	0.316	-	-
Proliferation (low/high)	0.39 (0.04-3.17)	0.383	-	-
Tumour Microenvironment Characteristics				
Klintrup-Makinen Grade (weak/strong)	0.97 (0.34-2.76)	0.956	-	-
Tumour stroma percentage (low/high)	3.00 (1.43-6.31)	**0.004**	2.41 (1.11-5.23)	**0.026**
Phenotypic subtypes (Immune/Canonical/Latent/Stromal)	1.28 (0.89-1.84)	0.177	-	-
Immune cell markers				
CD3 tumour (Low/High)	0.38 (0.18-0.80)	**0.012**	1.30 (0.45-3.74)	0.622
CD3 stroma (Low/High)	0.23 (0.05-0.99)	**0.048**	0.34 (0.08-1.47)	0.151
CD8 tumour (Low/High)	0.28 (0.13-0.59)	**0.001**	0.39 (0.18-0.85)	**0.018**
CD8 stroma (Low/High)	0.73 (0.17-3.06)	0.669	-	-
CD68 tumour (Low/High)	0.52 (0.15-1.74)	0.293	-	-
CD68 stroma (Low/High)	20.19 (0-8.40E+45)	0.954	-	-
CD66b tumour (Low/High)	0.81 (0.33-1.98)	0.653	-	-
CD66b stroma (Low/High)	1.61 (0.22-11.86)	0.636	-	-
Tumour immune score (CD3/CD68/CD66b)	0.66 (0.45-0.96)	**0.033**	1.23 (0.71-2.10)	0.448
Stroma immune score (CD3/CD68/CD66b)	0.50 (0.24-1.03)	0.061	-	-

HR=Hazard ration, CI=confidence intervals

3.12 Discussion

This study demonstrated that immune cells, both T-lymphocytes and myeloid cells high levels of infiltrate in early stage of disease and gradually decreased at later stages in tumour cell nests and tumour stroma. High numbers of cytotoxic T-lymphocytes ($CD8^+$) infiltration in tumour and stroma associated with improved CSS. $CD3^+$ infiltration within tumour cells could be independent prognostic factor, like results shown in a previous study (Ohtani, 2007). The presence of $FoxP3^+$ Tregs in stroma associated with improved CSS only. This agrees with other studies showing $FoxP3^+$ Tregs associated with improved prognosis in patients with CRC (Ladoire et al., 2011; Salama et al., 2009; Shang et al., 2015; Sun et al., 2017; Vlad et al., 2015). However, $FoxP3^+$ Tregs infiltration has been shown associated with poor prognosis in other types of tumours (Shang et al., 2015; Zhou et al., 2017). Our results are in the line with other studies that T-lymphocytes, cytotoxic T-lymphocytes and Tregs are beneficial to patient's survival in CRC regardless the locations, but high numbers are crucial to fight tumour cells. Overall, the data suggests that high levels of T-lymphocytes are important predictor of improved survival in patients with stage I-III CRC.

For myeloid cells, the present study showed that, high M1-like macrophages ($CD80^+$) was associated with improved CSS in both tumour and stroma, whereas high M2-like macrophages ($CD163^+$) in stroma was significantly associated with decreased CSS. Similarly, high granulocytes ($CD66b^+$) in tumour and stroma were associated with decreased CSS. M1-like macrophages known as a facilitator of cytotoxic T-lymphocytes function, presented high levels in tumour and stroma could benefit patient's survival. Whereas M2-like macrophages, known as could attract Tregs and help to create immunosuppressive environment, were presented low infiltration in the stroma in patients with improved CSS, however, high level in tumour cells nests were good and had the potential to significantly improved CSS. As for granulocytes, neutrophils are the most abundance in TME, which has been proposed having pro-tumorigenic and anti-tumorigenic characteristics. This study found that high granulocytes infiltration in tumour and stroma were associated with decreased CSS. This indicate that high M1 macrophages are needed, and low M2 macrophages, neutrophils individually are crucial for improving patient survival. However, the role of these in combination might cause distinct outcome. Overall, in multivariate, analysis only $CD3^+$ and $CD8^+$ T-lymphocytes were independently prognostic in the tumour cell nest and only $CD163^+$ M2-macrophages were independently prognostic in the tumour stroma.

To distinguish different immune landscapes, T-lymphocytes and myeloid cells were combined in tumour and stroma separately. The effects on prognosis showed that in tumour cell nests both T-lymphocytes and myeloid cells high group had a potentially better prognosis for CSS, whereas the

T-lymphocytes high only group had the worse prognosis. Whereas in stroma, T-lymphocytes high only group significantly had the best prognosis for CSS, while myeloid high only group clearly had the worse prognosis. This could indicate that in tumour cell nests both T-lymphocytes and myeloid are needed, or myeloid cells might need to enhance T-lymphocytes function when they become exhausted. This suggest that myeloid cells might have different role at different locations. In tumour cells, if patients present only myeloid cells strong will lead to poorer survival. On the other hand, if present with strong T-lymphocytes, it could enhance t-lymphocyte's function to eliminate tumour cells and improved patient's survival even better than T-lymphocytes strong only. Therefore, in tumour cells T-lymphocytes might need the co-operation with particular myeloid cells to reach greater effect for tumour cells eradication.

The correlation of T-lymphocytes populations and myeloid cells are in the current matter as they could affect patient's treatment which some studies show that the presence of myeloid cells related to poorer treatment outcomes (Awad et al., 2018). In pancreatic cancer showed that, myeloid cells could inhibit anti-tumour activity of cytotoxic T-lymphocytes (Guo et al., 2019). In addition, the role of myeloid cells, macrophages, in cancer immunotherapy has been proposed that monocytes/macrophages expressed PD-L1, which is receptor for PD-1 on T-lymphocytes, while tumour cells did not show high PD-L1 (Cantero-Cid et al., 2018). Suggest that monocytes/macrophages could interact with T-lymphocytes which trigger T-lymphocytes exhaustion, reduce T-lymphocytes proliferation, promote tumour progression, and induce resistance to anti PD-1/PD-L1 immunotherapy in CRC. However, the positive effect of innate and adaptive interplay has been reported. The association of $CD8^+$ T-lymphocytes and neutrophils has been proposed that there is interplay between $CD8^+$ T-lymphocytes and neutrophils, which can improve colorectal patient survival (Governa et al., 2017). Therefore, the effect of interplay between innate and adaptive immune response could be negative or positive in different cancer types and depends on particular cell types presented.

The role of myeloid cells in cancer immunotherapy is now one of the forefronts in research, as shown that targeting myeloid cells in immunotherapy in combination with conventional therapy and radiotherapy may lead to a better therapeutic outcome (Moynihan & Irvine, 2017). The combination between chemotherapy and immunotherapy targeting innate and adaptive immune cells has presented in ovarian cancer showed that could promote activated T-lymphocytes and reverse immunosuppression mediated by myeloid cells (Hartl et al., 2019). Recently, the dual target of immune checkpoint and novel molecule, CD47 has been proposed and now validated for cancer immunotherapy. CD47 is a do not eat me signal to protect tumour cells from innate immune system and escape from phagocytic cells such as macrophages. CD47 overexpression in multiple cancer

types, including CRC, and ovarian cancer. Inhibition results in increasing macrophages phagocytic activity leads to impaired tumour growth and limited metastasis (Takimoto et al., 2019). A number of studies found that dual blockade of CD47 and PD-L1 could enhance and bridge innate and adaptive immune response to cancer (Lian et al., 2019; B. Liu et al., 2018; X. Liu et al., 2018).

To validate the results, Norwegian cohort CRC patients was assessed, as it had similar patient characteristics, but the Norwegian cohort showed a low percentage of cancer death than the Scottish cohort. In addition, Norwegian patients had significantly elevated immune cells infiltration levels compared to the Scottish cohort for all cell types both in tumour and stroma. High levels of cytotoxic T-lymphocytes in tumour and stroma associate with improved CSS, while macrophages high infiltration in tumour cells nest significant improved CSS, but not in stroma. For multivariate analysis, $CD8^+$ T-lymphocytes in the tumour cell nests were independently prognostic validating the Scottish cohort results for $CD8^+$. As for immune landscapes, the significance presented in stroma, but not in tumour, which both T-lymphocyte high and myeloid cells high group had better survival than myeloid high only group. However, by lacking the other two groups the result might not be comparable to Scottish cohort. Although the two cohorts have similar results, the interesting point is that the high survival rate and high levels of immune cells infiltration, which Norwegian patients had both much higher than Scottish cohort. However, one limitation of this study may be the differences in prognosis seen between Scottish and Norwegian cohort, which might be due to the different immune cells infiltration levels seen between the two cohorts. This might be due to various factors between that could cause bias, for example, different diagnostic pathways, undergoing different surgery and perioperative care, different oncology treatments, specimens being processed differently, different TNM versions used, lifestyles factors, nutrition, or differences in systemic inflammation with Scottish patients more likely to be systemically inflamed than Norwegian patients (Park et al., 2020).

Interestingly, different immune cells associated with different phenotypic subtypes classifications that have been proposed to aid both prognosis and treatment. The immune subtype associated with higher levels of cytotoxic lymphocytes, whereas the canonical subtype associated with high levels of Tregs and macrophages. The latent and stromal subtypes generally associated with low levels of all immune cells. As this study developed immune landscapes and observed the relationship with patient's survival, which presented the distinct pattern in intratumorally and stromal areas. Therefore, differing immune landscapes within each subtype may contribute to their differing prognosis and may identify a subtype more likely to respond to immune-based therapies.

In conclusion, the present study confirms that different immune cell subtypes associate with different prognosis in stage I-III CRC patients. Elevated lymphoid cells always associate with improved prognosis independent of the presence of myeloid cells, whereas patients with only elevated myeloid cells have a poorer prognosis. The presence of both lymphoid and myeloid cells could reach better survival, however, depends on particular cell types presented and where they located. Besides, assessing different immune landscapes utilising broad markers for T-lymphocytes, macrophages, and granulocytes could aid clinicians with patient prognosis and help target appropriate patients for immunotherapy. However, further validation in a prospective setting across multiple research centres is needed to fully assess the prognostic value of the immune landscapes to assess if the cut-offs generated are appropriate in multiple populations before moving into clinical use.

Chapter 4 Adaptive and innate immune cells within CRC patients with different phenotypic subtype

4.1 Background

CRC prognosis, clinical classification and treatment strategies still mainly rely on tumour staging using the TNM method. However, clinical outcomes and treatment results are highly variable between patient with the same stage, which is one of the main problems for patients with CRC. To address this, Guiney et al. proposed a transcriptomics approach to classify patients into four molecular subtypes; CMS1: MSI Immune, CMS2: Canonical, CMS3: Metabolic, and CMS4: Mesenchymal. Another study also proposed an intrinsic subtype by using the pattern of full genome expression (Guinney, Dienstmann, Wang, de Reynies, Schlicker, Soneson, Marisa, Roepman, Nyamundanda, Angelino, Bot, Morris, Simon, Gerster, Fessler, De Sousa, et al., 2015; Roepman et al., 2014). However, due to the technical difficulties of translating transcriptomics into the clinical setting in a cost-effective manner, these methods are yet to be integrated into CRC clinical practice. Therefore, a CRC classification utilizing phenotypic characteristics could be the alternative way to classify CRC patients that accounts for both tumour and the surrounding microenvironment and utilises clinically utilised histological methods that could be readily translated to clinical practice. Roseweir et al. proposed such a classification called phenotypic subtypes that classify patients into four phenotypic subtypes: immune, canonical, latent, and stromal. These subtypes are independently prognostic for CRC and can predict patients likely to recur and respond to differing adjuvant chemotherapy regimens (Roseweir et al., 2020). However, to improve the predictive value of the phenotypic subtypes, they need further characterisation at both a genomic and proteomic level, including characterising the immune composition of each subtype.

As immune landscapes of T-lymphocytes and myeloid cells were developed; therefore, integration of differing immune landscapes into phenotypic subtypes may contribute to their differing prognosis and may identify a subtype more likely to respond to immune-based therapies such as immune checkpoint inhibitors (ICIs). This study aimed to explore the compositions and levels of T-lymphocytes and myeloid cells and the prognosis within CRC patients with stage I-III CRC.

4.2 Methods

Full sections and TMAs slide from stage I-III CRC patient samples of Scottish cohort were stained by utilising IHC technique. Positive stained cells were scored in tumour cell nests and tumour stroma. The final score for each marker was the average from three randomly selected areas in full sections, and four cores per patient for TMA. The agreement between two independent scorers were assessed by intra-class correlation coefficient (ICCC), scatter plot and Bland-Altman plot. Then the cut-off value for each marker were generated by Bioconductor R studio using the maximal log-rank method based on patients CSS and are the same as used in chapter 3. The analysis was performed for immune

cells markers in terms of the infiltration levels in each phenotypic subtype, CSS stratified by phenotypic subtype, associations with phenotypic subtypes, and multivariate analysis stratified by phenotypic subtype. The combination of T-lymphocytes and myeloid cells were also performed and analysed within phenotypic subtypes in the same manner.

4.3 Results

4.3.1 Patient characteristics

The same 930 Scottish patients with stage I-III CRC were included in the analysis used for the previous chapter (as shown in **Figure 3.1**). Patient characteristics for the cohort, briefly, 624 (67%) patients were over 65 years and 493 (53%) were male. 685 (73%) patients had colon cancer, and 238 (27%) had rectal cancer. 125 (13%) patients had stage I disease, 448 (48%) had stage II disease, with 357 (38%) stage III patients. 162 (18%) patients with MMR deficient. 298 (34%) had an immune subtype, 245 (28%) had a canonical subtype, 190 (21%) had a latent subtype and 156 (17%) had a stromal subtype. The median follows up for patients with stage I-III was 7.5 years (range 2 months -17 years) with 279 (30%) cancer-related deaths and 296 (32%) non-cancer related deaths (**Table 4.1**).

Table 4.1 - CRC patient's characteristics of stage I-III CRC with phonotypic subtypes in Scottish cohort (n=930)

Clinical characteristics	Number of patients (%)
Age	
<65	306 (33)
>65	624 (67)
Sex	
Female	437 (47)
Male	493 (53)
Tumour site	
Colon-right	377 (40)
Colon-left	308 (33)
Rectum	238 (27)
TNM-Stage	
I	125 (13)
II	448 (48)
III	357 (38)
MMR Deficiency	
Competent	739 (79)
Deficient	162 (18)
Missing	29 (3)
Phenotypic Subtype	
Immune	298 (32)
Canonical	245 (26)
Latent	190 (20)
Stromal	156 (17)
Missing	41 (5)
Survival	
Alive	355 (38)
Cancer death/recurrence	279 (30)
Non-cancer death	296 (32)

4.3.2 Immune compositions in CRC phenotypic subtypes

4.3.2.1 Tumour cell nests

The levels of T-lymphocytes and myeloid cells in tumour cell nests and checkpoint proteins were assessed. $CD3^+$ T-lymphocytes were significantly elevated in immune subtype (p=0.021, **Figure 4.1 A**). $CD8^+$ T-lymphocytes were significantly increased in the immune subtype (p<0.001, **Figure 4.1 B**). Whereas $FoxP3^+$ regulatory T-lymphocytes (Tregs) were significantly increased in the canonical subtype (p=0.010, **Figure 4.1 C**). For myeloid cells, $CD68^+$ macrophages were also significantly increased in the canonical subtype (p=0.016, **Figure 4.1 D**). $CD80^+$ M1-like macrophages were significantly greater in the canonical subtype than latent subtype (p=0.006, **Figure 4.1 E**). $CD163^+$ M2-like macrophages was significantly elevated in immune and canonical subtypes and depleted in the latent subtype (p=0.007, **Figure 4.1 F**). No significant difference was also observed for $CD66b^+$ granulocytes (p=0.164, **Figure 4.1 G**).

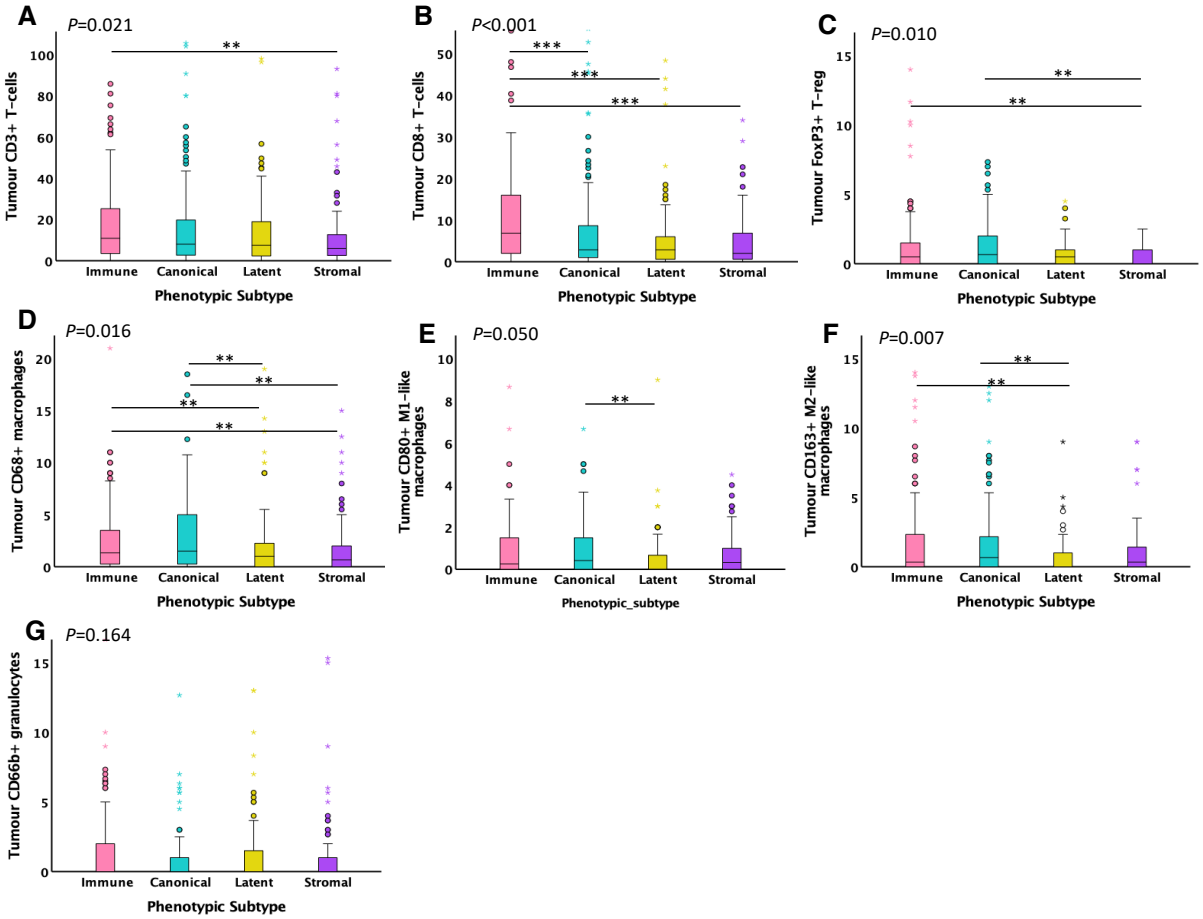

Figure 4.1 - T-lymphocytes and myeloid cells infiltration levels in tumour cell nests in CRC phenotypic subtypes (immune, canonical, latent, stromal) Scottish cohort (n=930); A. $CD3^+$ T-lymphocytes, **B.** $CD8^+$ T-lymphocytes, **C.** $FoxP3^+$ Tregs, **D.** $CD68^+$ macrophages, **E.** $CD80^+$ M1-like macrophages, **F.** $CD163^+$ M2-like macrophages, **G.** $CD66b^+$granulocytes, *p<0.05, **p<0.01, ***p<0.001

4.3.2.2 Tumour stroma

The levels of T-lymphocytes and myeloid cells in tumour stroma were also assessed. For T-lymphocytes, $CD3^+$, $CD8^+$ and $FoxP3^+$ Tregs were all significantly upregulated in immune subtype (p=0.002, p<0.001, and p=0.031, respectively, **Figure 4.2 A-C**). For myeloid cells, $CD68^+$ macrophages were significantly upregulated in the canonical subtype (p=0.016, **Figure 4.2 D**). However, $CD80^+$ M1-like macrophages present no significant difference among the four subtypes (p=0.296, **Figure 4.2 E**). Whereas $CD163^+$ M2-like macrophages were significantly depleted in the latent subtype (p=0.001, **Figure 4.2 F**). Similarly, $CD66b^+$ granulocytes were significantly downregulated in the canonical subtype (p=0.045, **Figure 4.2 G**). Overall, in tumour stroma T-lymphocytes are upregulated in immune subtype; whereas in canonical subtype was predominantly macrophages with depleted granulocytes; latent subtype had depleted M2-like macrophages, whereas stromal subtype presented intermediate level of all cell types.

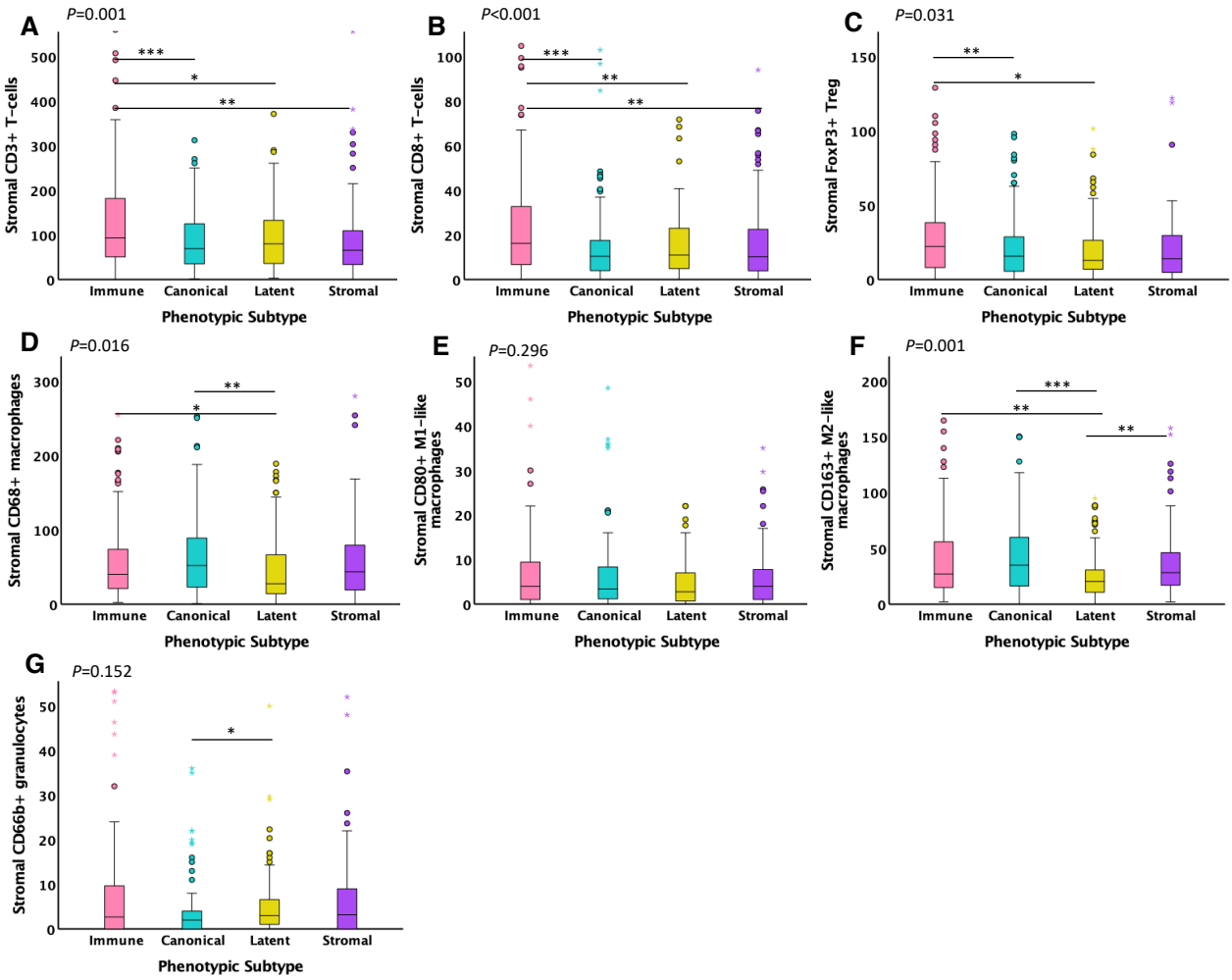

Figure 4.2 - T-lymphocytes and myeloid cells infiltration levels in tumour stroma in CRC phenotypic subtypes (immune, canonical, latent, stromal) Scottish cohort (n=930); A. $CD3^+$ T-lymphocytes, **B.** $CD8^+$ T-lymphocytes, **C.** $FoxP3^+$ Tregs, **D.** $CD68^+$ macrophages, **E.** $CD80^+$ M1-like macrophages, **F.** $CD163^+$ M2-like macrophages, **G.** $CD66b^+$ granulocytes, *p<0.05, **p<0.01, ***p<0.001

4.3.3 Relationship between immune cells in tumour cell nests and tumour stroma and CSS in CRC phenotypic subtypes

The prognostic value of T-lymphocytes, myeloid cells, in tumour cell nests and tumour stroma in each phenotypic subtype were assessed (**Table 4.2-4.4**).

4.3.3.1 Immune subtype

In tumour cell nests, high $CD3^+$ T-lymphocytes significantly associate with improved CSS in the immune subtype (HR 0.33, 95% CI 0.12-0.88, p=0.020, **Figure 4.3 A**) with 10-year CSS stratified from 93% (high) to 72% (low).

In tumour stroma, the presence of FoxP3$^+$ Tregs significantly improved CSS within the immune subtype (HR 0.20, 95% CI 0.04-0.89, *p*=0.020, **Figure 4.3 B**) with 10-year CSS stratified from 90% (present) to 78% (absent) (**Table 4.2**).

4.3.3.2 Canonical subtype

In tumour cell nests, high CD8$^+$ cytotoxic T-lymphocytes associated with significantly improved CSS in the canonical subtype (HR 0.48, 95% CI 0.23-0.99, *p*=0.044, **Figure 4.3 C**) with 10-year CSS stratified from 86% (high) to 76% (low).

In tumour stroma, not significantly associations with CSS were observed for CD3$^+$ T-lymphocytes, however, a trend toward significance was seen in the canonical subtype (HR 0.50, 95% CI 0.29-0.86, *p*=0.057) (**Table 4.2**). For myeloid cells in tumour stroma, CD68$^+$ macrophages trending toward significantly improved CSS in the canonical subtype (HR 1.46, 95% CI 1.08-1.97, *p*=0.080). Whereas CD163$^+$ M2-like macrophages trending toward significantly improved CSS in the canonical subtype (HR 2.06, 95% CI 1.20-3.55, *p*=0.065) (**Table 4.3**).

4.3.3.3 Latent subtype

In tumour cell nests, high CD66b$^+$ granulocytes were associated with significantly decreased CSS in latent subtype (HR 2.63, 95% CI 1.22-5.67, *p*=0.010, **Figure 4.3 D**) with 10-year CSS stratified from 66% (low) to 24% (high) (**Table 4.3**). As for the immune landscape scores developed in the previous chapter, the tumour immune landscape score was significantly associated with better survival in the latent subtype with both low group having the best survival (HR 0.88, 95% CI 0.69-1.11, *p*=0.003). No significant was observed in tumour stroma (**Table 4.4**).

4.3.3.4 Stromal subtype

In tumour cell nests, for myeloid cells, no significant associations were observed for high CD68$^+$ macrophages, however, there is a trend toward significantly improved CSS in the stromal subtype (HR 0.75, 95% CI 0.56-1.01, *p*=0.054). Similarly, no significant associations were observed for high CD80$^+$ M1-like macrophages, however, a trend toward significantly improve CSS in the stromal subtype (HR 0.53, 95% CI 0.36-0.92, *p*=0.090) was observed (**Table 4.3**).

In tumour stroma, the presence of FoxP3$^+$ Tregs significantly improved CSS within the stromal subtype (HR 0.21, 95% CI 0.25-0.87, *p*=0.018, **Figure 4.3 E**) with 10-year CSS stratified from 83% (present) to 43% (absent) (**Table 4.2**). However, high CD66b$^+$ granulocytes were significantly

associated with decreased CSS in the stromal subtype (HR 2.25, 95% CI 1.12-4.51, *p*=0.018, **Figure 4.3 F**) with 10-year CSS stratified from 58% (low) to 31% (high) (**Table 4.3**).

Table 4.2 - Relationship between phenotypic subtypes and T-lymphocytes in tumour cell nests and tumour stroma and CSS (% survival at 10 years) in stage I-III CRC Scottish cohort (n=930)

	T-lymphocytes								
	CD3+ (N=570)		*P*	CD8+ (N=560)		*P*	FoxP3+ (N=457)		*P*
	Low N (%)	High N (%)		Low N (%)	High N (%)		Absent N (%)	Present N (%)	
Tumour cell nests									
Immune	110 (60)	72 (40)	0.020	94 (53)	84 (47)	0.166	126 (83)	25 (17)	0.518
CSS (SE)	72 (6)	93 (3)		76 (6)	86 (5)		84 (4)	71 (15)	
Canonical	134 (69)	59 (31)	0.182	137 (72)	53 (28)	0.044	128 (83)	26 (17)	0.653
CSS (SE)	67 (4)	77 (6)		65 (4)	79 (6)		69 (4)	79 (8)	
Latent	69 (70)	30 (30)	0.644	82 (82)	18 (18)	0.744	72 (95)	4 (5)	0.218
CSS (SE)	59 (7)	64 (10)		56 (7)	66 (11)		56 (8)	100 (0)	
Stromal	77 (80)	19 (20)	0.521	72 (78)	20 (22)	0.837	75 (99)	1 (1)	0.405
CSS (SE)	46 (7)	58 (11)		47 (7)	48 (11)		49 (6)	100 (0)	
Tumour stroma									
Immune	135 (73)	49 (26)	0.834	73 (41)	105 (59)	0.133	103 (68)	48 (32)	0.020
CSS (SE)	78 (5)	83 (6)		73 (7)	85 (5)		78 (6)	90 (8)	
Canonical	172 (89)	21 (11)	0.057	119 (63)	71 (37)	0.480	127 (83)	27 (18)	0.202
CSS (SE)	68 (4)	87 (9)		67 (5)	72 (6)		68 (4)	83 (8)	
Latent	84 (85)	15 (15)	0.201	59 (59)	41 (41)	0.967	61 (80)	15 (20)	0.710
CSS (SE)	59 (7)	72 (15)		58 (8)	58 (9)		57 (9)	64 (13)	
Stromal	82 (85)	14 (15)	0.091	61 (66)	31 (34)	0.454	63 (83)	13 (17)	0.018
CSS (SE)	44 (6)	76 (12)		43 (8)	57 (10)		43 (7)	83 (11)	

N=number of patients, CSS=Cancer specific survival, SE= standard error

Table 4.3 - Association between phenotypic subtypes and myeloid cells in tumour cell nest and tumour stroma and CSS (% survival at 10 years) in stage I-III CRC Scottish cohort (n=930)

	Myeloid cells										
	CD68+ (N=544)		*P*	CD80+ (N=417)		*P*	CD163+ (411)		*P*	CD66b+ (N=392)		*P*
	Low N (%)	High N (%)		Low N (%)	High N (%)		Low N (%)	High N (%)		Low N (%)	High N (%)	
Tumour cell nests												
Immune	71 (39)	110 (61)	0.806	106 (80)	26 (20)	0.209	111 (85)	19 (15)	0.553	93 (74)	33 (26)	0.100
CSS (SE)	71 (9)	82 (4)		76 (6)	90 (7)		78 (6)	89 (8)		80 (6)	64 (10)	
Canonical	45 (37)	76 (63)	0.982	78 (78)	22 (22)	0.695	78 (82)	17 (18)	0.712	90 (81)	21 (19)	0.987
CSS (SE)	69 (7)	69 (6)		65 (6)	74 (10)		69 (6)	75 (11)		75 (5)	74 (10)	
Latent	64 (49)	66 (51)	0.249	88 (89)	11 (11)	0.257	95 (96)	4 (4)	0.569	63 (78)	18 (22)	**0.010**
CSS (SE)	48 (9)	66 (6)		54 (6)	67 (16)		52 (6)	75 (22)		66 (8)	24 (15)	
Stromal	57 (51)	55 (7)	0.054	76 (86)	12 (14)	0.090	80 (92)	7 (8)	0.287	57 (77)	17 (23)	0.119
CSS (SE)	55 (49)	47 (7)		33 (6)	67 (14)		36 (6)	57 (19)		55 (7)	39 (12)	
Tumour stroma												
Immune	115 (64)	66 (36)	0.513	95 (72)	37 (28)	0.167	20 (15)	110 (85)	0.483	89 (71)	37 (29)	0.581
CSS (SE)	80 (5)	71 (9)		75 (7)	89 (6)		89 (7)	77 (6)		77 (7)	75 (8)	
Canonical	62 (51)	59 (49)	0.080	76 (76)	24 (24)	0.235	10 (11)	85 (89)	0.065	99 (89)	12 (11)	0.611
CSS (SE)	76 (6)	62 (7)		63 (6)	80 (9)		100 (0)	67 (5)		74 (5)	82 (12)	
Latent	87 (67)	43 (33)	0.259	76 (78)	21 (22)	0.334	24 (24)	75 (76)	0.099	65 (81)	15 (18)	0.825
CSS (SE)	59 (7)	54 (8)		54 (6)	63 (13)		57 (15)	52 (6)		60 (8)	47 (21)	
Stromal	65 (58)	47 (42)	0.159	69 (78)	19 (22)	0.174	14 (16)	73 (84)	0.203	54 (73)	20 (27)	**0.018**
CSS (SE)	45 (7)	32 (7)		34 (6)	53 (11)		54 (14)	35 (6)		58 (7)	31 (11)	

N=number of patients, CSS=Cancer specific survival, SE= standard error

Table 4.4 - Association between phenotypic subtypes and immune landscape scores in tumour cell nest and tumour stroma and CSS (% survival at 10 years) in stage I-III CRC Scottish cohort (n=930)

	Immune landscape scores				
	Both low N (%)	Myeloid high N (%)	T-cells high N (%)	Both high N (%)	*P*
Tumour immune landscape (N=243)					
Immune	8 (11)	32 (44)	3 (4)	30 (41)	0.179
CSS (SE)	85 (14)	67 (10)	100 (0)	93 (5)	
Canonical	10 (14)	37 (51)	2 (3)	23 (32)	0.407
CSS (SE)	89 (10)	64 (9)	100 (0)	77 (9)	
Latent	4 (8)	27 (56)	1 (2)	16 (33)	**0.003**
CSS (SE)	67 (27)	56 (12)	-	62 (14)	
Stromal	9 (18)	33 (66)	2 (4)	6 (12)	0.256
CSS (SE)	53 (17)	46 (10)	0 (0)	67 (19)	
Stromal immune landscape (N=243)					
Immune	9 (12)	41 (54)	5 (7)	21 (27)	0.724
CSS (SE)	88 (12)	65 (14)	100 (0)	74 (12)	
Canonical	16 (21)	47 (62)	1 (1)	12 (16)	0.343
CSS (SE)	67 (14)	62 (7)	100 (0)	92 (8)	
Latent	3 (7)	36 (78)	2 (4)	5 (11)	0.226
CSS (SE)	100 (0)	44 (9)	0 (0)	80 (18)	
Stromal	7 (13)	40 (71)	2 (4)	7 (12)	0.229
CSS (SE)	69 (19)	34 (8)	50 (35)	69 (19)	

N=number of patients, CSS=Cancer specific survival, SE= standard error

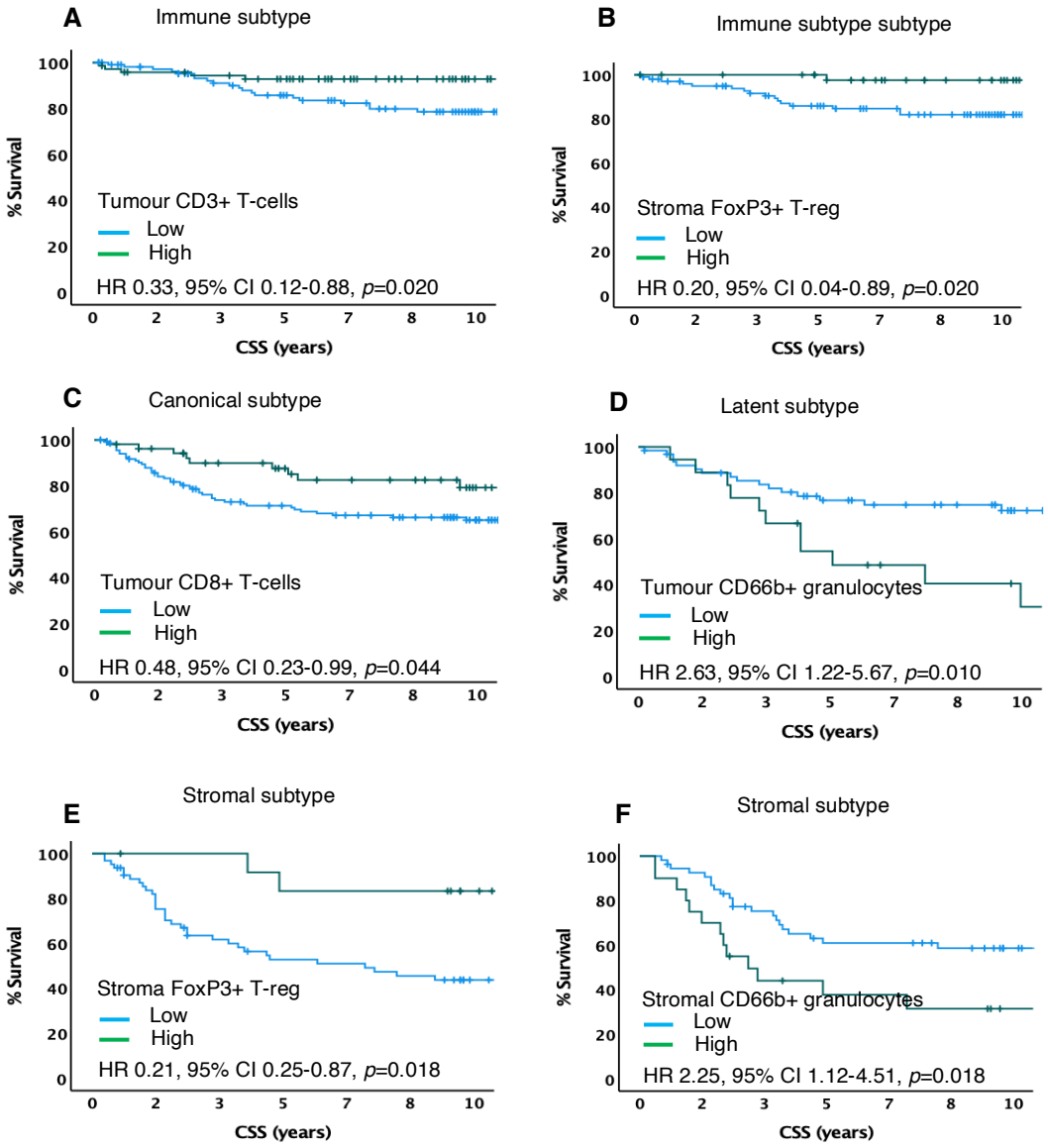

Figure 4.3 - KM plots of significant immune cells infiltration in tumour cell nests and tumour stroma to patients' survival in each phenotypic subtype. A. tumour $CD3^+$ T-lymphocytes in immune subtype, **B.** stromal $Foxp3^+$ Tregs in immune subtype, **C.** tumour $CD8^+$ T-lymphocytes in canonical subtype, **D.** tumour $CD66b^+$ granulocytes in latent subtype, **E.** stromal $FoxP3^+$ Tregs in stromal subtype, **F.** stromal $CD66b^+$ granulocytes in stromal subtype

4.3.4 Association between CRC phenotypic subtypes and immune cells infiltration in tumour cell nests and tumour stroma

4.3.4.1 Immune subtype

In tumour cell nests, immune subtype significantly associated with high $CD3^+$ (p=0.007), high $CD8^+$ (p<0.001), and present $FoxP3^+$ (p<0.001). In tumour stroma, again, the immune subtype significantly associated with high $CD3^+$ (p<0.001), high $CD8^+$ (p<0.001), and present $FoxP3^+$ (p=0.012) (**Table 4.5**).

4.3.4.2 Canonical subtype

In tumour cell nests, canonical subtype significantly associated with high $CD163^+$ M2-like macrophages (p=0.006) (**Table 4.6**).

4.3.4.3 Latent subtype

No significant associations were observed for T-lymphocytes in tumour cell nests. As for stromal immune landscape score, the myeloid high group significantly associated with the latent subtype (p=0.046) (**Table 4.7**).

4.3.4.4 Stromal subtype

No significant associations were observed for T-lymphocytes in tumour cell nests. In tumour stroma, the significant associations were observed for high $CD66b^+$ granulocytes in stromal subtypes (p=0.002) (**Table 4.6**).

Table 4.5 - Association between phenotypic subtypes and T-lymphocytes infiltration in tumour cell nests and tumour stroma in stage I-III CRC Scottish cohort (n=930)

	T-lymphocytes								
	CD3+ (N=570)		*P*	CD8+ (N=560)		*P*	FoxP3+ (N=457)		*P*
	Low N (%)	High N (%)		Low N (%)	High N (%)		Absent N (%)	Present N (%)	
Tumour cell nests									
Immune	110 (28)	72 (40)	**0.007**	94 (24)	84 (48)	**<0.001**	126 (31)	25 (45)	**<0.001**
Canonical	134 (34)	59 (33)		137 (36)	53 (30)		128 (32)	26 (46)	
Latent	69 (18)	30 (16)		82 (21)	18 (10)		72 (18)	4 (7)	
Stromal	77 (20)	19 (11)		72 (719)	20 (11)		75 (19)	1 (2)	
Tumour stroma									
Immune	135 (29)	49 (50)	**<0.001**	73 (23)	105 (42)	**<0.001**	103 (29)	48 (46)	**0.012**
Canonical	172 (36)	21 (21)		119 (38)	71 (29)		127 (36)	27 (26)	
Latent	84 (18)	15 (15)		59 (19)	41 (17)		61 (17)	15 (15)	
Stromal	82 (17)	14 (14)		61 (20)	31 (12)		63 (18)	13 (13)	

Table 4.6 - Association between phenotypic subtypes and myeloid cells infiltration in tumour cell nests and tumour stroma in stage I-III CRC Scottish cohort (n=930)

	Myeloid cells											
	CD68+ (N=544)		*P*	CD80+ (N=417)		*P*	CD163+ (N=411)		*P*	CD66b+ (N=392)		*P*
	Low N (%)	High N (%)		Low N (%)	High N (%)		Low N (%)	High N (%)		Low N (%)	High N (%)	
Tumour cell nests												
Immune	71 (30)	110 (36)	0.057	106 (31)	26 (37)	0.139	111 (31)	19 (40)	**0.006**	93 (31)	33 (37)	0.614
Canonical	45 (19)	76 (25)		78 (22)	22 (31)		78 (21)	17 (36)		90 (30)	21 (24)	
Latent	64 (27)	66 (22)		86 (25)	11 (15)		95 (26)	4 (9)		63 (20)	18 (20)	
Stromal	57 (24)	55 (17)		76 (22)	12 (17)		80 (22)	7 (15)		57 (19)	17 (19)	
Tumour stroma												
Immune	115 (35)	66 (31)	0.057	95 (30)	37 (36)	0.635	20 (29)	110 (32)	0.080	89 (29)	37 (44)	**0.002**
Canonical	62 (19)	59 (27)		76 (24)	24 (24)		10 (15)	85 (25)		99 (32)	12 (14)	
Latent	87 (26)	43 (20)		76 (24)	21 (21)		24 (35)	75 (22)		65 (21)	15 (18)	
Stromal	65 (20)	47 (22)		69 (22)	19 (19)		14 (21)	73 (21)		54 (18)	20 (24)	

Table 4.7 - Association between phenotypic subtypes and immune landscape scores in tumour cell nests and tumour stroma in stage I-III CRC Scottish cohort (n=930)

	Tumour immune landscape scores					Stromal immune landscape scores				
	Both low N (%)	**Myeloid high N (%)**	**T-cells high N (%)**	**Both high N (%)**	***P***	**Both low N (%)**	**Myeloid high N (%)**	**T-cells high N (%)**	**Both high N (%)**	***P***
Immune	8 (26)	32 (25)	3 (38)	30 (40)	0.083	9 (26)	41 (25)	5 (50)	21 (47)	**0.046**
Canonical	10 (32)	37 (29)	2 (25)	23 (31)		16 (46)	47 (29)	1 (10)	12 (27)	
Latent	4 (13)	27 (21)	1 (12)	16 (21)		3 (8)	36 (22)	2 (20)	5 (11)	
Stromal	9 (29)	33 (25)	2 (25)	6 (8)		7 (20)	40 (24)	2 (20)	7 (15)	

4.3.5 Multivariate analysis

Univariate analysis was performed to evaluate the relationship between CSS and clinical parameters, immune cells, T-lymphocytes and myeloid cells in tumour cell nests and tumour stroma in each subtype were analysed separately (**Table 4.8**). The significant parameters were then analysed for multivariate analysis for each phenotypic subtype. For immune subtype, stage (p=0.042) and tumour budding (p<0.001) were independent prognostic factors, with stromal FoxP3$^+$ Tregs trending towards independence (p=0.064). In canonical subtype, stage (p=0.005) and tumour budding (p<0.001) were independently prognostic factors. Whereas in latent subtype, stage (p=0.001) and tumour CD66b$^+$ granulocytes (p=0.032) were independent prognostic factors. However, in stromal subtype only tumour budding (p<0.001) were independent prognostic factors. Overall, tumour CD66b$^+$ granulocytes within the latent subtype was the only one immune cell with independent prognostic value seen.

Table 4.8 - Univariate and multivariate analysis of immune cells, clinicopathological characteristics, and CSS (% survival at 10 years) of phenotypic subtypes in stage I-III CRC Scottish cohort (n=930)

	CSS			
	Univariate HR (95% CI)	***P***	**Multivariate HR (95% CI)**	***P***
Immune subtype (n=298)				
Age (<65/>65)	1.30 (0.69-2.41)	0.407	-	-
Sex (female/male)	2.20 (1.21-4.00)	**0.009**	1.73 (0.49-6.07)	0.389
Tumour site (left/right/rectum)	1.00 (0.72-1.40)	0.963	-	-
Stage (1/2/3)	2.21 (1.45-3.36)	**<0.001**	2.33 (1.03-5.25)	**0.042**
Differentiation (no/yes)	3.14 (1.60-6.41)	**0.001**	0.39 (0.07-2.03)	0.263
Vascular invasion (no/yes)	1.64 (0.91-2.96)	0.096	-	-
Peritoneal Involvement (no/yes)	2.38 (1.32-4.28)	**0.004**	1.01 (0.21-4.74)	0.981
Mismatch Repair Status (competent/deficient)	1.76 (0.97-3.18)	0.062	-	-
Proliferation (low/high)	0.54 (0.30-0.95)	**0.034**	2.12 (0.36-12.48)	0.404
Tumour necrosis (low/high)	1.89 (1.08-3.31)	**0.026**	2.37 (0.83-6.73)	0.105
Tumour budding (low/high)	6.97 (3.86-12.58)	**<0.001**	37.16 (9.65-143.06)	**<0.001**
Tumour stroma percentage (low/high)	2.88 (1.62-5.11)	**<0.001**	3.04 (0.99-9.28)	0.050
KM grade (weak/strong)	0.47 (0.19-1.20)	0.119	-	-
Tumour CD3+ lymphocytes (low/high)	0.33 (0.12-0.88)	**0.027**	0.50 (0.13-1.93)	0.320
Stromal CD3+ lymphocytes (low/high)	0.91 (0.38-2.14)	0.834	-	-
Tumour CD8+ lymphocytes (low/high)	0.56 (0.25-1.27)	0.172	-	-
Stromal CD8+ lymphocytes (low/high)	0.55 (0.25-1.20)	0.139	-	-
Tumour FoxP3+ Tregs (absent/present)	1.43 (0.47-4.32)	0.520	-	-
Stromal FoxP3+ Tregs (absent/present)	0.20 (0.04-0.89)	**0.035**	0.22 (0.04-1.09)	0.064
Tumour CD68+ macrophages (low/high)	0.91 (0.44-1.88)	0.807	-	-
Stromal CD68+ macrophages (low/high)	1.27 (6.14-2.64)	0.514	-	-
Tumour CD80+ macrophages (low/high)	0.40 (0.09-1.74)	0.225	-	-
Stromal CD80+ macrophages (low/high)	0.43 (0.12-1.47)	0.180	-	-
Tumour CD163+ macrophages (low/high)	0.64 (0.15-2.78)	0.556	-	-
Stromal CD163+ macrophages (low/high)	1.67 (0.38-7.23)	0.489	-	-
Tumour CD66b+ granulocytes (low/high)	1.99 (0.86-4.61)	0.107	-	-
Stromal CD66b+ granulocytes (low/high)	1.27 (0.53-3.00)	0.582	-	-
TIL_score	0.62 (0.35-1.10)	0.104	-	-
SIL_score	0.98 (0.57-1.68)	0.967	-	-
Canonical subtype (n=245)				
Age (<65/>65)	1.31 (0.72-2.36)	0.366	-	-
Sex (female/male)	1.17 (0.72-1.90)	0.505	-	-
Tumour site (left/right/rectum)	0.99 (0.70-1.38)	0.953	-	-
Stages (1/2/3)	3.26 (2.09-5.11)	**<0.001**	2.12 (1.25-3.62)	**0.005**
Differentiation (no/yes)	1.59 (0.83-3.03)	0.158	-	-
Vascular Invasion (absent/present)	1.97 (1.22-3.17)	**0.005**	1.13 (0.62-2.06)	0.679
Peritoneal Involvement (no/yes)	2.88 (1.78-4.65)	**<0.001**	1.03 (0.55-1.92)	0.914
Mismatch Repair Status (competent/deficient)	0.49 (0.21-1.13)	0.097	-	-
Proliferation (low/high)	1.26 (0.78-2.03)	0.338	-	-
Tumour necrosis (low/high)	1.60 (0.99-2.58)	0.051	-	-
Tumour budding (low/high)	7.95 (4.68-13.52)	**<0.001**	7.09 (3.72-13.52)	**<0.001**
Tumour stroma percentage (low/high)	1.02 (0.99-1.04)	0.093	-	-
KM grade (weak/strong)	1.10 (0.60-2.01)	0.751	-	-
Tumour CD3+ lymphocytes (low/high)	0.64 (0.34-1.23)	0.186	-	-
Stromal CD3+ lymphocytes (low/high)	0.27 (0.06-1.14)	0.076	-	-
Tumour CD8+ lymphocytes (low/high)	0.48 (0.23-0.99)	**0.049**	0.66 (0.32-1.37)	0.268

	CSS		CSS	
	Univariate HR (95% CI)		Univariate HR (95% CI)	
Canonical subtype (n=245) (Cont.)				
Stromal CD8+ lymphocytes (low/high)	0.81 (0.45-1.44)	0.481	-	-
Tumour FoxP3+ Tregs (absent/present)	0.80 (0.31-2.06)	0.654	-	-
Stromal FoxP3+ Tregs (absent/present)	0.51 (0.18-1.45)	0.211	-	-
Tumour CD68+ macrophages (low/high)	1.00 (0.50-2.01)	0.982	-	-
Stromal CD68+ macrophages (low/high)	1.83 (0.92-3.67)	0.085	-	-
Tumour CD80+ macrophages (low/high)	0.82 (0.31-2.16)	0.696	-	-
Stromal CD80+ macrophages (low/high)	0.53 (0.18-1.53)	0.243	-	-
Tumour CD163+ macrophages (low/high)	0.81 (0.28-2.37)	0.713	-	-
Stromal CD163+ macrophages (low/high)	24.27 (0.12-4626.21)	0.234	-	-
Tumour CD66b+ granulocytes (low/high)	1.00 (0.37-2.68)	0.987	-	-
Stromal CD66b+ granulocytes (low/high)	0.68 (0.16-2.92)	0.613	-	-
TIL_score	1.00 (0.65-1.54)	0.974	-	-
SIL_score	0.73 (0.43-1.23)	0.250	-	-
Latent subtype (n=190)				
Age (<65/>65)	1.22 (0.73-2.01)	0.436	-	-
Sex (female/male)	1.00 (0.62-1.60)	0.993	-	-
Tumour site (left/right/rectum)	0.97 (0.72-1.32)	0.880	-	-
Stage (1/2/3)	2.34 (1.53-3.58)	**<0.001**	3.65 (1.74-7.64)	**0.001**
Differentiation (no/yes)	2.14 (1.09-4.19)	**0.026**	2.13 (0.61-7.38)	0.231
Vascular Invasion (absent/present)	1.73 (1.07-2.81)	**0.024**	1.44 (0.64-3.24)	0.368
Peritoneal Involvement (no/yes)	1.99 (1.23-3.22)	**0.005**	1.99 (0.91-4.31)	0.081
Mismatch Repair Status (competent/deficient)	0.55 (0.25-1.21)	0.139	-	-
Proliferation (low/high)	-	-	-	-
Tumour necrosis (low/high)	0.93 (0.57-1.51)	0.791	-	-
Tumour budding (low/high)	3.58 (2.19-5.86)	**<0.001**	1.50 (0.65-3.48)	0.335
Tumour stroma percentage (low/high)	1.00 (0.98-1.02)	0.789	-	-
KM grade (weak/strong)	1.04 (0.61-1.79)	0.866	-	-
Tumour CD3+ lymphocytes (low/high)	0.83 (0.38-1.79)	0.646	-	-
Stromal CD3+ lymphocytes (low/high)	0.47 (0.14-1.54)	0.213	-	-
Tumour CD8+ lymphocytes (low/high)	0.86 (0.36-2.07)	0.745	-	-
Stromal CD8+ lymphocytes (low/high)	0.98 (0.50-1.91)	0.967	-	-
Tumour FoxP3+ Tregs (absent/present)	0.04 (0-81.13)	0.419	-	-
Stromal FoxP3+ Tregs (absent/present)	0.83 (0.31-2.20)	0.711	-	-
Tumour CD68+ macrophages (low/high)	0.71 (0.40-1.26)	0.253	-	-
Stromal CD68+ macrophages (low/high)	1.39 (0.77-2.50)	0.262	-	-
Tumour CD80+ macrophages (low/high)	0.51 (0.15-1.66)	0.267	-	-
Stromal CD80+ macrophages (low/high)	0.65 (0.27-1.56)	0.339	-	-
Tumour CD163+ macrophages (low/high)	0.56 (0.07-4.13)	0.575	-	-
Stromal CD163+ macrophages (low/high)	1.95 (0.86-4.43)	0.106	-	-
Tumour CD66b+ granulocytes (low/high)	2.63 (1.22-5.67)	**0.013**	2.32 (1.07-5.01)	**0.032**
Stromal CD66b+ granulocytes (low/high)	1.11 (0.42-2.95)	0.825	-	-
TIL_score	0.95 (0.59-1.51)	0.828	-	-
SIL_score	0.85 (0.47-1.51)	0.586	-	-
Stromal subtype (n=156)				
Age (<65/>65)	1.14 (0.72-1.79)	0.557	-	-
Sex (female/male)	0.72 (0.45-1.13)	0.157	-	-
Tumour site (left/right/rectum)	1.02 (0.77-1.35)	0.871	-	-
Stage (1/2/3)	1.44 (0.97-2.14)	0.065	-	-
Differentiation (no/yes)	2.04 (1.01-4.11)	**0.044**	-	-
Vascular Invasion (absent/present)	2.13 (1.34-3.37)	**0.001**	1.30 (0.44-3.81)	0.628

	CSS		CSS	
	Univariate HR (95% CI)		Univariate HR (95% CI)	
Stromal subtype (n=156) (Cont.)				
Peritoneal Involvement (no/yes)	1.90 (1.21-2.98)	**0.005**	0.99 (0.32-3.08)	0.995
Mismatch Repair Status (competent/deficient)	0.90 (0.45-1.81)	0.778	-	-
Proliferation (low/high)	0.72 (0.43-1.18)	0.199	-	-
Tumour necrosis (low/high)	0.97 (0.58-1.61)	0.918	-	-
Tumour budding (low/high)	6.23 (3.53-11.01)	**<0.001**	11.89 (3.16-44.66)	**<0.001**
Tumour stroma percentage (low/high)	0.97 (0.94-1.00)	0.084	-	-
KM grade (weak/strong)	-	-	-	-
Tumour CD3+ lymphocytes (low/high)	0.77 (0.36-1.67)	0.524	-	-
Stromal CD3+ lymphocytes (low/high)	0.37 (0.11-1.22)	0.105	-	-
Tumour CD8+ lymphocytes (low/high)	1.07 (0.53-2.18)	0.838	-	-
Stromal CD8+ lymphocytes (low/high)	0.77 (0.39-1.51)	0.457	-	-
Tumour FoxP3+ Tregs (absent/present)	0.04 (0-2308.79)	0.581	-	-
Stromal FoxP3+ Tregs (absent/present)	0.21 (0.05-8.78)	**0.032**	0.20 (0.02-1.64)	0.136
Tumour CD68+ macrophages (low/high)	0.61 (0.37-1.01)	0.058	-	-
Stromal CD68+ macrophages (low/high)	1.42 (0.86-2.34)	0.164	-	-
Tumour CD80+ macrophages (low/high)	0.42 (0.15-1.18)	0.102	-	-
Stromal CD80+ macrophages (low/high)	0.61 (0.29-1.25)	0.180	-	-
Tumour CD163+ macrophages (low/high)	0.53 (0.16-1.72)	0.297	-	-
Stromal CD163+ macrophages (low/high)	1.72 (0.73-4.04)	0.211	-	-
Tumour CD66b+ granulocytes (low/high)	1.78 (0.85-3.73)	0.125	-	-
Stroma CD66b+ granulocytes (low/high)	2.25 (1.12-4.51)	**0.022**	0.63 (0.16-2.46)	0.510
TIL_score	0.90 (0.55-1.47)	0.691	-	-
SIL_score	0.88 (0.57-1.37)	0.596	-	-

HR=Hazard ratio, CI=Confidence intervals

4.4 Discussion

This study examined the relationship between CRC phenotypic subtypes and the prognosis of immune cells infiltration in tumour cell nests and tumour stroma. The results revealed that each subtype has differing immune cell compositions that impact on patient's prognosis. Immune subtype is mainly composed of T-lymphocytes and obtained highest survival rate. Canonical subtype has significantly increased of macrophages giving an intermediate survival rate. Whereas the latent and stromal subtypes have decreased levels of all immune cell types in tumour cell nests, but not in tumour stroma and possess the poorest survival. The univariate survival analysis suggested cytotoxic T-lymphocytes, Tregs, and granulocytes are significantly associated with patient's survival in each subtype. Furthermore, the multivariate analysis designated tumour granulocytes as independently prognostic for the latent subtype. Therefore, the immune and latent subtypes may be potential targets populations for immune-based therapies.

The CRC consensus molecular subtypes (CMS1-CMS4) and immune classifications are widely recognised today. However, due to the problems of adjuvant chemotherapy resistance, and

immunotherapy could benefit dMMR or MSI-High patients but still low response rate; therefore, has yet to applied to all CRC patients. In addition, due to the difficulties of translating transcriptomics into all routine clinical setting; therefore, CRC classification and the role of immune cells are needed to categorize patients and benefit their personalized therapy. Thus, the integration of CRC molecular classifications, immune cells signatures, and stromal compartment were proposed by many studies.

Becht et al. proposed the correlation between molecular subgroups and tumour microenvironment utilized transcriptomics of immune cells, fibroblast, and angiogenic microenvironment. They found good prognosis in CMS1, which had overexpression of genes for cytotoxic T-lymphocytes; and poor prognosis in CMS4, which expressed lymphocytes and monocytic origin cells, whereas CMS2 and CMS3 contained low immune and inflammatory signatures with intermediate prognosis (Becht et al., 2016). Soldevilla et al. proposed the immune subtypes by utilized transcriptomics and assessed the correlation with the consensus molecular subtypes. The five immune subtypes were observed in CRC, C1 77% (wound healing), C2 17% (IFN-gamma dominant), C3 7% (inflammatory), C4 4% (lymphocytes depleted), C6 2.3% (TGF-beta dominant). CMS1 found mainly C2, which increased CD4, CD8, Tregs, neutrophils, and M1/M2 polarisation; while CMS2 dominant for C1, CMS3 had highest C3 and C4, whereas CMS4 contained had C6 representation. From the application of complete immune characteristics, they reported this classification better prognosis than CMS system (Soldevilla et al., 2019). In addition, Chen et al. performed molecular subtyping to determine immune subtypes for immune checkpoint inhibitors treatment. They identified as low-risk and high-risk subtypes due to the significantly differ prognosis. The low-risk subtype presented high overall survival rate, which contain high PD-L1 mRNA expression, high proportion of TILs and tumour mutation burden. Also, the pathway analysis found the association to an activation of immune response, and antigen processing and presentation signalling pathways (Chen et al., 2020). In addition, the classifications based on the correlations between CMSs and other characteristics have been proposed, i.e., genome-scale DNA methylation (Fennell et al., 2019), gene expression microarray of stromal compartment (Shen et al., 2020), gene expression of metabolism-related genes (Lin et al., 2021).

Apart from CRC disease classification, the relapse prediction also has been proposed from the immune infiltration estimation in tumour utilising gene expression profiles. They compared immune cells, innate and adaptive immune cells, performance with molecular subtypes and found that immune infiltration superior to predict disease relapse than CMSs or clinical characteristics alone (Kamal et al., 2021). From the studies point out to CMS1 and CMS4 into interest as they have clearly distinct prognosis, and for therapy which is in line with others (Rodriguez-Salas et al., 2017), including our present finding for immune and latent subtypes. From these studies, although CMS

classification still being the main CRC subtypes, however, immune signatures are in the rising interest for alternative subtyping tools for more details of patient's immune status which could feasibly translate to clinical setting and benefit immune-based therapy. However, clearly, and well-defined phenotypes is needed for clinical practice.

The relationship between phenotypic subtypes, immune cells and survival were investigated. For the immune subtype, strong tumour $CD3^+$ and strong stromal $FoxP3^+$ Tregs were significantly improved CSS, suggesting the high survival rate of this subtype may be due to the high T-lymphocytes populations. This suggest that apart from cytotoxic T-lymphocytes which is the main effector cells in immune subtype, regulatory T-lymphocytes have a role in tumour stroma to cooperate with other cell types and benefit patient's CSS in immune subtype resulting in the best prognosis. Improved prognosis due to a strong T-lymphocyte infiltration has been proposed in multiple cancers (Braha et al., 2016; Gao et al., 2007). Whereas in canonical subtype presented strong tumour $CD8^+$ cytotoxic T-lymphocytes significantly improved CSS. This might suggest that canonical subtype have good prognosis due to high cytotoxic T-lymphocytes (Gao et al., 2007; Ohtani, 2007). As for latent subtype, high $CD66b^+$ granulocytes infiltration significantly decreased CSS, and this could be independent prognostic factor for this subtype.

The prognostic value of tumour associated neutrophils (Liu et al.) is also controversial with studies reporting both good and poor prognosis in CRC. Rao et al. (2012) observed that neutrophils increase within the tumour microenvironment and independently associate with CRC malignancy and low survival rate in CRC patients (Rao et al., 2012). Stromal subtype presented high stromal $Foxp3^+$ Tregs could significantly improve CSS; on the other hand, high stromal $CD66b^+$ granulocytes significantly decreased CSS. As Tregs are well recognised as an inhibitor of cytotoxic T-lymphocytes function, and maintain stability of the local immune response, conveying a poor prognosis in solid tumours such as breast cancer, however, in CRC they have been shown to convey a good prognosis (Ling et al., 2014). However, with high numbers of granulocytes might trigger Tregs role turning into negative result which cause poor prognosis in stromal subtype. The role of neutrophils to Tregs was proposed by Mishalian et al. that neutrophils recruit Tregs to tumour cell nests by secreting CCL17, which Tregs then inhibit antitumour immunity and promote tumour growth in mice, and this could occur in human as well (Mishalian et al., 2014). Therefore, this brought stromal subtype into interest as it has the worse prognosis subtype. There's a study proposed that tumour neutrophils could suppress tumour infiltrating T-lymphocytes proliferation by expressing genes associated with T-lymphocytes suppression in mice (Germann et al., 2020). Thus, granulocytes might have a distinct role in tumour cell nests and tumour stroma. This might result from myeloid cells present mainly

pro-tumour function, but less anti-tumour function or even enhance T-lymphocytes suppression role of Tregs in stromal subtype leading to the worse prognosis.

As for tumour-associated macrophages (TAM) within tumour microenvironment, thought to drive pro-tumorigenic effects (Kim & Bae, 2016). However, the prognostic role of myeloid cells within the tumour microenvironment is controversial with some studies suggested they enhance tumour progression and others proposed improved patient's survival (Elliott et al., 2017; Powell & Huttenlocher, 2016). This study found no significant of all macrophage's markers in patients CSS to any phenotypic subtypes.

In conclusion, present finding suggests that subtypes with high T-lymphocyte infiltration in both tumour cell nests, and tumour stroma have the best prognosis as seen in the immune subtype, whereas the canonical subtype that has high macrophages presented a slightly reduced prognosis. However, subtypes that have high granulocytes infiltrates and low lymphocyte infiltrates in cancer cell nests lead to a poor prognosis, as seen in the latent and stromal subtypes. Therefore, the immune, latent, and stromal subtypes might represent a population of patients for immune-based therapy. However, the limitation of this study was a small sample numbers of each phenotypic subtype which can affect the results. Therefore, validation in larger cohort with more cases for each subtype is required to strengthen the analysis. Overall, this study suggest that phenotypic subtype can be alternative tools for CRC classification due to different immune cell compositions for each subtype. Understanding the different genetic backgrounds of these immune landscapes, may provide novel biomarkers for each subtype.

Chapter 5 Mutational profiling of innate and adaptive immune cell landscapes in CRC patients

5.1 Background

Cancer is recognized as a genetic disease which is an evolutionary process developed as a result of accumulated alterations in the DNA sequence of cancer cells genome over the lifetime of patients (Stratton et al., 2009). The accumulation processes can be based on random intrinsic mutations which are continuously heritable from genetic variations occurring during cell division (Stratton et al., 2009). In general, somatic mutations of 33-66 genes on average would be expected to alter proteins in solid tumours such as breast, and colon (Vogelstein et al., 2013). Theses cancer genome mutations may comprise of distinct classes of alterations in the DNA sequence of a genes including nucleotide substitution (95%), deletions or insertions. Nucleotide substitutions, mainly present as missense mutation (90.7%), nonsense mutation (7.6%), and alterations of splice sites or untranslated regions adjacent to start and stop codon (1.7%) (Vogelstein et al., 2013).

Today, tumour mutation burden is at the forefront of research to observe the impact of somatic mutations in combination with immune cells infiltrate on patient's prognosis and response to immunotherapy in many types of cancer, i.e., advanced gastric cancer (Guo et al., 2021), and CRC (Zhou et al., 2021). Therefore, identification of genetic mutations in CRC associated with immune cells infiltration that impact patient prognosis could be of benefit as a biomarker or target for immune-based therapy.

The objective of this study was to assess mutational profiles, in CRC patients with stage I-III disease, utilising the four immune landscape grouping from chapter 3. To identify any significantly differentially mutated gene(s) specific to each group, which could be a prognostic marker for that specific group and could potentially influence a patient response to immune-based therapy.

5.2 Methods

Whole genome mutational profiling was performed on a subset of patients from the Scottish cohort (n=252). DNA was extracted from bulk tumour FFPE sections and mutational profiling performed using a 150-cancer specific array by GPOL for a previous study. Data was subsequently available for analysis within this thesis. M2aftools packages version 2.6.05 within R-studio version 4.0.5 was utilised. For visualization, *plotmafSummay* was applied to observe the summary of mutational burden of each group, and *coBarPlot* was utilized for the comparison between groups, respectively. As for the analysis, *mafCompare* function was utilized to compare the significant differentially mutated genes among two groups (Mayakonda et al., 2018). The data were first analysed for an overview mutation of all samples and each immune landscape group. Then the comparison between groups was generated to observe the differences of highly mutated genes in each group. Genes which presented significance differentially mutated in any group were then compared to the same group in tumour stroma to assess the differences mutation frequency between tumour cell nests and tumour stroma. Then one of the most significances differentially mutated gene was selected to investigate at the protein expression level using IHC staining and the histoscore method. Cut-offs were made utilising maximal rank statistics. The protein expression was compared to the mutational results then analysed in terms of CSS in the full cohort and stratified for mutational status or immune cell infiltrate, and for association with immune cells infiltrations utilising SPSS.

5.3 Results

135 samples were available to analyse for the mutational profiles in tumour cell nests of stage I-III CRC patients from the Scottish Cohort.

5.3.1 Summary of somatic mutations in tumour cell nests in a subset of Glasgow Cohort CRC patients

In general, for the randomly selected 135 patients, missense mutations were the most frequent classification of mutations (**Figure 5.1 A, E**). As for types of mutations, single nucleotide polymorphisms (SNP) presented at the highest frequency compared to deletions (DEL) and insertions (INS) (**Figure 5.1 B**). Furthermore, C > T was the main type of single nucleotide variant classification (SNV) (**Figure 5.1 C**). The median number of mutations per sample was six (**Figure 5.1 D**). The top 10 mutated genes among the samples including *APC* (51%), *TP53* (46%), *KRAS* (31%), *AR* (22%), *RNF43* (17%), *ARID1A* (15%), *FBXW7* (15%), *ATM* (13%), *PIK3CA* (13%), and *ATR* (13%) (**Figure 5.1 F**).

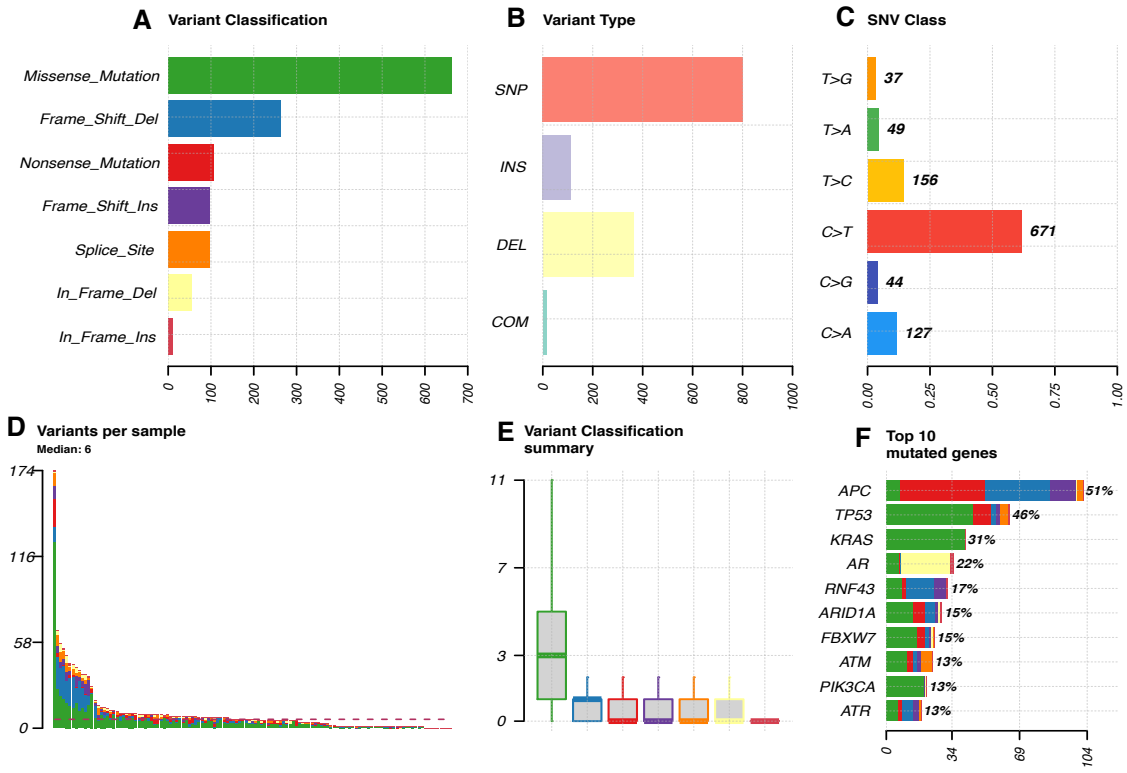

Figure 5.1- Summary of somatic mutational profiles in tumour cell nests in stage I-III CRC Scottish cohort (n=135); A. classification of mutation frequency, **B.** mutational variant type frequency, **C.** SNV class frequency, **D.** level of mutational variants per sample, **E.** summary of variants classification level, **F.** summary of top 10 mutated genes

5.3.2 Summary of somatic mutations in tumour immune landscape groups

Next, summaries of mutations for the four immune landscape groups were analysed into four groups, T-cells high (N=2), myeloid high (N=85), both high (N=33), and both low (N=15).

5.3.2.1 T-cells high

For T-cell high, missense mutations were the most frequent classification of mutations (**Figure 5.2 A, E**) and single nucleotide polymorphisms (SNP) presented at the highest frequency for mutation variant type (**Figure 5.2 B**). Again, C > T was the main type of single nucleotide variant classification (SNV) (**Figure 5.2 C**). The median number of variants per sample was 14.5 suggesting potential hypermutation status (**Figure 5.2 D**). As for the top 10 mutated genes, these were *ASXL1* (100%), *ERBB4* (100%), *CTCF* (50%), *CREBBP* (50%), *BRCA2* (50%), *BLM* (50%), *ATM* (50%), *AR* (50%), *APC* (50%), and *ALK* (50%) (**Figure 5.2 F**). Sample numbers were low with only two patients in the group, therefore more patient samples are needed to make any conclusions from this data.

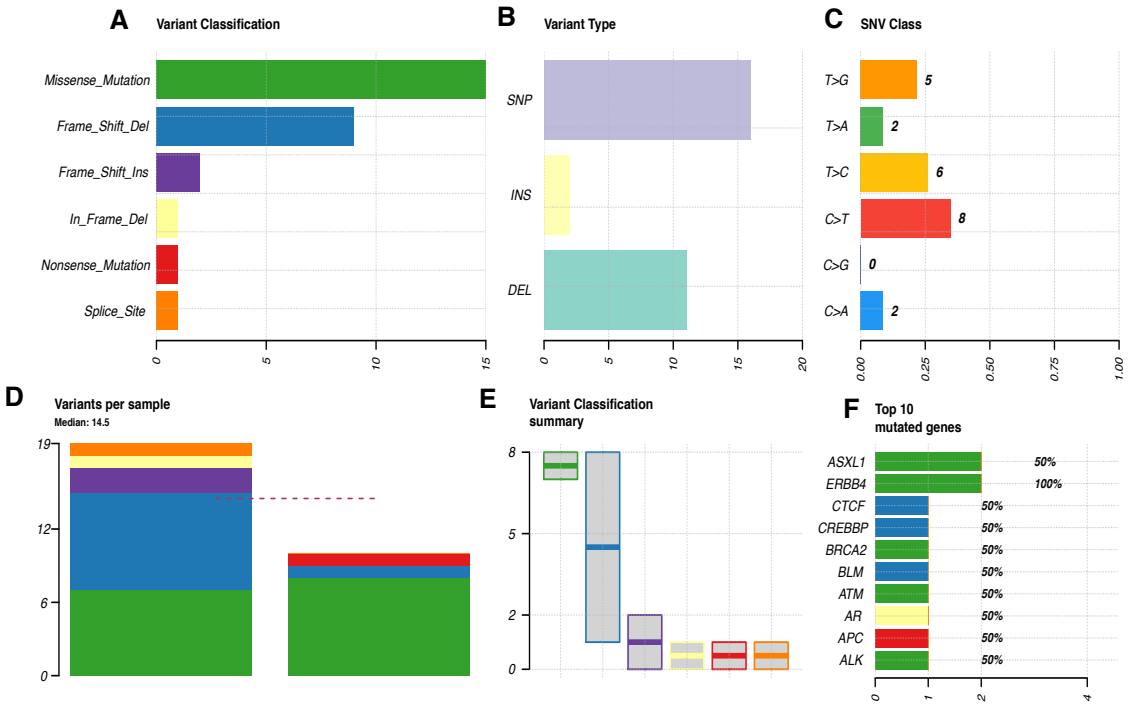

Figure 5.2 - Summary of somatic mutational profiles in T-cells high group in tumour cell nests in stage I-III CRC Scottish cohort (n=2); A. classification of mutation frequency, **B.** mutational variant type frequency, **C.** SNV class frequency, **D.** level of mutational variants per sample, **E.** summary of variants classification level, **F.** summary of top 10 mutated genes.

5.3.2.2 Myeloid high

As for myeloid high group, missense mutations were still the most frequent classification of mutations (**Figure 5.3 A, E**), and single nucleotide polymorphisms (SNP) still presented as the highest frequency of mutation variant type (**Figure 5.3 B**). C > T was still the main type of single nucleotide variant classification (SNV) (**Figure 5.3 C**). The median number of variants per sample was 7 (**Figure 5.3 D**). The top 10 mutated genes included *APC* (62%), *TP53* (60%), *KRAS* (40%), *FBXW7* (24%), *ARID1A* (24%), *AR* (24%), *ALK* (20%), *PIK3CA* (16%), *ASXL1* (18%), and *SMAD4* (18%) (**Figure 5.3 F**).

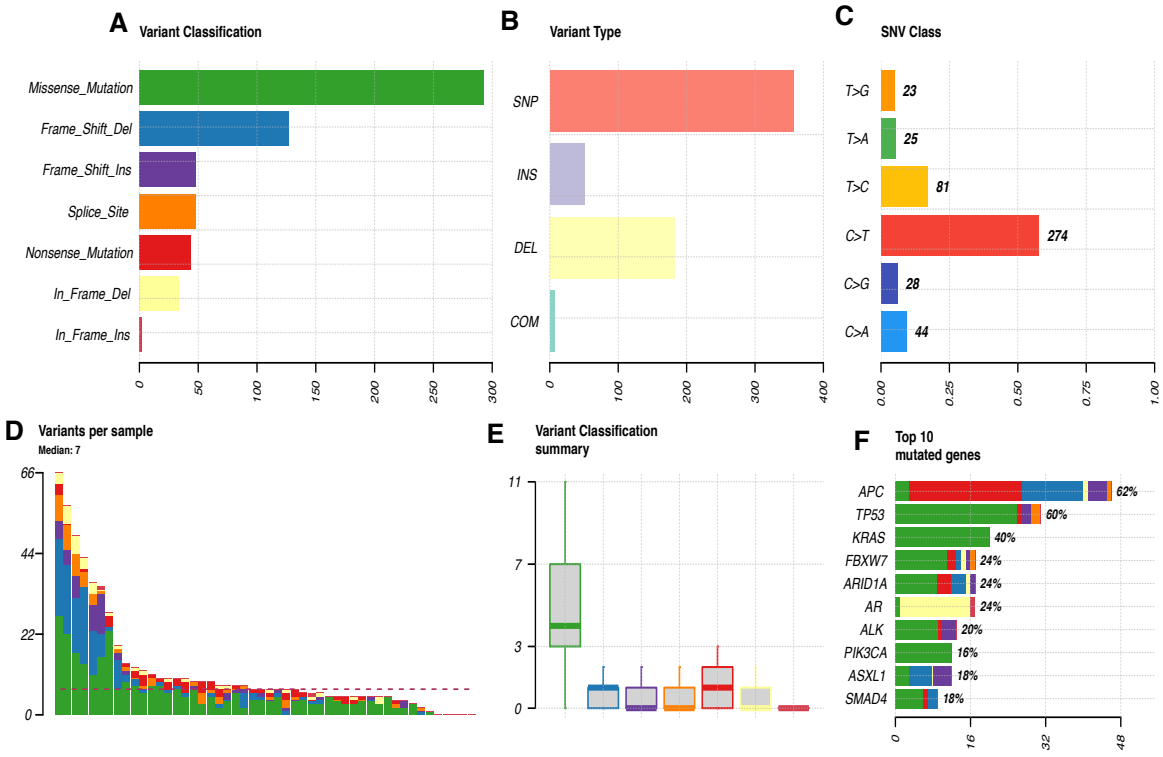

Figure 5.3 - Summary of somatic mutational profiles in myeloid cells high group in tumour cell nests in stage I-III CRC Scottish cohort (n=85); A. classification of mutation frequency, **B.** mutational variant type frequency, **C.** SNV class frequency, **D.** level of mutational variants per sample, **E.** summary of variants classification level, **F.** summary of top 10 mutated genes.

5.3.2.3 Both high

As for both high group, missense mutations were also the most frequent classification of mutations (**Figure 5.4 A, E**) and single nucleotide polymorphisms (SNP) presented at the highest frequency of mutation type (**Figure 5.4 B**). Again, C > T was the main type of single nucleotide variant classification (SNV) (**Figure 5.4 C**). The median number of variants per sample was 7 (**Figure 5.4 D**). The top 10 mutated genes included *APC* (64%), *TP53* (55%), *FBXW7* (30%), *ARID1A* (27%), *MSH2* (15%), *AR* (21%), *KRAS* (33%), *NOTCH1* (15%), *ASXL1* (15%), and *ATR* (18%), respectively (**Figure 5.4 F**).

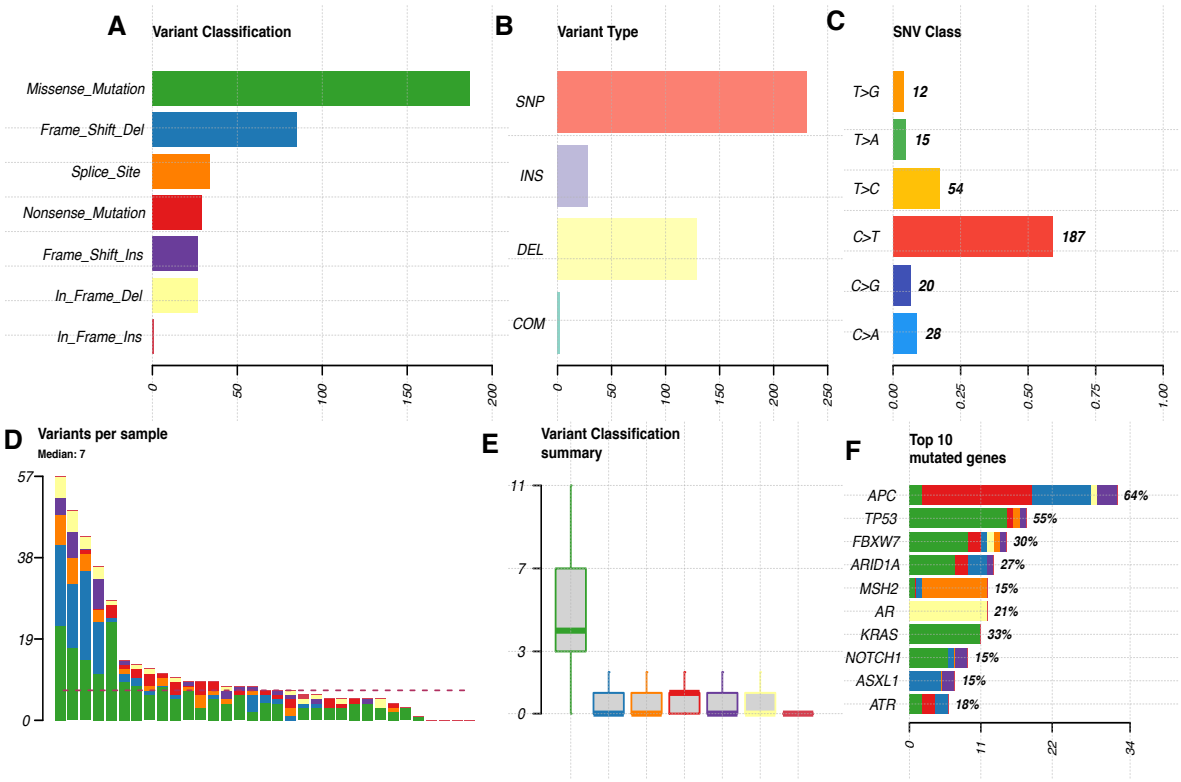

Figure 5.4 - Summary of somatic mutational profiles in both high group in tumour cell nest in stage I-III CRC Scottish cohort (n=33); A. classification of mutation frequency, **B.** mutational variant type frequency, **C.** SNV class frequency, **D.** level of mutational variants per sample, **E.** summary of variants classification level, **F.** summary of top 10 mutated genes.

5.3.2.4 Both Low

For the both low group, missense mutations were also the most frequent classification of mutations (**Figure 5.5 A, E**) and single nucleotide polymorphisms (SNP) presented at the highest frequency for mutation type (**Figure 5.5 B**). C > T was the main type of single nucleotide variant classification (SNV) (**Figure 5.5 C**). The median number of variants per sample was 7 (**Figure 5.5 D**). The top 10 mutated genes included *APC* (60%), *TP53* (73%), *KRAS* (53%), *ALK* (27%), *PIK3CA* (20%), *BRCA2* (20%), *ARID1A* (20%), *SMAD4* (27%), *AR* (27%), and *ASXL1* (20%), respectively (**Figure 5.5 F**).

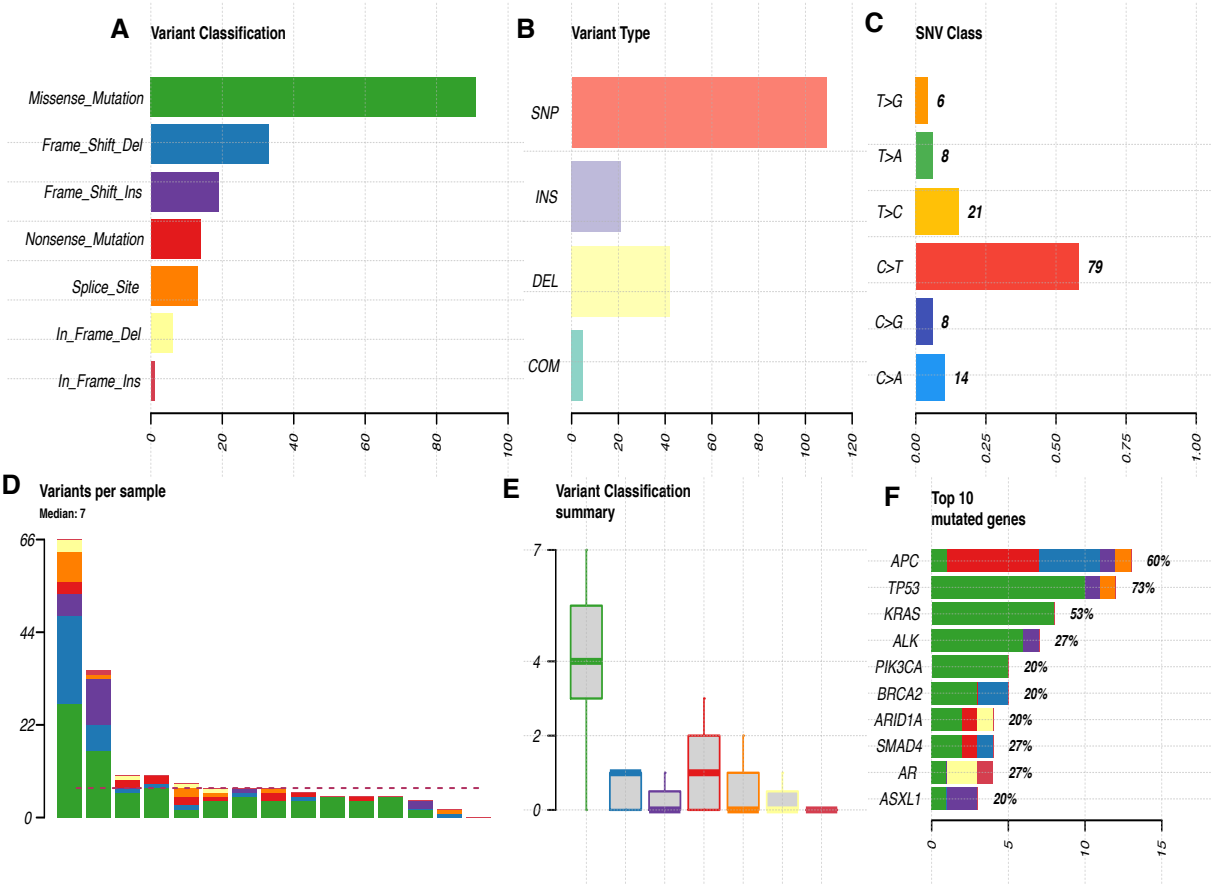

Figure 5.5 - Summary of somatic mutational profiles in both low group in tumour cell nests in stage I-III CRC Scottish cohort (n=15); A. classification of mutation frequency, **B.** mutational variant type frequency, **C.** SNV class frequency, **D.** level of mutational variants per sample, **E.** summary of variants classification level, **F.** summary of top 10 mutated genes.

5.3.3 Differentially mutated genes between tumour immune landscape groups

Next, to identify any differentially mutated genes between tumour immune landscape groups, comparisons between each group and all other samples were assessed. Fisher's exact tests were performed, and the results were visualised as co-bar plots to observe if any differentially mutated genes reached significance for a specific group.

5.3.3.1 T-cells high vs Others

Almost all 10 genes presented as highly mutated in T-cells high patients than in the others group including *ALK*, *AR*, *ATM*, *BLM*, *BRCA2*, *CREBBP*, *CTCF*, *ERBB4*, *ASXL1*, and *APC*. Among these, *ERBB4* was the only significantly differentially mutated gene, which present in 100% in T-cells high with only missense mutations, and 7% in other patients with a combinations of variant classes (**p<0.01) (**Figure 5.6**). Again, due to the low numbers of patients within T-cell high group (n=2) these results should be validated in a larger cohort.

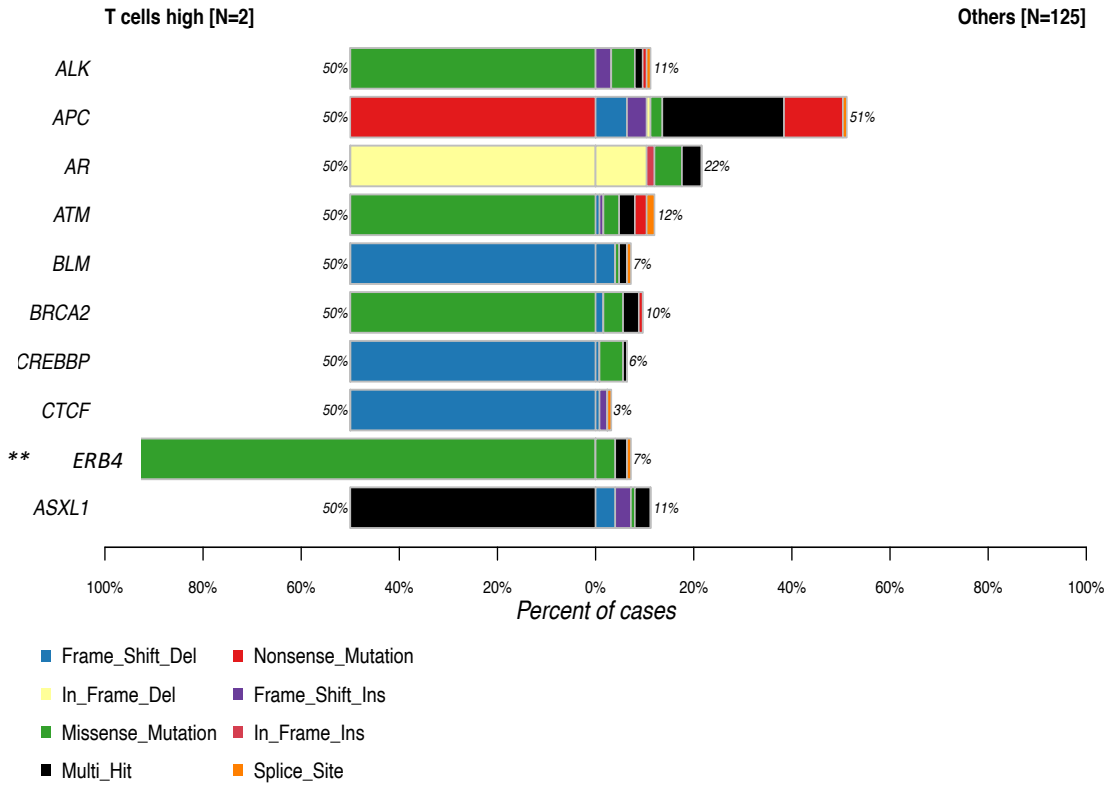

Figure 5.6 - Co-bar plot of top 10 mutated genes in T-cells high vs others; Among top 10 mutated genes, *ERBB4* is a differentially mutated gene 100% in T-lymphocytes high, and 7% in others (**p<0.01).

5.3.3.2 Myeloid cells high vs Others

Among the top 10 mutated genes, six were significantly differentially mutated including *SMAD4*, *ALK*, *ARID1A*, *FBXW7*, *TP53*, and *APC*. For all six genes, mutations were lower in the myeloid high group than the others group. Among these, *TP53* was the most significantly differentially mutated gene which presented in 34% of myeloid high patients, whereas 60% of patients in others group had a mutation in *TP53* (***p*<0.01) (**Figure 5.7**).

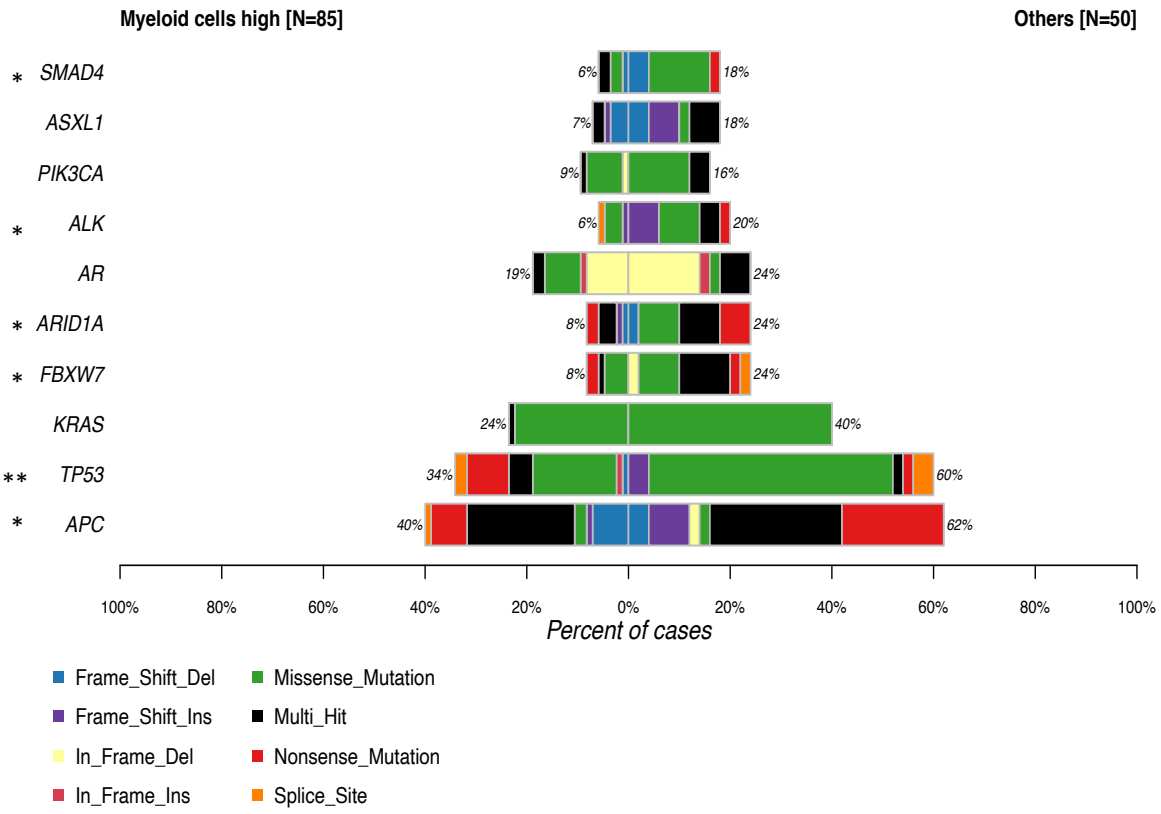

Figure 5.7 - Co-bar plot of top 10 mutated genes in myeloid cells high vs others; Among top 10 mutated genes, *TP53* is the most significance differentially mutated gene which presented in 34% of myeloid cells high, and 60% of others (***p*<0.01, **p*<0.05).

5.3.3.3 Both high vs Others

Among top 14 mutated genes, five were significantly differentially mutated including *BRCA1, MTOR, ARID1A, B2M*, and *FBXW7*. All five genes presented with more mutations in the both high group than the others group. Among these, *FBXW7* was the most significance differentially mutated gene which present in 30% of patients in both high group, and 9% of patients in others group (**p<0.01) (**Figure 5.8**).

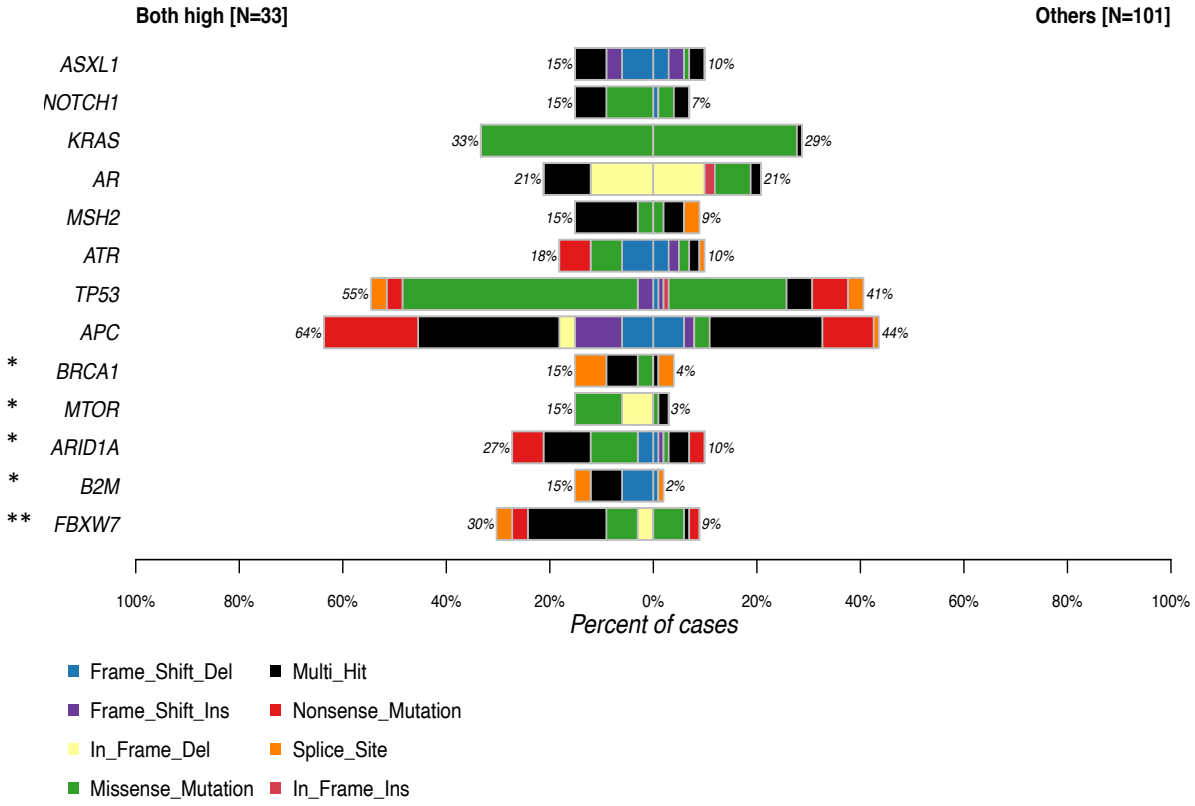

Figure 5.8 - Co-bar plot of top 10 mutated genes in both high vs others; Among top mutated genes, *FBXW7* is the most significance differentially mutated gene which presented in 30% of both high group, and 9% in others (**p<0.01, *p<0.05).

5.3.3.4 Both low vs Others

All the 10 mutated genes including *ASXL1*, *AR*, *SMAD4*, *ARID1A*, *BRCA2*, *PIK3CA*, *ALK*, *KRAS, TP53,* and *APC*, presented with more mutations in the both low group than the others group. Among these, *TP53* was the only significantly differentially mutated gene which presented in 73% of patients in both low group, and in 42% of other patients (*p<0.05) (**Figure 5.9**).

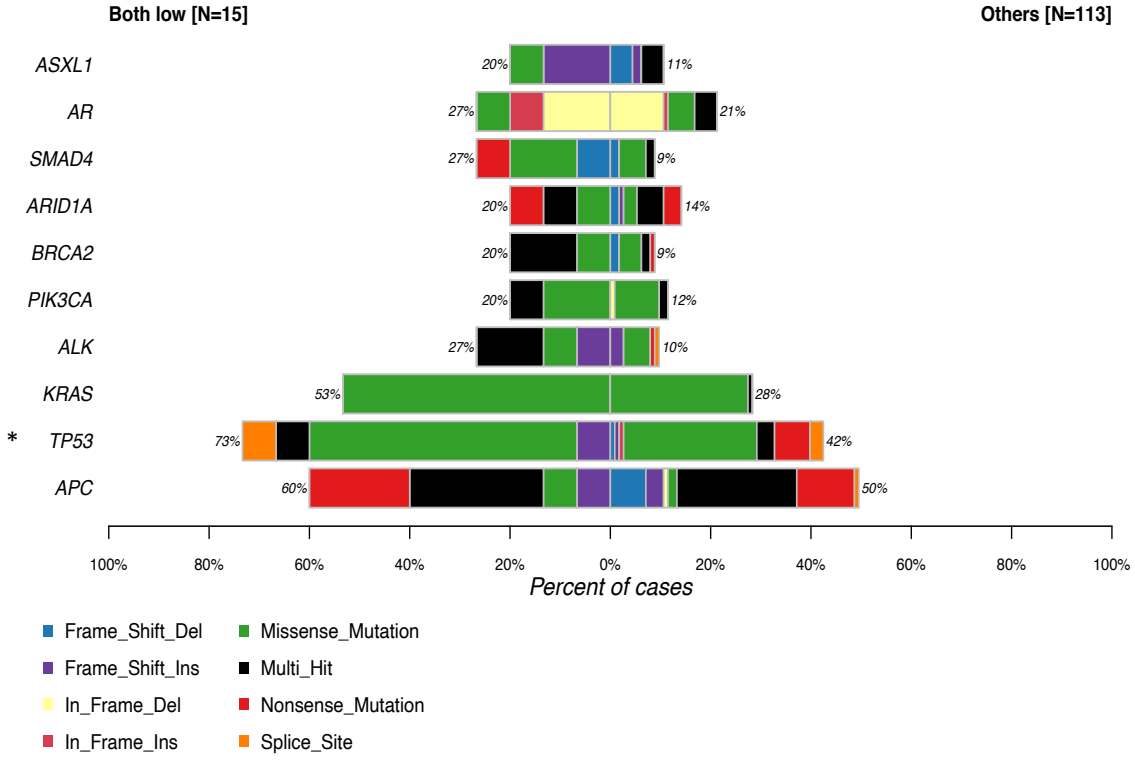

Figure 5.9 - Co-bar plot of top 10 mutated genes in both low vs others; Among top 10 mutated genes, *TP53* is the most significance differentially mutated gene which presented in 73% of both low group, and 42% in others (*p<0.05).

5.3.4 Comparison of differentially mutated genes between myeloid high groups and the other three immune landscape groups

From the comparison among immune landscape groups, interestingly, the myeloid high group had a much lower level of mutations compared to all other patients especially for *TP53*. To look at this in more detail, comparisons between the myeloid high group and the three other individual groups was performed to see whether this low mutation rate in myeloid high patients held out when compared to the other individual immune landscapes and assess if *TP53* was still highly significant.

5.3.4.1 Myeloid high vs T-cells high

The top 16 mutated genes between myeloid high and T-cells high groups were selected for comparison. These included *SMAD4*, *PIK3CA*, *ARID1A*, *FBXW7*, *KRAS*, *TP53*, *ALK*, *APC*, *AR*, *ATM*, *BLM*, *BRCA2*, *CREBBP*, *CTCF*, *ERBB4*, and *ASXL1*. No significantly differentially mutated genes were observed, which might be due to small number of T-cells high patients within the analysis, therefore, more patient samples are needed to make any conclusions. Overall, mutations were more frequent in the T-cells high group when comparison to the myeloid high group (**Figure 5.9**).

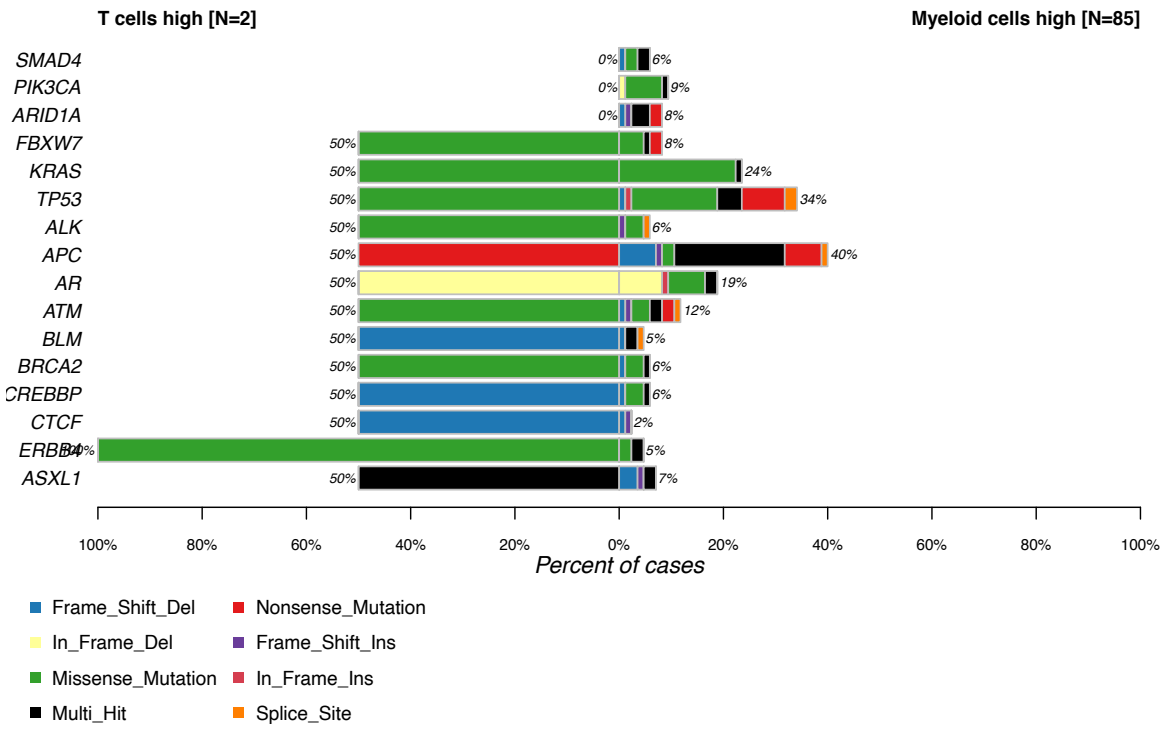

Figure 5.10 - Co-bar plot of top mutated genes in myeloid cells high vs T-cells high. Among top mutated genes, no significance differentially mutated genes were presented.

5.3.4.2 Myeloid high vs Both high

Next, the top 13 mutated genes from myeloid high and both high groups were selected for comparison. Three genes were significantly differentially mutated including *ARID1A*, *FBXW7*, and *APC*. All three genes presented at a lower frequency in the myeloid high group than the both high group. *FBXW7* was the most significantly differentially mutated gene which presented at 30% in the both high patients and 8% in the myeloid high patients (**p<0.01) (**Figure 5.10**).

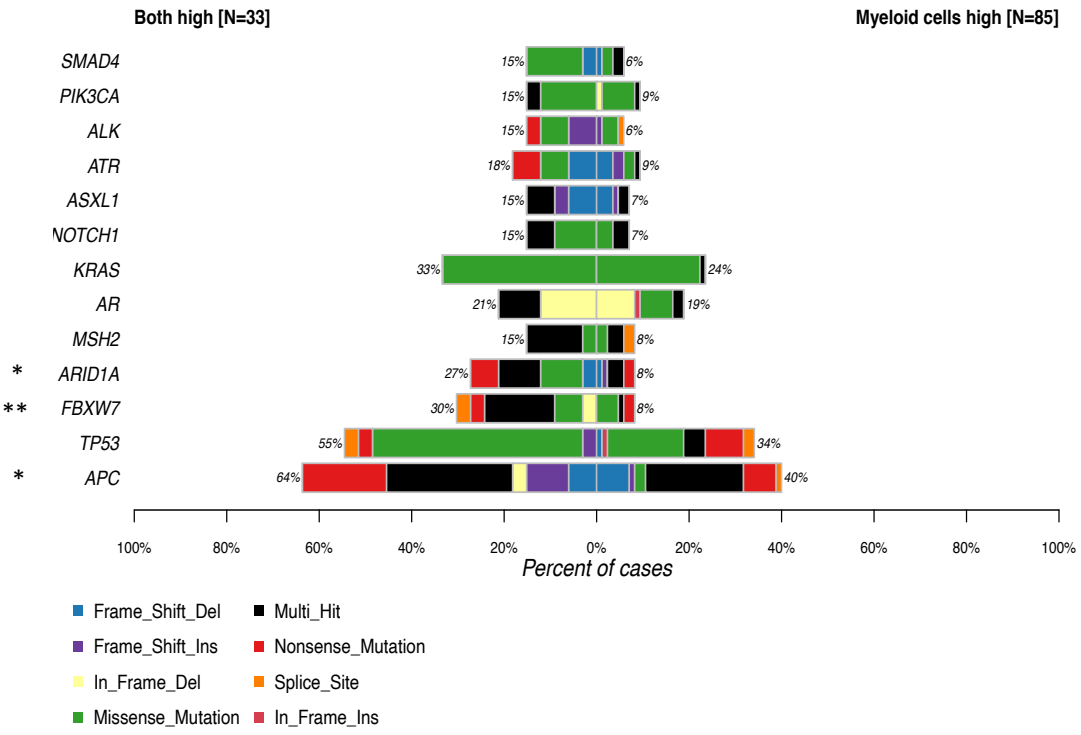

Figure 5.11 - Co-bar plot of top mutated genes in myeloid cells high vs both high. Among top mutated genes, *FBXW7* was the most significance differentially mutated gene which presented in 30% of both high patients, and 8% in myeloid cells high group (**p<0.01), followed by *APC*, and *ARID1A* (*p<0.05).

5.3.4.3 Myeloid cells high vs Both low

The top 11 mutated genes from the myeloid high and the both low groups were selected for comparison. Four genes were significantly differentially mutated including *SMAD4*, *AR*, *KRAS*, and *TP53*. All four genes were presented at a lower frequency in the myeloid high group but enriched in both low group. *TP53* was the most significantly differentially mutated gene which presented in 34% of the myeloid high group and 73% of the both low group (**p<0.01) (**Figure 5.11**).

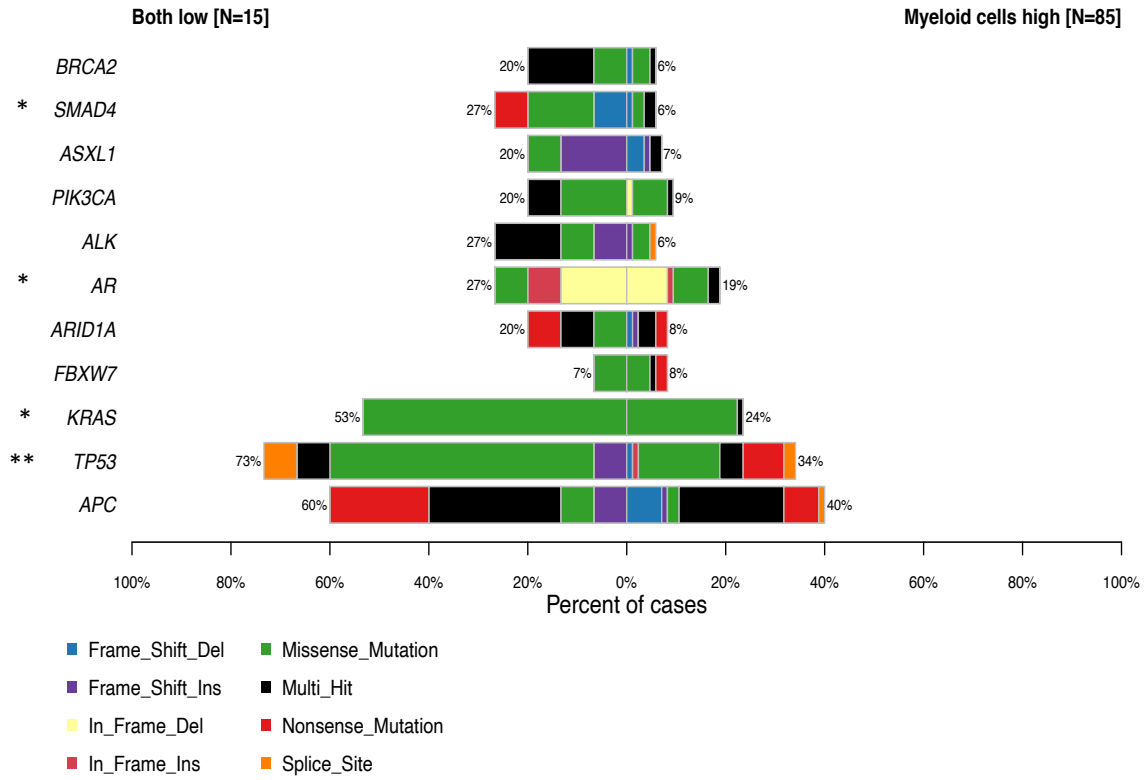

Figure 5.12 - Co-bar plot of top mutated genes in myeloid cells high vs both low; Among top mutated genes, *TP53* is the most significance differentially mutated gene which presented in 73% of both low patients, and 34% of myeloid cells high patients (**p<0.01).

5.3.5 Comparison of differentially mutated genes between myeloid high in tumour cell nests and tumour stroma

From the previous comparison, it was clear that the myeloid high group was harbouring significantly less mutations than the other groups. Interestingly, although *TP53* was one of the tops differentially mutated genes in all comparisons, it only reached significance when compared to the both low group. Therefore, the next step was to compare mutations within myeloid high group in tumour cell nests and tumour stroma to see whether there is a difference between these cells being present in the two locations. The top five significantly differentially mutated genes between the tumour cell nests and tumour stroma of patents classified as myeloid high were *BRCA2*, *KRAS*, *SMAD4*, *APC*, and *TP53*. All five genes were more highly mutated in samples with high myeloid cells in stroma when compared to samples with high myeloid cells in the tumour cell nests. Interestingly, *TP53* mutations was clearly the most significantly differentially mutated gene which presented with low mutations in the group with high myeloid cells in tumour cell nests (34%), whereas it was highly enriched (65%) in the group with high myeloid cells in tumour stroma (***p<0.001) (**Figure 5.12**). Therefore, *TP53* mutations seems to be connected to myeloid cell infiltration into tumour stroma rather than tumour cell nests.

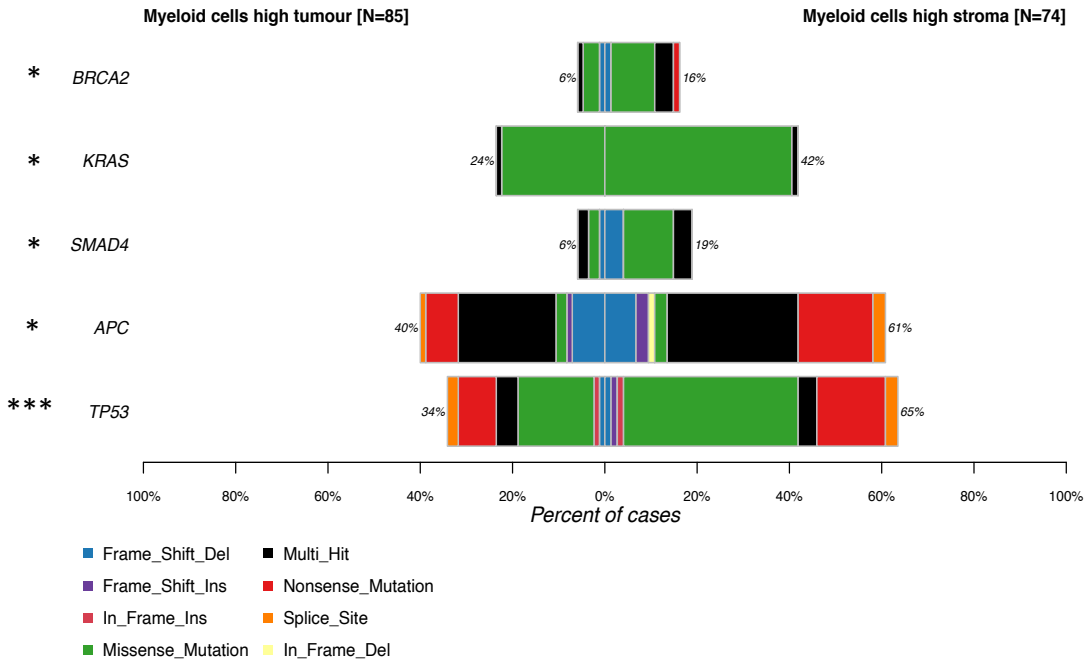

Figure 5.13 - Co-bar plot of top 5 mutated genes in myeloid cells high in tumour cell nests vs tumour stroma; Among top mutated genes, *TP53* was the most significance differentially mutated gene which presented low mutations in tumour cell nests (34%), but more mutations presented in tumour stroma (65%) (***p<0.001).

5.3.6 IHC for p53 expression

Given *TP53* mutations was the most significantly differentially mutated gene in myeloid high patients, and this was associated with stromal infiltration, protein expression of p53 was assessed for nuclear tumour expression. IHC for p53 expression was performed to observe the relationship between *TP53* mutation and its proteins p53 expression in our CRC patient's cohort with stage I-III disease (N=638). Among these patients, 111 (17%) patients carried *TP53* mutations, 84 (13%) patients presented no *TP53* mutations, and 443 (70%) patients with no mutation data available.

5.3.7 ICCC and cut-off point of nuclear p53 IHC in the full cohort

Correlation between the two nuclear p53 IHC scoring markers was performed. The standard ICCC testing exhibited great correlation between the two scorers (ICCC=0.965) (**Figure 5.13 A**). Bland-Altmann plot showed no differences out with 50 weighted histoscores **(Figure 5.13 B)**. The cut-off point was generated by maximal rank statistical analysis (142.5) based on patients CSS (**Figure 5.13 C**).

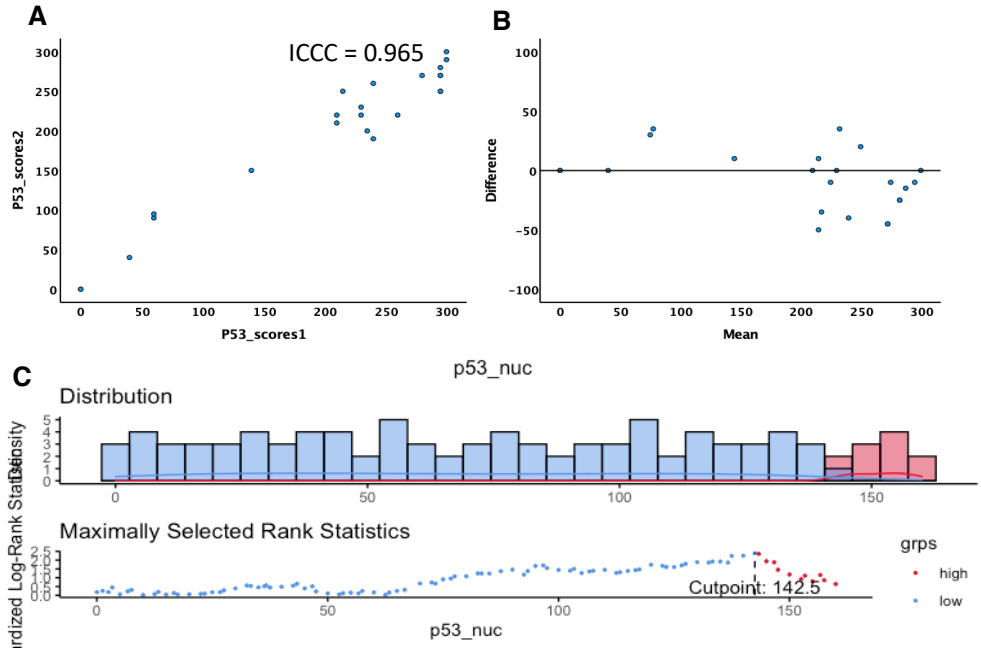

Figure 5.14 - ICCC, scatter plot, Bland-Altman plot of nuclear p53 expression in stage I-III CRC Scottish cohort TMAs (n=930); **A**. ICCC 0.965 and scatter plot, **B**. Bland-Altman plot, **C**. cut-off value 142.5

5.3.8 Correlation between TP53 mutations and p53 protein expression

A box plot comparing *TP53* mutation status and nuclear p53 expression level in the tumour was performed. Patients carrying *TP53* mutated had significantly increased p53 nuclear expression when compared to patients who has wild-type *TP53* (***p<0.001) (**Figure 5.14**).

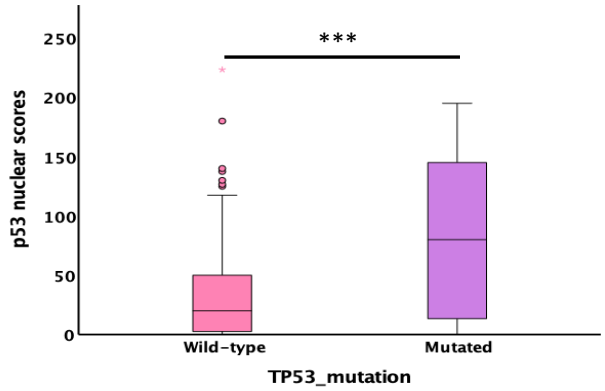

Figure 5.15 - Correlation between *TP53* mutations and p53 nuclear expression in stage I-III CRC Scottish cohort (n=930); Patients who carrying *TP53* mutations also presented significant increased p53 nuclear expression level when compared to wild type *TP53*(***p<0.001).

5.3.9 Survival analysis of nuclear p53 expression and CSS

The relationship between p53 nuclear expression and CSS was performed by KM plot and log-rank analysis. High p53 nuclear expression was associated with significantly improved CSS (HR 0.54, 95% CI 0.33-0.87, *p*=0.010, **Figure 5.15**) as expected from the role of p53 as a tumour suppressor.

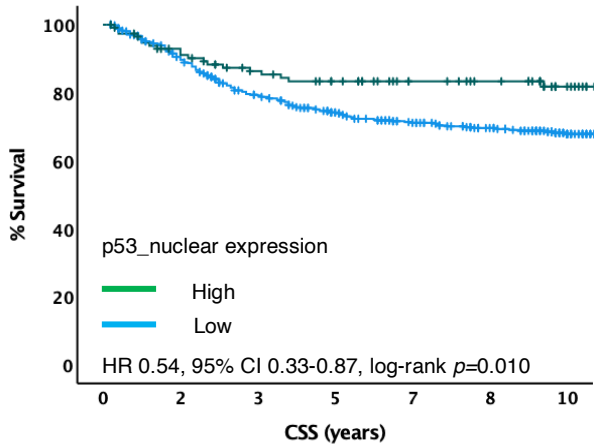

Figure 5.16 - KM plot of p53 nuclear expression and CSS (% survival at 10 years) in stage I-III CRC Scottish cohort (n=930). High p53 nuclear expression was significantly associated with improved CSS (*p*=0.010).

5.3.10 Nuclear p53 expression and CSS in TP53 mutated and TP53 wild type

Next, to observe whether there is a difference in nuclear p53 prognostic value for CSS if patients are carrying *TP53* mutations or are *TP53* wild-type, patients were stratified for mutational status. In *TP53* mutated patients, high p53 nuclear expression was significant associated with improved CSS (HR 0.40, 95% CI 0.18-0.89, *p*=0.016) (**Figure 5.16**). No significant difference was seen for wild-type patients, but this may be due to the low numbers of patients with high expression in this group. Therefore, *TP53* mutations are significantly correlated with high p53 nuclear expressions which associates with increased patient survival.

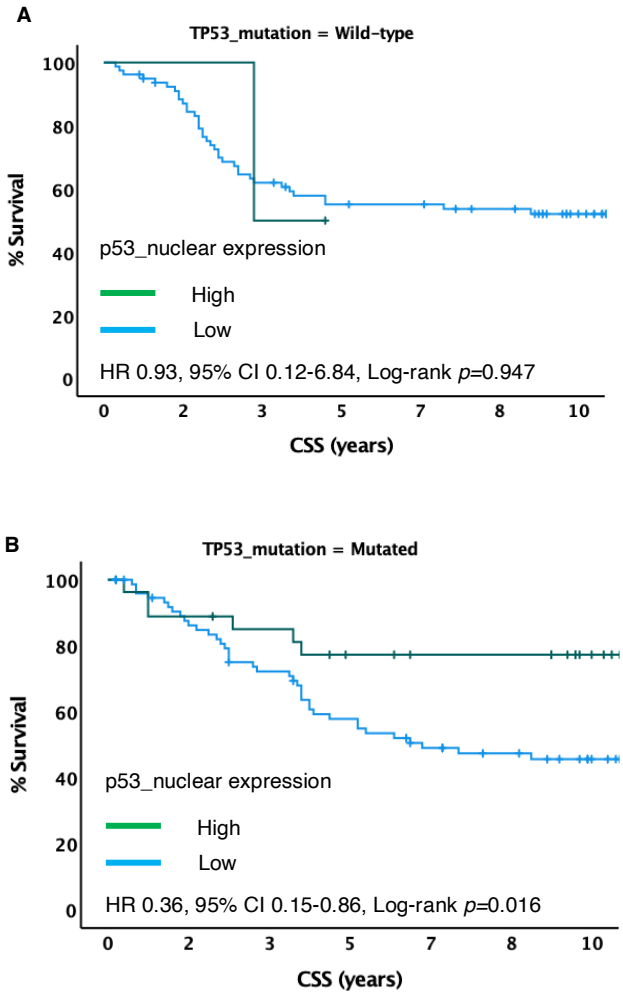

Figure 5.17 - KM plot of p53 nuclear expression and CSS (% survival at 10 years) in wild-type and mutated *TP53* in stage I-III CRC patients (n=930); A. In *TP53* wild type, no significant difference CSS observed between p53 high and p53 low (p=0.947). **B.** In *TP53* mutated, high p53 was significantly improved CSS (p=0.016).

5.3.11 Associations between nuclear p53 expression and immune cell infiltration in tumour and stroma

Next, the association between nuclear p53 expression and immune cells infiltration in tumour cell nests and tumour stroma was performed. No significant association were observed in either location. However, $CD68^+$ macrophages in tumour cell nests did trend toward significance, with low nuclear p53 expression associating with high $CD68^+$ infiltration (p=0.067) (**Table 5.1**).

Table 5.1 - Association between nuclear p53 expression and immune cells infiltration in tumour cell nests and tumour stroma in stage I-III CRC Scottish cohort (n=930)

	p53_Low N (%)	p53_High N (%)	*P*
Tumour cell nests			
$CD3^+$ lymphocytes (n=572)			0.992
Low	322 (68)	69 (68)	
High	149 (32)	32 (32)	
$CD8^+$ lymphocytes (n=558)			0.644
Low	314 (68)	69 (71)	
High	147 (32)	28 (29)	
$FoxP3^+$ Tregs (n=462)			0.480
Absent	335 (88)	71 (86)	
Present	44 (12)	12 (14)	
$CD68^+$ macrophages (n=299)			0.067
Low	85 (34)	23 (48)	
High	166 (66)	25 (52)	
$CD80^+$ M1-like macrophages (n=291)			0.889
Low	185 (76)	37 (76)	
High	57 (24)	12 (24)	
$CD163^+$ M2-like macrophages (n=285)			0.534
Low	205 (86)	41 (89)	
High	34 (14)	5 (11)	
$CD66b^+$ granulocytes (n=272)			0.796
Low	185 (84)	44 (83)	
High	34 (16)	9 (17)	
Tumour stroma			
$CD3^+$ lymphocytes (n=574)			0.763
Low	390 (83)	84 (82)	
High	81 (17)	19 (18)	
$CD8^+$ lymphocytes (n=558)			0.315
Low	250 (54)	58 (60)	
High	211 (26)	39 (40)	
$FoxP3^+$ Tregs (n=462)			0.162
Absent	297 (78)	59 (71)	
Present	82 (22)	24 (29)	
$CD68^+$ macrophages (n=299)			0.449
Low	85 (34)	19 (40)	
High	166 (66)	29 (60)	
$CD80^+$ M1-like macrophages (n=291)			0.350
Low	165 (68)	30 (61)	
High	77 (32)	19 (39)	
$CD163^+$ M2-like macrophages (n=285)			0.646
Low	40 (17)	9 (20)	
High	199 (83)	37 (80)	
$CD66b^+$ granulocytes (n=272)			0.996
Low	186 (85)	45 (85)	
High	33 (15)	8 (15)	

5.3.12 Correlation between p53 expression, immune cells infiltration and CSS

Next, the relationship between nuclear p53 expression, immune cells infiltration, and patient survival was assessed (**Table 5.2**). Nuclear p53 prognostic value was assessed in patients stratified for low and high levels of individual immune cell types, to assess if the good prognostic value of p53 was associated with a specific immune cell infiltration.

5.3.12.1 In tumour cell nests

For T-lymphocytes, in patients with low $CD3^+$ infiltration, high nuclear p53 level significantly improved CSS (HR 0.43, 95% CI 0.25-0.75, p=0.001) with 10 years survival stratified by 58% for low p53 to 86% for high p53. This was not seen in patients with high $CD3^+$. No differences in nuclear p53 prognosis were noted between low and high $CD8^+$ infiltration with nuclear p53 associating with improved survival in both patients with low (HR 0.36, 95% CI 0.20-0.65, p=0.010) and high (HR 0.36, 95% CI 0.20-0.65, p=0.008) $CD8^+$. However, in the absent of $FoxP3^+$, high p53 expression was associated with significantly improved CSS (HR 0.38, 95% CI 0.20-0.74, p=0.004) with 10 years survival stratified by 65% at low p53 to 84% for high p53. This was not seen in patients with FoxP3 present.

For myeloid cells, no associations were noted for $CD68^+$ or $CD66b^+$. However, in patients with low infiltration of $CD80^+$ M1-like macrophages, high nuclear p53 was associated with improved CSS (HR 0.40, 95% CI 0.17-0.93, p=0.028, **Figure 5.17 A**) with 10 years survival stratified by 55% for low p53 to 82% for high p53. Whereas no associations were observed for $CD80^+$ high (HR 0.72, 95% CI 0.16-3.29, p=0.678, **Figure 5.17 B**). Similarly, in patients with low $CD163^+$ M2-like macrophages, high nuclear p53 was associated with improved CSS (HR 0.49, 95% CI 0.23-1.02, p=0.045) with 10 years survival stratified from 59% for low p53 to 80% for high p53. This was not seen in patients with high CD163.

5.3.12.2 In tumour stroma

For T-lymphocytes, in patients with low $CD3^+$ infiltration, high nuclear p53 was associated with improved CSS (HR 0.46, 95% CI 0.27-0.79, p=0.005) with 10 years survival stratified by 62% for low p53 to 83% for high p53. This was not seen in patients with high $CD3^+$. Like in tumour cell nests, no differences in nuclear p53 prognosis were noted between low and high CD8 infiltration with nuclear p53 associating with improved survival in both patients with low (HR 0.36, 95% CI 0.20-0.65, p=0.032) and high (HR 0.36, 95% CI 0.20-0.65, p=0.002) $CD8^+$. Furthermore, in patients with an absence of $FoxP3^+$ Tregs, high nuclear p53 was associated with improved CSS (HR 0.41,

95% CI 0.21-0.79, *p*=0.016) with 10 years survival stratified by 61% for low p53 to 83% for high p53. This was not seen in patients with FoxP3 present.

As for myeloid cells, only in patients with low $CD80^+$ M1-like macrophages infiltration did high nuclear p53 associate with improved CSS (HR 0.29, 95% CI 0.10-0.79, *p*=0.011, **Figure 5.17 C**) with 10 years survival stratified by 53% for low p53 to 86% for high p53. Whereas no significance was observed for $CD80^+$ high (HR 1.09, 95% CI 0.36-3.30, *p*=0.868, **Figure 5.17 D**).

Table 5.2 - Relationship between p53 expression and immune cells infiltration and CSS (% survival at 10 years) in stage I-III CRC Scottish cohort (n=930)

	p53 low		p53 high		*P*
	N (%)	CSS (SE)	N (%)	CSS (SE)	
Tumour cell nests					
$CD3^+$ lymphocytes (n=572)					
Low	322 (68)	58 (3)	69 (68)	86 (4)	0.001
High	149 (32)	79 (4)	32 (32)	81 (8)	0.653
$CD8^+$ lymphocytes (n=558)					
Low	314 (68)	59 (3)	69 (71)	80 (5)	0.010
High	147 (32)	74 (4)	28 (29)	100 (0)	0.008
$FoxP3^+$ Tregs (n=462)					
Absent	335 (88)	65 (3)	71 (86)	84 (5)	0.008
Present	44 (12)	71 (11)	12 (14)	100 (0)	0.126
$CD68^+$ macrophages (n=299)					
Low	85 (34)	53 (7)	23 (48)	78 (9)	0.112
High	166 (66)	66 (4)	25 (52)	79 (9)	0.223
$CD80^+$ M1-like macrophages (n=291)					
Low	185 (76)	55 (4)	37 (76)	82 (7)	0.028
High	57 (24)	78 (6)	12 (24)	80 (13)	0.678
$CD163^+$ M2-like macrophages (n=285)					
Low	205 (86)	59 (4)	41 (89)	80 (7)	0.045
High	34 (14)	74 (8)	5 (11)	75 (22)	0.982
$CD66b^+$ granulocytes (n=272)					
Low	185 (84)	73 (3)	44 (83)	86 (6)	0.076
High	34 (16)	66 (11)	9 (17)	74 (16)	0.881
Tumour stroma					
$CD3^+$ lymphocytes (n=574)					
Low	390 (83)	62 (3)	84 (82)	83 (4)	0.005
High	81 (17)	80 (5)	19 (18)	85 (10)	0.496
$CD8^+$ lymphocytes (n=558)					
Low	250 (54)	59 (4)	58 (60)	80 (5)	0.032
High	211 (26)	70 (4)	39 (40)	95 (5)	0.002
$FoxP3^+$ Tregs (n=462)					
Absent	297 (78)	61 (3)	59 (71)	83 (5)	0.016
Present	82 (22)	80 (6)	24 (29)	93 (7)	0.160
$CD68^+$ macrophages (n=299)					
Low	85 (34)	75 (5)	19 (40)	84 (11)	0.243
High	166 (66)	55 (5)	29 (60)	73 (9)	0.237
$CD80^+$ M1-like macrophages (n=291)					
Low	165 (68)	53 (5)	30 (61)	86 (6)	0.011
High	77 (32)	77 (5)	19 (39)	71 (13)	0.868
$CD163^+$ M2-like macrophages (n=285)					
Low	40 (17)	73 (9)	9 (20)	100 (0)	0.176
High	199 (83)	59 (4)	37 (80)	75 (8)	0.147
$CD66b^+$ granulocytes (n=272)					
Low	186 (85)	72 (4)	45 (85)	87 (6)	0.071
High	33 (15)	71 (8)	8 (15)	64 (21)	0.755

N=number of patients, CSS=Cancer specific survival, SE=standard error

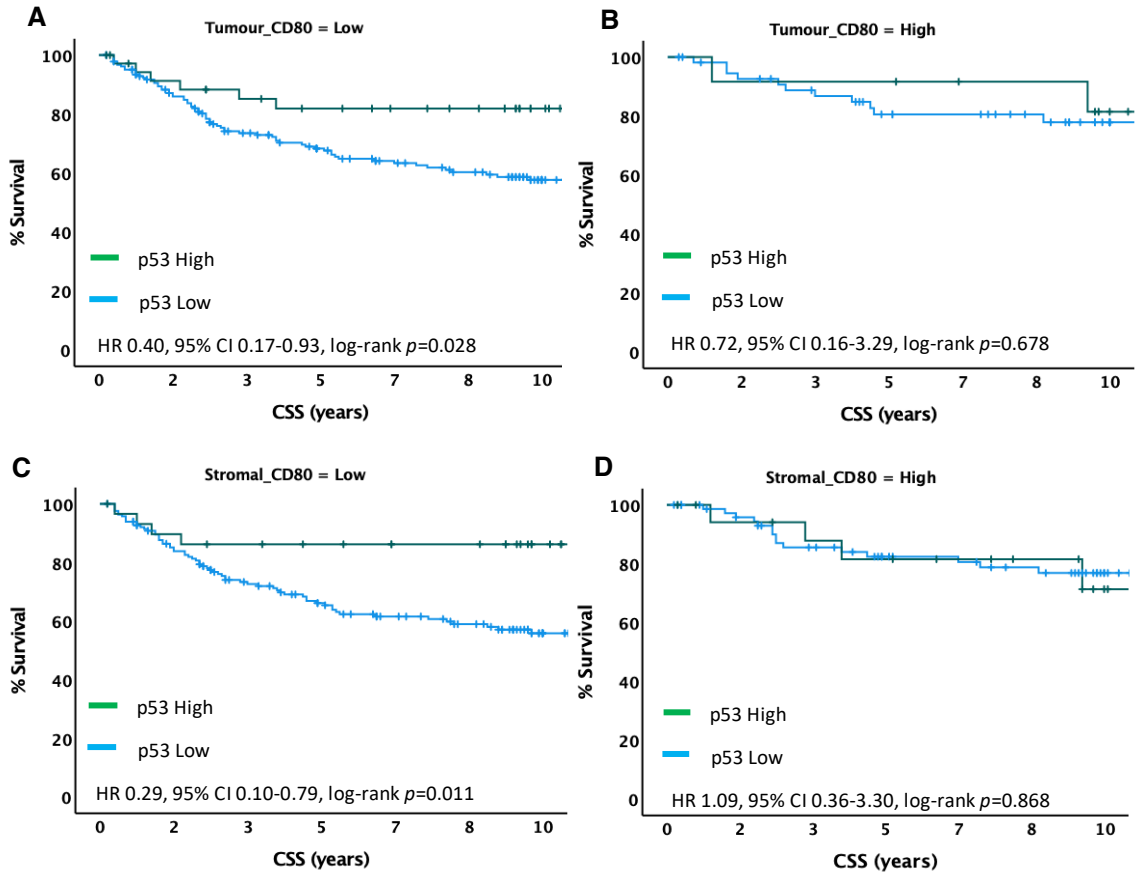

Figure 5.18 - KM plots of p53 nuclear expression and CSS (% survival at 10 years) in high CD80 and low CD80 in tumour cell nests and tumour stroma in stage I-III CRC Scottish cohort (n=930); A. high p53 was significant associated with improved CSS at low CD80 in tumour cell nests, (p=0.028), **B.** no significant at high CD80 in tumour cell nests, **C.** high p53 was significant associated with improved CSS at low CD80 in tumour stroma, (p=0.011), **D.** no significant at high CD80 in tumour stroma.

5.3.13 Comparison between mutations in low and high CD80⁺ M1-like macrophages in tumour cell nests and tumour stroma

From the IHC results, $CD80^+$ M1-like macrophages were associated with differences p53 prognosis in both the tumour cell nests and stroma. When M1-like macrophages are low, low p53 is bad for the patient, however, when M1-like macrophages are high, this poor prognostic effect of low p53 is lost and all patients do well. Therefore, mutational profiles for low and high $CD80^+$ M1-like macrophage infiltrates were compared to see whether there is a difference between *TP53* mutation in these two groups in either tumour cell nests or tumour stroma.

5.3.13.1 In tumour cell nests

For CD80$^+$ M1-like macrophages in tumour cell nests, there were 13 significantly differentially mutated genes included *CREBBP*, *MSH2*, *MARCA4*, *APC*, *BLM*, *TGFBR2*, *RPL22*, *MSH6*, *FBXW7*, *SMAD4*, *BRCA2*, *ERBB3*, and *B2M*. All mutated genes presented with more mutations in high CD80$^+$ patients than low CD80$^+$ patients (**Figure 5.18**). However, among 13 significant differentially mutated genes *TP53* mutation were not included. This suggest that *TP53* is not associated with CD80$^+$ infiltration within tumour cell nests at the DNA level.

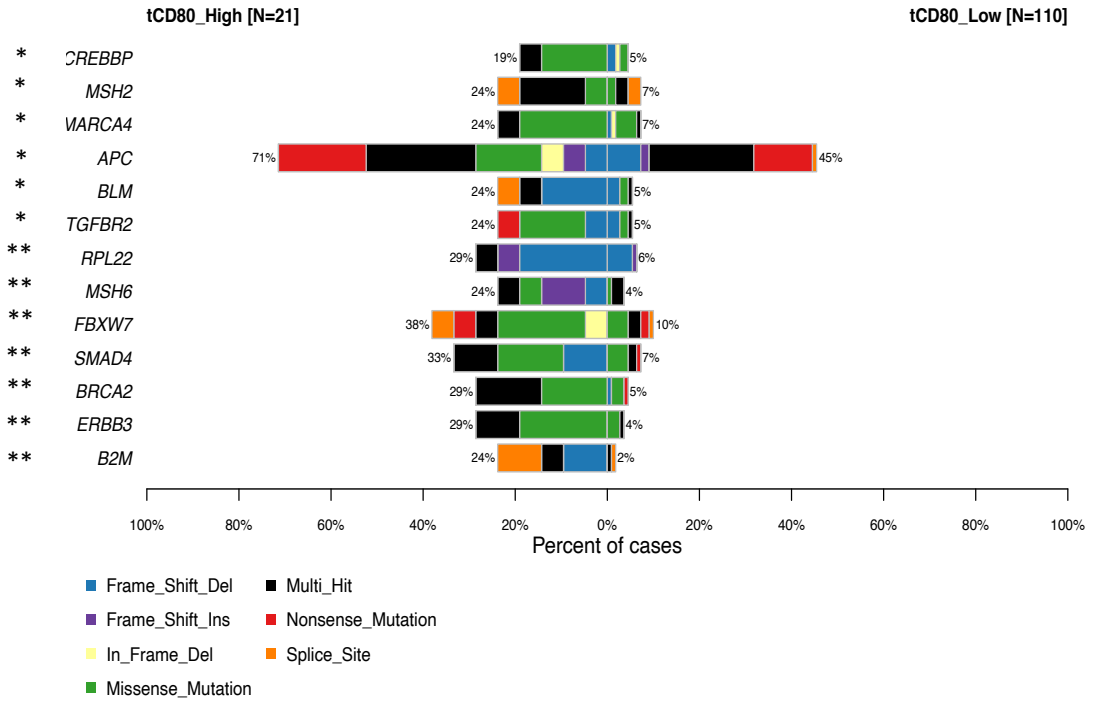

Figure 5.19 - Co-bar plot of high mutated genes in high and low CD80 infiltration in tumour cell nests; Thirteen significantly differentially mutated genes presented more mutations in high CD80$^+$ than low CD80$^+$ patients (**p<0.01, *p<0.05).

5.3.13.2 In tumour stroma

For CD80$^+$ M1-like macrophages in tumour stroma, of the top 13 mutated genes, four were significantly differentially mutated including *ALK*, *ARID1A*, *TP53*, and *APC*. All 4 genes were presented as significantly increase mutated frequency in high CD80$^+$ patients than low CD80$^+$ patients (all *p<0.05) (**Figure 5.19**). *TP53* was significantly differentially mutated with 60% of CD80$^+$ high patients carrying a mutation compared to 37% of CD80 low patients. This suggests that *TP53* mutations are associated with CD80$^+$ infiltration into the tumour stroma.

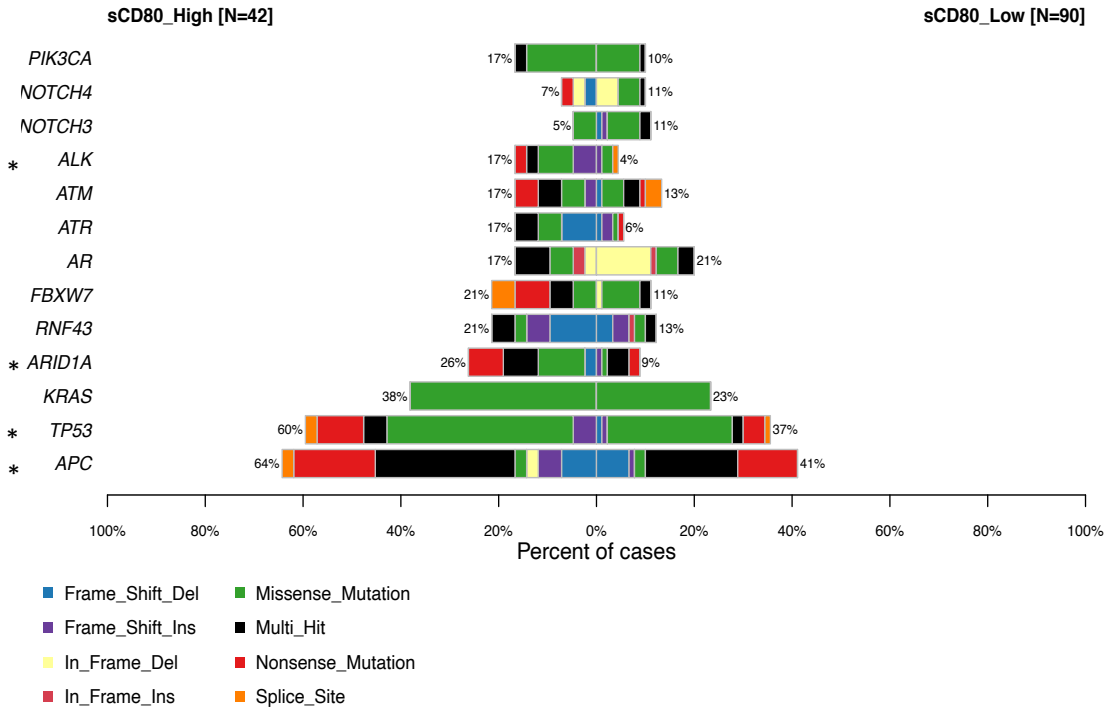

Figure 5.20 - Co-bar plot of high mutated genes in high and low CD80$^+$ infiltration in tumour stroma. Among top mutated genes, *APC*, *TP53*, *ARID1A*, and *ALK* mutated were significantly presented in high CD80$^+$ greater than low CD80$^+$ patients (**p*<0.05).

5.3.14 Correlation between p53 expression and phenotypic subtypes

In terms of phenotypic subtypes, the correlation between p53 expression and CRC phenotypic subtypes was evaluated. The result showed p53 expression level was significantly decreased in latent subtypes when compared to canonical subtype (***p* < 0.01).

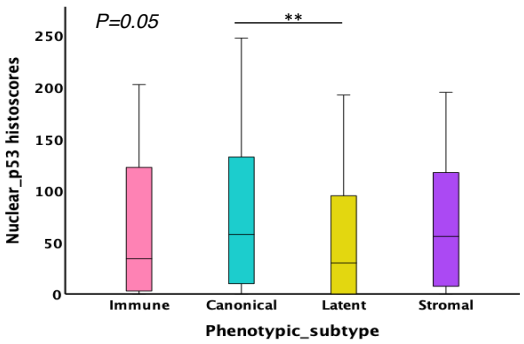

Figure 5.21 - Correlation between p53 expression and CRC phenotypic subtypes; p53 expression was significantly decreased in latent subtypes (***p*<0.01).

5.4 Discussion

Currently, tumour immunotherapy is at the forefront of research searching for new strategies to reach successful treatment outcomes, together with overcome drug resistance in many types of solid tumours. Besides, due to the reduction in cost of whole genome sequencing (WGS) (Huang et al., 2019; Mayakonda et al., 2018; Wu et al., 2012) and a variety of convenient bioinformatic tools packages that were developed over the past few decades to analyse high throughput complex dataset from large cohort's studies in minutes, the use of genomic analysis in the clinic is becoming ever closer (Branco & Choupina, 2021; Brenner, 2019; Cole et al., 2021; Mayakonda et al., 2018). Therefore, today the trend of cancer genomics and genetic alteration studies are an arising approach to predict potential tumour neoantigens as new drug targets (Huang et al., 2019), prognostic biomarkers (Wang et al., 2020; Zhao et al., 2020), or predictive biomarkers for treatment response (Jiang et al., 2012; Koncina et al., 2020) to guide immunotherapy use (Bupathi & Wu, 2016; Mukherjee, 2019), all of which is crucial to eliminate tumours and improve patient survival.

As our study is interested in the role of T-lymphocytes and myeloid cells infiltration in CRC patients and has developed immune cells landscapes grouping based on their infiltration level in tumour cell nests and tumour stroma. The aim of this chapter was to examine whether there are any significantly differentially mutated genes in each immune landscapes grouping. The results from whole genome sequencing data presented that, in general, the top three mutated genes in our patient's cohort were *APC* (51%), *TP53* (46%), and *KRAS* (31)%, as expected from their role in CIN pathway in CRC tumorigenesis (Tariq & Ghias, 2016). Normally in colorectal cancer, the top three mutated genes are *APC*, *KRAS*, and *TP53*. *APC*, is the most important tumour suppressor gene, around 75% of CRC cases have mutation in this gene (Tariq & Ghias, 2016). *KRAS,* is another important gene, mutated *KRAS* is found around 35-42% of CRC cases. Whereas, *TP53*, impairment presents in around 50-75% in CRC cases (Worthley & Leggett, 2010).

In order to identified specific mutated genes for each landscape groups, the comparison between mutational profiles in each immune landscape group was performed. The mutational profiles of the most statistically significant differentially mutated genes in each group obtained that, in T-cells high group, the most significant differentially mutated gene was *ERBB4* (100%) (erb-b2 receptor tyrosine kinase 4 or HER4), however, there is only 2 cases in this group, which need more cases to validate this result. Whereas, the myeloid high group, presented six significantly differentially mutated genes, all of which showed lower mutations in this group compared to the others, of which *TP53* was the most significant. Whereas the both high group presented five significant differentially mutated genes, of which *FBXW7* (F-Box And WD Repeat Domain Containing 7), was the most significant differentially mutated with higher levels of mutations in this group. Lastly, in both low group, only

TP53 was significantly differentially mutated, with high mutation levels in this group. Therefore, as the myeloid group appeared to have low levels of mutations and *TP53* mutations where one of the most significantly differentially mutated between groups these were taken forward for further analysis. From this it was found that myeloid high has significantly less *TP53* mutations than both low group and therefore it could be extrapolated that myeloid low patients have more *TP53* mutations. After observing *TP53* mutations in patients with high myeloid cell infiltration into tumour cell nests, this was compared to patient with high myeloid cell infiltration into tumour stroma and indicated that *TP53* mutations in patients with infiltration within the stroma were significantly higher than in patients with infiltration within tumour cell nests. However, the effect of *TP53* mutations and immune cells infiltration for our patient's cohort was not clear at this point. As *TP53* is a most significant tumour suppressor gene, therefore, the hypothesis was its enriched mutations might result in a negative outcome in tumour stroma compared tumour nests with high myeloid cell infiltration.

The role of *TP53* mutations, and immune response has been studied. As *TP53* is well-recognized as the guardian of genome and more than 50% of cancers cases harbor somatic mutations in this gene, mostly missense mutations causing single amino acid alterations leading to expanding the tumour cells half-life by accumulating in cell, whereas it would rapidly degrade in normal cells (Olivier et al., 2010; Wang & Sun, 2017). High p53 expression has been proposed to be used as a marker for *TP53* missense mutations in high-grade serious ovarian cancer (Cole et al., 2016). Mostly, the result from mutations is altering conformational change in p53 proteins which impair DNA binding capacity and finally loss of p53 function and reduce apoptosis (Cui & Guo, 2016). Another effect of conformational change is stabilized p53 protein resulting in increased p53 level in tumour that triggers cell stress leading negative results. Therefore, p53 mutation could promote tumour progression from both loss-of-function (LOF) and gain-of-functions(GOF) mutations (Michel et al., 2021).

Therefore, we assessed the correlation between *TP53* mutations and p53 protein expression level, and found that *TP53* mutations was significantly correlate with high p53 expression, suggest that in our cohort *TP53* mutations result in elevated p53 expression, which is in line with other reports that elevated p53 proteins could be indicator of *TP53* mutations (Menendez et al., 2013). However, a limitation of this study was the antibody used in p53 IHC staining bound to both wild type and mutant p53, therefore, p53 expression was from a mixed population of wild type and mutant p53, so it was not possible to say what percentage of patients had the mutant p53 protein. However, survival analysis revealed that high p53 expression was significantly associated with improved patient's survival as expected from its role for tumour suppressor function suggesting the majority of the p53

pick up by the antibody was wild type. However, when we stratified for mutated versus wild type *TP53* mutations, only patients with mutated *TP53* had improved survival.

As we want to see the effect of immune cells infiltration on p53 expression, the relationship between p53 expression and immune cells infiltration was observed, however, no significant association was noted, suggesting there was not a direct linking between the two. However, when the relationship between p53 expression and patient's survival was stratified for immune cell infiltrate, interesting associations were observed. With high immune cell infiltrates, there is no significant change in survival rate between low and high p53. Interestingly, low levels of $CD80^+$, together with low p53 could decrease survival when compared to high $CD80^+$ in both tumour cell nests and tumour stroma. This suggests that if $CD80^+$ is low, high levels of p53 are needed to improve patients' survival, however, when $CD80^+$ cells are high, p53 is no longer important and all patients do well.

There is a strong connection between p53 and the innate immune response, through p53 mediating innate immune system to orchestrate clearance of DNA damaged cells which eliminates tumour cells (Guo & Cui, 2015; Menendez et al., 2013). Recently, the role of p53 in tumour cells and the association with myeloid lineage cells has been studied. Cooks et al. reported that human mutant p53 tumour cells can reprogram macrophages into anti-inflammatory state, M2-macrophages, which support tumour progression through intercellular interactions by shedding exosomes with miR-1246-enriched. Later macrophages which uptake these exosomes then trigger miR-1246-dependent reprogram into a tumour promoting state which support anti-inflammatory immunosuppression leading to poor survival (Cooks et al., 2018). Therefore, the role of p53 to myeloid cells could result in poor survival.

However, in our study, p53 was linked to M1-like macrophages in both tumour cell nests and tumour stroma. As discussed above high p53, together with low M1-like macrophages could improve survival in both tumour cell nests and tumour stroma, but when M1-macrophages are high, p53 levels are no longer important. This suggests that M1-like macrophages may compete with p53 to result in improve patient survival. However, when *TP53* mutations were assessed in high and low $CD80^+$ M1-like macrophages, it was found that high $CD80^+$ group was significantly enriched for *TP53* mutations only in tumour stroma, whereas in tumour cell nests, *TP53* mutations did not appear among thirteen significantly differentially mutated genes in high $CD80^+$ in tumour cell nests. Therefore, at DNA level, enriched *TP53* mutation could be detected in patients with high M1-like macrophage in stroma, but not in tumour cell nest. Whereas high p53 expression presented similar effect on patients' survival in both locations. This suggests that the prognostic role of *TP53* mutations and p53 expression in patients with stromal infiltration of M1-like macrophages may be of more importance

of than in patients with tumour nest infiltration. But as our antibody detected both mutant and wild type p53 protein this effect may be hidden in the IHC results and needs validated with a mutant specific antibody.

In conclusion, at DNA level, there were differences between *TP53* mutations in patients with only high levels of myeloid cells, with more mutations were presented in patients when high numbers of myeloid cells in the stroma, suggesting *TP53* mutations might affect myeloid infiltration into the stroma. *TP53* mutated was correlated with high p53 expression when compared to wild-type *TP53* at the protein expression level. In addition, low p53 expression was a poor prognostic factor in patients with low levels of M1-macrophages, but this was negated when M1-macrophage levels are high. However, at DNA level, *TP53* mutations were more frequent in patients with high stromal M1-like macrophages, denoting *TP53* mutations could be a prognostic factor in patients with high myeloid cells infiltration into tumour stroma.

Chapter 6 Differential gene expression of innate and adaptive immune cell landscapes in stage I-III CRC

6.1 Background

CRC is a heterogeneous disease, the heterogeneity can be linked to various phenotypes and clinicopathological features, which are controlled by several factors varying from genetics to epigenetics, and tumour microenvironment (Picard et al., 2020; Saleh et al., 2020). The tumour microenvironment is complex consisting of stromal cells and several immune cell compositions which function as pro-tumorigenic or anti-tumorigenic depends on which cell types presented. Therefore, studies of gene expressions are rising focusing on integrating gene expression signatures and immune cells, in multiple tumours including CRC to create prognostic and predictive markers, i.e., developing immune-related gene expression signatures to predict response to chemotherapy, which might improve patient's prognosis and benefit therapeutic responses, ranging from chemotherapy and radiotherapy, to immunotherapy (Chen et al., 2020; Choe et al., 2021; Li et al., 2020; Tan et al., 2021; Wang et al., 2020; Zhao et al., 2021). In addition, an integration of genomic and transcriptome data to identify somatic mutation-driven immune cells has been reported (Jiang et al., 2021).

In chapter 5, the immune landscape grouping was integrated into mutational analysis, and found that *TP53* mutations were significant in the myeloid high group which had more mutations presented in patients with high level of myeloid cells in the stroma, suggesting *TP53* mutations might impact myeloid infiltration into the stroma. Mutations in *TP53* were specifically higher in patients with high stromal M1-like macrophages.

The aim of this chapter was to examine transcriptomic data, to assess whether there are patterns of differentially expressed genes which could be used as potential prognostic or predictive markers for each immune landscape grouping.

6.2 Method

Whole transcriptome RNA-Seq was performed by BioClavis Glasgow by utilising the novel TempO-Seq technique (Biospyder Technologies, Carlsbad, CA, USA) on a FFPE full section tissue from subset of patients from the Glasgow combined cohort (n=100). The pre-processing quality control of FastQ files and the Mahalanobis distance outliers' analysis were performed by BioClavis Glasgow and has determined the 9 outliers which were excluded from the final raw gene counts for downstream analysis. Data analysis was done using R studio version 4.0.5. RNA-Seq raw counts data normalization and differential expressed genes (DEGs) were performed by utilizing DESeq2 packages (Love et al., 2014) version 1.30.1 for the full ~22,000 gene transcriptome. Differentially expressed genes tables were performed for each immune landscape groups (both low, t-cell high,

myeloid high, both high) compared to all other patients. PCA plot and samples clustering were generated to explore the sample-to-sample distance relationship. The hierarchical clustering of gene expressions was constructed by *pheatmap* package. Box plot was performed to observe gene expression level in each group. Volcano plots and MA plots were generated to visualise DEGs by displaying mean expression levels, log 2-fold changes, and *p*-value. Significant DEGs was set if adjusted *p*-value < 0.05 with log 2-fold changes > 1 for significant upregulated genes, while adjusted *p*-value < 0.05 with log 2-fold changes < 1 was set for significant downregulated genes. Venn diagram was generated to observe the overlapping of differentially expressed genes between groups. Over-representative analysis (ORA) of enriched gene sets were performed by *enrichGO* function and *cnet* function was utilised for gene-concept networks plots to observe biological processes involves. Protein-protein interactions (PPIs) was generated by STRING functional enrichment analysis online tool. Boxplots were constructed to assess the correlation between mutations and DEGs expression levels.

6.3 Results

From RNA-Sequencing data of 100 samples available from the Scottish cohort, after potentially 9 outliers were excluded, raw read counts of 48 samples were available for the subsequent analysis after grouping by immune landscape (**Figure 6.1**).

6.3.1 Transcriptomics analysis of the tumour immune landscape groups

First, analysis was performed in the 48 patient samples based on the four tumour immune landscape groups generated from chapter 3: T-cells high (N=3), myeloid high (N=24), both high (N=14), and both low (N=7) (**Figure 6.1**).

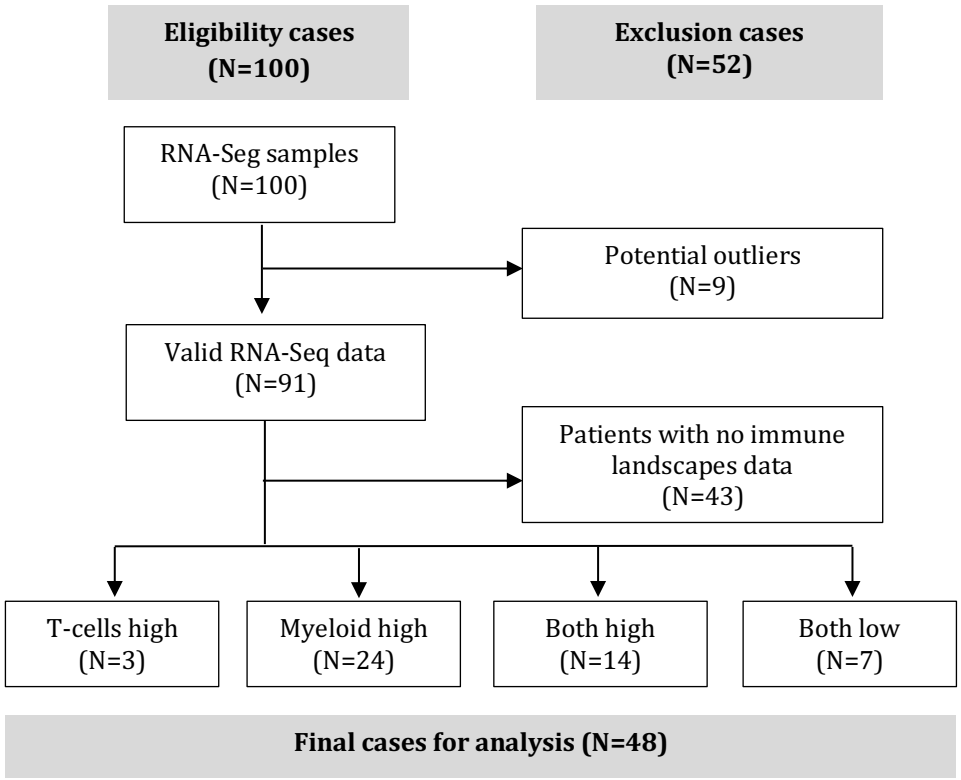

Figure 6.1 - Consort diagram of RNA-Sequencing data of Scottish cohort patients; Showing 48 valid RNA-Sequencing data from patient samples were available in the study with excluding criteria by potential outliers, and patients with no immune landscapes data.

6.3.2 Correlation between immune cells level and related gene expression

The correlation between tumour T-lymphocytes and macrophages expression level and genes correlated with each cell were observed by boxplots. For T-lymphocytes, high CD3 was associated with CD3E_16113 expression (**Figure 6.2 A**), and high CD8 was associated with CD8A_1152 expression (**Figure 6.2 B**). For macrophages markers, CD68 expression was not associated with CD68_20756 expression (**Figure 6.2 C**), whereas high CD80 was significantly associated with CD80_88562 expression (**Figure 6.2 D**). However, CD163 was not associated with CD163_14001 expression (**Figure 6.2 E**). Due to low patient numbers, markers did not reach significant.

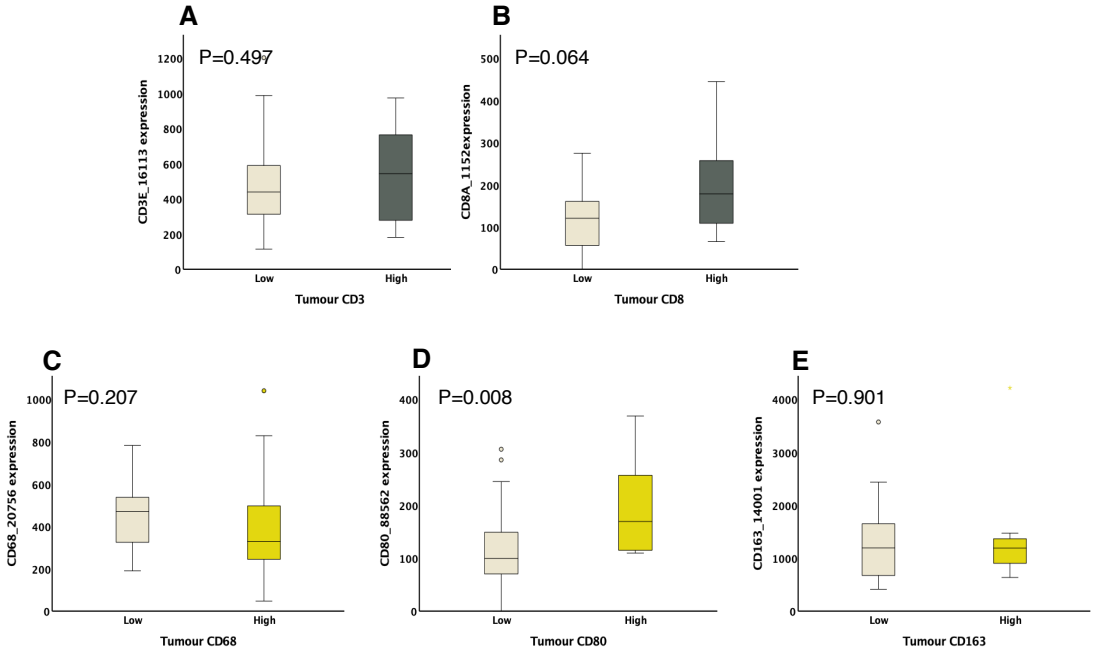

Figure 6.2 - The correlation between immune cells expression level and immune cells related genes expression; showing high CD3 and CD8 expression were correlated with high expression of CD3E_16113 (**A**) and CD8A_1152 (**B**), respectively. CD68 expression level was not correlated with CD68_20756 expression (**C**). High CD80 was significant correlated with CD80_88562 (**D**). CD163 expression was not correlated with CD163_14001 (**E**).

6.3.3 Principal component analysis (PCA) of immune landscape groups

Principal component analysis and gene clustering was generated by *stat_ellipse* function on *ggplot2* packages, the result revealed potential gene clusters for myeloid high (green ellipse), both high (blue ellipse), and both low (purple ellipse) groups. However, no potential gene clustering for T-cells high group (red dots) was observed potentially due to the small sample number (**Figure 6.3**).

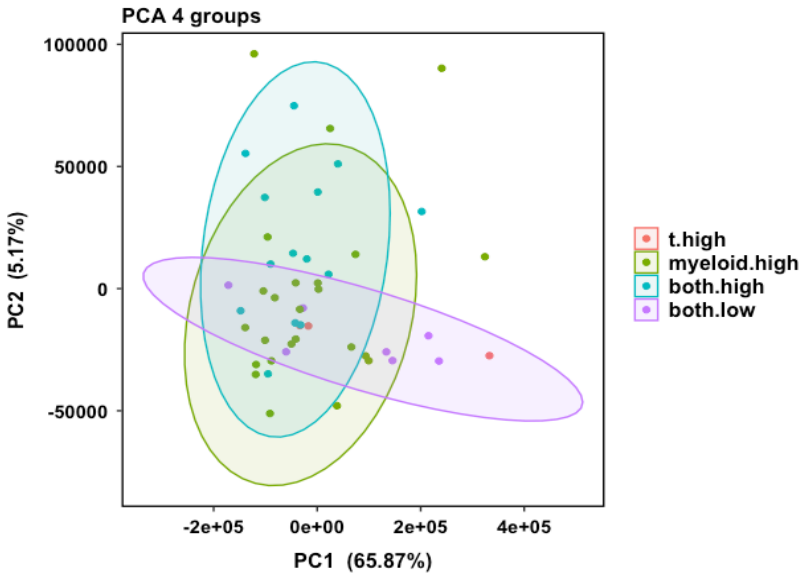

Figure 6.3 - PCA plot of 4 immune landscape groups in stage I-III CRC Scottish cohort (n=48); PCA presented potential gene clustering for myeloid high (green), both high (blue), and both low (purple). No potential clustering for T-cells high group (red) due to small sample numbers.

6.3.4 Analysis of candidate top 40 genes expressed in the four tumour immune landscape groups

Next, a heatmap plot was generated to observe the pattern of expression of the top 40 genes across the four groups. In general, the heatmap plot showing 3 distinct patterns of sample groups, group A showing high expression, group B showing low expression, and group C showing intermediate expression. However, sample group B predominantly consisted of patients from the myeloid high group, whereas the other two groups consisted of the mixed populations of the other groups (**Figure 6.4**).

To observe the expression pattern of top 40 genes among the four groups, box plots were generated. The result indicated that in T-cells high group there was low expression from most genes. However, due to the small number of samples in this group this would need to be confirmed in a larger cohort. Whereas, myeloid high, both high, and both low groups showed similar expression patterns. Some genes, i.e., FAM3B_11565, were downregulated in the T-cells high group but upregulated in the myeloid high and both high groups, with intermediate expression in the both low group (**Figure 6.5**). This suggests the expression pattern of the both high group might be influenced by myeloid high group. However, due to low sample size within the T-cells high group, validation in a larger patient cohort is needed to clarify these results.

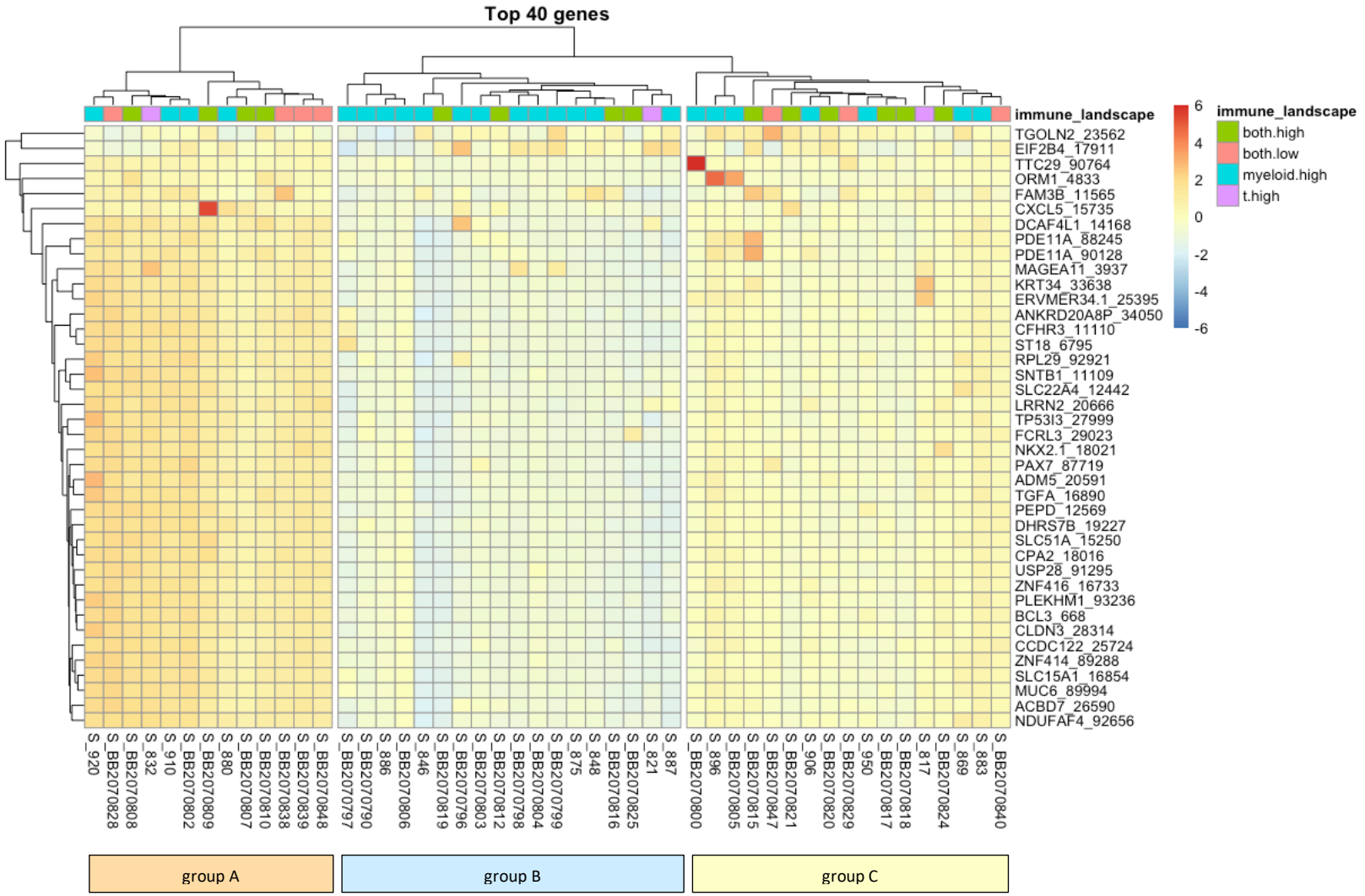

Figure 6.4 - Top 40 genes expression in 4 immune landscape groups; Heatmap showing top 40 gene expression patterns presented 3 distinct patterns among sample groups, group A showing high expression, group B showing low expression, and group C showing intermediate expression. The group A, B, C represented sample groups. The gene names are listed on the right.

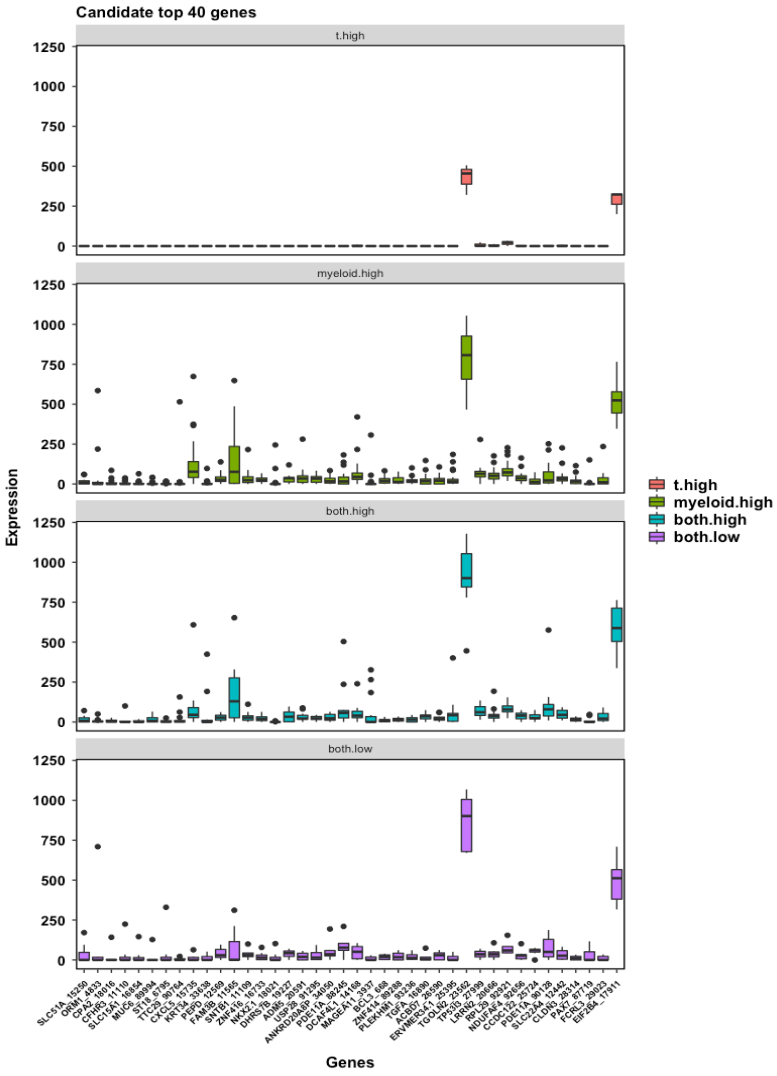

Figure 6.5 - Expression of top 40 genes in each immune landscape group; in T-cells high group given low expression from most of genes. Whereas, myeloid high, both high, and both low groups presented almost similar expression patterns.

6.3.5 Comparison of differentially expressed genes between T-cells high vs others

Next, to observe differentially expressed genes, the comparison between each immune landscape group and others were analysed. In the comparison between T-cells high and others groups, the results revealed 17 significantly differentially expressed genes which were downregulated in T-cells high group (**Table 6.1**). Among 17 genes, the top 5 most significant, (REG3A_22026, REG3G_88681, PEPD_12569, NXF2_25593, CXCL5_15735) were labelled on Volcano plot and MA plot, of which *REG3A*, *REG3G*, and *NFX2* represented the top 3 highest fold changes in expression levels (**Figure 6.6 A, B**). Again, due to the low sample size within this group, validation in a larger cohort is needed.

Table 6.1 – Significantly downregulated genes in T-cells high group from DE T-cells high vs others

Gene name	Mean expression	Log2FoldChange	Pvalue	Padj
REG3A_22026	128.21062	-23.09025171	1.76E-17	3.52E-13
REG3G_88681	38.15083	-19.71353786	2.23E-11	2.23E-07
PEPD_12569	31.48458	-7.444128812	3.32E-07	0.001749385
NXF2_25593	13.50833	-20.43945814	3.50E-07	0.001749385
CXCL5_15735	141.11583	-9.003716244	5.73E-07	0.002292599
FAM3B_11565	137.98438	-9.576396834	1.37E-06	0.004314644
PDE11A_88245	56.65812	-8.292316418	1.51E-06	0.004314644
SNTB1_11109	32.43854	-7.482625537	2.49E-06	0.00621764
ANKRD20A8P_34050	28.53229	-7.302170518	3.19E-06	0.007086093
ZNF416_16733	22.69958	-6.973028879	4.03E-06	0.008067713
DHRS7B_19227	31.14500	-7.430319462	4.44E-06	0.008077978
USP28_91295	26.60625	-7.204052087	1.03E-05	0.017138656
ADM5_20591	33.32042	-7.523706994	1.24E-05	0.019016025
DCAF4L1_14168	59.59917	-4.41888204	1.68E-05	0.024074749
PDE11A_90128	68.85354	-5.211721529	1.97E-05	0.026245807
CCDC122_25724	25.44000	-7.138193392	2.80E-05	0.034966712
TGOLN2_23562	926.72458	-1.167803131	3.23E-05	0.037994092

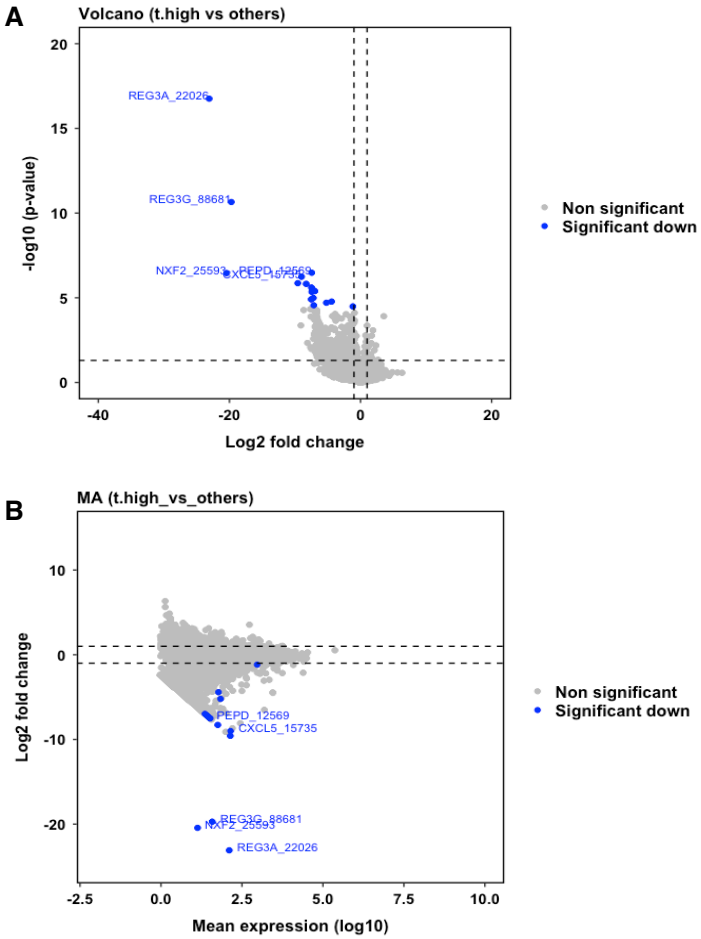

Figure 6.6 – Volcano and MA plots for significant downregulated genes for DE T-cells high vs others; A. Volcano plot showing 17 significant genes in T-cells high group, **B.** MA plot showing log2 fold change and average of expression level of significant genes, top 5 most significant downregulated genes were labelled in blue.

6.3.5.1 Analysis of expression of 17 significantly downregulated genes

A box plot was generated to observe the expression level from normalized raw gene counts, the result showed that among 17 genes showing low expression in T-cells high group, REG3A_22026 and REG3G_88681 were the most significant expressed genes with highest fold changes (**Figure 6.7**). Further analysis is needed to validate these results due to the small sample size.

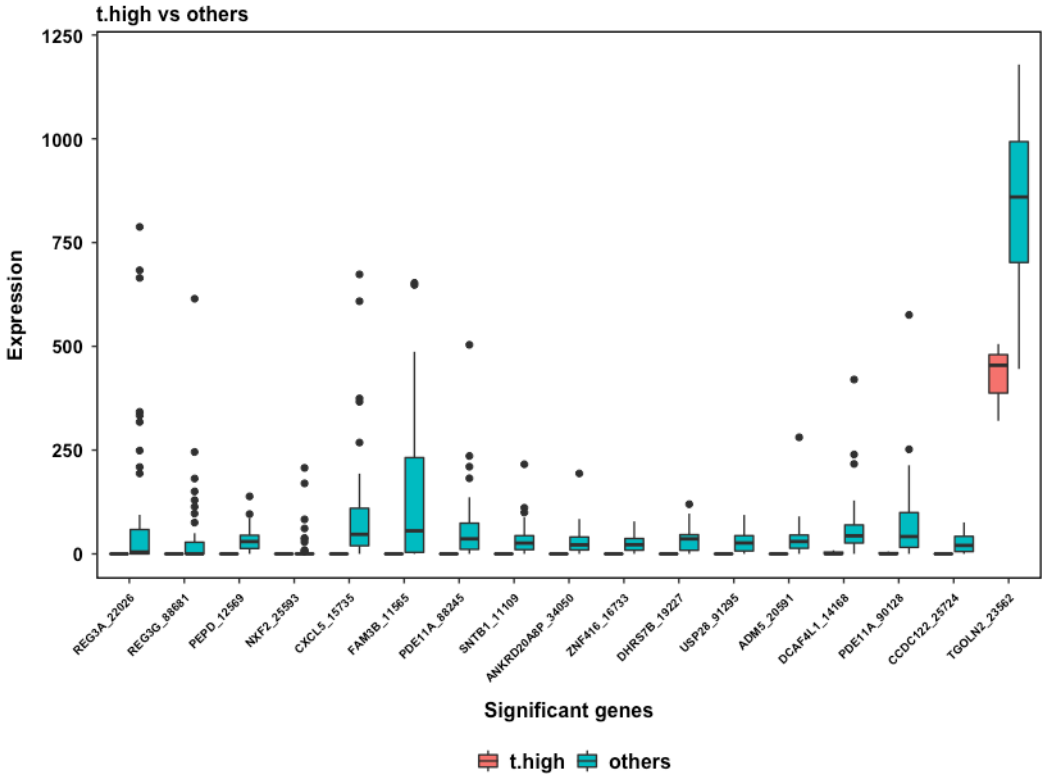

Figure 6.7 - Expression level of 17 significant downregulated genes in DE T-cells high vs others; From normalized raw gene counts data, *REG3A*, *REG3G*, and *PEPD* were top 3 most significant genes.

6.3.5.2 Analysis of Gene-Concept network for 17 significantly downregulated genes

The gene-concept network by cnet plot for significant differentially expressed genes was analysed, the result revealed that 3 out of 17 significant genes, REG3A_22026, REG3G_88681, and CXCL5_15735, appear in the network linkage for biological processes related to immune response, i.e., humoral immune responses, acute inflammatory response, regulation of wound healing and regulation of response to wound healing (**Figure 6.8**).

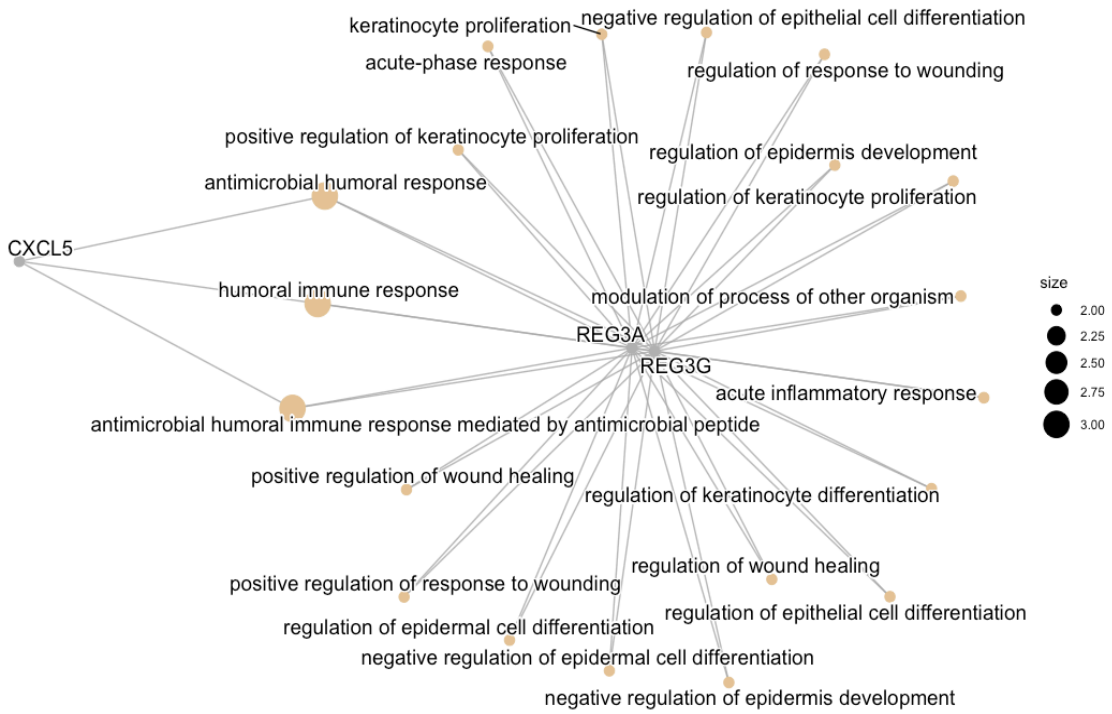

Figure 6.8 - Network plot for enriched 17 significant differentially expressed downregulated genes in T-cells high group; Enrichment genes cnet plot showing the network linking of biological processes from 3 out of 17 genes, *REG3A*, *REG3G*, *CXCL5*, participated in immune response processes, i.e., humoral immune responses, antimicrobial humoral response, acute inflammatory response, regulation of wound healing, cell proliferation, cell differentiation, cell development.

6.3.6 Comparison of differentially expressed genes between myeloid high vs others

In the comparison between myeloid high and others group, the results revealed only 1 significantly differentially expressed gene, IGF2BP1_24044, which was downregulated in myeloid high group (**Table 6.2**). The log2 fold change and average of expression were shown in Volcano plot and MA plot (**Figure 6.9 A, B**).

Table 6.2 – Significantly downregulated gene in myeloid high group from DE myeloid high vs others

Gene name	Mean expression	Log2FoldChange	Pvalue	Padj
IGF2BP1	9.278125	-6.408081	2.327016e-06	0.0479

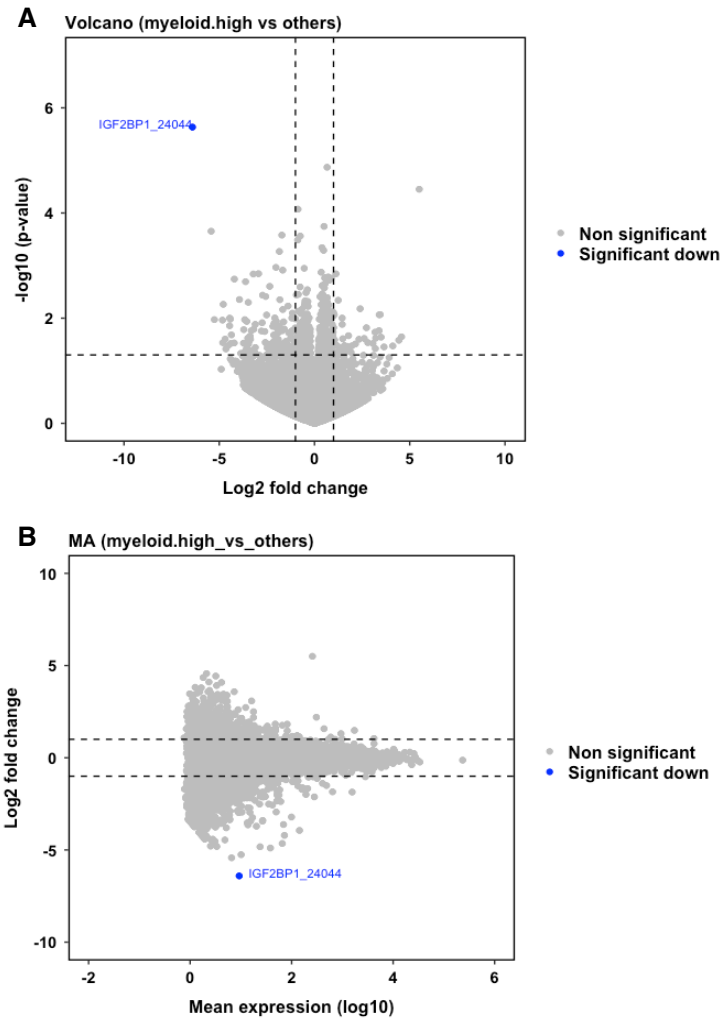

Figure 6.9 - Significant differentially expressed genes for myeloid high vs others; A. Volcano plot showing 1 significant differentially expressed gene, IGF2BP1_24044, downregulated in myeloid high group, **B.** MA plot showing log2 fold change and average of expression level, gene name with blue colour labelled represented downregulated expressed gene.

6.3.6.1 Analysis of the expression level of the *IGF2BP1* gene

When observed, the normalized raw gene counts found that IGF2BP1_24044 show very low expression in myeloid high group compared to the others group (**Figure 6.10**).

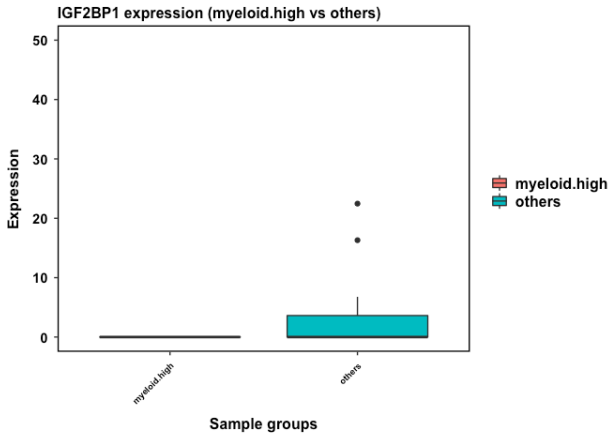

Figure 6.10 - Expression level of IGF2BP1_24044 significant downregulated gene in DE myeloid high vs others; IGF2BP1_24044 was the only one significant downregulated gene expressed in myeloid high group.

6.3.6.2 Analysis of Gene-Concept network for the *IGF2BP1* gene

The gene-concept network cnet plot for IGF2BP1_24044 was analysed, the result indicated that *IGF2BP1* participating in the biological processes network relating to RNA and mRNA, i.e., the regulation of RNA stability, mRNA stabilization and RNA localisation, and transport, i.e., nucleic acid transport, RNA transport and mRNA transport. (**Figure 6.11**).

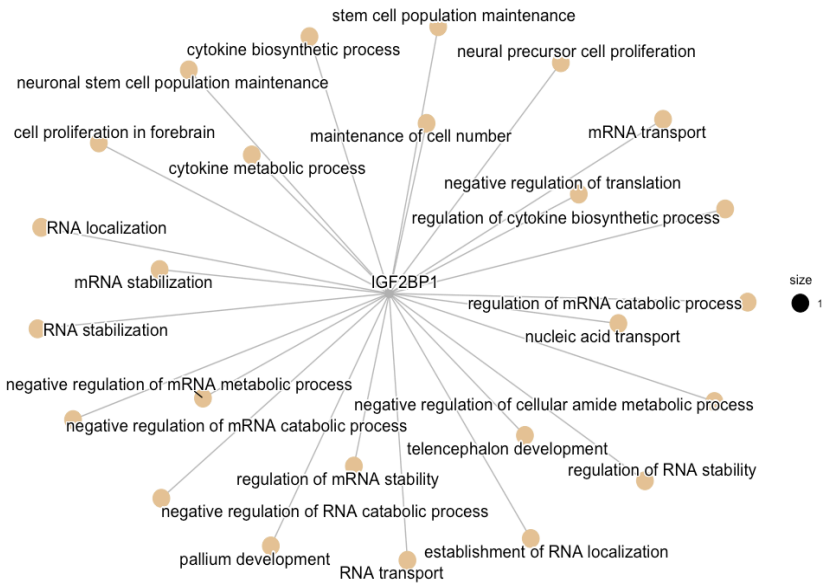

Figure 6.11 - Network plot for *IGF2BP1* significant differentially expressed downregulated gene in myeloid high group; enrichment cnet network plot showing the network linking of *IGF2BP1* genes participated in many biological processes.

6.3.7 Comparison of differentially expressed genes between both high vs others

In the comparison between both high and others groups, the results revealed only 1 significantly differentially expressed gene, HLA-DRB5_15922, which was downregulated in the both high group (**Table 6.3**). The log2 fold change and average of expression were shown in Volcano plot and MA plot (**Figure 6.12 A, B**).

Table 6.3 - Significantly downregulated gene in both high group from DE both high vs others

Gene name	Mean expression	Log2FoldChange	Pvalue	Padj
HLA-DRB5	947.3431	-1.407805	4.474593e-07	0.00278

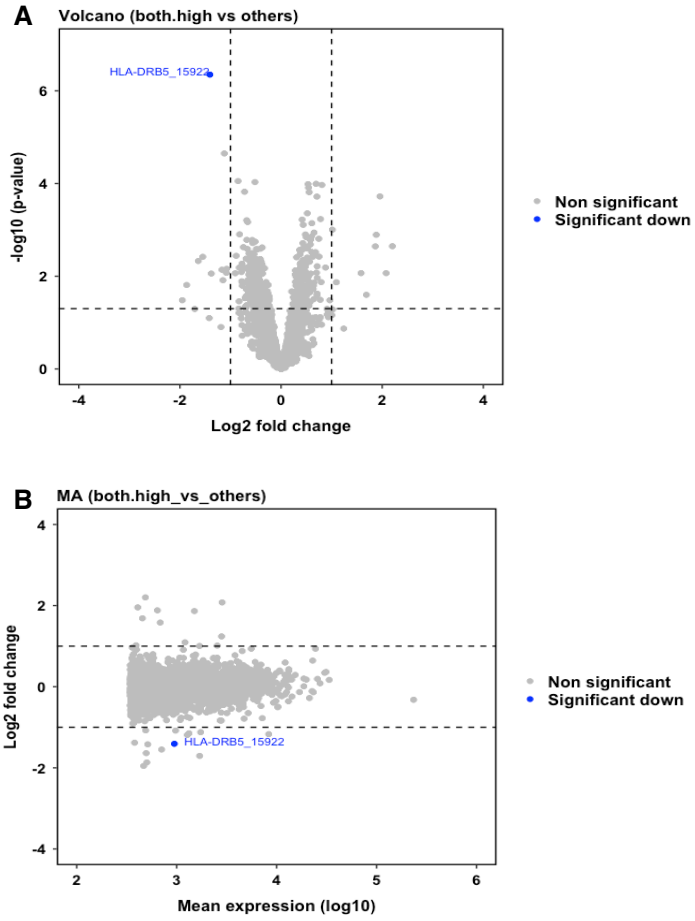

Figure 6.12 – Volcano and MA plots for significant genes of DE both high vs others; A. Volcano plot showing HLA-DRB5, downregulated in myeloid high group, **B.** MA plot showing log2 fold change and average of gene expression, gene name with blue colour labelled represented downregulated expressed gene.

6.3.7.1 Analysis of the expression level of the HLA-DRB5 gene

When observed, the normalized raw gene counts found that HLA-DRB5_15922 was downregulated in the both high group when compared to the others group (**Figure 6.13**).

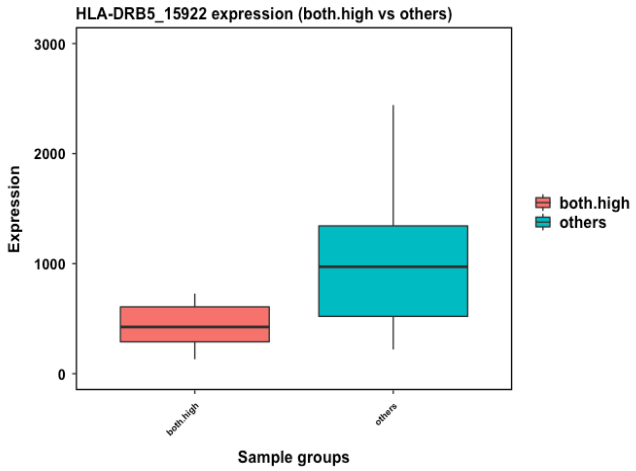

Figure 6.13 - Expression level of HLA-DRB5 significant downregulated genes in DE both high vs others; HLA-DRB5_15922 was the only one gene showing downregulated gene in both high group.

6.3.7.2 Analysis of Gene-Concept network for the *HLA-DRB5* genes

The gene-concept network cnet plot for HLA-DRB5 was analysed, the result revealed that *HLA-DRB5* participating in the network of biological processes relating to antigen presentation pathways, i.e., T-cell receptor signalling pathway, antigen-receptor mediated signalling pathway and interferon-gamma-mediated signalling pathway. (**Figure 6.14**).

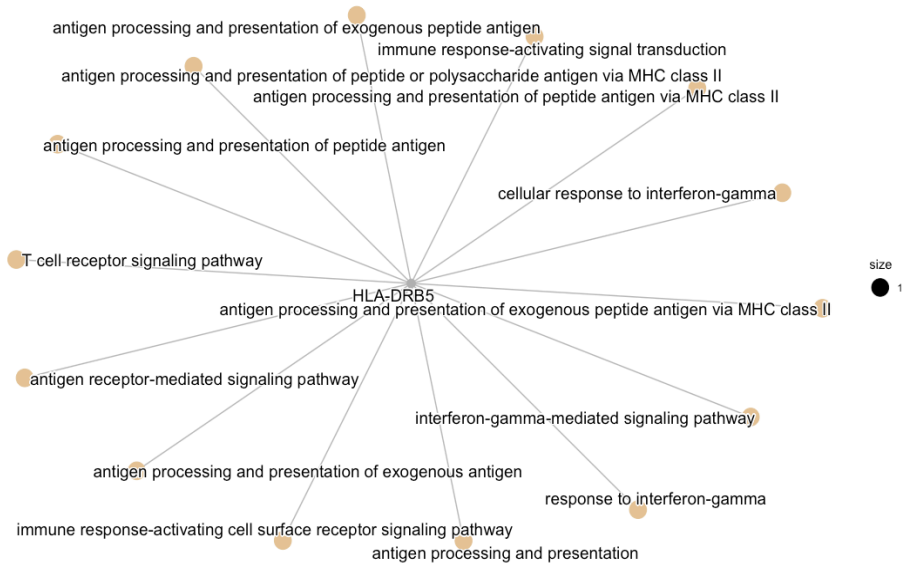

Figure 6.14 - Network plot for HLA-DRB5 significant differentially expressed genes in both high group; Enrichment network, cnet, plot showing the network linking of biological processes of *HLA-DRB5* genes participated in immune response signalling pathways.

6.3.8 Comparison of differentially expressed genes between both low vs others

For the comparison between both low and others groups, the results revealed 29 significant differentially expressed genes, of which 13 genes were upregulated, and 16 genes were downregulated in both low group. For upregulated genes, *S100A4*, *CSPG4*, *HDAC4*, *SLC19A3*, and *PDK4* were top 5 most significant genes (**Table 6.4**). Whereas for downregulated genes, *REG1A*, *SVOPL*, *IGLV5-45*, *IDH2*, and *ELAVL4* were top 5 most significant genes (**Table 6.5**). The log2 fold change and average of expression were shown in Volcano plot and MA plot (**Figure 6.15 A, B**).

Table 6.4 - Significantly upregulated genes in both low group from DE both low vs others

Gene_names	Mean expression	Log2FoldChange	Pvalue	Padj
S100A4_6083	1224.593542	2.67202116	1.02E-08	9.24E-05
CSPG4_24558	382.8702083	1.322040486	8.32E-08	0.000504668
HDAC4_25787	348.090625	1.166686461	6.18E-07	0.002250351
SLC19A3_11343	358.265625	2.47494838	1.00E-06	0.003042794
PDK4_28868	377.6641667	1.380413525	1.41E-06	0.003668626
AKAP12_24261	400.0241667	1.339064323	2.42E-06	0.005031098
TNXA_20709	487.7483333	1.251562614	7.44E-06	0.012320925
CD109_19701	356.1014583	1.870337732	2.50E-05	0.021635943
MST1L_22368	1272.423542	1.183543635	2.83E-05	0.022393497
EPHA4_16068	42.6525	3.407306135	5.50E-05	0.033360297
MLLT11_4193	103.706875	1.331344772	6.45E-05	0.03354161
CACNA1H_19299	563.6945833	1.133414548	8.38E-05	0.042279942
AFAP1L2_26435	602.2014583	1.593498256	0.000101698	0.047479902

Table 6.5 - Significantly downregulated genes in both low group from DE both low vs others

Gene_names	Mean expression	Log2FoldChange	Pvalue	Padj
REG1A_5790	434.27625	-10.62314472	2.74E-15	4.98E-11
SVOPL_88522	14.65229167	-6.557299014	5.13E-07	0.002250351
IGLV5-45_90843	82.073125	-7.798278008	9.14E-06	0.013015936
IDH2_24565	1917.377917	-1.056529605	9.29E-06	0.013015936
ELAVL4_88663	10.83645833	-5.706788784	1.11E-05	0.014490601
TNPO2_14787	6.8525	-5.463564748	1.65E-05	0.019141455
KCNIP2_18588	8.142708333	-5.709718405	1.95E-05	0.020893062
IGLV1_28171	1210.710625	-2.565292392	2.29E-05	0.021635943
CLN6_25567	641.733125	-1.155781054	2.41E-05	0.021635943
REG3G_88681	38.15083333	-7.938903943	3.26E-05	0.023740522
BLM_716	608.5389583	-1.141726103	5.07E-05	0.032987381
TP63_21790	7.642916667	-5.623734004	5.37E-05	0.033360297
ADGRL1_23280	239.4547917	-1.086636783	6.12E-05	0.03354161
HSD3B1_90693	11.55583333	-6.214151558	6.23E-05	0.03354161
KCNJ10_12722	13.62520833	-6.04077744	6.42E-05	0.03354161
TMPRSS7_17846	10.55791667	-6.081502273	0.000108398	0.049342711

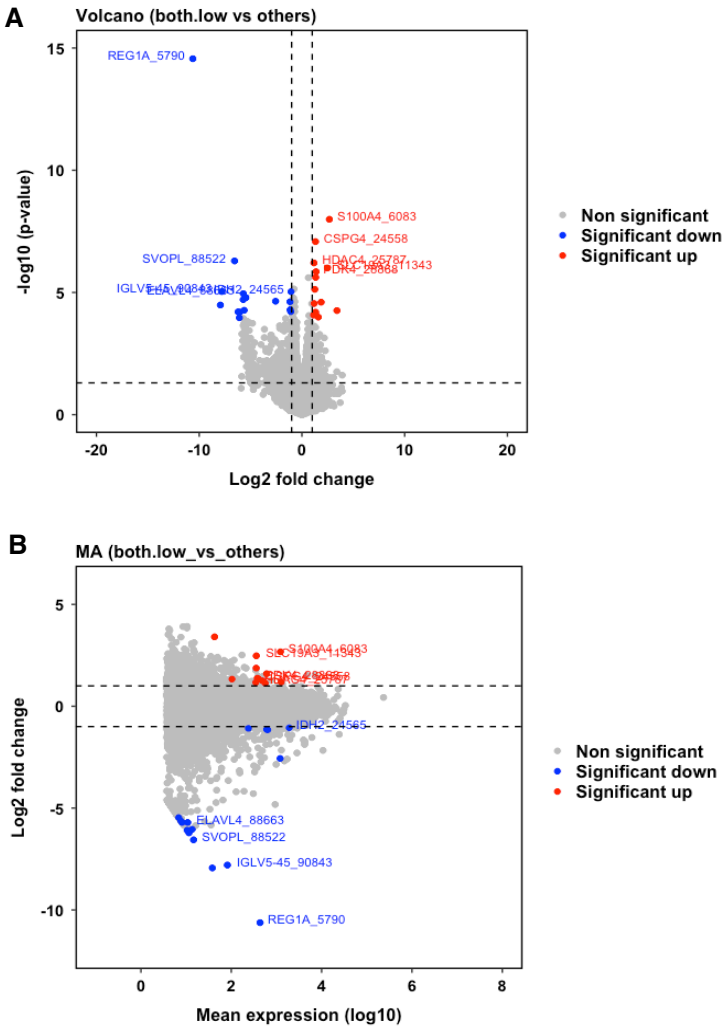

Figure 6.15 – Volcano and MA plots of significant genes for DE both low vs others; A. Volcano plot showing 13 upregulated gene (gene name with red labelled), and 7 downregulated genes (gene name with blue labelled), **B.** MA plot showing log2 fold change and average of expression level.

6.3.8.1 Analysis of expression levels of the 13 significantly upregulated genes

Among 13 significant upregulated genes, S100A4_6083, CSPG4_24558, and HDAC4_25787 were top 3 most significant genes presented high expression in the both low group when compared to others group. However, when observing the expression level, MST1L_22368 showed highest expression level (**Figure 6.16**).

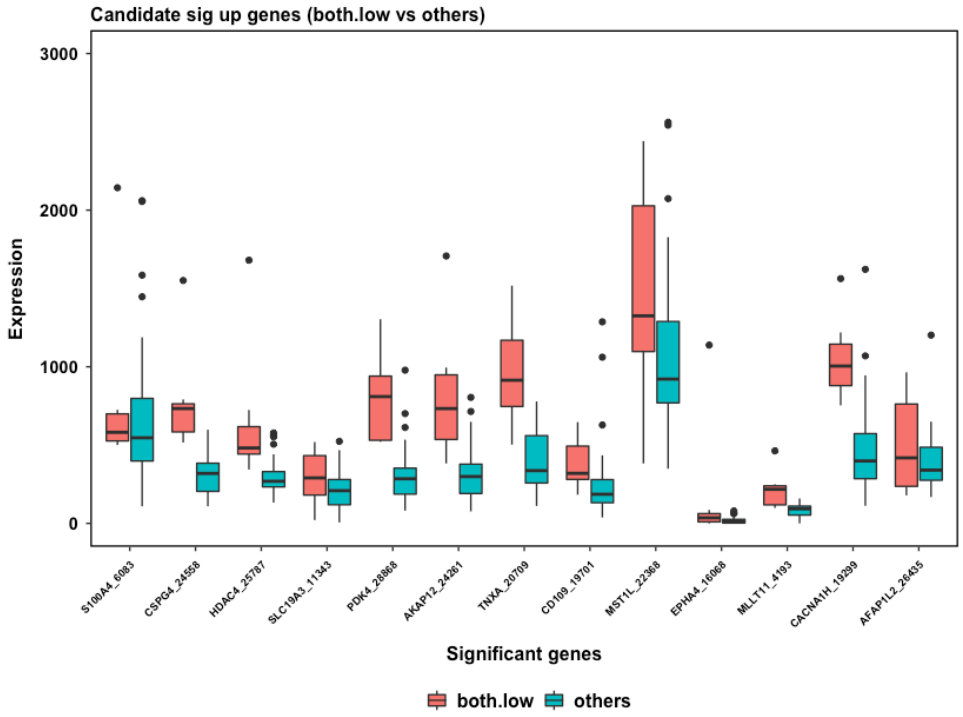

Figure 6.16 - Expression level of 13 significant upregulated genes in DE both low vs others; Among 13 significant upregulated genes, *MST1L*, *TNXA*, *CACNA1H*, *AKAP12*, and *ODK4* were the top 5 genes presented high expression.

6.3.8.2 Analysis of Gene-Concept network for the 13 significant upregulated genes

The gene-concept network cnet plot for significant upregulated genes was analysed, the result revealed 2 clusters of networks. The first network is *CD109* and *CACNA1H* participated in cell-cell fusion, syncytium formation and plasma membrane fusion. Whereas *CACNA1H* and *HDAC4* participated in positive regulation of multi-organism process. The second network is *CSPG4*, *EPHA4*, and *AFAP1L2* participated in positive regulation of peptidyl-tyrosine phosphorylation. Whereas *AFAP1L2* and *EPHA4* participated in positive regulation of protein tyrosine kinase activity (**Figure 6.17**).

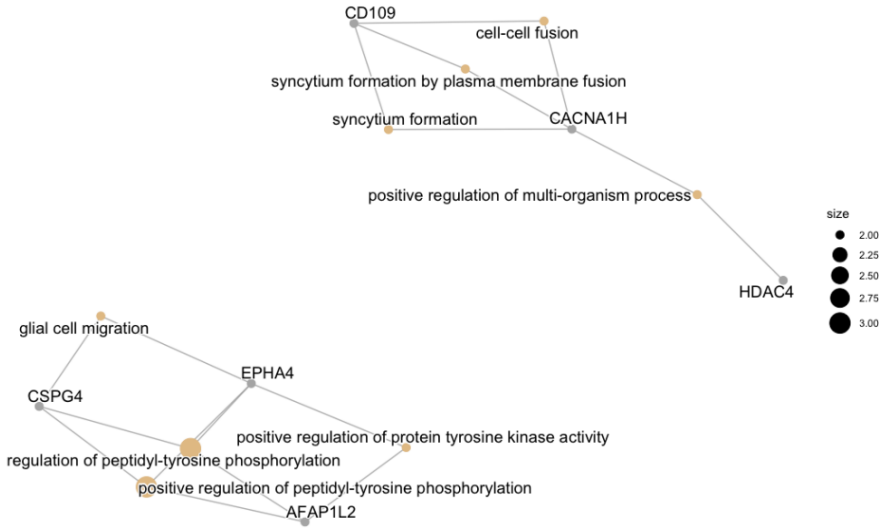

Figure 6.17 - Network plot for enriched 13 significant upregulated genes in both low group; Enrichment cnet network plot showing 2 networks linking to biological processes from 6 out of 13 genes.

6.3.8.3 Analysis of the expression level of the 16 significantly downregulated genes

For downregulated genes, among 16 significantly downregulated genes, REG1A_5790, SVOPL_88522, and IGLV5-45_90843 were top 3 most significant genes. However, IDH2_24565 showed highest expression level in both low group (**Figure 6.18**).

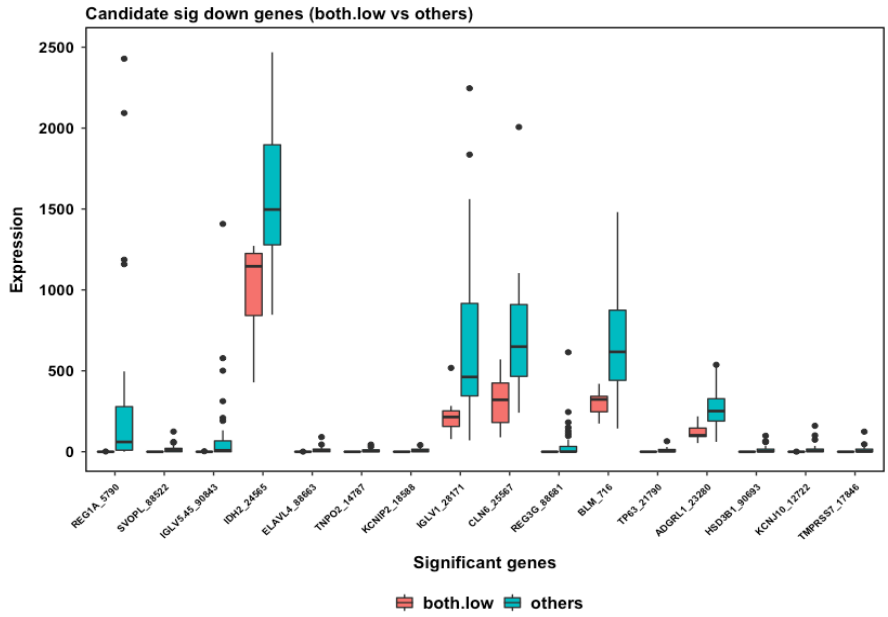

Figure 6.18 - Expression level of 16 significant downregulated genes in DE both low vs others. Showing 16 significant downregulated genes in both low group.

6.3.8.4 Analysis of Gene-Concept network for the 16 significantly downregulated genes

The gene-concept network cnet plot for 16 significant genes was analysed, the result revealed that 2 out of 16 significant genes, *TP63* and *REG3G* appearing in the network linking for negative regulation of epidermal cell differentiation, negative regulation of epidermis development, and positive regulation of keratinocyte proliferation (**Figure 6.19**)

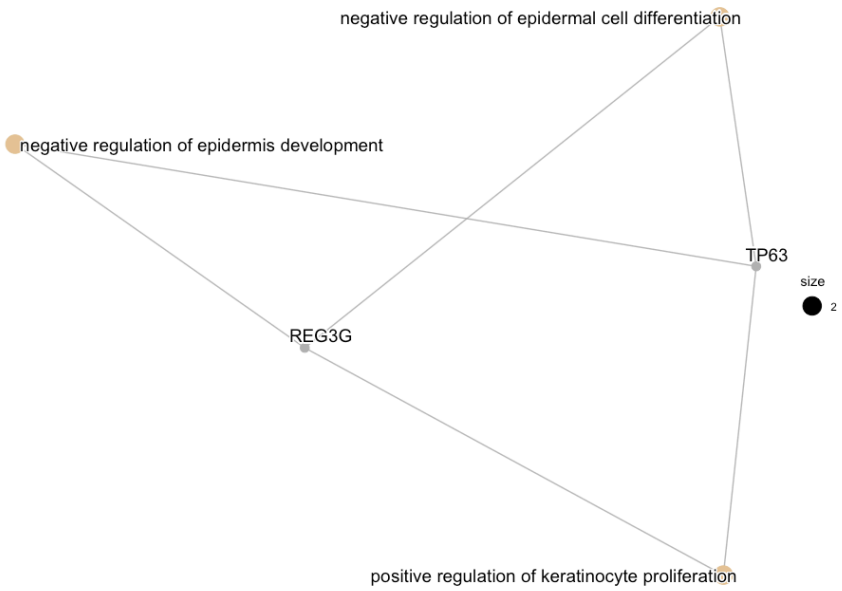

Figure 6.19 - Network plot for enriched 16 significant downregulated genes in both low group; Enrichment network, cnet, plot showing the network linking of biological processes from 3 of 16 genes participated in immune responses.

6.3.9 Venn diagram showing overlapping gene expression between groups

Given the heatmap of top 40 genes expression pointed to the clustering of myeloid high group and the boxplot of expression pattern indicated a solid pattern of high expression in myeloid high group. Therefore, to observe whether there are overlapping of significant genes expressed between myeloid group and the other 3 groups, the size proportional Venn diagram was constructed from 3 DE comparison between myeloid high and the other groups, DE myeloid high vs T-cells high, DE myeloid high vs both high, and DE myeloid high vs both low group. The result designated no overlapping genes expression from all significant differentially expressed 44 genes (**Figure 6.20**). Suggesting that in myeloid high group might develops distinct gene expression pattern depends on which immune cell compositions presented around them in the microenvironment. However, this comparison should be performed for T-cell high with against other groups as well, unfortunately, our data contained only 3 samples available for analysis which could not give conclusive results.

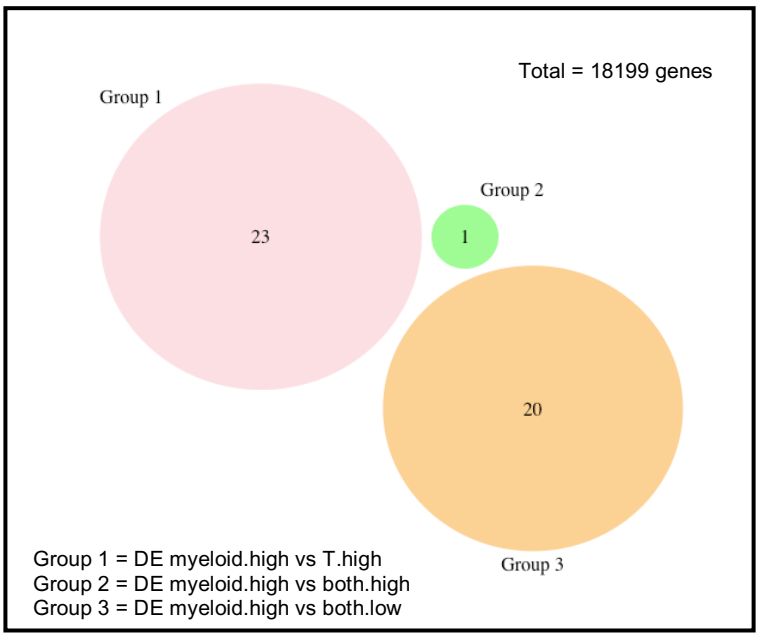

Figure 6.20 - Venn diagram of overlapping of significant differentially expressed genes for 4 tumour immune landscape groups; The size proportional Venn diagram showing no overlapping genes appeared from all significant differentially expressed genes when compare between groups.

6.3.10 Comparison of differentially expressed genes between myeloid high vs T-cells high

Next, DE table was extracted to clarify the significantly differentially expressed genes for myeloid high versus T-cells high. The result showed 23 significantly differentially expressed gene, with upregulation in myeloid high group. Of which, SLC51A_15250, ORM1_4833, CPA2_18016, CFHR3_11110, SLC15A1_16854, MUC6_89994, ST18_6795, TTC29_90764 were the top significant genes with elevated fold changes (**Table 6.6**). The log2 fold change and average of expression were shown in Volcano plot and MA plot (**Figure 6.21 A, B**).

Table 6.6 - Significantly upregulated genes in myeloid high group from DE myeloid high vs T-cells high

Gene names	Mean expression	Log2FoldChange	Pvalue	Padj
SLC51A_15250	17.109792	20.37958535	1.48E-21	2.69E-17
ORM1_4833	103.345833	21.85353622	2.46E-20	2.24E-16
CPA2_18016	8.859583	19.56959836	2.08E-12	1.26E-08
CFHR3_11110	11.023125	19.23110008	3.95E-12	1.80E-08
SLC15A1_16854	7.423542	19.0738721	9.26E-11	3.37E-07
MUC6_89994	10.200625	18.6325807	1.34E-10	4.07E-07
ST18_6795	10.524375	18.21218713	2.43E-10	6.32E-07
TTC29_90764	60.894167	21.14858488	3.71E-10	8.44E-07
CXCL5_15735	141.115833	9.371800351	1.64E-07	0.00033164
KRT34_33638	19.037500	19.20393792	3.25E-07	0.000591472
PEPD_12569	31.484583	7.48393439	4.35E-07	0.000719074
FAM3B_11565	137.984375	9.6508985	2.12E-06	0.003222498
SNTB1_11109	32.438542	7.498449263	3.95E-06	0.005534823
ZNF416_16733	22.699583	7.079290703	4.52E-06	0.00587623
NKX2-1_18021	10.701875	20.76148117	6.53E-06	0.007919455
DHRS7B_19227	31.145000	7.336738079	9.62E-06	0.010875819
ADM5_20591	33.320417	7.751699785	1.05E-05	0.010875819
USP28_91295	26.606250	7.352923418	1.08E-05	0.010875819
ANKRD20A8P_34050	28.532292	6.907758987	1.19E-05	0.011372914
DCAF4L1_14168	56.658125	4.582241376	1.51E-05	0.013113321
PDE11A_88245	59.599167	7.490958725	1.45E-05	0.013113321
MAGEA11_3937	26.639375	18.27053149	2.68E-05	0.022153121
BCL3_668	18.228750	6.986311705	2.89E-05	0.022831886

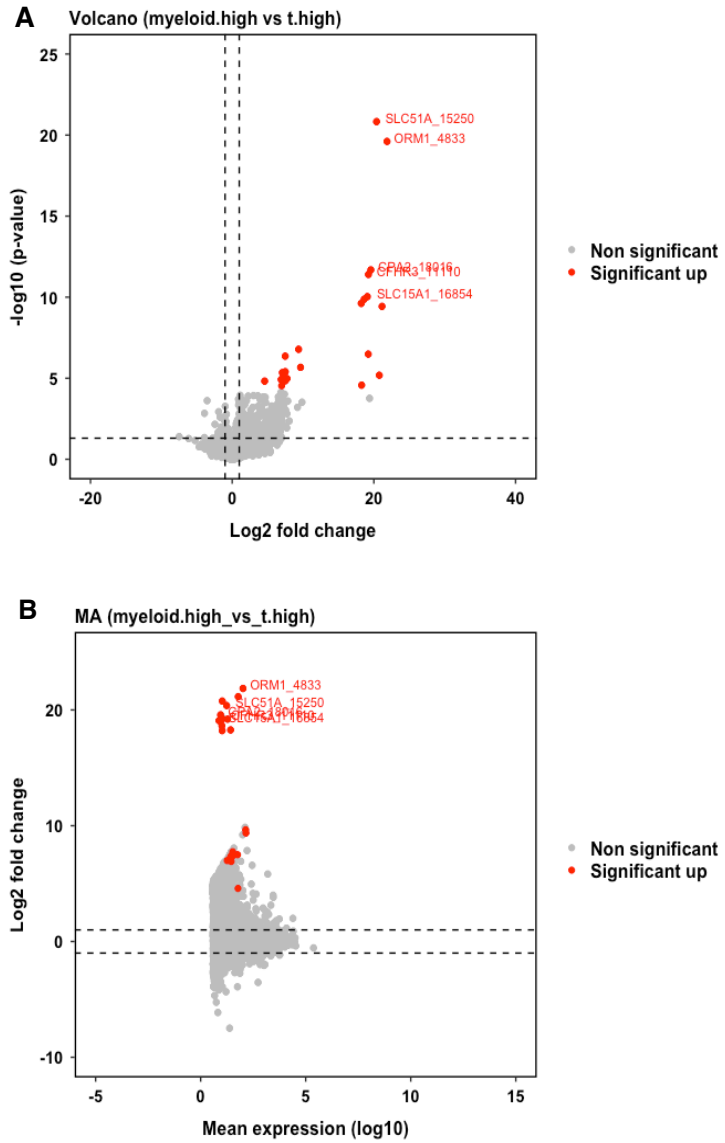

Figure 6.21 - Significant differentially expressed genes for DE myeloid high vs T-cells high; A. Volcano plot showing 23 significant differentially expressed upregulated genes in myeloid high group, **B.** MA plot showing log2 fold change and average of expression level. The labelled gene name in red were top 5 most significant upregulated genes.

6.3.11 Comparison of differentially expressed genes between myeloid high vs both high

Again, DE table was extracted to clarify the significantly differentially expressed genes for myeloid high versus both high group. The result showed 1 significantly differentially expressed gene, with upregulation in myeloid high group, HLA-DRB5_15922 (**Table 6.7**). The log2 fold change and average of expression were shown in Volcano plot and MA plot (**Figure 6.22 A-B**).

Table 6.7 - Significantly upregulated genes in myeloid high group from DE myeloid high vs both high

Gene names	Mean expression	Log2FoldChange	Pvalue	Padj
HLA-DRB5	947.3431	1.441622	1.143194e-06	0.02346062

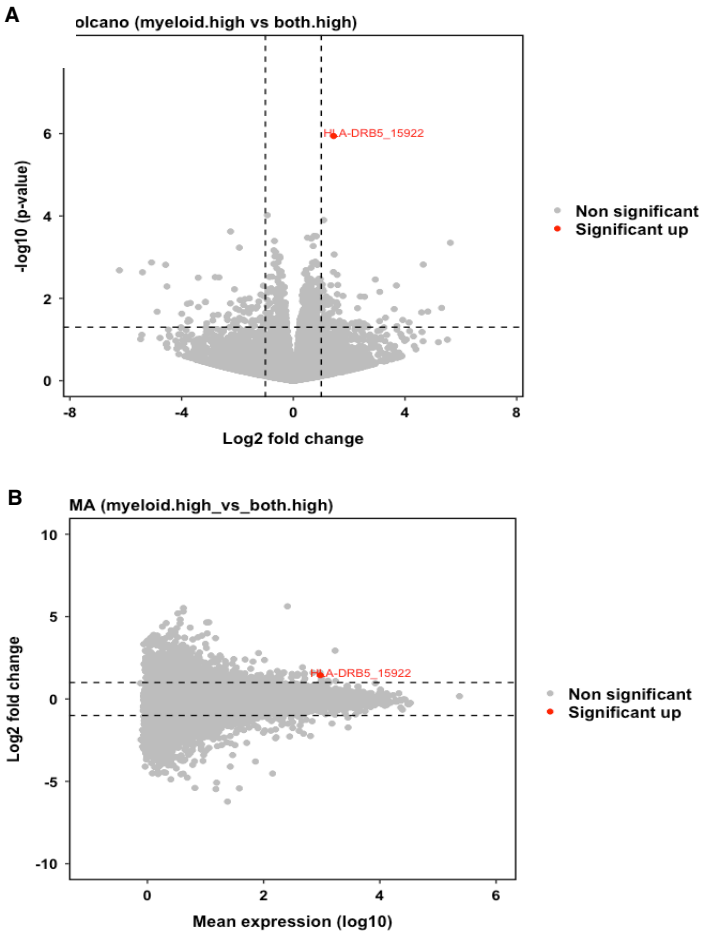

Figure 6.22 - Significant differentially expressed genes for DE myeloid high vs both high; A. Volcano plot showing *HLA-DRB5* was the one significant differentially expressed upregulated genes in myeloid high group, **B.** MA plot showing log2 fold change and average of expression level.

6.3.12 Comparison of differentially expressed genes between myeloid high vs both low

Next, DE table was extracted to clarify the significantly differentially expressed genes for myeloid high versus both low group. The result showed 20 significantly differentially expressed genes, of which 16 genes were upregulated, and 7 genes were downregulated in myeloid high group. For upregulated genes, ART3_25022, REG1A_5790, and ANKRD30B_10482 were the most top 3

significant genes with high log2 fold change (**Table 6.8**). As for significant downregulated genes, S100A4_6083 and PDK4_28868 were the most significant genes (**Table 6.9**). The log2 fold change and average of expression were shown in Volcano plot and MA plot (**Figure 6.23 A, B**).

Table 6.8 - Significantly upregulated genes in myeloid high group from DE myeloid high vs both low

Gene_names	Mean expression	Log2FoldChange	Pvalue	Padj
ART3_25022	7.342708	19.34399499	3.03E-17	6.21E-13
REG1A_5790	434.276250	10.97843849	1.45E-15	1.49E-11
ANKRD30B_10482	23.891667	17.17168515	1.51E-10	1.04E-06
SVOPL_88522	14.652292	6.641055089	1.36E-06	0.003495798
PES1_92441	244.842292	1.053018334	4.23E-06	0.008680336
ELAVL4_88663	6.852500	6.059343251	7.13E-06	0.012200781
TNPO2_14787	10.836458	5.8713582	6.90E-06	0.012200781
IGLV5-45_90843	82.073125	8.124953543	8.07E-06	0.012732927
HIST1H2AL_20843	785.046458	1.06275607	1.30E-05	0.016451333
REG3G_88681	38.150833	8.14847785	3.25E-05	0.035109359
ADGRL1_23280	239.454792	1.184360139	3.43E-05	0.035223761
KCNIP2_18588	8.142708	5.720402585	4.44E-05	0.041994388
MKKS_17700	474.676042	1.010235686	5.16E-05	0.046014596

Table 6.9 - List of 7 significantly upregulated genes in myeloid high group from DE myeloid high vs both low

Gene_names	Mean expression	Log2FoldChange	Pvalue	Padj
S100A4_6083	1224.5935	-2.725496467	4.56E-08	0.00023379
PDK4_28868	377.6642	-1.575000194	1.03E-07	0.000422191
CSPG4_24558	348.0906	-1.25512772	1.24E-06	0.003495798
HDAC4_25787	382.8702	-1.216699873	1.05E-06	0.003495798
SLC19A3_11343	358.2656	-2.509902906	3.52E-06	0.008016024
AKAP12_24261	400.0242	-1.331770018	1.07E-05	0.014600646
AFAP1L2_26435	602.2015	-1.797176623	2.70E-05	0.030807274

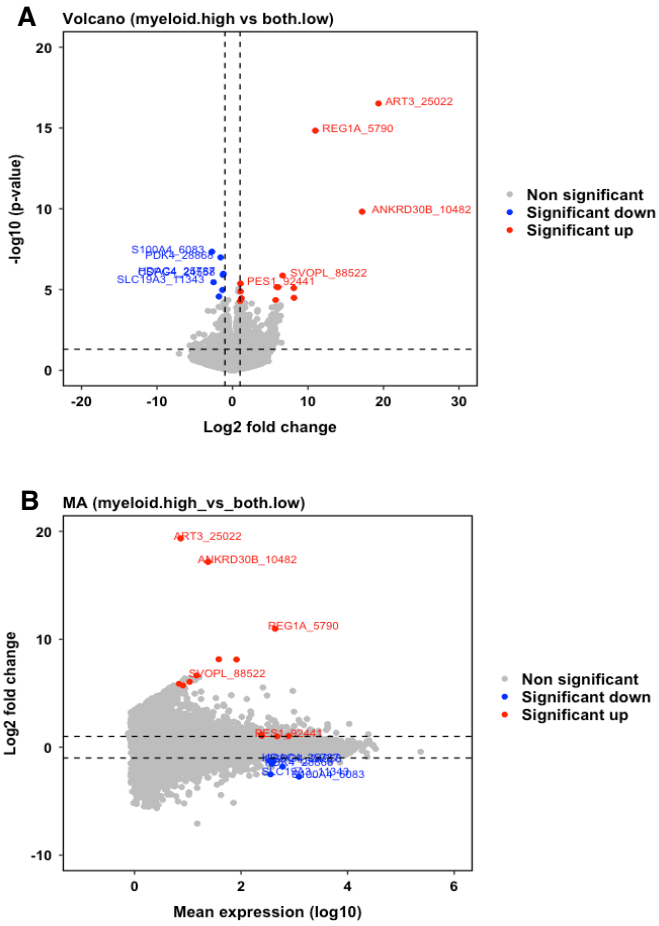

Figure 6.23 - Significant differentially expressed genes for DE myeloid high vs both low; A. Volcano plot showing 13 significant differentially expressed upregulated genes, and 7 genes downregulated genes in myeloid high group, **B.** MA plot showing log2 fold change and average of expression level. The labelled gene name in red were top 5 most significant upregulated genes, and labelled gene name in blue were the top 5 most significant downregulated genes.

6.3.13 Analysis of Protein-proteins interaction (PPI) networks for significant genes across all immune landscapes

As the aim of this chapter was to identify differentially expressed genes in each immune landscape grouping, and the results presented distinct sets of gene expression between groups, especially for myeloid high group. Therefore, the PPI networks for significant differentially expressed gene sets was constructed with modifying by adding more genes for clarification of networks involve (**Figure 6.24**). The interaction network plot showing most of significant genes from study could be linked to a TP53 network including IDH2, S100A4, TP63, KRT34, IGF2BP1, ELAVL4, NKX2-1, USP28, AKAP12, MUC6, HDAC4, PES1, and SLC19A3. The other network groups consisted of REG3G-REG3A-REG1A for regenerating islet-derived (REGs) proteins network have been implicated in a variety of diseases including diabetes, various types of cancer of the digestive tract, and Alzheimer disease; KCNIP2-CACNA1H-KCNJ10 for potassium and calcium channel-interacting proteins; NFX2-TNPO2 for nuclear transcription factor and transportin protein; SLC15A1-SLC51A for intestinal hydrogen peptide cotransporter localized to the brush border membrane of the intestinal epithelium plays an important role in the uptake and digestion of dietary proteins.

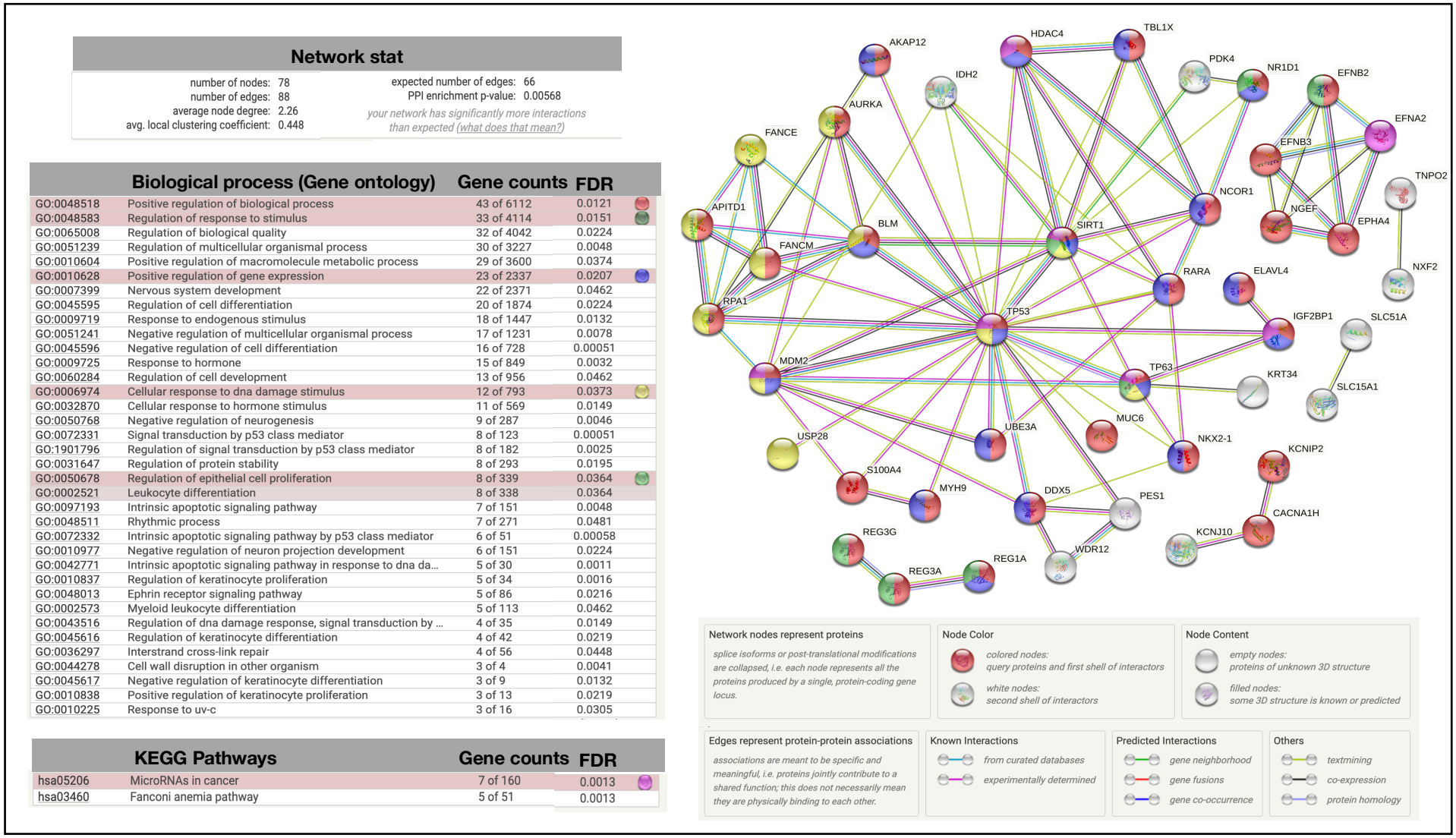

Figure 6.24 - STRING interaction network plot for all significant differentially expressed genes from all DE comparison groups. STRING interaction network for all significant genes with modifying by adding more genes for network clarification showing most of significant genes from study could be linked to TP53 network including TP63, IGF2BP1, ELAVL4, NKX2-1, KRT34, USP28, AKAP12, MUC6, HDAC4, PES1, SLC19A3, BLM, IDH2, S100A.

6.3.14 Association between TP53 mutation and significant gene expressions

Finally, from PPI network, the most of proteins of interest were predominantly related to *TP53* network. Therefore, the associations between *TP53* mutations and normalized raw counts of genes of interest from each immune landscape group were assessed. *TP53* mutations were available for 32/48 samples for this analysis, of which 19 were mutants and 13 were wild-type *TP53*.

Firstly, the correlation between p53 protein levels and *TP53* gene expression levels was checked to validate the transcriptomics data.

6.3.14.1 *TP53* gene expression and nuclear p53 protein expression

As *TP53* mutation chapter 5 found that *TP53* mutation was significantly associated with high nuclear p53 expression. Therefore, the correlation between TP53_7287 expression and p53 protein expression was observed. A boxplot showed high nuclear p53 expression was correlated with high TP53_7287 expression level (**Figure 6.25**).

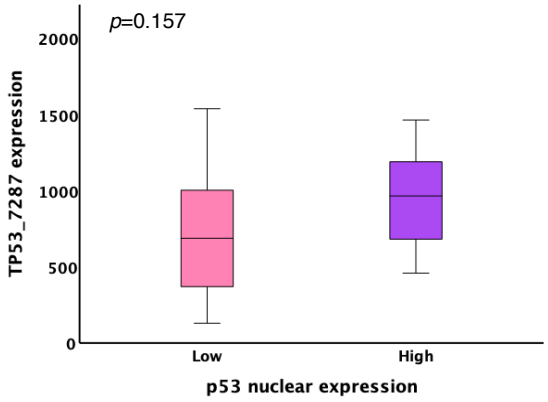

Figure 6.25 - Association between TP53_7287 gene expression and nuclear p53 expression. High TP53_7287 expression was correlated with high nuclear p53 expression.

6.3.14.2 *TP53* mutations and upregulated genes in myeloid high - *REG1A*, *REG3A*, *REG3G*

From the myeloid high group, 3 genes were assessed which were upregulated, REG1A_5790 (**Figure 6.26 A**), REG3A_22026 (**Figure 6.26 B**), and REG3G_88681 (**Figure 6.26 C**). All three genes were downregulated in the presence of *TP53* mutations when compared to wild-type *TP53*. However, these differences between mutant and wildtype p53 were non-significant which might be due to small

patient numbers in the analysis. Therefore, a larger cohort are needed to validate these results. As REGs proteins have a pro-tumorigenic function in gastrointestinal tract, therefore, downregulating their expression in p53 mutant tumours might influence the patient's better prognosis seen in the previous chapter.

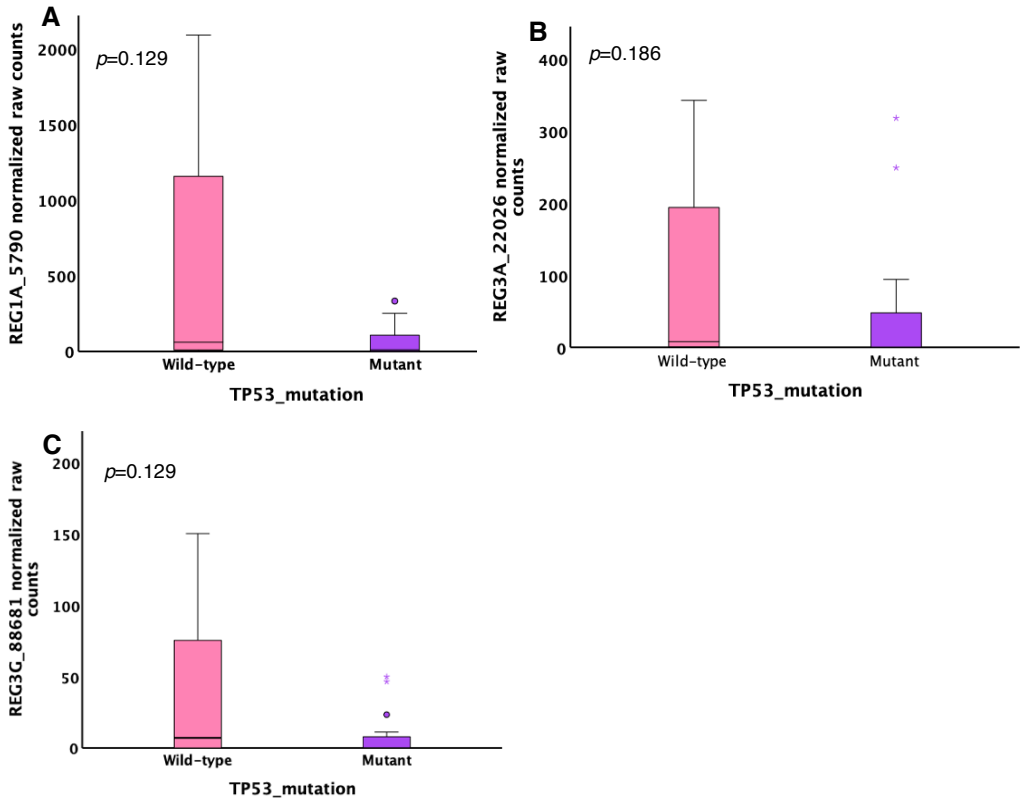

Figure 6.26 - Association between *TP53* mutations and REG1A, REG3A, REG3G genes expression, significant differentially upregulated in myeloid high group; A. REG1A_5790, **B.** REG3A_22026, and **C**. REG3G_88681 expressions were downregulated in *TP53* mutant when compared to wild-type *TP53*.

6.3.14.3 *TP53* mutations and downregulated genes in myeloid high - *IGF2BP1*

As for a downregulated gene in myeloid high group, IGF2BP1_24044, was found to be upregulated in patients with *TP53* mutations however, this was not significant (**Figure 6.27**). Again, a larger cohort are needed for further elucidation of these result.

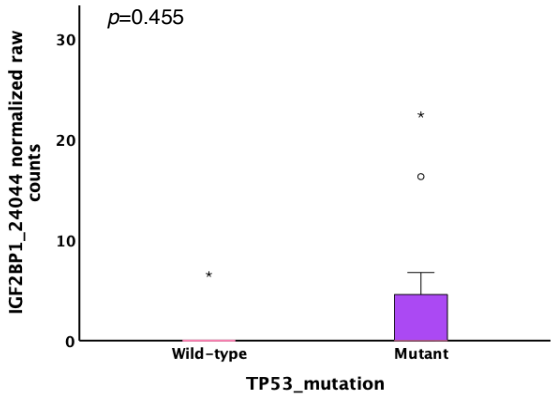

Figure 6.27 - Association between *TP53* mutations and IGF2BP1_24044 significant differentially downregulated gene in myeloid high group; *TP53* mutations associated with upregulation of IGF2BP1 gene in myeloid high group.

6.3.14.4 *TP53* mutations and downregulated genes in both-high – *HLA-DRB5*

For the downregulated gene in both high group, HLA-DRB5_15922, TP53 mutations did not affect the expression level as expression in wild-type and mutant p53 patients was similar. A larger cohort is also needed to clarify this result (**Figure 6.28**).

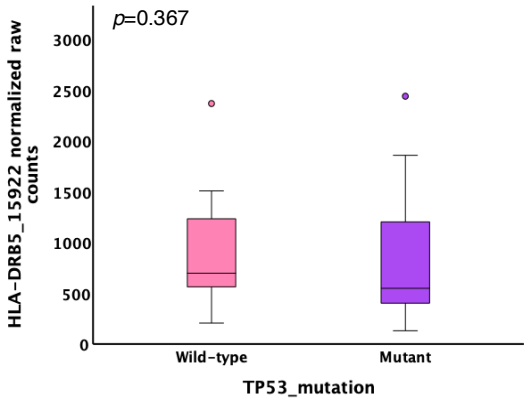

Figure 6.28 - Association between *TP53* mutations and HLA-DRB5_15922 significant differentially downregulated gene in both high group; *TP53* mutations presented no effect to *HLA-DRB5* expression level in both high group.

6.4 Discussion

The results from current study indicated different patterns of gene expression in each tumour immune landscape grouping. In general, PCA analysis and gene clustering revealed potential gene clusters for myeloid high, both high, and both low groups, but not for T-cells high group due to small sample numbers. When observed the heatmap of top 40 genes expression revealed 3 expression patterns, from which low expression was potentially predominantly made up of patients from the myeloid high group, whereas the other two groups consisted of the mix populations of other groups. When observed boxplot for patterns of gene expression, the results presented high expression levels in myeloid cells high, whereas low expression in T-cells high group. A similar pattern to myeloid high occurred in both high and both low groups, suggesting that the expression pattern of these 2 groups might be influenced by myeloid high group.

When assessing the DEGs in T-cells high groups when compared to others group, the results showed downregulation of multiple genes which participating in immune response and would healing. This might because T-cells high is a good prognosis group. Whereas in myeloid high group showed downregulated in a gene *IGF2BP1*, which participating in RNA manipulation, i.e., stabilization, transport, etc. This might account for the pro-tumorigenic effect of myeloid high, disruption of RNA transcription. Whereas in both high group presented with downregulation of a gene *HLA-DRB5*, which participating in T-lymphocytes receptor signalling and other antigen presenting signalling pathways. This might because with high mixed immune cells infiltration the killing function is intact, and antigens can be recognised. Whereas in both low group there was both upregulation and downregulation of multiple genes, that need more investigation as the biological processes recognised were not easily associated with cancer or the immune system. This suggests that different gene expression patterns from each group participated in different biological processes which might be specific to each biological condition dependant on which immune cell compositions are being orchestrated in the tumour and its microenvironment.

As myeloid high might be an important driver for gene expression pattern among the four groups, it was decided to observe more specifically for the DEGs between myeloid high groups and the three others was performed. First, when compared myeloid high with T-cells high, found 23 significant differentially upregulated genes. Whereas, if compared myeloid high to both high group, only one significant upregulated gene, *HLA-DRB5*, was found. As this gene was downregulated in both high group, it suggests this gene may be upregulated in the myeloid high group. Lastly, when compared myeloid high to both low group, the results revealed 20 significant differentially expressed genes, of which, 13 genes were upregulated, and 7 genes were downregulated in myeloid high. From Venn

diagram displayed no overlapping gene expressions from 44 significant DEGs based on myeloid high group, therefore, myeloid high might be an important factor influencing different gene expression pattern dependant on the other immune cells within the tumour microenvironment. When a mix of immune cells as seen in both high, not many genes are differentially expressed suggesting myeloid high is the over-riding factor in this group. Whereas when compared to T-cell high or both low, where myeloid high is not involved, many genes are differentially expressed.

Next protein-protein interaction networks from significant genes, with modification by adding more genes during generated STRING networks were analysed. The main link was a *TP53* network, with some genes forming a few other independent linkages. This suggest that most of the significant genes found in this study are part of a *TP53* network. As we have the results showing *TP53* mutations are associated with a stromal myeloid landscape from chapter 5, therefore, the correlation between *TP53* mutations and these DEGs expression level were constructed.

When looking at the downregulated gene found in myeloid high group, IGF2BP1_24044, it was found that patients with *TP53* mutations appeared to have higher expression level, though this did not reach significance. *IGF2BP1* (Insulin-like growth factor 2 mRNA-binding protein 1) is a crucial regulator of tumour and stem cell fate and its elevated expression in a multitude of tumour is associated with poor prognosis (Glass et al., 2021). As *IGF2BP1* participated in RNA stability, downregulation might cause mutations and differential expression at protein level, therefore, upregulation in patients with *TP53* mutations could stabilise mRNA and contribute to the good outcomes seen in these patients.

HLA-DRB5 is a gene encoding for classical major histocompatibility complex (MHC) class II molecule and antigen-presenting cells. Again, this gene may be upregulated in the myeloid high, however in the both high group, with both T-lymphocytes and myeloid cells high, this gene was downregulated, and showed no differential expression between *TP53* mutations and wildtype patients. Recently, Schaafsma et.al. proposed the comprehensive analysis of HLA gene expression from multiple databases in combination with patient's cohorts receiving immune-checkpoint blockade treatment involving in 33 cancer types. They found that elevated HLA gene expression is associated with prolong survival in several cancer types, and HLA class II expression during treatment is associated with response to immune checkpoint blockade. Therefore, HLA gene expression is important for patients prognosis (Schaafsma et al., 2021). Therefore, it is interesting that *HLA-DRB5* is down-regulated in the both high group which has a good prognosis, suggesting it may play a different role in these patients.

Interestingly, among DEGs, the REGs genes; *REG1A*, *REG3A*, and *REG3G* presented upregulation in wild type *TP53* and downregulation in *TP53* mutated patients. REGs, Regenerating Islet-Derived, genes and proteins have arisen to obtain multifunction include pro-proliferative, anti-apoptotic, differentiation-inducing, and anti-bacterial properties. REGs protein family has been shown to have affects in multiple organs, and as pro-tumorigenic in colon tissues (Chen et al., 2019; Sun et al., 2021). Therefore, downregulated causing by *TP53* mutation might could turn down the tumorigenic state into normal state in colon tissue. However, this was not statistically significant even though the high differences expression level was observed, this might be due to small sample numbers. Therefore, the large cohort is needed to validate the results.

In conclusion, this study presented the potential gene expression pattern which might be driven by myeloid cells in CRC patient's cohort. The results revealed significant DEGs specific for immune landscapes, especially in myeloid high group. REGs genes, *REG1A*, *REG3A*, *REG3G*, were significantly upregulated in myeloid high and downregulated in T-cells high groups. *HLA-DRB5* was upregulated in myeloid high group but downregulated in both high group, whereas *IGF2BP1* was downregulated in myeloid high group. Most of significant DEGs were connected to *TP53* networks. *TP53* mutation was associated with downregulation of REGs genes, and upregulation of the *IGF2BP1* gene. Therefore, this might influence the good prognosis of p53 mutations in the tumour microenvironment where we see an influx of myeloid cells. However, a larger cohort of patients are needed to validate the present results.

Chapter 7 Establishment of 3-D co-culture model using CRC and immune cell lines to assess immune checkpoint inhibitors (anti-PD-1/anti-PD-L1)

7.1 Background

Immune checkpoints are well recognized as negative regulators of T-lymphocytes function and play a crucial role in limiting anti-tumour immune responses. Two types of co-inhibitory proteins that are widely studied are programmed cell death protein 1 (PD-1: bind to specific ligand called PD-L1), and cytotoxic T-lymphocyte antigen 4 (CTLA-4) (Buchbinder & Desai, 2016). Immune checkpoint interactions can be blocked with anti-PD-1/anti-PD-L1/anti-CTLA-4 lead to immune cell re-activation and a coordinated T-lymphocytes anti-tumour response. Therefore, immunotherapy is now a main focus for many cancer types (Farkona S, 2016; Stanley J. Oiseth, 2017b). Pembrolizumab, nivolumab, and cemiplimab are approved anti-PD-1 immune checkpoint inhibitors for use within the clinical setting. Atezolizumab, durvalumab, and avelumab are also approved anti-PD-L1. Ipilimumab is an approved anti-CTLA-4 for clinical use.

3-dimentional (3D) multicellular tumour models, tumour spheroids and tumour organoids are becoming promising tools in cancer research as they are a better representative of *in vivo* solid tumour than 2D monolayer models (Fitzgerald et al., 2020). 2D models lack the complexity of tumour characteristics and the microenvironment, whereas co-culture 3D models mimic several aspects of tumour physiology and the microenvironment (Han et al., 2021; Vis et al., 2020). Furthermore, 3D co-culture models are thought to be superior in terms of monitoring drug effects as they represent an *in vivo*-like human tissue better and should be employed alongside animal models (Goers et al., 2014). Therefore, tumour 3D models are a promising approach in various types of studies including co-culture of cancer cells with other cells in TME such as immune cells, and fibroblast mimicking *in vivo* status for multiple tumour types including CRC (Bauleth-Ramos et al., 2020; Franchi-Mendes et al., 2021; Koh et al., 2019; Venter & Niesler, 2018). This chapter, therefore, aimed to establish a 3-D co-culture model comprising a CRC tumour cell line and immune cell lines (T-lymphocytes and macrophages) in double or triple co-cultures. These 3-D co-culture models were then treated with anti-PD-1/anti-PD-L1 individually and in combinations to see the effects of immunotherapy on different cell compositions that mimic the immune landscape groups developed in chapter 3.

7.2 Method

Firstly, PD-L1 expression on HT29, PD-1 expression on Jurkat E6-1 t-cell line, and CD163 expression on RAW264.7 macrophage cell line was assessed to investigate the suitability of the cell lines for co-culture. Next, HT29 spheroid formation was assessed to investigate the optimal spheroid size and seeding density. Then, the best media for co-cultures was checked by varying the media normally used for each cell line and assessing growth and health of the cells. Immune cell line

infiltration into spheroids was then observed to estimate the immune cell seeding density for use in both double and triple co-cultures. Next, anti-PD-1 (Pembrolizumab, Nivolumab) and anti-PD-L1 (Atezolizumab) inhibitors were tested in each cell line to assess the optimal non-toxic concentration when tumour (HT29) and immune cells (Jurkat E6-1 human T-lymphocytes, RAW264.7 murine macrophage) were grown alone. Double and triple co-cultures of HT29 and Jurkat E6-1 T-lymphocytes or/and RAW264.7 macrophage were performed to assess the response to each inhibitor by observing the effects on proliferation and apoptosis. Effects of combinations of anti-PD-1 and anti-PD-L1 treatment on the co-cultures were also assessed.

7.3 Results

7.3.1 Determining immune checkpoint expression on CRC and immune cell lines

7.3.1.1 PD-L1 expression on HT29 cells

Firstly, PD-L1 expression on HT29 tumour cells was performed by immunoblotting. Protein extraction was performed from HT29 cells culturing in T75 flasks. Anti-PD-L1 antibody concentration was used at 1:1000. Two other colon tumour cell lines, DLD1 and SW620 were used as positive control as stated to express PD-L1 in literature. Molecular weight (Mboowa et al.) for PD-L1 is ~40-50kDa. The result showed positive PD-L1 expression for all cell lines, DLD1, SW620, and HT29 (**Figure 7.5**). Tubulin protein was used as the housekeeping control, unfortunately, there was a problem with saving of this image making it unavailable for publication in this thesis.

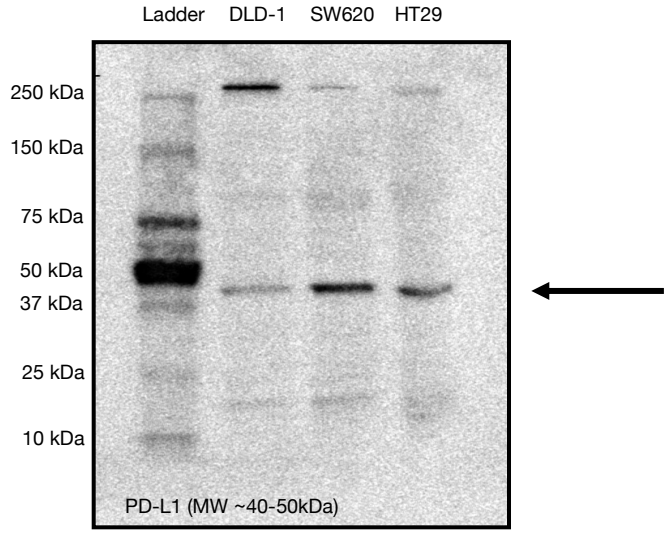

Figure 7.1 – PD-L1 expression on HT29 colorectal cancer cell line; PD-L1 expression was determined on HT29, with DLD-1 and SW620 run as positive control cell lines. The molecular weight of PD-L1 is ~40-50kDa, showing positive PD-L1 bands for DLD-1, SW620, and HT29 as shown by arrow.

7.3.1.2 PD-1 expression on Jurkat E6-1 human T-lymphocytes cell line

PD-1 expression was assessed using Jurkat cell pellets. PD-1 DNA plasmid transfection was employed as a positive control. Three conditions were used to assess PD-1 expression in Jurkat cell pellets: Jurkat cells in control media only (**Figure 7.6 A**), Jurkat cells with lipofectamine transfection reagent control (**Figure 7.6 B**), and Jurkat cells with PD-1 DNA plasmid transfection (**Figure 7.6 C**). Due to the small size of some of the cell pellets, the Observer microscope was utilized at 20x magnification to assess PD-1 expression. The results showed positive PD-1 expression for all conditions. The slide with Jurkat cells in media control was then scanned (**Figure 7.6 D**) to allow closer magnification, and comparison to a positively stained colon tissue section (**Figure 7.6 E**). This confirmed Jurkat E6-1 T-lymphocytes express PD-1 protein.

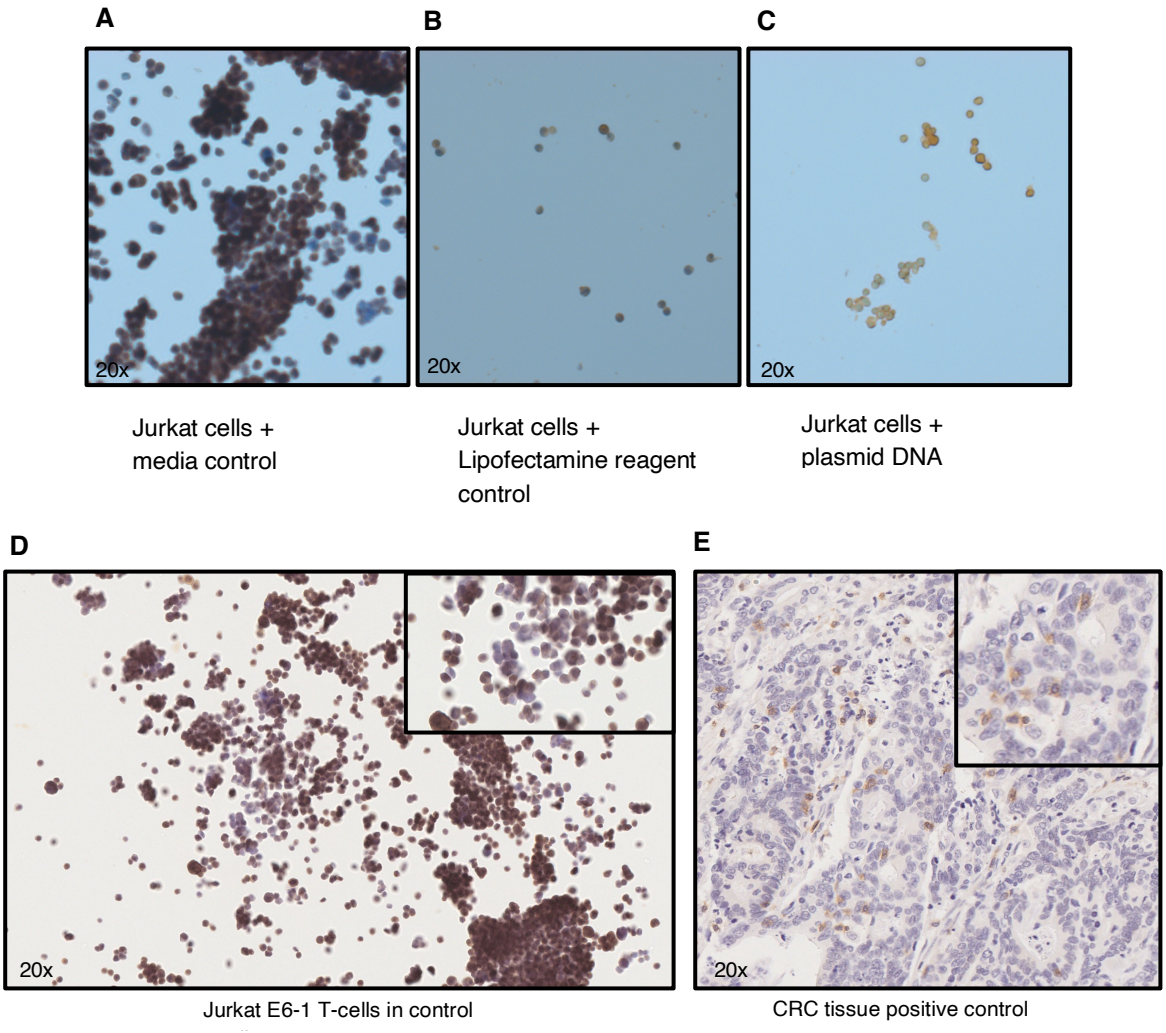

Figure 7.2 - PD-1 expression on normal and transfected Jurkat E6-1 T-lymphocytes; IHC stained for PD-1 expression on Jurkat E6-1 cell pellets. Jurkat cells from all conditions showed positive PD-1 expression, Jurkat in control media (**A**), reagent control (**B**), with plasmid DNA transfection (**C**), when observed by Observer microscope at 20x magnification. The Jurkat in control media (**D**) and positive stained from colon tissue (**E**) were observed from scanner at 20x and 40x (insert) magnification.

7.3.2 Determining CD163 expression on RAW264.7 murine macrophage cell line

To check the phenotype of RAW264.7 macrophages, conditioned media collected after 1 day of HT29 spheroid culturing was added to RAW264.7 macrophage culture. The cells were then collected when they reached confluency and were prepared as cell pellets for IHC staining. CD163 staining for M2 macrophage phenotype was performed on RAW264.7 cell pellets and colon tissue control. The results were observed by Observer microscope at 10x magnification, showing positive staining for both, colon tissue (**Figure 7.7 A**), and RAW264.7 in conditioned media from HT29 culture (**Figure 7.7 B**). This suggest that RAW264.7 macrophage may polarize into $CD163^{+}$ M2-like macrophages after co-culture with HT29 tumour cells.

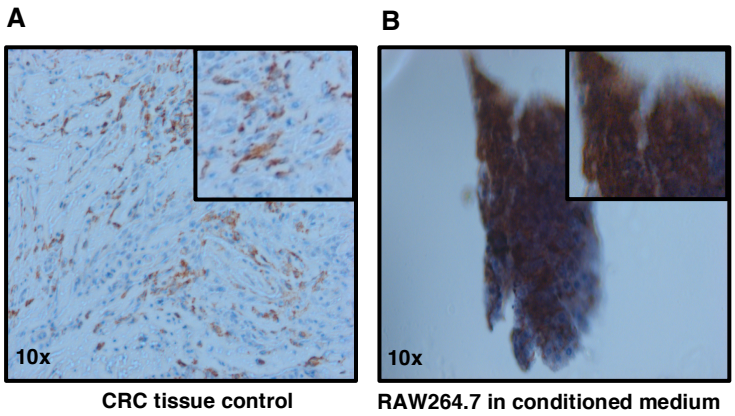

Figure 7.3 – CD163 (M2 phenotype) expression on RAW264.7 murine macrophage cell line; IHC for CD163 was performed on RAW264.7 macrophage cultured in conditioned media from HT29 and CRC tissue as positive control (**A**), RAW264.7 macrophages showing positive for CD163 (**B**). The picture was captured from Observer microscope at 10x optical magnification.

7.3.3 Spheroids formation from HT29 CRC cell line

Next formation of HT29 spheroids was assessed after reviewing methods for spheroid formation in the literature. An ultralow-attachment 96-well U-plate was selected for all experiments for spheroids and co-cultures with immune cell lines. First, HT29 seeding density gradient from $1x10^3$ – $1x10^4$ cells/well were performed. The spheroid size was measured over 5 days and viability checked at the same time points by utilized Cell-titer® Glo 3D Viability Assay.

7.3.3.1 Spheroid size and viability

This experiment was performed with 3 replicates as preliminary study. Due to the capacity of viability assay kit, an optimal spheroid size for this study was set at ~500 µm in diameter (shown by

red line). The results showed at HT29 seeding density 2.5x10^3 cells/well was the best density which reached ~500 µm in diameter over the 5 days with least necrosis seen (**Figure 7.1 A**). For viability, the best spheroids viability was at day 1 and day 2 (**Figure 7.1 B**). Therefore, the optimal time selected for adding immune cells to the co-culture was after 1 day of spheroid formation.

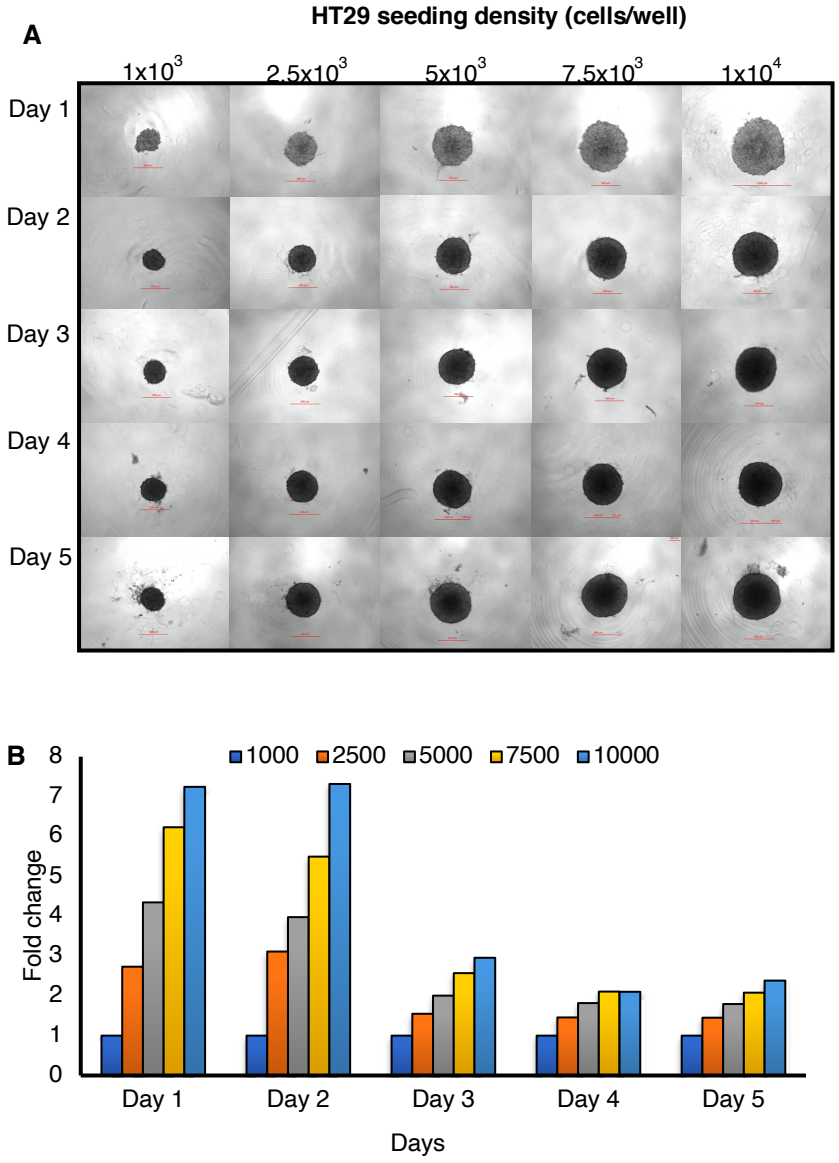

Figure 7.4 - Optimization for optimal spheroid size and viability. HT29 seeding density was varying from 1x10^3 – 1x10^4 cells/well. Spheroid size and viability were assessed from day 1-5. The optimal spheroid size was ~500 µm in diameter (2500 cells/well) (**A**), and the optimal time for adding immune cells for co-culture was at day 1 after spheroid formation (**B**).

7.3.4 Determining the medium for co-cultures

7.3.4.1 Jurkat E6-1 T-lymphocytes viability in RPMI1640 and McCoy's 5A medium

As the common medium for Jurkat E6-1 is RPMI1640 medium, whereas McCoy's 5A medium is used for HT29, the viability of Jurkat E6-1 in both media was performed to see which one was optimal for HT29 and Jurkat cell co-culture. The optimal Jurkat cells seeding density in co-culture was observed at the same time. As the seeding density for HT29 spheroid forming was $2.5x10^3$cells/well with highest viability rate at day 1 and day 2. These experiments were set for varying Jurkat seeding density from $2x10^3$-$1x10^4$ cells/well added 1 day after HT29 spheroid formation and viability was observed for 3 days, over 3 separate experiment repeats. The result showed at day 2 of McCoy's 5A medium, at seeding density $2x10^3$ and $4x10^3$ cells/well giving the highest viable rate. Therefore, Jurkat cells at seeding density $2.5x10^3$ cells/well was selected for co-culturing with HT29 at day 1 in McCoy's 5A medium to get 1:1 ratio of cell lines (**Figure 7.5**).

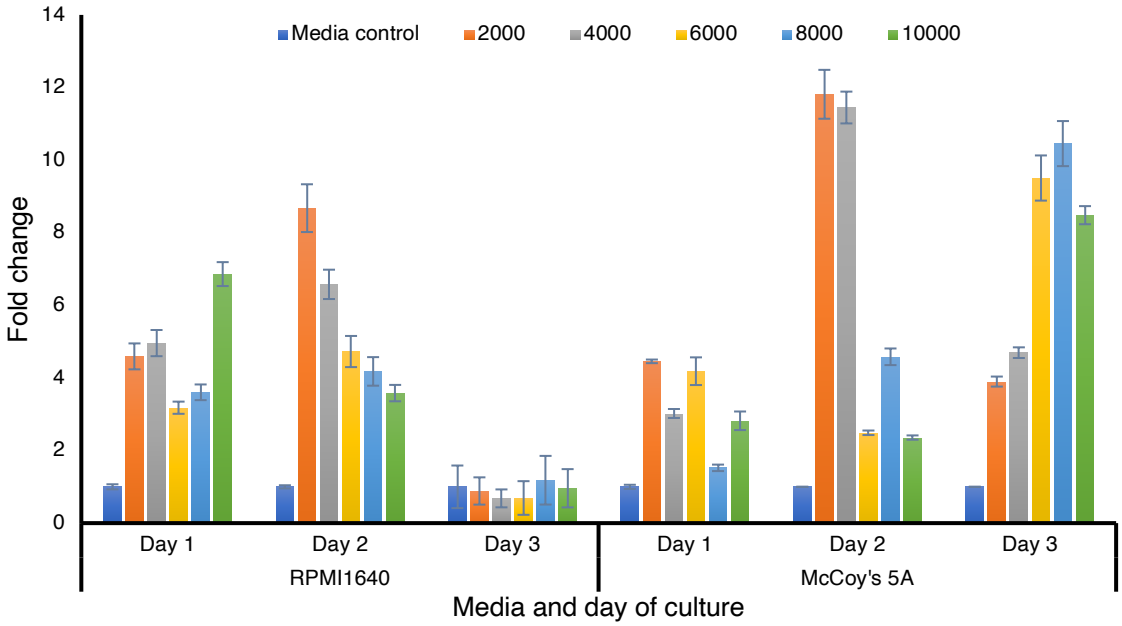

Figure 7.5 - Jurkat E6-1 T-lymphocytes viability from varying seeding density in RPMI and McCoy's 5A; Jurkat cells were cultured at varying seeding density in RPMI1640 and McCoy's 5A medium with HT29 spheroids and viability observed for 3 days. The results show that seeding density 2000-4000 cells/well in McCoy's 5A medium had the best viability when co-cultured with HT29 spheroids.

7.3.4.2 Determining medium for RAW264.7 murine macrophage cell line

As the medium utilized for HT29 and RAW264.7 are different. Therefore, the optimal medium for co-culture were tested before experiments. Spheroid characteristics were observed over 6 days in varying media conditions as cell viability was unable to be assessed due to supply issues. Similarly,

Jurkats, RAW264.7 cells were added after 1 day of HT29 spheroid formation in DMEM only, McCoy only, McCoy's 5A followed by DMEM, and McCoy's 5A followed by DMEM + McCoy's 5A. The results showed similar growth for all conditions (**Figure 7.3**). Therefore, McCoy's 5A was selected for further experiments to keep the media the same as used for Jurkat cell co-culture.

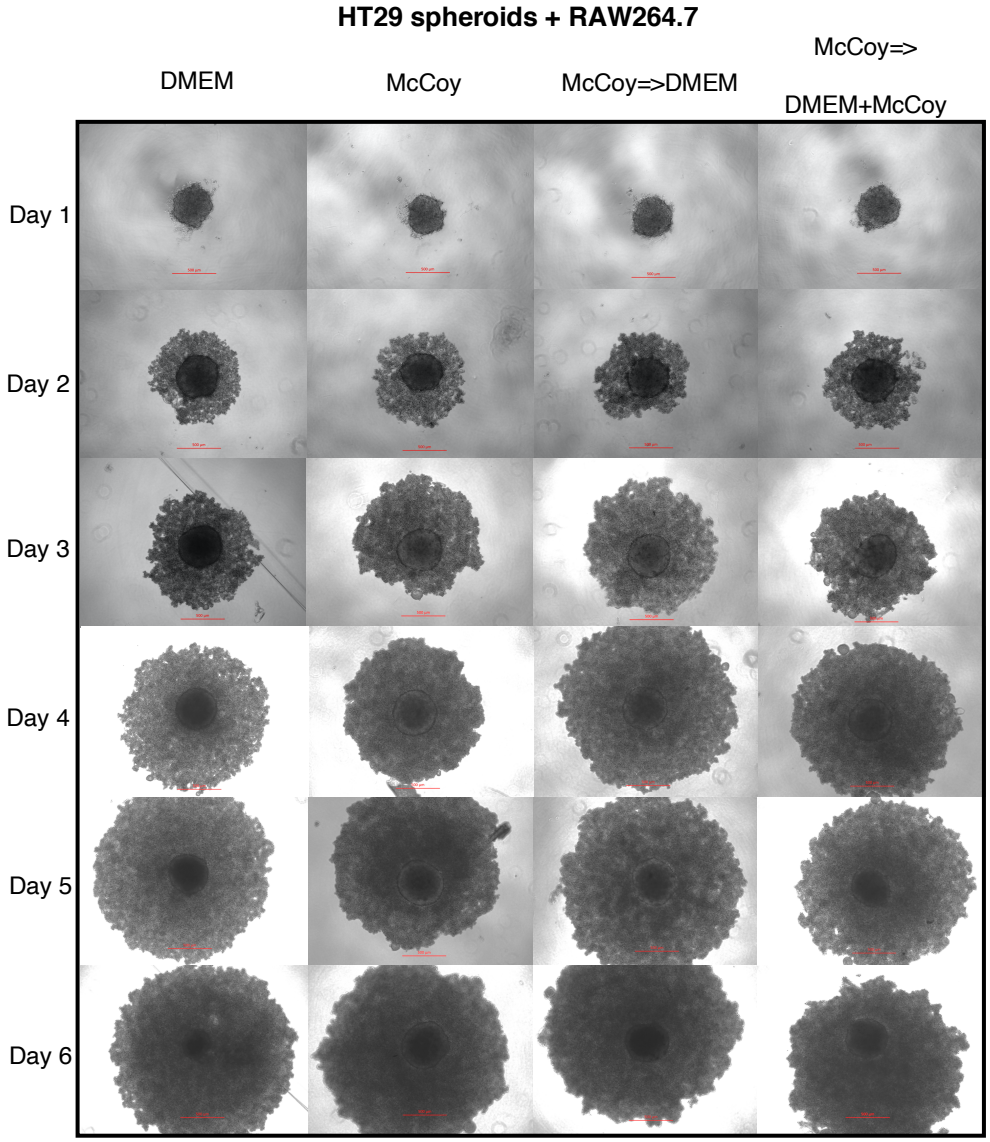

Figure 7.6 - Optimization for optimal medium for HT29 spheroid with RAW264.7 macrophages; HT29 spheroids were co-cultured with RAW264.7 macrophages in DMEM and McCoy's 5A medium. The optimal medium selected was McCoy's 5A.

7.3.4.3 Determining medium for HT29, Jurkat E6-1, and RAW264.7 co-cultures

Again, the optimal medium for triple co-culture were tested before experiments. For triple co-cultures to maintain a 1:1 seeding density of immune cells to CRC cells, 1250 cells/well of each

immune cell type were added to maintain the 2500 cells/well total immune cell density. The conditions used for adding Jurkat E6-1 (1250 cells/well) and RAW264.7 (1250 cells/well) after 1 day of HT29 (2500 cells/well) spheroid formation were DMEM only, McCoy only, McCoy's 5A followed by DMEM, and McCoy's 5A followed by DMEM + McCoy's 5A. Spheroid's characteristics were again observed over 6 days. The results showed similar growth for all conditions (**Figure 7.4**). Therefore, McCoy's 5A was selected for further triple co-culture experiments to keep the media consistent across all future experiments.

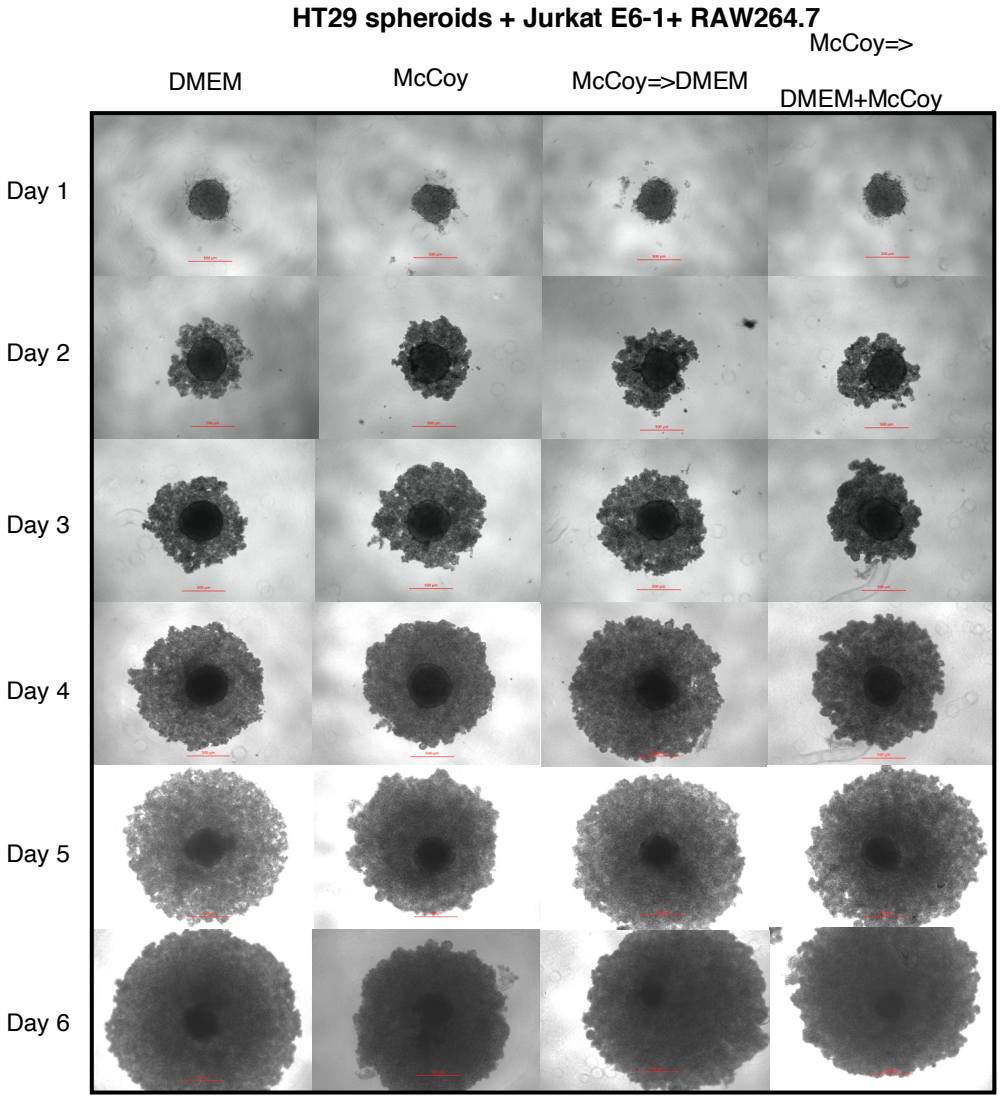

Figure 7.7 - Optimization for optimal medium for HT29 spheroid with Jurkat E6-1 and RAW264.7 macrophages triple co-cultures; HT29 spheroids were co-cultured with Jurkat E6-1 T-lymphocytes and RAW264.7 macrophages in DMEM and McCoy's 5A medium. The optimal medium selected was McCoy's 5A.

7.3.5 Immune cells infiltration into HT29 spheroids

Next, the infiltration of labelled immune cells was assessed to ensure the immune cells where mixing with the HT29 cells in the spheroid to replicate *in vivo* conditions. Jurkat E6-1 or RAW264.7 cells labelled with Cell tracker green dye were added into HT29 spheroids wells and incubated for 24 hours. The experiments were performed in double co-cultures of HT29 spheroids with labelled immune cells and in triple co-cultures with HT29 cells, one labelled immune cell line and one unlabeled immune cell line. The results showed high infiltration of both immune cell lines into HT29 spheroids for both double co-cultures with Jurkat E6-1 (**Figure 7.8 A**), or RAW264.7 (**Figure 7.8 B**). Similarly, infiltration of both cells lines was seen within triple co-cultures of all three cell lines (**Figure 7.8 C, D**).

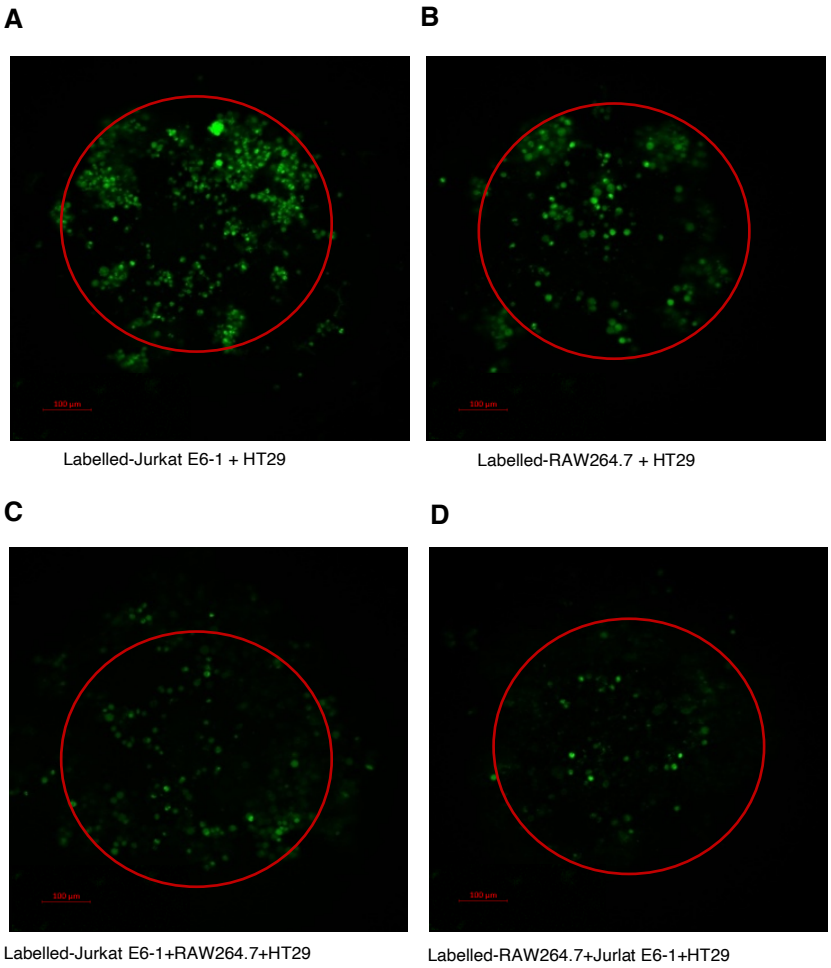

Figure 7.8 – Checking for immune cells infiltrated into HT29 spheroids; GFP labelled-Jurkat E6-1 and labelled- RAW264.7 infiltrated in HT29 spheroids (all seeding density at $2.5x10^5$ cells/well), double and triple co-culture. Showing both Jurkat E6-1 T-lymphocytes and RAW264.7 macrophages were well-infiltrated into spheroids in double co-culture (**A, B**), and in triple co-cultures (**C, D**). Red circle represented spheroid size.

7.3.6 Effect of anti-PD-1/anti-PD-L1 on HT29 CRC cell line

First, effect of anti-PD-1 and anti-PD-L1 to HT29 cell line were performed by WST-1 to determine an optimal concentration of each inhibitor for further experiments. These experiments were performed in 3 different experiments with 6 replicates per condition. The optimal concentration was selected as the concentration which showed no effect to tumour cells viability.

HT29 cell line were treated with anti-PD-1/anti-PD-L1 at concentrations varying from 1-100 µg/ml. WST-1 cell viability assay was performed at 24h. The optimal concentration for Pembrolizumab (**Figure 7.9 A**), Nivolumab (**Figure 7.9 B**), and Atezolizumab (**Figure 7.9 C**) was selected at 1 µg/mL.

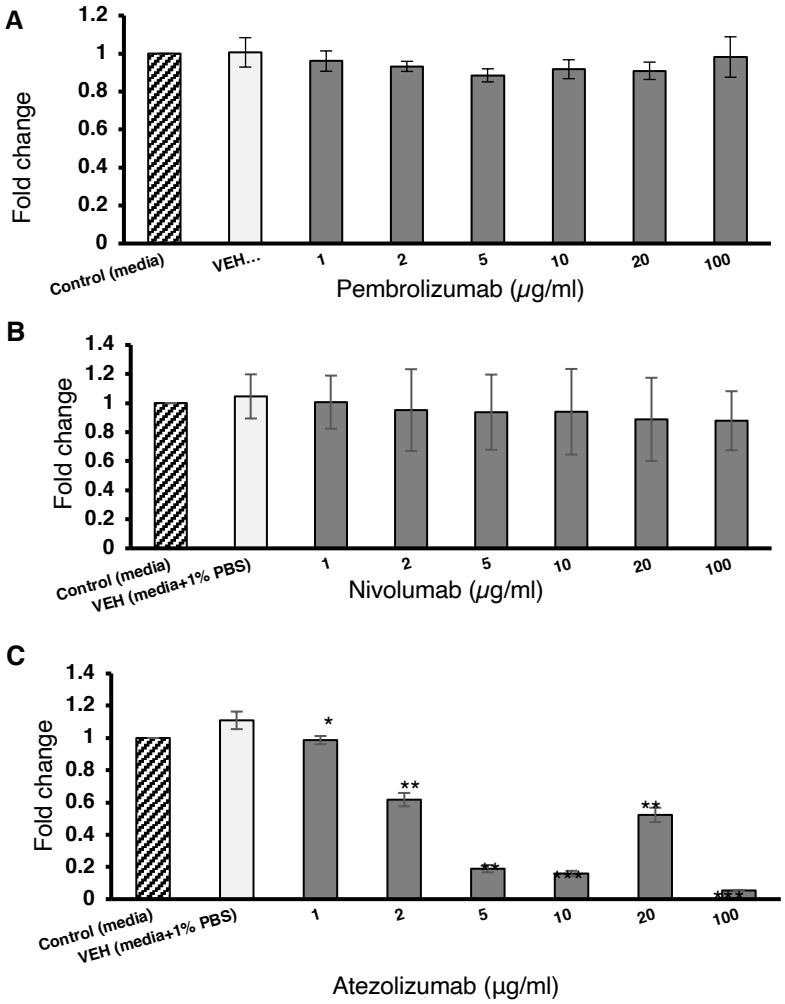

Figure 7.9 - Effect of anti-PD-1/anti-PD-L1 on HT29 colorectal cancer cell line; Effect of anti-PD-1 (Pembrolizumab) (**A**), (Nivolumab) (**B**), and anti-PD-L1 (Atezolizumab) (**C**) to HT29 colon tumour cell line at concentrations varying from 1-100 µg/ml with McCoy5A as media control (no inhibitors), and McCoy5A+1%PBS as vehicle control (no inhibitors), *p<0.05, **p<0.01, ***p<0.001.

7.3.7 Effect of anti-PD-1/anti-PD-L1 on immune cell lines

Next, effect of anti-PD-1 and anti-PD-L1 on immune cell lines were performed by WST-1 or CellTiter Glo® Viability Assay to determine an optimal concentration of each inhibitor. These experiments were performed in 3 different experiments with 6 replicates per condition. The optimal concentration was selected at a concentration which showing no effect to immune cells viability.

7.3.7.1 Effect of anti-PD-1/anti-PD-L1 on Jurkat E6-1 human T-lymphocytes cell line

Jurkat E6-1 cells were treated with anti-PD-1/anti-PD-L1 at concentrations varying from 1-100 µg/ml. WST-1 cell viability assay was performed at 24h. The optimal concentration for Pembrolizumab (**Figure 7.10 A**), Nivolumab (**Figure 7.10 B**), and Atezolizumab (**Figure 7.10 C**) was selected at 1 µg/mL.

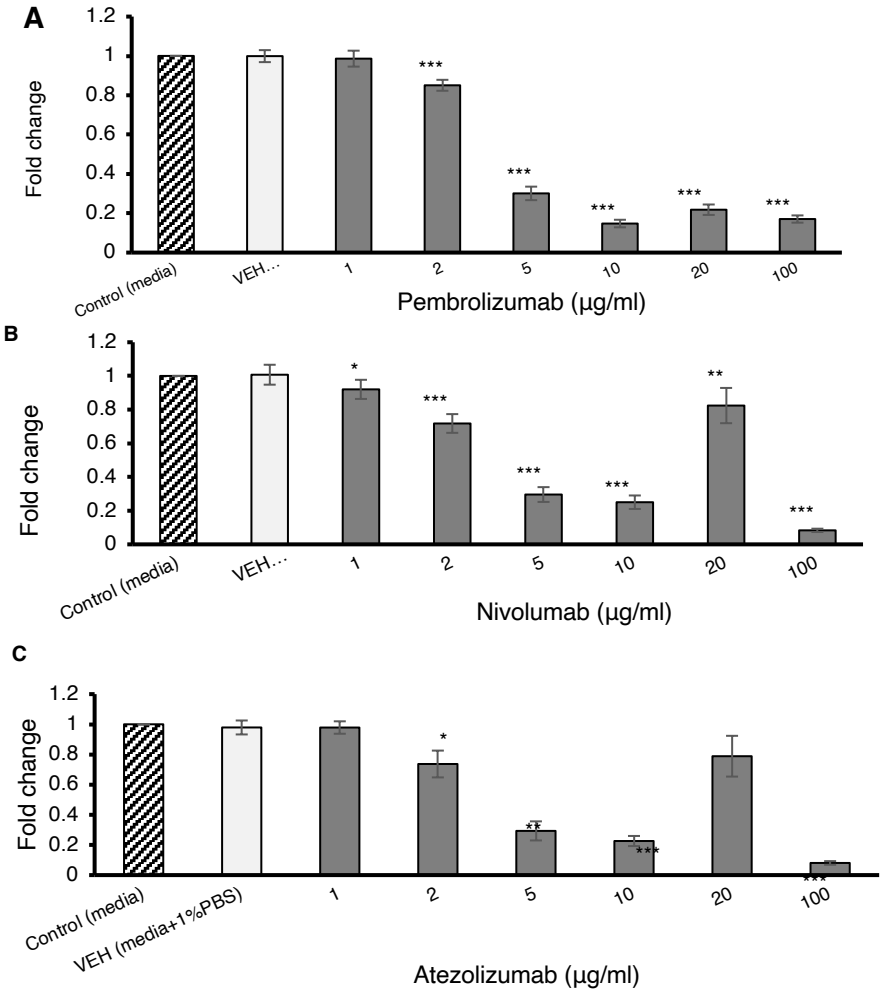

Figure 7.10 - Effect of anti-PD-1/anti-PD-L1 to Jurkat E6-1 cell line. Effect of anti-PD-1 (Pembrolizumab) (**A**), (Nivolumab) (**B**), and anti-PD-L1 (Atezolizumab) (**C**) to Jurkat E6-1 t-cell line at concentrations varying from 1-100 µg/ml with McCoy5A as media control (no inhibitors), and McCoy5A+1%PBS as vehicle control (no inhibitors), *p<0.05, **p<0.01, ***p<0.001.

7.3.7.2 Effect of anti-PD-1/anti-PD-L1 on RAW264.7 murine macrophages

As 1 ug/ml had been optimal for both HT29 and Jurkat E6-1, it was decided to first test this concentration on RAW264.7 cells to assess if this concentration could be used for all further experiments. Therefore, RAW264.7 cells were treated with anti-PD-1/anti-PD-L1 at a concentration of 1 µg/ml. CellTiter Glo® Viability Assay was performed at 24h. The result showed no effect of all 3 inhibitors on RAW264.7 macrophage viability confirming the applicability of this concentration to all future experiments (**Figure 7.11**).

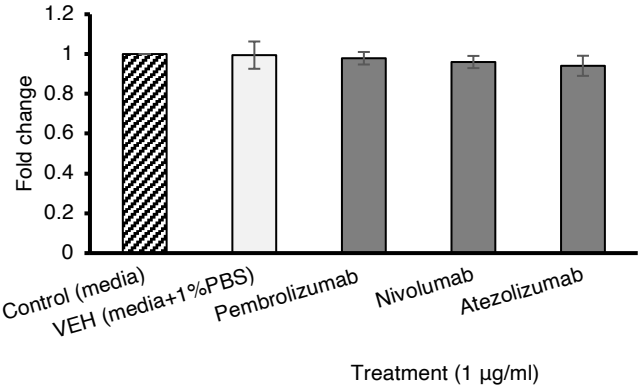

Figure 7.11 - Effect of anti-PD-1/anti-PD-L1 to RAW264.7 murine macrophage cell line; Effect of anti-PD-1 (Pembrolizumab), (Nivolumab, and anti-PD-L1 (Atezolizumab) to RAW264.7 macrophage cell line at concentrations 1 µg/ml in DMEM as media control (no inhibitors), and DMEM+1%PBS as vehicle control (no inhibitors).

7.3.8 Time scale for co-culture and anti-PD-1/anti-PD-L1 treatment

After testing for the optimal conditions for co-cultures, the proposed schedule for co-cultures and drug testing was as follows: HT29 (2500 cells/well) were plated on day 0, Jurkat E6-1 and/or RAW264.7 cells (2500 cells/well) added on day 1, then anti-PD-1/anti-PD-L1 added at a concentration of 1 µg/mL on day 2. CellTiter® Glo viability performed at day 4 (48hrs) and day 6 (96hrs). Media was replaced at the time of adding immune cells (day 1) and inhibitors (day 2), and half at day 4 (**Figure 7.12**).

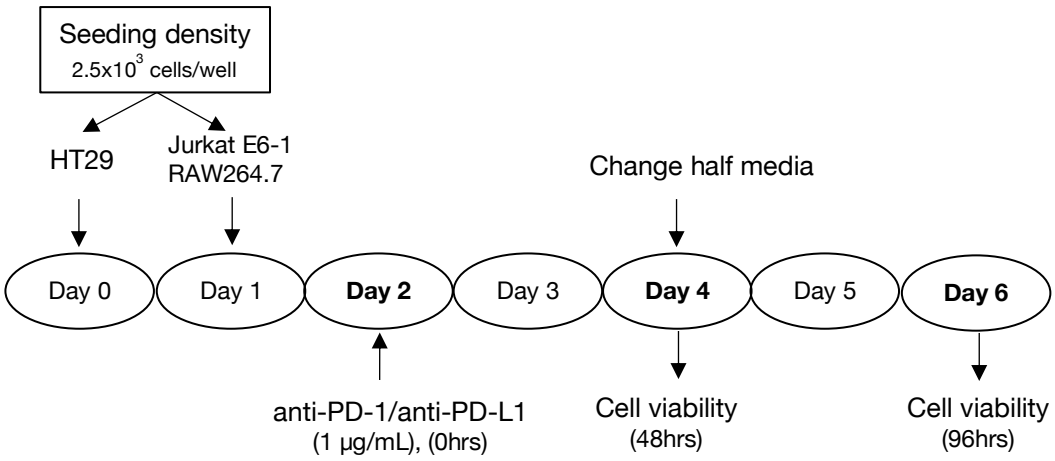

Figure 7.12 - Time scale for co-culture and anti-PD-1/anti-PD-L1 treatment experiments; HT29 was seeding at $2.5x10^3$ cells/well at Day 0, immune cells were added at Day 1, anti-PD-1/anti-PD-L1 were added at Day 2 (0hrs). Cell viability was tested at Day 4 (48hrs), and Day 6 (96hrs).

7.3.9 Effect of anti-PD1/anti-PD-L1 on double and triple co-cultures

Finally, the effect of inhibitors on double and triple co-cultures was assessed over 3 different inter-experimental repeats with 6 intra-experimental replicates per condition. The conditions were spheroid with control media only, spheroid with vehicle control, co-culture with control media, co-culture with vehicle control, co-culture treated with inhibitors individually, and co-culture treated with combinations of inhibitors. The results of treated conditions were normalized to co-culture with media control.

In general, for all 3 experiments showed significantly difference between spheroids only and co-culture, which is expected from higher cell numbers in co-cultures. For double co-culture of HT29 spheroid and Jurkat E6-1, showed significantly difference between spheroids in vehicle control and co-culture in media at 48hrs ($p<0.05$) and 96hrs ($p<0.05$). The result of treated conditions showed not significant effect of inhibitors on viability at either 48hrs or 96hrs when compared to co-culture with media control (**Figure 7.13 A**). The double co-culture of HT29 and RAW264.7 macrophages, showed significant difference between spheroids in vehicle control and co-culture in media at 48hrs ($p<0.01$) and 96hrs ($p<0.01$). The result showed no significant differences between treated conditions at either 48hrs and 96hrs, however, the viability was higher than for the HT29 and Jurkat E6-1 co-culture (**Figure 7.13 B**). The triple co-culture of all 3 cell types, showed significantly difference between spheroids in vehicle control and co-culture in media at 48hrs ($p<0.05$) and 96hrs ($p<0.01$). The results of treated conditions showed no significant differences between treated conditions at

either 48hrs and 96hrs, however, the viability was slightly decreased when compared to HT29 and RAW264.7 co-culture (**Figure 7.13 C**).

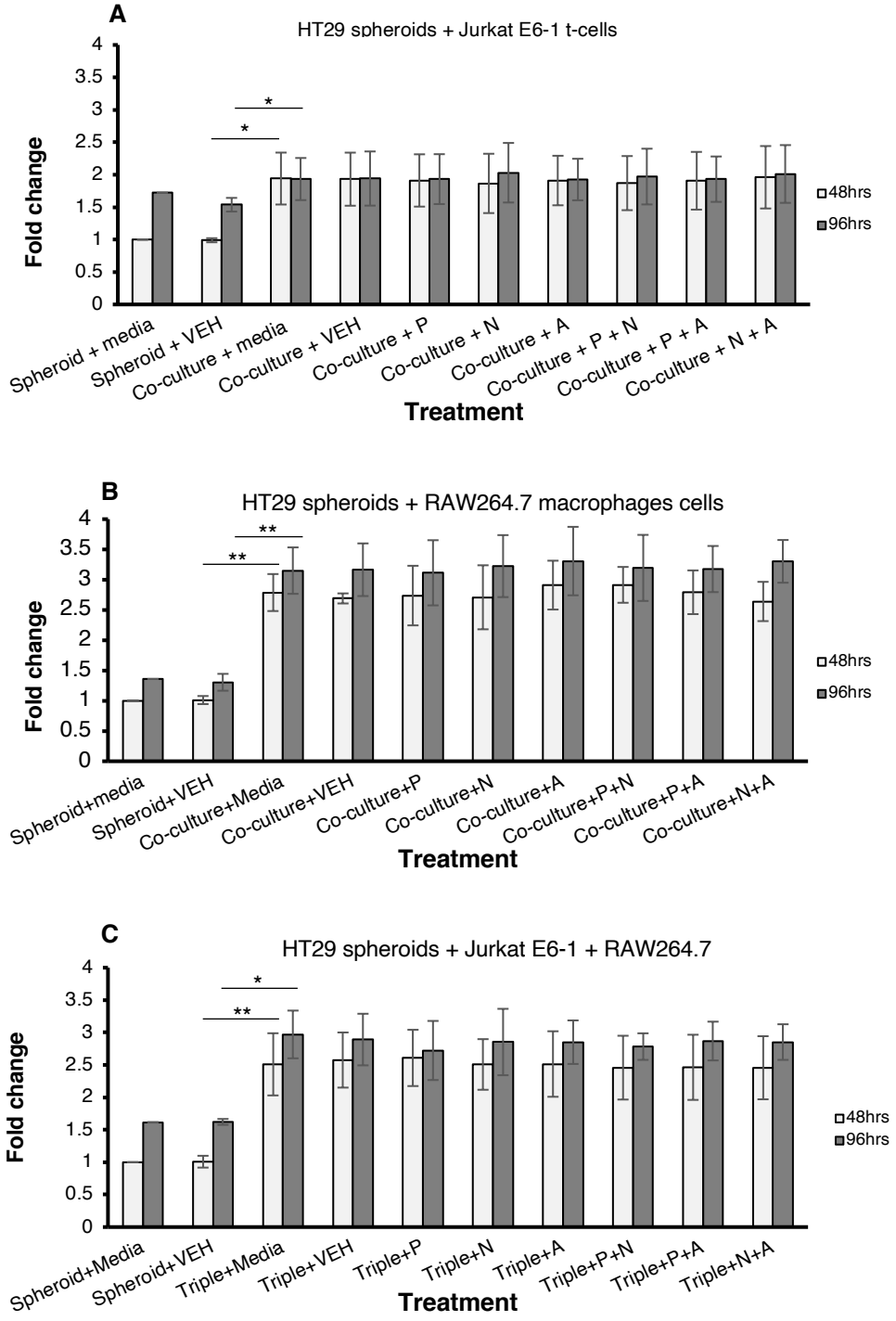

Figure 7.13 - Effect of anti-PD-1/anti-PD-L1 to HT29 spheroids and immune cells co-cultures; Effect of anti-PD-1, Pembrolizumab, and anti-PD-L1, Nivolumab, Atezolizumab to HT29 CRC cell line and Jurkat E6-1, RAW264.7 macrophage cell line co-cultures at concentrations 1 µg/ml, P=pembrolizumab, N=nivolumab, A=atezolizumab, *p<0.05, **p<0.01, ***p<0.001.

7.4 Discussion

As immune landscapes based on the combination of T-lymphocytes and myeloid cells were developed, which showed the different survival rate and gene expression pattern for each group. This chapter established 3-D multicellular spheroids from a CRC cell line co-cultured with a human t-cell line and/or murine macrophages cell line. These co-cultures were then treated with anti-PD-1/anti-PD-L1 to assess differences in cell viability. The results showed there were no significant differences between tumour cells for any inhibitors at 48hrs and 96hrs. This may be due to the optimal conditions not being reached within the co-culture development as discussed below.

The first step was checking for PD-L1 protein expression on HT29, PD-1 pression on Jurkat E6-1 T-lymphocytes, and CD163 expression on RAW264.7 macrophages to confirm immune checkpoint proteins were expressed on all cell lines, which all presented positive results. Although, this could confirm the expression of proteins of interest, the stimulation of immune cells prior to co-culture with tumour cells might be needed. The hypothesis was set that during HT29 tumour culture, the tumour might secrete chemokines or cytokines to enabling signalling or released tumour antigens to activate or stimulate immune cells as would be present in the human tumour. From the present results, immune cell stimulation might be essential for M2-like macrophage differentiation which might influence the co-culture. Therefore, replacing media when adding immune cells, may be affecting this process and may not be optimal for the co-culture.

The next step was performing spheroid formation in ultra-low attachment well plate and observed spheroid sizes and viability for 5 days to get optimal seeding density and spheroid size for the best 3D tumour viability assay. According to company's optimization (Promega), spheroid size at ~500-600 μm in diameter have shown highest luminescence signals, this also confirmed by other study (Zanoni et al., 2016) suggesting this step may be optimal.

Then the medium for co-culture system was assessed as all cell line commonly grow in different medium, i.e., McCoy's 5A for HT29, RPMI1640 for Jurkat E6-1, and DMEM for RAW264.7 macrophages. Therefore, the optimal medium composition for double and triple co-culture were tested to assess the influence on cell growth. The impact of media composition, media volume, and media exchange to co-culture are crucial as it could change cell fate and affect the results (Vis et al., 2020). Therefore, this step needs to be taken into consideration when optimizing, the co-culture further. A limitation of this study was that for spheroid viability and for Jurkat cell co-cultures cell viability was utilised to assess media conditions. However, due to supply issues and time constraints, RAW264.7 + HT29 co-cultures and triple co-cultures in different media were mainly observed using

microscopy to assess sizes and characteristics of spheroids which might not be enough to get accurate results. Therefore, repeating these two experiments utilising cell viability may give more accurate results to improve the co-culture protocol.

Next, checking the optimal ratio of seeding density for co-culture experiments, which ratio 1:1 for HT29 and each immune cell double co-culture, and 1:0.5:0.5 for HT29 and both immune cells triple co-culture to keep a 1:1 ratio. At this point, normally the cell composition should be set to mimic normal human condition for optimum cell-cell interactions (Goers et al., 2014). However, as immune cells infiltration into HT29 spheroids was suitable at this ratio, the study decided to proceed with 1:1 ratio for co-culture. However, this might need more optimization to account for patients with low or high immune cell infiltration as seen in our three immune landscape groups. It may be best to always have all three cell lines in triple culture but to change the immune cell rations to mimic the immune landscapes more accurately.

Another point that may affect the results is the concentration of inhibitors selected for treatment, as no effect was seen for any inhibitor on combination in this study. This study was tested for optimal concentration of each inhibitor by treating tumour cells and immune cells individually with each inhibitor. Then the concentration which does not harm tumour cells or immune cells alone at the beginning was selected from the hypothesis that once anti-PD-1/anti-PD-L1's action is to inhibit the interactions between co-stimulatory of PD-1 on T-lymphocytes and PD-L1 on tumour cells to inhibit their negative regulator of immune response, not to induce tumour cell death directly. Therefore, without interaction between tumour and T-lymphocytes, the inhibitors shouldn't harm the cells, therefore, the viability of each cell should remain the same. The decreased cell viability then might result from high chemical substance concentration which is toxic to cells. However, maybe choosing a concentration with a slight effect on the cells alone, may allow for synergy to be seen when they are in co-culture. Furthermore, the experiment may need to perform on other CRC cell lines to assess the optimal CRC line for this co-culture model. Also, the time scale for viability test, 48-96hrs, might not enough to see the clearly effect of inhibitors.

In conclusion, this study develops a co-culture system model of 3D tumour spheroid from human cell line co-culture with different immune cell types from human and murine sources. After checking for multiple factors which might affect cell growth, co-culture system, and anti-PD-1/anti-PD-L1 treatment, the results showed no significant differences on tumour cells viability between 48hrs and 96hrs time points. As discussed above, co-culture could be affected by several factors from medium compositions thorough to time scale of treatment. Therefore, optimization of the process is needed to allow further investigation of the inhibitors. However, it may suggest that this is not the most

optimal model for this purpose. This study had planned to also utilise 3D tumour spheroids from patient derived cells to test the drugs with and without co-cultures with immune cell lines to compare the differences between cell line and patient-derived organoids. Unfortunately, due to Covid 19 pandemic during the final stage of experiments, this was not able to be performed. Therefore, for future work, a co-culture model from patient's derived tumour tissue and autologous immune cells treated with known immune checkpoint inhibitors would be the next step, potentially alongside the use of animal models of the immune landscape groups.

Chapter 8 General Discussion and Future work

8.1 General Discussion

CRC classification currently relies on TNM staging to identify tumour characteristics that inform prognosis and is widely used in clinical setting along with tumour grading. In cancer research, molecular subtyping based on gene expression is widely used by multiple research groups worldwide. However, due to the lack of a gold standard method and the inconsistency of results, the CRC subtyping consortium was then formed and combined the various classifications from different research groups into four consensus molecular subtypes: CMS1 to CMS4 with distinct characteristics (Guinney, Dienstmann, Wang, de Reynies, Schlicker, Soneson, Marisa, Roepman, Nyamundanda, Angelino, Bot, Morris, Simon, Gerster, Fessler, De Sousa, et al., 2015). Recently, another molecular subtyping was proposed called cancer-intrinsic subtypes (CRIS). This system was developed in patient-derived xenografts (PDXs) to assess cancer cell intrinsic transcriptional landscapes and classified into five subtypes from CRIS-A to CRIS-E (Isella et al., 2017). Later CMS and CRISs systems have been validated in patients biopsies from different sampling methodologies implemented in clinical setting and found that CRIS can provided better results than CMS to subtype CRC primary tumour tissues (Alderdice et al., 2018). The two molecular subtyping are successfully clarified as CRC subtypes and widely implemented internationally in research and have the potential to translate to clinical setting especially the CRIS system. However, both methods utilise transcriptomics approaches which need high-cost equipment and experienced personnel for data analysis. Therefore, a simpler clinically translatable method is still required.

Tumour staging now relies on TNM classification, this method is the most widely used for CRC staging as well as for the basis of treatment decision. However, it is now known that patients with the same stage of disease can develop different clinical and treatment outcomes. Therefore, another classification method is now widely used based on histopathology of the tumour microenvironment called Immunoscore. Immunoscore focuses on the local immune response as the impact of immune response has been recognized as involved in regulating tumour progression. This method is widely used now for assessing patient's prognosis in research (Galon et al., 2012). Later, the standardized consensus found that Immunoscore was a strong prognostic factor for DFS, DSS, and OS including in early-stage CRC superior to conventional TNM classification (Galon et al., 2014). From the strength of prognostic, Immunoscore could be introduced into clinical setting and could potentially classify and predict patients likely to respond and benefit from immunotherapy (Galon & Lanzi, 2020). However, the system requires the user to buy a specific set of reagents and software package to analyse this score, which would not be considered cost-effective when compared to conventional methods in a routine clinical setting.

Glasgow microenvironment score (GMS) is another method for CRC classification. GMS is a tumour microenvironment based prognostic score based on assessment of inflammatory cells infiltrate in tumour stroma in primary operable CRC patients (Park et al., 2015). GMS has been validated in two cohorts: TNM I-III CRC validation cohort and TNM II-III CRC adjuvant chemotherapy cohort (TransSCOT) in association with DFS and RFS as primary endpoint assessment and adjuvant chemotherapy interaction as exploratory endpoint. The result showed that GMS is independently associated with DFS and RFS significantly. In addition, GMS0 significantly associated with improved DFS in patients receiving FOLFOX when compared to CAPOX chemotherapy (Alexander et al., 2021).

Recently, CRC phenotypic features related to CMS subtypes which associated with each molecular subtype and are associated with patient outcome was proposed by Roseweir et al. They utilised three of these features; immune infiltrate, proliferation rate and stromal invasion to propose a simple phenotypic subtyping method with four groups: immune, canonical, latent, and stromal. The effect of the phenotypic subtypes on DFS and recurrence risk (RR) was assessed and observed; the result found strong association. Of these, immune presented a good prognosis, canonical and latent having intermediate prognosis, while stromal showed the worst prognosis (Roseweir et al., 2020). Furthermore, the immune subtype could stratify response to chemotherapy, with the immune subtype patients responding better to FOLFOX than CAPOX, similar to GMS0. From the results, phenotypic subtypes could be used in routine clinical pathology for CRC patient's prognosis and response to chemotherapy.

One common factor between all these histological scores is the use of the local immune response. Generally, tumour tissue is infiltrated with inflammatory cells, which is the normal reaction of the host immune response reacting to the foreign tumour cells. The immune cells consist of cells in the lymphoid lineage and myeloid lineage. Lymphoid lineage cells are mostly T-lymphocytes, B-lymphocytes, and NK cells. Myeloid lineage cells are TAMs, MDSCs, TANs, and mast cells (Balkwill et al., 2012). In early-stage tumours, immune cells participate in preventing tumour progression by detecting tumour cells and destroy them, however, these cells can be hijacked by the tumour to perform another role promoting cancer development, by dampening the lymphoid immune response and promoting the myeloid immune cells, which have been shown to be crucial for tumour progression (Edmondson et al.; Grivennikov & Karin, 2010).

The local immune response has been recognized as being involved in regulating tumour progression and classification by using immune status is now widely accepted. In addition, it is crucial to investigating the CRC classification method which can easily translating to clinical setting.

Therefore, this thesis aims consist of two parts, part one is to investigate immune landscape of stage I-III CRC patients from the association of individual immune cell types and patient's prognosis. Then part two consist of three objectives; 1) to investigate the immune landscapes and their prognosis in each phenotypic subtype, 2) to assess transcriptomics and mutational profiles between immune landscapes to investigate potential biomarkers for each landscape and to examine the most significantly dysregulated genes at a protein level, and 3) to assess the effect of immune checkpoint inhibitors targeting PD-1/PD-L1 in CRC cell lines co-cultures with different immune cell lines which model immune landscapes to mimic patients normal status to examine if there is a difference efficacy between each immune landscape.

From part one of the aims, to investigate immune landscape of stage I-III CRC patients from the association of individual immune cell types and patient's prognosis. IHC staining of immune cells markers from T-lymphocytes populations (CD3, CD8, FoxP3) and myeloid cells populations (CD68, CD80, CD163, CD66b) were performed and analysed in association with patients' cancer specific survival (CSS), and overall survival (OS). The results found both T-lymphocytes and myeloid cells showed high infiltration in both tumour cell nests and tumour stroma at early stage of disease and gradually declined at advanced stages.

For T-lymphocyte populations, high $CD8^+$ cytotoxic T-lymphocytes infiltration in both tumour and stroma associated with improved CSS, with $CD3^+$ T-lymphocytes infiltration within tumour cells being an independent prognostic factor. $FoxP3^+$ Tregs in tumour stroma associated with improved CSS, which is in line with other studies on the role of Tregs in in CRC (Vlad et al., 2015), whereas it can cause poor prognosis in other cancer types (Shang et al., 2015; Zhou et al., 2017). The current study results are in the line with other studies that cytotoxic T-lymphocytes and Tregs can benefit CRC patient's survival regardless of the locations, but high level of infiltration is crucial. Overall, the data suggests that high levels of T-lymphocytes are important to predict if CRC patient's survival will be improved.

As for myeloid cells, high M1-like macrophages are associated with improved CSS in both tumour cell nests and tumour stroma. As M1-like macrophages known as a facilitator of cytotoxic T-lymphocytes function, presented high levels in tumour and stroma could benefit patient's survival. Whereas high M2-like macrophages in stroma significantly decreased CSS. As M2-like macrophages could attract Tregs and help to create immunosuppressive environment, presented high infiltration in the stroma in patients resulting in decreased CSS. However, the current study showed that presence of $FoxP3^+$ Tregs was significantly associated with improved CSS, and OS in tumour stroma. This might be due to the ratio of infiltration of Tregs to M2-like macrophages, as Tregs were

had significantly different infiltration levels at each stage of disease. Whereas $CD163^+$ M2-like macrophages had a similar infiltration level at each stage, suggesting the ration between the two would differ over time effecting the interaction between the two cell types. While high granulocytes in tumour cell nest and tumour stroma are associated with decreased CSS. For granulocytes, neutrophils are the most abundant cells in TME, and has been proposed having both pro-tumorigenic and anti-tumorigenic characteristics.

From the results, indicated that high T-lymphocytes, high M1 macrophages, low M2 macrophages, and low granulocytes or neutrophils individually are crucial to improve patient's survival. However, the role of these cells in combination might cause distinct outcome depends on other factors in TME. Therefore, the combination of T-lymphocytes and myeloid cells were generated from $CD3^+$ combined with $CD68^+$ and $CD66b^+$ and produced four immune landscapes which are T-lymphocytes high only (T-cells high), myeloid cells high only (myeloid high), both T-lymphocytes and myeloid cells high (both high), and both T-lymphocytes and myeloid cells low (both low) in tumour cell nests and tumour stroma separately.

The prognostic analysis showed that in tumour cell nests, the both high present potentials to reach better prognosis for CSS, whereas T-cells high had the worse prognosis, however, this was not significant. In tumour stroma, T-cells high significantly had the best prognosis for CSS, whereas myeloid high had the worse prognosis significantly. This suggest that myeloid cells might have different role at different locations and dependent on the other immune cells present. In tumour cells, if patients present with only myeloid cells strong will lead to poorer survival. On the other hand, if present with strong T-lymphocytes, it could enhance T-lymphocyte's function to eliminate tumour cells and improved patient's survival even better than T-lymphocytes strong only. Therefore, in tumour cells if T-lymphocytes co-operated with particular myeloid cells they might could reach greater effect for tumour cells eradication. Therefore, the role of myeloid cells is now one of the forefronts of research into cancer immunotherapy.

The results from Scottish discovery cohort have been validated in Norwegian validation cohort because of the similar patient's characteristics. However, Norwegian cohort presented decreased death cases when compared to Scottish cohort. Furthermore, Norwegian cohort had significantly increased immune cells infiltration for all cell types evaluated in both tumour cell nests and tumour stroma. For T-lymphocytes, high cytotoxic T-lymphocytes infiltrated in tumour cell nests and tumour stroma were associated with improved CSS as shown in Scottish cohort. Whereas myeloid cells, macrophages high infiltrated in tumour cell nests was significantly improved CSS, but not seen in tumour stroma. The immune landscape prognosis was significant in tumour stroma only with both-

high group having better survival than myeloid high group, but this cannot compare to Scottish cohort from small samples due to lack of the other two groups. Even though the two cohorts had similar results, however, Norwegian cohort had higher immune cells infiltration and higher survival rate than Scottish cohort. Therefore, this brought into interest about the other different factors underlying between two cohorts which resulting in differences in immune cells infiltration and survival rate.

From the results of both cohorts showed different immune cell types and different immune landscapes were associated with different prognosis in CRC patients with stage I-III disease. High T-lymphocytes are always associate with improved patient's prognosis independent of myeloid cells attending, whereas elevated myeloid cells only have poorer prognosis. The presence of both T-lymphocytes and myeloid cells together can result in better survival depending on cell types presented and their locations.

The next objective was to investigate the prognostic value of immune landscapes to phenotypic subtypes which were developed by Roseweir et al. and termed immune, canonical, latent, and stromal subtypes. The current study investigated the association between CRC phenotypic subtypes and the prognostic value of immune cells infiltration and immune landscapes in tumour cell nests and tumour stroma. The results showed each subtype was infiltrated by differing immune cell types. Immune subtype is predominantly composed of T-lymphocytes and showed the best survival rate. Canonical subtype has elevated macrophages and provided intermediate survival rate. Latent and stromal subtype have declined levels of all immune cell types, especially in tumour cell nests, and obtained poor prognosis. In addition, the univariate analysis revealed that cytotoxic T-lymphocytes, Tregs, and granulocytes are significantly associated with patient's survival in each phenotypic subtype. The multivariate analysis designated granulocytes infiltration in tumour cell nests is an independent prognostic factor for the latent subtype.

The present finding suggests that subtypes with high T-lymphocyte infiltration in both tumour cell nests, and tumour stroma have the best prognosis as seen in the immune subtype, whereas the canonical subtype that has high macrophages presented a slightly reduced prognosis. However, subtypes that have high granulocytes infiltrates and low lymphocyte infiltrates in cancer cell nests lead to a poor prognosis, as seen in the latent and stromal subtypes. Therefore, the immune, latent, and stromal subtypes might represent a population of patients for immune-based therapy. Overall, this study suggest that phenotypic subtype can be alternative tools for CRC classification due to significant immune cell compositions for each subtype which are easily assessed using a simple, clinically utilised method, and benefit patient's therapy.

As the study found significant survival differences between the four immune landscapes and different infiltration in the four phenotypic subtypes, it was decided to look for underlying difference between these immune landscapes. Therefore, the next objective is to assess mutational profiles in CRC patients with stage I-III disease based on four immune landscape grouping from chapter 3 to investigate any potential underlying differences that could be used as biomarkers for each immune landscape and then to examine the most significantly dysregulated genes at a protein level. From whole genome sequencing of stage I-III CRC patients cohort, it was found that top three mutated genes were *APC* (51%), *TP53* (46%), and *KRAS* (31%) as commonly present in CRC tumorigenesis (Tariq & Ghias, 2016) (Worthley & Leggett, 2010). This could be used to confirm the further analysis as the initial results showed as expected sequential genes mutations in CIN pathway of CRC tumorigenesis. Therefore, the identification of genes mutation was analysed for each immune landscape. In T-cells high group, *ERBB4* (100%) was the most significant mutated gene. However, due to only two samples available in this group, more cases are needed to validate the result. In myeloid high group, a low mutation frequency of *TP53* was found among six significantly mutated genes. In both high group, high mutation frequency of *FBXW7* was the most significant seen among five significantly differentially mutated genes. Whereas in both low group showed high mutation frequency only for *TP53*.

Interestingly, *TP53* was less differentially mutated in myeloid high group patients and had increased mutations in the both low group patients. Further analysis by comparing *TP53* mutations in both groups found that myeloid high patients had less *TP53* mutations than both low patients, suggesting *TP53* mutations have a higher frequency in patients with low myeloid cells. The next question was whether there was a difference in *TP53* mutation frequency between patients with high level of myeloid cells infiltration in tumour cell nest and those with infiltration into tumour stroma. Further analysis found that *TP53* mutations where more frequent in patients with high myeloid cell infiltration into tumour stroma than in patients with high myeloid cell infiltration into tumour cell nests. By the fact that *TP53* is a significant tumour suppressor gene, high mutations along with high myeloid cells infiltrations into tumour stroma might lead to negative outcome. To address this, therefore, the correlation between *TP53* mutations and the expression at protein level was performed by p53 performing p53 IHC in our patient's cohort. The results found that *TP53* mutations was significantly correlate with high level of p53 expression. This in line with others that p53 overexpression is an indicator for *TP53* mutations (Menendez et al., 2013). This study cannot characterize wild type and mutant p53 due to antibody limitation which could bind both wild type and mutant p53. However, survival analysis showed high p53 expression was significantly associated with improved patient's survival and only patients with mutated *TP53* had improved survival. Therefore, *TP53* mutations in this study provide positive outcome to patient's survival.

In terms of p53 expression and immune cells infiltration no significant correlation was seen, suggesting that it might not a direct interaction between them. However, when assessing the relationship between p53 expression and patient's survival with immune cells infiltrate stratification. It was found that in patients with high immune cells infiltration, no significant change in patient's survival was observed between low and high p53 expression. However, in patients with low $CD80^+$ M1-like macrophages and low p53 expression a decreased survival in tumour cell nests and tumour stroma was observed when compared to high $CD80^+$. This suggests that if $CD80^+$ M1-like macrophages are low, high levels of p53 are needed to improve patients' survival, however, when $CD80^+$ cells are high, p53 is no longer important and as all patients are doing well. As M1-like macrophages is known for anti-tumour function, therefore, at high level they can function effectively and do not need p53 action. Whereas it is the opposite in case of low M1-like macrophage levels, they need p53 function to maintain anti-tumour effects as proposed in another study showing a strong connection between them (Guo & Cui, 2015; Menendez et al., 2013). This suggest that p53 expression was linked to M1-like macrophages resulting in a positive outcome in our study. However, there is a report that the combined role of p53 and myeloid cells can have negative outcomes leading to poor survival (Cooks et al., 2018).

When assessing the correlation between $CD80^+$ M1-like macrophages infiltration level and *TP53* mutations it was found that high $CD80^+$ was significantly enriched for *TP53* mutations when infiltrating into tumor stroma only, whereas it did not appear amongst the 13 significant genes for patients with high $CD80^+$ infiltration into tumour cell nests. Therefore, enriched *TP53* mutations can be detected at DNA level only in patients with high levels of $CD80^+$ M1-like macrophages infiltration into the tumour stroma. Whereas at protein expression level, high p53 expression showed same effect on patient's survival in patients with $CD80^+$ infiltration into both tumour cell nests and tumour stroma. Therefore, this suggested that *TP53* mutations and p53 expression had distinct prognostic value in tumour microenvironment, which might be more important and predictive in patients with high $CD80^+$ M1 macrophage infiltration into tumour stroma. This suggest that *TP53* mutations might affect myeloid cells infiltration into tumour stroma including M1 macrophages and could be a prognostic factor for high myeloid cells in tumour stroma.

To further assess biomarkers for each immune landscape, the next objective was to investigate gene expression profiles between immune landscapes to identify differentially expressed genes for each landscape which could be used as potential prognostic or predictive biomarker for specific immune landscape grouping. The result from our patient cohort revealed diverse gene expression patterns for each immune landscape as shown in gene clustering in PCA plot for myeloid high, both high, and

both low, but none for T-cells high due to small sample number. Of which, myeloid high group presented high gene expression level, whereas T-cells high presented low gene expression level, whereas other two groups, both high and both low showed similar pattern as myeloid high. This suggest that myeloid high might influenced the expression of both high and both low groups independent of T-lymphocytes presented.

As for differentially expressed genes in each immune landscape group when compared to others, in T-cells high group showed downregulated genes for immune response and wound healing. Whereas in myeloid high there was a downregulation in a gene involved in RNA manipulation. The both high group showed downregulation of a gene involved in T-lymphocytes receptor signaling and other antigen presenting signaling pathways. Whereas the both low group showed both upregulation and downregulation genes, however, the biological processes of these genes were not associated with cancer or immune system, therefore, more investigations are needed. These results suggest that each immune landscape group had different gene expression pattern which might due to the differences of biological condition result from the composition of immune cells infiltration in tumour microenvironment in order to maintain anti-tumour activity.

As myeloid cells high might influence gene expression pattern among the four groups, therefore, the comparison of gene expression patterns between myeloid high and other three groups were performed. For myeloid high and T-cells high, showed 23 significant differentially upregulated genes, whereas when compared to both high group found only 1 upregulated gene presented. For the comparison between myeloid high and both low group, found that 20 genes were significantly expressed, which 13 genes were upregulated, and 7 genes were downregulated in myeloid high group. From all 44 significant differentially expressed genes from 4 immune landscapes, no overlapping expression was observed. Therefore, this could confirm that myeloid cells high can influence gene expression pattern depend on other immune cell composition in tumour microenvironment. Interestingly, in a mixed of immune cells in both high group, not many genes are differentially expressed. Whereas when in T-cell high or both low, where myeloid high is not elaborated, many genes are differentially expressed. Suggesting myeloid cells high is the over-riding factor in both high group, but not T-cells high. However, this result needs more validation as small sample number for T-lymphocytes high group might affect the analysis.

To observe the biological processes of differentially expressed genes, the protein-protein interaction network was generated and found that the centre of network was TP53. Suggesting most of differentially expressed genes in our study were linked to TP53 network with a few independent linkages out with TP53 network. As chapter 5 indicated that *TP53* mutation was associated with

stromal myeloid cells high landscape, therefore, the correlation between *TP53* mutations and all differentially expressed genes expression level were observed. Interestingly, among all DEGs, the REG genes family; *REG1A*, *REG3A*, and *REG3G* presented upregulated in wild type *TP53* and downregulated in mutated *TP53*. As *REGs* genes and proteins have been reported having multifunction as pro-tumorigenic in colon tissues as well as affects in multiple organs (Chen et al., 2019; Sun et al., 2021). Therefore, downregulated of these genes in mutated *TP53* condition, which associated with high p53 expression, might alter colon tissues from tumorigenic status into normal status and improved patient's survival. Overall, this study presented potential gene expression pattern might be influenced by myeloid cells high group and most of significant genes were link to TP53 network. As *TP53* mutation was associated with *REGs* genes downregulation. Therefore, the prognostic role of p53 in tumour microenvironment might be good due to the influx of myeloid cells.

As missense mutations can induce loss of p53 function by inactivation of p53 binding property, this can lead to cell transformation and negative outcomes (Lopez et al., 2012). In normal cell condition, the expression of p53 is very low, and not generally detected by IHC. Whereas mutations can cause a shift to elevated p53 accumulation making it detectable. The current study assessed p53 nuclear expression by IHC and divided expression into low and high. However, the results showed that high *TP53* mutations were correlated with high p53 expression as expected but associated with improved patients CSS. This potentially suggests that splitting p53 expression into low or high levels by IHC in this study might not the appropriate as it may miss some of the lower level expression and these results need to be validated utilising another method to classify p53 expression levels.

The final objective of this thesis is to assess the effect of immune checkpoint inhibitors targeting PD-1/PD-L1 in CRC cell lines co-culture with different immune cell lines (T-lymphocytes cell line and macrophages cell line) to model the immune landscapes developed in chapter 3 and mimicking patient's normal state to examine if there is a difference efficacy between each immune landscape. 3- D multicellular spheroids from a CRC cell line were developed and co-cultured with T-lymphocytes cell line or macrophages cell line and combination of the three cell lines. These co-cultures were then treated with anti-PD-1/anti-PD-L1 or a combination of them. The results showed there were no significant differences between tumour cells viability for any inhibitors at 48hrs and 96hrs. This may be due to the optimal conditions not being reached within the co-culture development. Therefore, by varying factors within the co-cultures further to obtain an optimal research model could allow observation of better treatment results.

8.2 Future work

From the studies, except common IHC for each immune cell marker, the immune landscapes from T-lymphocytes and myeloid cells combination were covered small sample numbers which might affect the subsequence analysis for phenotypic subtypes, genomics, and transcriptomics analysis. Therefore, in future work, more cases are needed for each immune landscape to clarify and confirm the results.

For genomics analysis, the study at protein level of significantly mutated genes was performed for *TP53*. However, for transcriptomics analysis, due to time limitations with COVID-19 pandemic, the confirmation at protein expression level was unable to perform. Therefore, IHC staining for *REG1A*, *REG3A*, *REG3G*, and/or *IGF2BP1* are needed to confirm the correlation with gene expression level and to assess the association with patients' survival. However, as *REG*s genes are associated with colon tissues, therefore, IHC results performing in normal tissues and compare with CRC disease tissues might clarify the role of these genes in CRC patients' survival. In addition, genomics and transcriptomics analysis for each immune cell marker might identify the most significant genes specific to each immune cells. However, this might not correlate with normal state as human body contain a mixed population of immune cells and they are co-operating in normal function of immune response. Therefore, the analysis for these results in other patient cohort is needed which might confirm the results.

For cell culture part, there are many aspects need future work to complete the experiments. First, cell lines used for spheroid formation, this study was performed in only HT29 CRC cell line which not enough to confirm the results because of different cell line has different characteristics. Therefore, 3-D spheroids formation should be performed from other CRC cell lines to compare the characteristics which might affect immune checkpoint inhibitors treatment. In addition, IHC for PD-1 and PD-L1 in co-cultures cell pellets or patients' TMAs might be the other way to check if checkpoints are active within the model and available for intervention with checkpoint inhibitors. At first, apart from 3-D tumour spheroids model from CRC cell line, the study in patient-derived organoid was planned to compare ICI treatment in cell lines and patient's cells, due to coronavirus pandemic, this part was cancelled. Another level of cell work is patient-derived xenografts (PDXs) which is the most suitable model for CRC study today to assess ICI treatment which will be the most model closely mimic CRC primary tumour. For ICIs treatment, the study was performed to assess tumour viability for 48hrs and 96hrs which might not enough for the action and changing of cell viability to observe. Therefore, the longer period for treatment might needed. Therefore, this needs

more validation for 3-D spheroid forming and spheroid viability checking to maintain tumour cell viability at all treatment time period. Followed by translation into the other models mentioned above.

Bibliography

Aguiar, P. N., Santoro, I. L., Tadokoro, H., Lopes, G. D., Filardi, B. A., Oliveira, P., Mountzios, G., & de Mello, R. A. (2016, Apr). The role of PD-L1 expression as a predictive biomarker in advanced non-small-cell lung cancer: a network meta-analysis. *Immunotherapy, 8*(4), 479-488. https://doi.org/10.2217/imt-2015-0002

Ahmad, M., Rees, R. C., & Ali, S. A. (2004, Oct). Escape from immunotherapy: possible mechanisms that influence tumor regression/progression. *Cancer Immunology Immunotherapy, 53*(10), 844-854. https://doi.org/10.1007/s00262-004-0540-x

Ahmad, S. M., Larsen, S. K., Svane, I. M., & Andersen, M. H. (2014, Jan). Harnessing PD-L1-specific cytotoxic T cells for anti-leukemia immunotherapy to defeat mechanisms of immune escape mediated by the PD-1 pathway. *Leukemia, 28*(1), 236-238. https://doi.org/10.1038/leu.2013.261

Alderdice, M., Richman, S. D., Gollins, S., Stewart, J. P., Hurt, C., Adams, R., McCorry, A. M., Roddy, A. C., Vimalachandran, D., Isella, C., Medico, E., Maughan, T., McArt, D. G., Lawler, M., & Dunne, P. D. (2018, May). Prospective patient stratification into robust cancer-cell intrinsic subtypes from colorectal cancer biopsies. *Journal of Pathology, 245*(1), 19-28. https://doi.org/10.1002/path.5051

Alexander, P. G., Roseweir, A. K., Pennel, K. A. F., van Wyk, H. C., Powell, A., McMillan, D. C., Horgan, P. G., Kelly, C., Hay, J., Sansom, O., Harkin, A., Roxburgh, C. S. D., Graham, J., Church, D. N., Tomlinson, I., Saunders, M., Iveson, T. J., Edwards, J., & Park, J. H. (2021, Feb). The Glasgow Microenvironment Score associates with prognosis and adjuvant chemotherapy response in colorectal cancer. *Br J Cancer, 124*(4), 786-796. https://doi.org/10.1038/s41416-020-01168-x

Alsaab, H. O., Sau, S., Alzhrani, R., Tatiparti, K., Bhise, K., Kashaw, S. K., & Iyer, A. K. (2017, Aug 23). PD-1 and PD-L1 Checkpoint Signaling Inhibition for Cancer Immunotherapy: Mechanism, Combinations, and Clinical Outcome. *Frontiers in Pharmacology, 8*. https://doi.org/ARTN 561

10.3389/fphar.2017.00561

Armaghany, T., Wilson, J. D., Chu, Q., & Mills, G. (2012, Jan). Genetic alterations in colorectal cancer. *Gastrointest Cancer Res, 5*(1), 19-27. https://www.ncbi.nlm.nih.gov/pubmed/22574233

ASCO.org. (2021a). *Colorectal Cancer: Stages*. Retrieved December 7 from https://www.cancer.net/cancer-types/colorectal-cancer/stages

ASCO.org. (2021b). *Colorectal Cancer: Types of Treatment*. https://www.cancer.net/cancer-types/colorectal-cancer/types-treatment

Awad, R. M., De Vlaeminck, Y., Maebe, J., Goyvaerts, C., & Breckpot, K. (2018). Turn Back the TIMe: Targeting Tumor Infiltrating Myeloid Cells to Revert Cancer Progression. *Front Immunol, 9*, 1977. https://doi.org/10.3389/fimmu.2018.01977

Babcock, B. D., Aljehani, M. A., Jabo, B., Choi, A. H., Morgan, J. W., Selleck, M. J., Luca, F., Raskin, E., Reeves, M. E., Garberoglio, C. A., Lum, S. S., & Senthil, M. (2018, Jul). High-Risk Stage II Colon Cancer: Not All Risks Are Created Equal. *Ann Surg Oncol, 25*(7), 1980-1985. https://doi.org/10.1245/s10434-018-6484-8

Bajorin, D. F., Plimack, E. R., Siefker-Radtke, A. O., Choueiri, T. K., De Wit, R., Sonpavde, G., Gipson, A., Brown, H., Mai, Y. B., Pang, L., Perini, R. F., & Bellmunt, J. (2015, May 20). KEYNOTE-052: Phase 2 study of pembrolizumab (MK-3475) as first-line therapy for patients (pts) with unresectable or metastatic urothelial cancer ineligible for cisplatin-based therapy. *Journal of Clinical Oncology, 33*(15). <Go to ISI>://WOS:000358036904764

Balkwill, F. R., Capasso, M., & Hagemann, T. (2012, Dec 1). The tumor microenvironment at a glance. *Journal of Cell Science, 125*(23), 5591-5596. https://doi.org/10.1242/jcs.116392

Baptista, M. Z., Sarian, L. O., Derchain, S. F. M., Pinto, G. A., & Vassal, J. (2016, Jan). Prognostic significance of PD-L1 and PD-L2 in breast cancer. *Human Pathology, 47*(1), 78-84. https://doi.org/10.1016/j.humpath.2015.09.006

Bauleth-Ramos, T., Feijao, T., Goncalves, A., Shahbazi, M. A., Liu, Z., Barrias, C., Oliveira, M. J., Granja, P., Santos, H. A., & Sarmento, B. (2020, Jul 10). Colorectal cancer triple co-culture spheroid model to assess the biocompatibility and anticancer properties of polymeric nanoparticles. *J Control Release, 323*, 398-411. https://doi.org/10.1016/j.jconrel.2020.04.025

Becht, E., de Reynies, A., Giraldo, N. A., Pilati, C., Buttard, B., Lacroix, L., Selves, J., Sautes-Fridman, C., Laurent-Puig, P., & Fridman, W. H. (2016, Aug 15). Immune and Stromal Classification of Colorectal Cancer Is Associated with Molecular Subtypes and Relevant for Precision Immunotherapy. *Clin Cancer Res, 22*(16), 4057-4066. https://doi.org/10.1158/1078-0432.CCR-15-2879

Bendell, J. C., Powderly, J. D., Lieu, C. H., Eckhardt, S. G., Hurwitz, H., Hochster, H. S., Murphy, J. E., Funke, R. P., Rossi, C., Wallin, J., Waterkamp, D., & Pishvaian, M. J. (2015, Jan 20). Safety and efficacy of MPDL3280A (anti-PDL1) in combination with bevacizumab (bev) and/or FOLFOX in patients (pts) with metastatic colorectal cancer (mCRC). *Journal of Clinical Oncology, 33*(3). https://doi.org/DOI 10.1200/jco.2015.33.3_suppl.704

Berry, R. S., Xiong, M. J., Greenbaum, A., Mortaji, P., Nofchissey, R. A., Schultz, F., Martinez, C., Luo, L., Morris, K. T., & Hanson, J. A. (2017). High levels of tumor-associated neutrophils are associated with improved overall survival in patients with stage II colorectal cancer. *PLoS One, 12*(12), e0188799. https://doi.org/10.1371/journal.pone.0188799

Blair, G. E., & Cook, G. P. (2008, Oct 6). Cancer and the immune system: an overview - Introduction. *Oncogene, 27*(45), 5868-5868. https://doi.org/10.1038/onc.2008.277

Boland, C. R., & Goel, A. (2010, Jun). Microsatellite instability in colorectal cancer. *Gastroenterology, 138*(6), 2073-2087 e2073. https://doi.org/10.1053/j.gastro.2009.12.064

Boland, P. M., & Ma, W. W. (2017, May). Immunotherapy for Colorectal Cancer. *Cancers, 9*(5). https://doi.org/ARTN 50

10.3390/cancers9050050

Braha, M., Chikman, B., Habler, L., Shapira, Z., Vasyanovich, S., Tolstov, G., Halevy, A., Sandbank, J., & Lavy, R. (2016, Feb). Lymphocytic Infiltration as a Prognostic Factor in Patients With Colon Cancer. *International Journal of Surgical Pathology, 24*(1), 16-23. https://doi.org/10.1177/1066896915596808

Branco, I., & Choupina, A. (2021, Feb). Bioinformatics: new tools and applications in life science and personalized medicine. *Appl Microbiol Biotechnol, 105*(3), 937-951. https://doi.org/10.1007/s00253-020-11056-2

Bray, F., Ferlay, J., Soerjomataram, I., Siegel, R. L., Torre, L. A., & Jemal, A. (2018, Nov). Global cancer statistics 2018: GLOBOCAN estimates of incidence and mortality worldwide for 36 cancers in 185 countries. *CA Cancer J Clin, 68*(6), 394-424. https://doi.org/10.3322/caac.21492

Brenner, C. (2019, Oct 24). Applications of Bioinformatics in Cancer. *Cancers (Basel), 11*(11). https://doi.org/10.3390/cancers11111630

Brenner, H., Kloor, M., & Pox, C. P. (2014, Apr 26). Colorectal cancer. *Lancet, 383*(9927), 1490-1502. https://doi.org/10.1016/S0140-6736(13)61649-9

Bretthauer, M. (2011, Aug). Colorectal cancer screening. *J Intern Med, 270*(2), 87-98. https://doi.org/10.1111/j.1365-2796.2011.02399.x

Broggio, S. J. a. J. (2019, 12 August 2019). Cancer survival in England: adult, stage at diagnosis and childhood - patients follow up to 2018 [Health and social care]. https://www.ons.gov.uk/peoplepopulationandcommunity/healthandsocialcare/conditionsanddiseases/bulletins/cancersurvivalinengland/stageatdiagnosisandchildhoodpatientsfollowedupto2018

Buchbinder, E. I., & Desai, A. (2016, Feb). CTLA-4 and PD-1 Pathways Similarities, Differences, and Implications of Their Inhibition. *American Journal of Clinical Oncology-Cancer Clinical Trials, 39*(1), 98-106. https://doi.org/10.1097/Coc.0000000000000239

Buikhuisen, J. Y., Torang, A., & Medema, J. P. (2020, Jul 9). Exploring and modelling colon cancer inter-tumour heterogeneity: opportunities and challenges. *Oncogenesis, 9*(7), 66. https://doi.org/10.1038/s41389-020-00250-6

Bupathi, M., & Wu, C. (2016, Oct). Biomarkers for immune therapy in colorectal cancer: mismatch-repair deficiency and others. *J Gastrointest Oncol, 7*(5), 713-720. https://doi.org/10.21037/jgo.2016.07.03

Campos, F., Figueiredo, M. N., Monteiro, M., Nahas, S. C., & Cecconello, I. (2017, Mar-Apr). Incidence of colorectal cancer in young patients. *Rev Col Bras Cir, 44*(2), 208-215. https://doi.org/10.1590/0100-69912017002004

Cantero-Cid, R., Casas-Martin, J., Hernandez-Jimenez, E., Cubillos-Zapata, C., Varela-Serrano, A., Avendano-Ortiz, J., Casarrubios, M., Montalban-Hernandez, K., Villacanas-Gil, I., Guerra-Pastrian, L., Peinado, B., Marcano, C., Aguirre, L. A., & Lopez-Collazo, E. (2018, Oct 3). PD-L1/PD-1 crosstalk in colorectal cancer: are we targeting the right cells? *BMC Cancer, 18*(1), 945. https://doi.org/10.1186/s12885-018-4853-0

Cardoso, R., Guo, F., Heisser, T., Hackl, M., Ihle, P., De Schutter, H., Van Damme, N., Valerianova, Z., Atanasov, T., Majek, O., Muzik, J., Nilbert, M. C., Tybjerg, A. J., Innos, K., Magi, M., Malila, N., Bouvier, A. M., Bouvier, V., Launoy, G., Woronoff, A. S., Cariou, M., Robaszkiewicz, M., Delafosse, P., Poncet, F., Katalinic, A., Walsh, P. M., Senore, C., Rosso, S., Vincerzevskiene, I., Lemmens, V., Elferink, M. A. G., Johannesen, T. B., Korner, H., Pfeffer, F., Bento, M. J., Rodrigues, J., Alves da Costa, F., Miranda, A., Zadnik, V., Zagar, T., Lopez de Munain Marques, A., Marcos-Gragera, R., Puigdemont, M., Galceran, J., Carulla, M., Chirlaque, M. D., Ballesta, M., Sundquist, K., Sundquist, J., Weber, M., Jordan, A., Herrmann, C., Mousavi, M., Ryzhov, A., Hoffmeister, M., & Brenner, H. (2021, Jul). Colorectal cancer incidence, mortality, and stage distribution in European countries in the colorectal cancer screening era: an international population-based study. *Lancet Oncology, 22*(7), 1002-1013. https://doi.org/10.1016/S1470-2045(21)00199-6

Cartwright, T. H. (2012, Sep). Treatment decisions after diagnosis of metastatic colorectal cancer. *Clin Colorectal Cancer, 11*(3), 155-166. https://doi.org/10.1016/j.clcc.2011.11.001

Chen, G., Wang, L., Diao, T. W., Chen, Y., Cao, C. B., & Zhang, X. D. (2020, Jul). Analysis of immune-related signatures of colorectal cancer identifying two different immune phenotypes: Evidence for immune checkpoint inhibitor therapy. *Oncology Letters, 20*(1), 517-524. https://doi.org/10.3892/ol.2020.11605

Chen, Z., Downing, S., & Tzanakakis, E. S. (2019). Four Decades After the Discovery of Regenerating Islet-Derived (Reg) Proteins: Current Understanding and Challenges. *Front Cell Dev Biol, 7*, 235. https://doi.org/10.3389/fcell.2019.00235

Choe, E. K., Lee, S., Kim, S. Y., Shivakumar, M., Park, K. J., Chai, Y. J., & Kim, D. (2021, Feb 11). Prognostic Effect of Inflammatory Genes on Stage I-III Colorectal Cancer-Integrative Analysis of TCGA Data. *Cancers (Basel), 13*(4). https://doi.org/10.3390/cancers13040751

Chung, D. C. (2000, Sep). The genetic basis of colorectal cancer: insights into critical pathways of tumorigenesis. *Gastroenterology, 119*(3), 854-865. https://doi.org/10.1053/gast.2000.16507

Chung, H. C., Schellens, J. H. M., Delord, J. P., Perets, R., Italiano, A., & Shapira-Frommer, R. (2018, May 20). Pembrolizumab treatment of advanced cervical cancer: Updated results from the phase 2 KEYNOTE-158 study. *Journal of Clinical Oncology, 36*(15). https://doi.org/DOI 10.1200/JCO.2018.36.15_suppl.5522

Church, S. E., & Galon, J. (2015, Oct 20). Tumor Microenvironment and Immunotherapy: The Whole Picture Is Better Than a Glimpse. *Immunity, 43*(4), 631-633. https://doi.org/10.1016/j.immuni.2015.10.004

Cohen, E. E. W., Machiels, J. P. H., Harrington, K. J., Burtness, B., Shin, S. W., Gause, C. K., Swift, A. M., Brown, H., Perrone, A. M., Cheng, J. D., Swaby, R. F., & Le Tourneau, C. (2015, May 20). KEYNOTE-040: A phase III randomized trial of pembrolizumab (MK-3475) versus standard treatment in patients with recurrent or metastatic head and neck cancer. *Journal of Clinical Oncology, 33*(15). <Go to ISI>://WOS:000358036904810

Cole, A. J., Dwight, T., Gill, A. J., Dickson, K. A., Zhu, Y., Clarkson, A., Gard, G. B., Maidens, J., Valmadre, S., Clifton-Bligh, R., & Marsh, D. J. (2016, May 18). Assessing mutant p53 in primary high-grade serous ovarian cancer using immunohistochemistry and massively parallel sequencing. *Sci Rep, 6*, 26191. https://doi.org/10.1038/srep26191

Cole, J. J., Faydaci, B. A., McGuinness, D., Shaw, R., Maciewicz, R. A., Robertson, N. A., & Goodyear, C. S. (2021, Aug 19). Searchlight: automated bulk RNA-seq exploration and visualisation using dynamically generated R scripts. *BMC Bioinformatics, 22*(1), 411. https://doi.org/10.1186/s12859-021-04321-2

Colussi, D., Brandi, G., Bazzoli, F., & Ricciardiello, L. (2013, Aug 7). Molecular pathways involved in colorectal cancer: implications for disease behavior and prevention. *Int J Mol Sci, 14*(8), 16365-16385. https://doi.org/10.3390/ijms140816365

Comin-Anduix, B., Escuin-Ordinas, H., & Ibarrondo, F. J. (2016). Tremelimumab: research and clinical development. *Oncotargets and Therapy, 9*. https://doi.org/10.2147/Ott.S65802

Cooks, T., Pateras, I. S., Jenkins, L. M., Patel, K. M., Robles, A. I., Morris, J., Forshew, T., Appella, E., Gorgoulis, V. G., & Harris, C. C. (2018, Feb 22). Mutant p53 cancers reprogram macrophages to tumor supporting macrophages via exosomal miR-1246. *Nat Commun, 9*(1), 771. https://doi.org/10.1038/s41467-018-03224-w

Correa, L. H., Correa, R., Farinasso, C. M., de Sant'Ana Dourado, L. P., & Magalhaes, K. G. (2017). Adipocytes and Macrophages Interplay in the Orchestration of Tumor Microenvironment: New Implications in Cancer Progression. *Front Immunol, 8*, 1129. https://doi.org/10.3389/fimmu.2017.01129

Cui, Y., & Guo, G. (2016, Nov 19). Immunomodulatory Function of the Tumor Suppressor p53 in Host Immune Response and the Tumor Microenvironment. *Int J Mol Sci, 17*(11). https://doi.org/10.3390/ijms17111942

D.T. Le, J. N. U., H. Wang, B.R. Bartlett, H. Kemberling, A.D. Eyring, A.D. Skora, B.S., Luber, N. S. A., D. Laheru, B. Biedrzycki, R.C. Donehower, A. Zaheer, G.A. Fisher, T.S., Crocenzi, J. J. L., S.M. Duffy, R.M. Goldberg, A. de la Chapelle, M. Koshiji, F. Bhaijee, T., Huebner, R. H. H., L.D. Wood, N. Cuka, D.M. Pardoll, N. Papadopoulos, K.W. Kinzler, S., Zhou, T. C. C., J.M. Taube, R.A. Anders, J.R. Eshleman, B. Vogelstein, and L.A. Diaz, & Jr. (2015). PD-1 Blockade in Tumors with Mismatch-Repair Deficiency. *The New England Journal of Medicine, 372*(26), 12.

de la Chapelle, A., & Hampel, H. (2010, Jul 10). Clinical relevance of microsatellite instability in colorectal cancer. *J Clin Oncol, 28*(20), 3380-3387. https://doi.org/10.1200/JCO.2009.27.0652

Delyon, J., Mateus, C., Lefeuvre, D., Lanoy, E., Zitvogel, L., Chaput, N., Roy, S., Eggermont, A. M. M., Routier, E., & Robert, C. (2013, Jun). Experience in daily practice with ipilimumab for the treatment of patients with metastatic melanoma: an early increase in lymphocyte and eosinophil counts is associated with improved survival. *Annals of Oncology, 24*(6), 1697-1703. https://doi.org/10.1093/annonc/mdt027

Di Giacomo, A. M., Calabro, L., Danielli, R., Fonsatti, E., Bertocci, E., Pesce, I., Fazio, C., Cutaia, O., Giannarelli, D., Miracco, C., Biagioli, M., Altomonte, M., & Maio, M. (2013, Jun). Long-term survival and immunological parameters in metastatic melanoma patients who responded to ipilimumab 10 mg/kg within an expanded access programme. *Cancer Immunology Immunotherapy, 62*(6), 1021-1028. https://doi.org/10.1007/s00262-013-1418-6

Diaz, L., Marabelle, A., Kim, T. W., Geva, R., Van Cutsem, E., Andre, T., Ascierto, P. A., Maio, M., Delord, J. P., Gottfried, M., Guimbaud, R., Jaeger, D., Elez, E., Yoshino, T., Joe, A., Lam, B., Ding, J., Pruitt, S., Kang, S. P., & Le, D. T. (2017, Sep). Efficacy of pembrolizumab in phase 2 KEYNOTE-164 and KEYNOTE-158 studies of microsatellite instability high cancers. *Annals of Oncology, 28*. <Go to ISI>://WOS:000411324001046

Dine, J., Gordon, R., Shames, Y., Kasler, M. K., & Barton-Burke, M. (2017, Apr-Jun). Immune Checkpoint Inhibitors: An Innovation in Immunotherapy for the Treatment and Management of Patients with Cancer. *Asia-Pacific Journal of Oncology Nursing, 4*(2), 127-135. https://doi.org/10.4103/apjon.apjon_4_17

Dougan, M., & Dougan, S. K. (2017, Oct). Targeting Immunotherapy to the Tumor Microenvironment. *J Cell Biochem, 118*(10), 3049-3054. https://doi.org/10.1002/jcb.26005

Dvorak, H. F. (2015, Jan). Tumors: Wounds That Do Not Heal-Redux. *Cancer Immunology Research, 3*(1), 1-11. https://doi.org/10.1158/2326-6066.Cir-14-0209

Dyson, J. K., & Rutter, M. D. (2012, Aug 7). Colorectal cancer in inflammatory bowel disease: what is the real magnitude of the risk? *World J Gastroenterol, 18*(29), 3839-3848. https://doi.org/10.3748/wjg.v18.i29.3839

Edmondson, R., Broglie, J. J., Adcock, A. F., & Yang, L. (2014, May). Three-dimensional cell culture systems and their applications in drug discovery and cell-based biosensors. *Assay Drug Dev Technol, 12*(4), 207-218. https://doi.org/10.1089/adt.2014.573

Edwards, M. S., Chadda, S. D., Zhao, Z., Barber, B. L., & Sykes, D. P. (2012, Feb). A systematic review of treatment guidelines for metastatic colorectal cancer. *Colorectal Disease, 14*(2), e31-e47. https://doi.org/10.1111/j.1463-1318.2011.02765.x

Elliott, L. A., Doherty, G. A., Sheahan, K., & Ryan, E. J. (2017). Human Tumor-Infiltrating Myeloid Cells: Phenotypic and Functional Diversity. *Front Immunol, 8*, 86. https://doi.org/10.3389/fimmu.2017.00086

Ewing, I., Hurley, J. J., Josephides, E., & Millar, A. (2014, Jan). The molecular genetics of colorectal cancer. *Frontline Gastroenterol, 5*(1), 26-30. https://doi.org/10.1136/flgastro-2013-100329

Farkona S, D. E., Blasutig IM. (2016). Cancer immunotherapy: the beginning of the end of cancer? *Bmc Medicine, 14*. https://doi.org/10.1186/s12916-016-0623-5

Fearon, E. R., & Vogelstein, B. (1990, Jun 1). A genetic model for colorectal tumorigenesis. *Cell, 61*(5), 759-767. https://doi.org/10.1016/0092-8674(90)90186-i

Fehrenbacher, L., Spira, A., Ballinger, M., Kowanetz, M., Vansteenkiste, J., Mazieres, J., Park, K., Smith, D., Artal-Cortes, A., Lewanski, C., Braiteh, F., Waterkamp, D., He, P., Zou, W., Chen, D. S., Yi, J., Sandler, A., Rittmeyer, A., & Grp, P. S. (2016, Apr 30). Atezolizumab versus docetaxel for patients with previously treated non-small-cell lung cancer (POPLAR): a multicentre, open-label, phase 2 randomised controlled trial. *Lancet, 387*(10030), 1837-1846. https://doi.org/10.1016/S0140-6736(16)00587-0

Feinberg, A. P., Ohlsson, R., & Henikoff, S. (2006, Jan). The epigenetic progenitor origin of human cancer. *Nat Rev Genet, 7*(1), 21-33. https://doi.org/10.1038/nrg1748

Fennell, L., Dumenil, T., Wockner, L., Hartel, G., Nones, K., Bond, C., Borowsky, J., Liu, C., McKeone, D., Bowdler, L., Montgomery, G., Klein, K., Hoffmann, I., Patch, A. M., Kazakoff, S., Pearson, J., Waddell, N., Wirapati, P., Lochhead, P., Imamura, Y., Ogino, S., Shao, R., Tejpar, S., Leggett, B., & Whitehall, V. (2019). Integrative Genome-Scale DNA Methylation Analysis of a Large and Unselected Cohort Reveals 5 Distinct Subtypes of Colorectal Adenocarcinomas. *Cell Mol Gastroenterol Hepatol, 8*(2), 269-290. https://doi.org/10.1016/j.jcmgh.2019.04.002

Ferris, R. L., Blumenschein, G., Fayette, J., Guigay, J., Colevas, A. D., Licitra, L., Harrington, K., Kasper, S., Vokes, E. E., Even, C., Worden, F., Saba, N. F., Docampo, L. C. I., Haddad, R., Rordorf, T., Kiyota, N., Tahara, M., Monga, M., Lynch, M., Geese, W. J., Kopit, J., Shaw, J. W., & Gillison, M. L. (2016, Nov 10). Nivolumab for Recurrent Squamous-Cell Carcinoma of the Head and Neck. *New England Journal of Medicine, 375*(19), 1856-1867. https://doi.org/10.1056/NEJMoa1602252

Fitzgerald, A. A., Li, E., & Weiner, L. M. (2020, Dec 28). 3D Culture Systems for Exploring Cancer Immunology. *Cancers (Basel), 13*(1). https://doi.org/10.3390/cancers13010056

Franchi-Mendes, T., Eduardo, R., Domenici, G., & Brito, C. (2021, Sep 14). 3D Cancer Models: Depicting Cellular Crosstalk within the Tumour Microenvironment. *Cancers (Basel), 13*(18). https://doi.org/10.3390/cancers13184610

Fuchs, C. S., Doi, T., Jang, R. W., Muro, K., Satoh, T., Machado, M., Sun, W. J., Jalal, S. I., Shah, M. A., Metges, J. P., Garrido, M., Golan, T., Mandala, M., Wainberg, Z. A., Catenacci, D. V., Ohtsu, A., Shitara, K., Geva, R., Bleeker, J., Ko, A. H., Ku, G., Philip, P., Enzinger, P. C., Bang, Y. J., Levitan, D., Wang, J. D., Rosales, M., Dalal, R. P., & Yoon, H. H. (2018, May). Safety and Efficacy of Pembrolizumab Monotherapy in Patients With Previously Treated Advanced Gastric and Gastroesophageal Junction Cancer Phase 2 Clinical KEYNOTE-059 Trial. *Jama Oncology, 4*(5). https://doi.org/ARTN e180013

10.1001/jamaoncol.2018.0013

Galluzzi, L., Vacchelli, E., Bravo-San Pedro, J. M., Buque, A., Senovilla, L., Baracco, E. E., Bloy, N., Castoldi, F., Abastado, J. P., Agostinis, P., Apte, R. N., Aranda, F., Ayyoub, M., Beckhove, P., Blay, J. Y., Bracci, L., Caignard, A., Castelli, C., Cavallo, F., Celis, E., Cerundolo, V., Clayton, A., Colombo, M. P., Coussens, L., Dhodapkar, M. V., Eggermont, A. M., Fearon, D. T., Fridman, W. H., Fucikova, J., Gabrilovich, D. I., Galon, J., Garg, A., Ghiringhelli, F., Giaccone, G., Gilboa, E., Gnjatic, S., Hoos, A., Hosmalin, A., Jager, D., Kalinski, P., Karre, K., Kepp, O., Kiessling, R., Kirkwood, J. M., Klein, E., Knuth, A., Lewis, C. E., Liblau, R., Lotze, M. T., Lugli, E., Mach, J. P., Mattei, F., Mavilio, D., Melero, I., Melief, C. J., Mittendorf, E. A., Moretta, L., Odunsi, A., Okada, H., Palucka, A. K., Peter, M. E., Pienta, K. J., Porgador, A., Prendergast, G. C., Rabinovich, G. A., Restifo, N. P., Rizvi, N., Sautes-Fridman, C., Schreiber, H., Seliger, B., Shiku, H., Silva-Santos, B., Smyth, M. J., Speiser, D. E., Spisek, R., Srivastava, P. K., Talmadge, J. E., Tartour, E., Van der Burg, S. H., Van den Eynde, B. J., Vile, R., Wagner, H., Weber, J. S., Whiteside, T. L., Wolchok, J. D., Zitvogel, L., Zou, W. P., & Kroemer, G. (2014, Dec 30). Classification of current anticancer immunotherapies. *Oncotarget, 5*(24), 12472-12508. https://doi.org/10.18632/oncotarget.2998

Galon, J., & Lanzi, A. (2020, Jun). Immunoscore and its introduction in clinical practice. *Q J Nucl Med Mol Imaging, 64*(2), 152-161. https://doi.org/10.23736/S1824-4785.20.03249-5

Galon, J., Mlecnik, B., Bindea, G., Angell, H. K., Berger, A., Lagorce, C., Lugli, A., Zlobec, I., Hartmann, A., Bifulco, C., Nagtegaal, I. D., Palmqvist, R., Masucci, G. V., Botti, G., Tatangelo, F., Delrio, P., Maio, M., Laghi, L., Grizzi, F., Asslaber, M., D'Arrigo, C., Vidal-Vanaclocha, F., Zavadova, E., Chouchane, L., Ohashi, P. S., Hafezi-Bakhtiari, S., Wouters, B. G., Roehrl, M., Nguyen, L., Kawakami, Y., Hazama, S., Okuno, K., Ogino, S., Gibbs, P.,

Waring, P., Sato, N., Torigoe, T., Itoh, K., Patel, P. S., Shukla, S. N., Wang, Y., Kopetz, S., Sinicrope, F. A., Scripcariu, V., Ascierto, P. A., Marincola, F. M., Fox, B. A., & Pages, F. (2014, Jan). Towards the introduction of the 'Immunoscore' in the classification of malignant tumours. *Journal of Pathology, 232*(2), 199-209. https://doi.org/10.1002/path.4287

Galon, J., Pages, F., Marincola, F. M., Angell, H. K., Thurin, M., Lugli, A., Zlobec, I., Berger, A., Bifulco, C., Botti, G., Tatangelo, F., Britten, C. M., Kreiter, S., Chouchane, L., Delrio, P., Arndt, H., Asslaber, M., Maio, M., Masucci, G. V., Mihm, M., Vidal-Vanaclocha, F., Allison, J. P., Gnjatic, S., Hakansson, L., Huber, C., Singh-Jasuja, H., Ottensmeier, C., Zwierzina, H., Laghi, L., Grizzi, F., Ohashi, P. S., Shaw, P. A., Clarke, B. A., Wouters, B. G., Kawakami, Y., Hazama, S., Okuno, K., Wang, E., O'Donnell-Tormey, J., Lagorce, C., Pawelec, G., Nishimura, M. I., Hawkins, R., Lapointe, R., Lundqvist, A., Khleif, S. N., Ogino, S., Gibbs, P., Waring, P., Sato, N., Torigoe, T., Itoh, K., Patel, P. S., Shukla, S. N., Palmqvist, R., Nagtegaal, I. D., Wang, Y., D'Arrigo, C., Kopetz, S., Sinicrope, F. A., Trinchieri, G., Gajewski, T. F., Ascierto, P. A., & Fox, B. A. (2012, Oct 3). Cancer classification using the Immunoscore: a worldwide task force. *J Transl Med, 10*, 205. https://doi.org/10.1186/1479-5876-10-205

Gao, Q., Qiu, S. J., Fan, J., Zhou, J., Wang, X. Y., Xiao, Y. S., Xu, Y., Li, Y. W., & Tang, Z. Y. (2007, Jun 20). Intratumoral balance of regulatory and cytotoxic T cells is associated with prognosis of hepatocellular carcinoma after resection. *Journal of Clinical Oncology, 25*(18), 2586-2593. https://doi.org/10.1200/Jco.2006.09.4565

Garon E, R. N., Hui R, Leighl N, Balmanoukian A, Eder J. (2015). Pembrolizumab for the Treatment of Non–Small-Cell Lung Cancer. *N Engl J Med, 372*(21), 11. https://doi.org/doi: 10.1056/NEJMoa1501824

Garvey, C. M., Chen, O., & Mumenthaler, S. M. (2017, Jul). Cancer-associated fibroblast driven drug resistance in colorectal cancer. *Cancer Research, 77*. https://doi.org/10.1158/1538-7445.Am2017-5908

Germann, M., Zangger, N., Sauvain, M. O., Sempoux, C., Bowler, A. D., Wirapati, P., Kandalaft, L. E., Delorenzi, M., Tejpar, S., Coukos, G., & Radtke, F. (2020, Jan 9). Neutrophils suppress tumor-infiltrating T cells in colon cancer via matrix metalloproteinase-mediated activation of TGF beta. *Embo Molecular Medicine, 12*(1). https://doi.org/ARTN e10681

10.15252/emmm.201910681

Glass, M., Misiak, D., Bley, N., Muller, S., Hagemann, S., Busch, B., Rausch, A., & Huttelmaier, S. (2021). IGF2BP1, a Conserved Regulator of RNA Turnover in Cancer. *Front Mol Biosci, 8*, 632219. https://doi.org/10.3389/fmolb.2021.632219

Goers, L., Freemont, P., & Polizzi, K. M. (2014, Jul 6). Co-culture systems and technologies: taking synthetic biology to the next level. *J R Soc Interface, 11*(96). https://doi.org/10.1098/rsif.2014.0065

Governa, V., Trella, E., Mele, V., Tornillo, L. G., Amicarella, F., Cremonesi, E., Muraro, M. G., Xu, H., Droeser, R., Daster, S. R., Bolli, M., Rosso, R., Oertli, D., Eppenberger-Castori, S., Terracciano, L. M., Iezzi, G., & Spagnoli, G. C. (2017, Jul 15). The Interplay Between Neutrophils and CD8(+) T Cells Improves Survival in Human Colorectal Cancer. *Clinical Cancer Research, 23*(14), 3847-3858. <Go to ISI>://WOS:000405678400040

Grivennikov, S. I., & Karin, M. (2010, Feb). Inflammation and oncogenesis: a vicious connection. *Current Opinion in Genetics & Development, 20*(1), 65-71. https://doi.org/10.1016/j.gde.2009.11.004

Guinney, J., Dienstmann, R., Wang, X., de Reynies, A., Schlicker, A., Soneson, C., Marisa, L., Roepman, P., Nyamundanda, G., Angelino, P., Bot, B. M., Morris, J. S., Simon, I. M., Gerster, S., Fessler, E., De Sousa, E. M. F., Missiaglia, E., Ramay, H., Barras, D., Homicsko, K., Maru, D., Manyam, G. C., Broom, B., Boige, V., Perez-Villamil, B., Laderas, T., Salazar, R., Gray, J. W., Hanahan, D., Tabernero, J., Bernards, R., Friend, S. H., Laurent-Puig, P., Medema, J. P., Sadanandam, A., Wessels, L., Delorenzi, M., Kopetz, S., Vermeulen, L., & Tejpar, S. (2015, Nov). The consensus molecular subtypes of colorectal cancer. *Nat Med, 21*(11), 1350-1356. https://doi.org/10.1038/nm.3967

Guinney, J., Dienstmann, R., Wang, X., de Reynies, A., Schlicker, A., Soneson, C., Marisa, L., Roepman, P., Nyamundanda, G., Angelino, P., Bot, B. M., Morris, J. S., Simon, I. M., Gerster, S., Fessler, E., Melo, F. D. E., Missiaglia, E., Ramay, H., Barras, D., Homicsko, K., Maru, D., Manyam, G. C., Broom, B., Boige, V., Perez-Villamil, B., Laderas, T., Salazar, R., Gray, J. W., Hanahan, D., Tabernero, J., Bernards, R., Friend, S. H., Laurent-Puig, P., Medema, J. P., Sadanandam, A., Wessels, L., Delorenzi, M., Kopetz, S., Vermeulen, L., & Tejpar, S. (2015, Nov). The consensus molecular subtypes of colorectal cancer. *Nature Medicine, 21*(11), 1350-1356. https://doi.org/10.1038/nm.3967

Guo, G., & Cui, Y. (2015). New perspective on targeting the tumor suppressor p53 pathway in the tumor microenvironment to enhance the efficacy of immunotherapy. *J Immunother Cancer, 3*, 9. https://doi.org/10.1186/s40425-015-0053-5

Guo, G. F., Wang, Y. X., Zhou, Y. X., Quan, Q., Zhang, Y. J., Wang, H. H., Zhang, B., & Xia, L. P. (2019, Jul 12). Immune cell concentrations among the primary tumor microenvironment in colorectal cancer patients predicted by clinicopathologic characteristics and blood indexes. *Journal for Immunotherapy of Cancer, 7*. https://doi.org/ARTN 179

10.1186/s40425-019-0656-3

Guo, X., Liang, X., Wang, Y., Cheng, A., Zhang, H., Qin, C., & Wang, Z. (2021). Significance of Tumor Mutation Burden Combined With Immune Infiltrates in the Progression and Prognosis of Advanced Gastric Cancer. *Front Genet, 12*, 642608. https://doi.org/10.3389/fgene.2021.642608

Gupta, R., Sinha, S., & Paul, R. N. (2018, Nov). The impact of microsatellite stability status in colorectal cancer. *Curr Probl Cancer, 42*(6), 548-559. https://doi.org/10.1016/j.currproblcancer.2018.06.010

Hagland, H. R., Lea, D., Watson, M. M., & Soreide, K. (2017, Feb). Correlation of Blood T-Cells to Intratumoural Density and Location of CD3(+) and CD8(+) T-Cells in Colorectal Cancer. *Anticancer Res, 37*(2), 675-683. https://doi.org/10.21873/anticanres.11363

Hamid, O., Schmidt, H., Nissan, A., Ridolfi, L., Aamdal, S., Hansson, J., Guida, M., Hyams, D. M., Gomez, H., Bastholt, L., Chasalow, S. D., & Berman, D. (2011, Nov 28). A prospective phase II trial exploring the association between tumor microenvironment biomarkers and clinical activity of ipilimumab in advanced melanoma. *Journal of Translational Medicine, 9*. https://doi.org/Artn 204

10.1186/1479-5876-9-204

Hammers, H. J., Plimack, E. R., Sternberg, C., McDermott, D. F., Larkin, J. M. G., Ravaud, A., Rini, B. I., Sharma, P., Bhagavatheeswaran, P., Gagnier, P., & Motzer, R. (2015, May 20). CheckMate 214: A phase III, randomized, open-label study of nivolumab combined with ipilimumab versus sunitinib monotherapy in patients with previously untreated metastatic renal cell carcinoma. *Journal of Clinical Oncology, 33*(15). <Go to ISI>://WOS:000358036904770

Han, S. J., Kwon, S., & Kim, K. S. (2021, Mar 4). Challenges of applying multicellular tumor spheroids in preclinical phase. *Cancer Cell Int, 21*(1), 152. https://doi.org/10.1186/s12935-021-01853-8

Hanahan, D., & Coussens, L. M. (2012, Mar 20). Accessories to the crime: functions of cells recruited to the tumor microenvironment. *Cancer Cell, 21*(3), 309-322. https://doi.org/10.1016/j.ccr.2012.02.022

Hanahan, D., & Weinberg, R. A. (2011, Mar 4). Hallmarks of Cancer: The Next Generation. *Cell, 144*(5), 646-674. https://doi.org/10.1016/j.cell.2011.02.013

Hartl, C. A., Bertschi, A., Puerto, R. B., Andresen, C., Cheney, E. M., Mittendorf, E. A., Guerriero, J. L., & Goldberg, M. S. (2019, Jul 30). Combination therapy targeting both innate and adaptive immunity improves survival in a pre-clinical model of ovarian cancer. *Journal for Immunotherapy of Cancer, 7*. <Go to ISI>://WOS:000477971400001

Hirst, Y., Stoffel, S., Baio, G., McGregor, L., & von Wagner, C. (2018, Nov). Uptake of the English Bowel (Colorectal) Cancer Screening Programme: an update 5 years after the full roll-out. *Eur J Cancer, 103*, 267-273. https://doi.org/10.1016/j.ejca.2018.07.135

Hodi, F. S., O'Day, S. J., McDermott, D. F., Weber, R. W., Sosman, J. A., Haanen, J. B., Gonzalez, R., Robert, C., Schadendorf, D., Hassel, J. C., Akerley, W., van den Eertwegh, A. J. M., Lutzky, J., Lorigan, P., Vaubel, J. M., Linette, G. P., Hogg, D., Ottensmeier, C. H., Lebbe, C., Peschel, C., Quirt, I., Clark, J. I., Wolchok, J. D., Weber, J. S., Tian, J., Yellin, M. J., Nichol, G. M., Hoos, A., & Urba, W. J. (2010, Aug 19). Improved Survival with Ipilimumab in Patients with Metastatic Melanoma. *New England Journal of Medicine, 363*(8), 711-723. https://doi.org/10.1056/NEJMoa1003466

Hopkins, A. M., Rowland, A., Kichenadasse, G., Wiese, M. D., Gurney, H., McKinnon, R. A., Karapetis, C. S., & Sorich, M. J. (2017, Sep 26). Predicting response and toxicity to immune checkpoint inhibitors using routinely available blood and clinical markers. *British Journal of Cancer, 117*(7), 913-920. https://doi.org/10.1038/bjc.2017.274

Hori, S., Nomura, T., & Sakaguchi, S. (2003, Feb 14). Control of regulatory T cell development by the transcription factor Foxp3. *Science, 299*(5609), 1057-1061. https://doi.org/10.1126/science.1079490

Housman, G., Byler, S., Heerboth, S., Lapinska, K., Longacre, M., Snyder, N., & Sarkar, S. (2014, Sep). Drug Resistance in Cancer: An Overview. *Cancers, 6*(3), 1769-1792. https://doi.org/10.3390/cancers6031769

Hu, G., Li, Z., & Wang, S. (2017, Sep 26). Tumor-infiltrating FoxP3(+) Tregs predict favorable outcome in colorectal cancer patients: A meta-analysis. *Oncotarget, 8*(43), 75361-75371. https://doi.org/10.18632/oncotarget.17722

Huang, C., Ma, J., Wu, C., & Zhu, Y. (2019, Jul 25). [A new bioinformatics approach for prediction of potential tumor neoantigens based on the cancer genome atlas dataset]. *Sheng Wu Gong Cheng Xue Bao, 35*(7), 1295-1306. https://doi.org/10.13345/j.cjb.190025

Isella, C., Brundu, F., Bellomo, S. E., Galimi, F., Zanella, E., Porporato, R., Petti, C., Fiori, A., Orzan, F., Senetta, R., Boccaccio, C., Ficarra, E., Marchionni, L., Trusolino, L., Medico, E., & Bertotti, A. (2017, May 31). Selective analysis of cancer-cell intrinsic transcriptional traits defines novel clinically relevant subtypes of colorectal cancer. *Nat Commun, 8*, 15107. https://doi.org/10.1038/ncomms15107

Ishii, G., Ochiai, A., & Neri, S. (2016, Apr 1). Phenotypic and functional heterogeneity of cancer-associated fibroblast within the tumor microenvironment. *Adv Drug Deliv Rev, 99*(Pt B), 186-196. https://doi.org/10.1016/j.addr.2015.07.007

James D.B., M. K. G., Christian W. (2017). TNM Classification of Malignant Tumours, Eighth Edition. *Union for International Cancer Control (UICC)*. https://www.legeforeningen.no/contentassets/201604933ce448e888a101ab969a4205/tnm-classification-of-malignant-tumours-8th-edition.pdf

Jean H. Hoffman-Censits , P. G., Michiel Simon Van Der Heijden , Robert Dreicer , Yohann Loriot , Margitta Retz , Nicholas J. Vogelzang , Jose Luis Perez-Gracia , Arash Rezazadeh , Sergio Bracarda , Evan Y. Yu , Christopher J. Hoimes , Joaquim Bellmunt , David I. Quinn , Daniel Peter Petrylak , Syed A. Hussain , Na Cui , Sanjeev Mariathasan , Oyewale O. Abidoye , Jonathan E. Rosenberg. (2016). IMvigor 210, a phase II trial of atezolizumab (MPDL3280A) in platinum-treated locally advanced or metastatic urothelial carcinoma (mUC). *Journal of Clinical Oncology, 34*(2_suppl), 1.

Jenkins, R. W., Barbie, D. A., & Flaherty, K. T. (2018, Jan 9). Mechanisms of resistance to immune checkpoint inhibitors. *British Journal of Cancer, 118*(1), 9-16. https://doi.org/10.1038/bjc.2017.434

Jensen, C., & Teng, Y. (2020). Is It Time to Start Transitioning From 2D to 3D Cell Culture? *Front Mol Biosci, 7*, 33. https://doi.org/10.3389/fmolb.2020.00033

Jiang, W. Q., Fu, F. F., Li, Y. X., Wang, W. B., Wang, H. H., Jiang, H. P., & Teng, L. S. (2012, Sep). Molecular biomarkers of colorectal cancer: prognostic and predictive tools for clinical practice. *J Zhejiang Univ Sci B, 13*(9), 663-675. https://doi.org/10.1631/jzus.B1100340

Jiang, Y., Zheng, B., Yang, Y., Li, X., & Han, J. (2021). Identification of Somatic Mutation-Driven Immune Cells by Integrating Genomic and Transcriptome Data. *Front Cell Dev Biol, 9*, 715275. https://doi.org/10.3389/fcell.2021.715275

Kamal, Y., Dwan, D., Hoehn, H. J., Sanz-Pamplona, R., Alonso, M. H., Moreno, V., Cheng, C., Schell, M. J., Kim, Y., Felder, S. I., Rennert, H. S., Melas, M., Lazaris, C., Bonner, J. D., Siegel, E. M., Shibata, D., Rennert, G., Gruber, S. B., Frost, H. R., Amos, C. I., & Schmit, S. L. (2021, Mar 9). Tumor immune infiltration estimated from gene expression profiles predicts colorectal cancer relapse. *Oncoimmunology, 10*(1), 1862529. https://doi.org/10.1080/2162402X.2020.1862529

Kaufman, H. L., Russell, J., Hamid, O., Bhatia, S., Terheyden, P., D'Angelo, S. P., Shih, K. C., Lebbe, C., Linette, G. P., Milella, M., Brownell, I., Lewis, K. D., Lorch, J. H., Chin, K., Mahnke, L., von Heydebreck, A., Cuillerot, J. M., & Nghiem, P. (2016, Oct). Avelumab in patients with chemotherapy-refractory metastatic Merkel cell carcinoma: a multicentre, single-group, open-label, phase 2 trial. *Lancet Oncology, 17*(10), 1374-1385. https://doi.org/10.1016/S1470-2045(16)30364-3

Kazandjian, D., Suzman, D. L., Blumenthal, G., Mushti, S., He, K., Libeg, M., Keegan, P., & Pazdur, R. (2016, May). FDA Approval Summary: Nivolumab for the Treatment of Metastatic Non-Small Cell Lung Cancer With Progression On or After Platinum-Based Chemotherapy. *Oncologist, 21*(5), 634-642. https://doi.org/10.1634/theoncologist.2015-0507

Kefford, R., Ribas, A., Hamid, O., Robert, C., Daud, A., Wolchok, J. D., Joshua, A. M., Hodi, F. S., Gangedher, T. C., Hersey, P., Weber, J. S., Dronca, R. S., Patnaik, A., Zarour, H. M., Dolled-Filhart, M., Lunceford, J., Emancipator, K., Ebbinghaus, S., Rang, S. P., & Hwu, W. J. (2014, May 20). Clinical efficacy and correlation with tumor PD-L1 expression in patients (pts) with melanoma (MEL) treated with the anti-PD-1 monoclonal antibody MK-3475. *Journal of Clinical Oncology, 32*(15). <Go to ISI>://WOS:000358613202897

Kelderman, S., Heemskerk, B., van Tinteren, H., van den Brom, R. R. H., Hospers, G. A. P., van den Eertwegh, A. J. M., Kapiteijn, E. W., de Groot, J. W. B., Soetekouw, P., Jansen, R. L., Fiets, E., Furness, A. J. S., Renn, A., Krzystanek, M., Szallasi, Z., Lorigan, P., Gore, M. E., Schumacher, T. N. M., Haanen, J. B. A. G., Larkin, J. M. G., & Blank, C. U. (2014, May). Lactate dehydrogenase as a selection criterion for ipilimumab treatment in metastatic

melanoma. *Cancer Immunology Immunotherapy, 63*(5), 449-458. https://doi.org/10.1007/s00262-014-1528-9

Kim, E. R., & Chang, D. K. (2014, Aug 7). Colorectal cancer in inflammatory bowel disease: the risk, pathogenesis, prevention and diagnosis. *World J Gastroenterol, 20*(29), 9872-9881. https://doi.org/10.3748/wjg.v20.i29.9872

Kim, J., & Bae, J. S. (2016). Tumor-Associated Macrophages and Neutrophils in Tumor Microenvironment. *Mediators Inflamm, 2016*, 6058147. https://doi.org/10.1155/2016/6058147

Koh, B., Jeon, H., Kim, D., Kang, D., & Kim, K. R. (2019, Feb). Effect of fibroblast co-culture on the proliferation, viability and drug response of colon cancer cells. *Oncol Lett, 17*(2), 2409-2417. https://doi.org/10.3892/ol.2018.9836

Koncina, E., Haan, S., Rauh, S., & Letellier, E. (2020, Jan 30). Prognostic and Predictive Molecular Biomarkers for Colorectal Cancer: Updates and Challenges. *Cancers (Basel), 12*(2). https://doi.org/10.3390/cancers12020319

Koo, S., Neilson, L. J., Von Wagner, C., & Rees, C. J. (2017). The NHS Bowel Cancer Screening Program: current perspectives on strategies for improvement. *Risk Manag Healthc Policy, 10*, 177-187. https://doi.org/10.2147/RMHP.S109116

Korneev, K. V., Atretkhany, K. S. N., Drutskaya, M. S., Grivennikov, S. I., Kuprash, D. V., & Nedospasov, S. A. (2017, Jan). TLR-signaling and proinflammatory cytokines as drivers of tumorigenesis. *Cytokine, 89*, 127-135. https://doi.org/10.1016/j.cyto.2016.01.021

Ladoire, S., Martin, F., & Ghiringhelli, F. (2011, Jul). Prognostic role of FOXP3+ regulatory T cells infiltrating human carcinomas: the paradox of colorectal cancer. *Cancer Immunology Immunotherapy, 60*(7), 909-918. https://doi.org/10.1007/s00262-011-1046-y

Le, D. T., Durham, J. N., Smith, K. N., Wang, H., Bartlett, B. R., Aulakh, L. K., Lu, S., Kemberling, H., Wilt, C., Luber, B. S., Wong, F., Azad, N. S., Rucki, A. A., Laheru, D., Donehower, R., Zaheer, A., Fisher, G. A., Crocenzi, T. S., Lee, J. J., Greten, T. F., Duffy, A. G., Ciombor, K. K., Eyring, A. D., Lam, B. H., Joe, A., Kang, S. P., Holdhoff, M., Danilova, L., Cope, L., Meyer, C., Zhou, S., Goldberg, R. M., Armstrong, D. K., Bever, K. M., Fader, A. N., Taube, J., Housseau, F., Spetzler, D., Xiao, N., Pardoll, D. M., Papadopoulos, N., Kinzler, K. W., Eshleman, J. R., Vogelstein, B., Anders, R. A., & Diaz, L. A., Jr. (2017, Jul 28). Mismatch repair deficiency predicts response of solid tumors to PD-1 blockade. *Science, 357*(6349), 409-413. https://doi.org/10.1126/science.aan6733

Le, D. T., Yoshino, T., Jager, D., Andre, T., Bendell, J. C., Wang, R. X., Kang, S. P., Koshiji, M., & Diaz, L. A. (2016, Feb 1). KEYNOTE-164: Phase II study of pembrolizumab (MK-3475) for patients with previously treated, microsatellite instability-high advanced colorectal carcinoma. *Journal of Clinical Oncology, 34*(4). https://doi.org/DOI 10.1200/jco.2016.34.4_suppl.tps787

Leach D, K. M., Allison J. (1996). Enhancement of anti- tumor immunity by CTLA-4 blockade. *Science, 271*, 3. https://doi.org/doi: 10.1126/science.271.5256.1734

Lee, J. J., Sun, W. J., Bahary, N., Ohr, J., Rhee, J. C., Stoller, R. G., Marks, S. M., Lernbersky, B. C., Beasley, H. S., Drummond, S., Streeter, N., Shuai, Y. L., Lin, Y., Herman, J., & Chu, E. (2017, May 20). Phase 2 study of pembrolizumab in combination with azacitidine in subjects with metastatic colorectal cancer. *Journal of Clinical Oncology, 35*. https://doi.org/10.1200/JCO.2017.35.15_suppl.3054

Lenz, H. J., Van Cutsem, E., Luisa Limon, M., Wong, K. Y. M., Hendlisz, A., Aglietta, M., Garcia-Alfonso, P., Neyns, B., Luppi, G., Cardin, D. B., Dragovich, T., Shah, U., Abdullaev, S., Gricar, J., Ledeine, J. M., Overman, M. J., & Lonardi, S. (2021, Oct 12). First-Line Nivolumab Plus Low-Dose Ipilimumab for Microsatellite Instability-High/Mismatch Repair-Deficient Metastatic Colorectal Cancer: The Phase II CheckMate 142 Study. *J Clin Oncol*, JCO2101015. https://doi.org/10.1200/JCO.21.01015

Li, B., Geng, R., Wu, Q., Yang, Q., Sun, S., Zhu, S., Xu, Z., & Sun, S. (2020). Alterations in Immune-Related Genes as Potential Marker of Prognosis in Breast Cancer. *Front Oncol, 10*, 333. https://doi.org/10.3389/fonc.2020.00333

Lian, S., Xie, R., Ye, Y., Xie, X., Li, S., Lu, Y., Li, B., Cheng, Y., Katanaev, V. L., & Jia, L. (2019, Apr). Simultaneous blocking of CD47 and PD-L1 increases innate and adaptive cancer immune responses and cytokine release. *EBioMedicine, 42*, 281-295. https://doi.org/10.1016/j.ebiom.2019.03.018

Lin, D. G., Fan, W. H., Zhang, R. X., Zhao, E., Li, P. S., Zhou, W. H., Peng, J. H., & Li, L. R. (2021, Jun 30). Molecular subtype identification and prognosis stratification by a metabolism-related gene expression signature in colorectal cancer. *Journal of Translational Medicine, 19*(1). https://doi.org/ARTN 279

10.1186/s12967-021-02952-w

Ling, A., Edin, S., Wikberg, M. L., Oberg, A., & Palmqvist, R. (2014, May 13). The intratumoural subsite and relation of CD8(+) and FOXP3(+) T lymphocytes in colorectal cancer provide important prognostic clues. *British Journal of Cancer, 110*(10), 2551-2559. https://doi.org/10.1038/bjc.2014.161

Liu, B., Guo, H., Xu, J., Qin, T., Guo, Q., Gu, N., Zhang, D., Qian, W., Dai, J., Hou, S., Wang, H., & Guo, Y. (2018, Feb/Mar). Elimination of tumor by CD47/PD-L1 dual-targeting fusion protein that engages innate and adaptive immune responses. *MAbs, 10*(2), 315-324. https://doi.org/10.1080/19420862.2017.1409319

Liu, M., Xu, J., Souza, P., Tanswell, B., Tanswell, A. K., & Post, M. (1995, Dec). The effect of mechanical strain on fetal rat lung cell proliferation: comparison of two- and three-dimensional culture systems. *In Vitro Cell Dev Biol Anim, 31*(11), 858-866. https://doi.org/10.1007/BF02634570

Liu, X., Liu, L., Ren, Z., Yang, K., Xu, H., Luan, Y., Fu, K., Guo, J., Peng, H., Zhu, M., & Fu, Y. X. (2018, Aug 21). Dual Targeting of Innate and Adaptive Checkpoints on Tumor Cells Limits Immune Evasion. *Cell Rep, 24*(8), 2101-2111. https://doi.org/10.1016/j.celrep.2018.07.062

Lonardi, S., Andre, T., Wong, K. Y. M., Morse, M., McDermott, R., Hill, A., Hendlisz, A., Lenz, H., Leach, J., Moss, R. A., Cao, Z. A., Ledeine, J., Kopetz, S., & Overman, M. (2017, Oct). Combination of nivolumab (nivo) 1 ipilimumab (ipi) in the treatment of patients (pts) with deficient DNA mismatch repair (dMMR)/high microsatellite instability (MSI-H) metastatic colorectal cancer (mCRC): CheckMate 142 Study. *Annals of Oncology, 28*, 3-3. <Go to ISI>://WOS:000414493900006

Long, G. V., Atkinson, V., Ascierto, P. A., Robert, C., Hassel, J. C., Rutkowski, P., Savage, K. J., Taylor, F., Coon, C., Gilloteau, I., Dastani, H. B., Waxman, I., & Abernethy, A. P. (2015, Aug). CHECKMATE 066: effect of nivolumab (NIVO) on quality of life (QoL) in patients (pts) with treatment-naive advanced melanoma (MEL) *Asia-Pacific Journal of Clinical Oncology, 11*, 58-58. <Go to ISI>://WOS:000357957300042

Lopez, I., L, P. O., Tucci, P., Alvarez-Valin, F., R, A. C., & Marin, M. (2012, May 10). Different mutation profiles associated to P53 accumulation in colorectal cancer. *Gene, 499*(1), 81-87. https://doi.org/10.1016/j.gene.2012.02.011

Loughrey, M. B., Arends, M., Brown, I., Burgart, L.J., Cunningham, C., Flejou, J.F., Kakar, S., Kirsch, R., Kojima, M., Lugli, A., Rosty, C., Sheahan, K., West, N.P., Wilson, R., Nagtegaal, I.D. (2020). Colorectal Cancer Histopathology Reporting Guide [International Collaboration on Cancer Reporting; Sydney, Australia]. http://www.iccr-cancer.org/datasets/published-datasets/digestive-tract/colorectal

Loughrey, M. B., Quirke, P., Shepherd, N.A. (2018). Standards and datasets for reporting cancers, Dataset for histopathological reporting of colorectal cancer. https://www.rcpath.org/uploads/assets/c8b61ba0-ae3f-43f1-85ffd3ab9f17cfe6/G049-Dataset-for-histopathological-reporting-of-colorectal-cancer.pdf

Love, M. I., Huber, W., & Anders, S. (2014). Moderated estimation of fold change and dispersion for RNA-seq data with DESeq2. *Genome Biol, 15*(12), 550. https://doi.org/10.1186/s13059-014-0550-8

Manson, G., Norwood, J., Marabelle, A., Kohrt, H., & Houot, R. (2016, Jul). Biomarkers associated with checkpoint inhibitors. *Annals of Oncology, 27*(7), 1199-1206. https://doi.org/10.1093/annonc/mdw181

Mariani, F., Sena, P., & Roncucci, L. (2014, Aug 21). Inflammatory pathways in the early steps of colorectal cancer development. *World Journal of Gastroenterology, 20*(29), 9716-9731. https://doi.org/10.3748/wjg.v20.i29.9716

Markowitz, S. D., & Bertagnolli, M. M. (2009, Dec 17). Molecular origins of cancer: Molecular basis of colorectal cancer. *N Engl J Med, 361*(25), 2449-2460. https://doi.org/10.1056/NEJMra0804588

Mayakonda, A., Lin, D. C., Assenov, Y., Plass, C., & Koeffler, H. P. (2018, Nov). Maftools: efficient and comprehensive analysis of somatic variants in cancer. *Genome Res, 28*(11), 1747-1756. https://doi.org/10.1101/gr.239244.118

Mboowa, G., Mwesigwa, S., Kateete, D., Wayengera, M., Nasinghe, E., Katagirya, E., Katabazi, A. F., Kigozi, E., Kirimunda, S., Kamulegeya, R., Kabahita, J. M., Luutu, M. N., Nabisubi, P., Kanyerezi, S., Bagaya, B. S., & Joloba, M. L. (2021). Whole-genome sequencing of SARS-CoV-2 in Uganda: implementation of the low-cost ARTIC protocol in resource-limited settings. *F1000Res, 10*, 598. https://doi.org/10.12688/f1000research.53567.1

McMillan, D. C. (2013, Aug). The systemic inflammation-based Glasgow Prognostic Score: A decade of experience in patients with cancer. *Cancer Treatment Reviews, 39*(5), 534-540. https://doi.org/10.1016/j.ctrv.2012.08.003

Menendez, D., Shatz, M., & Resnick, M. A. (2013, Jan). Interactions between the tumor suppressor p53 and immune responses. *Curr Opin Oncol, 25*(1), 85-92. https://doi.org/10.1097/CCO.0b013e32835b6386

Michel, M., Kaps, L., Maderer, A., Galle, P. R., & Moehler, M. (2021, May 11). The Role of p53 Dysfunction in Colorectal Cancer and Its Implication for Therapy. *Cancers (Basel), 13*(10). https://doi.org/10.3390/cancers13102296

Michot, J. M., Armand, P., Ding, W., Ribrag, V., Christian, B., Marinello, P., Chlosta, S., Zhang, Y., Shipp, M., & Zinzani, P. L. (2016, Nov). KEYNOTE-170: Phase 2 study of pembrolizumab in patients with relapsed/refractory primary mediastinal large B-cell lymphoma (rrPMBCL) or relapsed or refractory Richter syndrome (rrRS). *Annals of Oncology, 27*. <Go to ISI>://WOS:000392830300050

Mishalian, I., Bayuh, R., Eruslanov, E., Michaeli, J., Levy, L., Zolotarov, L., Singhal, S., Albelda, S. M., Granot, Z., & Fridlender, Z. G. (2014, Sep 1). Neutrophils recruit regulatory T-cells into tumors via secretion of CCL17-A new mechanism of impaired antitumor immunity. *International Journal of Cancer, 135*(5), 1178-1186. https://doi.org/10.1002/ijc.28770

Mitchell, E. P. (2013, Jun). Targeted therapy for metastatic colorectal cancer: role of aflibercept. *Clin Colorectal Cancer, 12*(2), 73-85. https://doi.org/10.1016/j.clcc.2012.08.001

Moss, S. F., & Blaser, M. J. (2005, Feb). Mechanisms of disease: Inflammation and the origins of cancer. *Nat Clin Pract Oncol, 2*(2), 90-97; quiz 91 p following 113. https://doi.org/10.1038/ncponc0081

Motzer, R. J., Escudier, B., Mcdermott, D. F., George, S., Hammers, H. J., Srinivas, S., Tykodi, S. S., Sosman, J. A., Procopio, G., Plimack, E. R., Castellano, D., Gurney, H., Donskov, F., Bono, P., Wagstaff, J., Gauler, T. C., Ueda, T., Xu, L. A., Waxman, I. M., Sharma, P., & Invest, C. (2015, Dec). CheckMate 025: a randomized, open-label, phase Ill study of nivolumab versus everolimus in advanced renal cell carcinoma (RCC). *Bju International, 116*, 17-17. <Go to ISI>://WOS:000366284900033

Moynihan, K. D., & Irvine, D. J. (2017, Oct 1). Roles for Innate Immunity in Combination Immunotherapies. *Cancer Research, 77*(19), 5215-5221. <Go to ISI>://WOS:000412138300001

Mukherjee, S. (2019, Oct). Genomics-Guided Immunotherapy for Precision Medicine in Cancer. *Cancer Biother Radiopharm, 34*(8), 487-497. https://doi.org/10.1089/cbr.2018.2758

Nguyen, H. T., & Duong, H. Q. (2018, Jul). The molecular characteristics of colorectal cancer: Implications for diagnosis and therapy. *Oncol Lett, 16*(1), 9-18. https://doi.org/10.3892/ol.2018.8679

Ohtani, H. (2007, Feb 21). Focus on TILs: prognostic significance of tumor infiltrating lymphocytes in human colorectal cancer. *Cancer Immun, 7*, 4. https://www.ncbi.nlm.nih.gov/pubmed/17311363

Olivier, M., Hollstein, M., & Hainaut, P. (2010, Jan). TP53 mutations in human cancers: origins, consequences, and clinical use. *Cold Spring Harb Perspect Biol, 2*(1), a001008. https://doi.org/10.1101/cshperspect.a001008

Overman, M. J., Lonardi, S., Wong, K. Y. M., Lenz, H. J., Gelsomino, F., Aglietta, M., Morse, M., Van Cutsem, E., McDermott, R. S., Hill, A. G., Sawyer, M. B., Hendlisz, A., Neyns, B., Svrcek, M., Atasoy, A., Zhao, H. Y., Lei, M., Kopetz, S., & Andre, T. (2019, Feb 1). Nivolumab (NIVO) plus low-dose ipilimumab (IPI) in previously treated patients (pts) with microsatellite instability-high/mismatch repair-deficient (MSI-H/dMMR) metastatic colorectal cancer (mCRC): Long-term follow-up. *Journal of Clinical Oncology, 37*(4). https://doi.org/DOI 10.1200/JCO.2019.37.4_suppl.635

Overman, M. J., Lonardi, S., Wong, K. Y. M., Lenz, H. J., Gelsomino, F., Aglietta, M., Morse, M. A., Van Cutsem, E., McDermott, R., Hill, A., Sawyer, M. B., Hendlisz, A., Neyns, B., Svrcek, M., Moss, R. A., Ledeine, J. M., Cao, Z. A., Kamble, S., Kopetz, S., & Andre, T. (2018, Mar 10). Durable Clinical Benefit With Nivolumab Plus Ipilimumab in DNA Mismatch Repair-Deficient/Microsatellite Instability-High Metastatic Colorectal Cancer. *J Clin Oncol, 36*(8), 773-779. https://doi.org/10.1200/JCO.2017.76.9901

Palaghia, M., Mihai, C., Danciu, M., Tarcoveanu, E., Crumpei, F., & Prelipcean, C. C. (2015, Apr-Jun). Liver Metastasis of a Gastrointestinal Stromal Tumor of Large Bowel: Case Report. *Rev Med Chir Soc Med Nat Iasi, 119*(2), 395-400. https://www.ncbi.nlm.nih.gov/pubmed/26204643

Papadopoulos, K. P., Owonikoko, T. K., Johnson, M., Brana, I., Martin, M. G., & Perez, R. P. (2018, Feb 10). Cemiplimab (REGN2810): A fully human anti-PD-1 monoclonal antibody for patients with unresectable locally advanced or metastatic cutaneous squamous cell carcinoma (CSCC)-Initial safety and efficacy from expansion cohorts (ECs) of phase I study. *Journal of Clinical Oncology, 36*(5). https://doi.org/DOI 10.1200/JCO.2018.36.5_suppl.195

Pardoll, D. M. (2012, Apr). The blockade of immune checkpoints in cancer immunotherapy. *Nature Reviews Cancer, 12*(4), 252-264. https://doi.org/10.1038/nrc3239

Park, E. J., & Baik, S. H. (2016, Jan). Robotic Surgery for Colon and Rectal Cancer. *Current Oncology Reports, 18*(1). https://doi.org/10.1007/s11912-015-0491-8

Park, J. H., Fuglestad, A. J., Kostner, A. H., Oliwa, A., Graham, J., Horgan, P. G., Roxburgh, C. S. D., Kersten, C., & McMillan, D. C. (2020, Aug). Systemic Inflammation and Outcome in 2295 Patients with Stage I-III Colorectal Cancer from Scotland and Norway: First Results from the ScotScan Colorectal Cancer Group. *Ann Surg Oncol, 27*(8), 2784-2794. https://doi.org/10.1245/s10434-020-08268-1

Park, J. H., McMillan, D. C., Powell, A. G., Richards, C. H., Horgan, P. G., Edwards, J., & Roxburgh, C. S. (2015, Feb 15). Evaluation of a tumor microenvironment-based prognostic score in primary operable colorectal cancer. *Clin Cancer Res, 21*(4), 882-888. https://doi.org/10.1158/1078-0432.CCR-14-1686

Park, J. H., Powell, A. G., Roxburgh, C. S., Horgan, P. G., McMillan, D. C., & Edwards, J. (2016, Mar 1). Mismatch repair status in patients with primary operable colorectal cancer: associations with the local and systemic tumour environment. *Br J Cancer, 114*(5), 562-570. https://doi.org/10.1038/bjc.2016.17

Park, J. H., Watt, D. G., Roxburgh, C. S., Horgan, P. G., & McMillan, D. C. (2016, Feb). Colorectal Cancer, Systemic Inflammation, and Outcome: Staging the Tumor and Staging the Host. *Ann Surg, 263*(2), 326-336. https://doi.org/10.1097/SLA.0000000000001122

Passardi, A., Canale, M., Valgiusti, M., & Ulivi, P. (2017, Jun). Immune Checkpoints as a Target for Colorectal Cancer Treatment. *International Journal of Molecular Sciences, 18*(6). https://doi.org/ARTN 1324

10.3390/ijms18061324

Patel, M. R., Ellerton, J., Agrawal, M., Gordon, M., Dirix, L., Lee, K. W., Infante, J., Schlichting, M., Chin, K., & Apolo, B. (2016, Oct 1). Avelumab (MSB0010718C; anti-PD-L1) in patients with metastatic urothelial carcinoma progressed after platinum-based therapy or platinum ineligible. *Annals of Oncology, 27*. https://doi.org/10.1093/annonc/mdw373.5

Picard, E., Verschoor, C. P., Ma, G. C. W., & Pawelec, G. (2020, Mar 6). Relationships Between Immune Landscapes, Genetic Subtypes and Responses to Immunotherapy in Colorectal Cancer. *Frontiers in Immunology, 11*. https://doi.org/ARTN 369

10.3389/fimmu.2020.00369

Pitt, J. M., Marabelle, A., Eggermont, A., Soria, J. C., Kroemer, G., & Zitvogel, L. (2016, Aug). Targeting the tumor microenvironment: removing obstruction to anticancer immune responses and immunotherapy. *Annals of Oncology, 27*(8), 1482-1492. <Go to ISI>://WOS:000383182800016

Pollheimer, M. J., Kornprat, P., Lindtner, R. A., Harbaum, L., Schlemmer, A., Rehak, P., & Langner, C. (2010, Dec). Tumor necrosis is a new promising prognostic factor in colorectal cancer. *Human Pathology, 41*(12), 1749-1757. https://doi.org/10.1016/j.humpath.2010.04.018

Potdar, P. D., & Chaudhary, S. (2017). Molecular characterization of cancer-associated fibroblasts isolated from human colorectal cancer as a major stromal cell component promoting metastasis. *Journal of Unexplored Medical Data, 2*, 1-8. https://doi.org/10.20517/2572-8180.2016.10

Powell, D. R., & Huttenlocher, A. (2016, Jan). Neutrophils in the Tumor Microenvironment. *Trends Immunol, 37*(1), 41-52. https://doi.org/10.1016/j.it.2015.11.008

R J Seager, C. H., Fabian Spill, Roger D Kamm, Muhammad H Zaman. (2017). Dynamic interplay between tumour, stroma and immune system can drive or prevent tumour progression. *Convergent Science Physical Oncology, 3*. https://doi.org/https://doi.org/10.1088/2057-1739/aa7e86

Raedler, L. A. (2015). Opdivo (Nivolumab): Second PD-1 inhibitor receives FDA Approval for unresectable or metastatic melanoma *Am Health Drug Benefits, 8*, 4.

Raguz, S., & Yague, E. (2008, Jul 29). Resistance to chemotherapy: new treatments and novel insights into an old problem. *British Journal of Cancer, 99*(3), 387-391. https://doi.org/10.1038/sj.bjc.6604510

Rao, H. L., Chen, J. W., Li, M., Xiao, Y. B., Fu, J., Zeng, Y. X., Cai, M. Y., & Xie, D. (2012, Jan 25). Increased Intratumoral Neutrophil in Colorectal Carcinomas Correlates Closely with Malignant Phenotype and Predicts Patients' Adverse Prognosis. *PLoS One, 7*(1). <Go to ISI>://WOS:000301640600056

Reidy, E., Leonard, N. A., Treacy, O., & Ryan, A. E. (2021, Jan 10). A 3D View of Colorectal Cancer Models in Predicting Therapeutic Responses and Resistance. *Cancers (Basel), 13*(2). https://doi.org/10.3390/cancers13020227

Ribas, A., Kefford, R., Marshall, M. A., Punt, C. J. A., Haanen, J. B., Marmol, M., Garbe, C., Gogas, H., Schachter, J., Linette, G., Lorigan, P., Kendra, K. L., Maio, M., Trefzer, U., Smylie, M., McArthur, G. A., Dreno, B., Nathan, P. D., Mackiewicz, J., Kirkwood, J. M., Gomez-Navarro, J., Huang, B., Pavlov, D., & Hauschild, A. (2013, Feb 10). Phase III Randomized Clinical Trial Comparing Tremelimumab With Standard-of-Care Chemotherapy in Patients

With Advanced Melanoma. *Journal of Clinical Oncology, 31*(5), 616-622. https://doi.org/10.1200/Jco.2012.44.6112

Richards, C. H., Roxburgh, C. S., Anderson, J. H., McKee, R. F., Foulis, A. K., Horgan, P. G., & McMillan, D. C. (2012a, Feb). Prognostic value of tumour necrosis and host inflammatory responses in colorectal cancer. *Br J Surg, 99*(2), 287-294. https://doi.org/10.1002/bjs.7755

Richards, C. H., Roxburgh, C. S. D., Anderson, J. H., Mckee, R. F., Foulis, A. K., Horgan, P. G., & McMillan, D. C. (2012b, Feb). Prognostic value of tumour necrosis and host inflammatory responses in colorectal cancer. *British Journal of Surgery, 99*(2), 287-294. https://doi.org/10.1002/bjs.7755

Richards, C. H., Roxburgh, C. S. D., Powell, A. G., Foulis, A. K., Horgan, P. G., & McMillan, D. C. (2014, Jan). The clinical utility of the local inflammatory response in colorectal cancer. *European Journal of Cancer, 50*(2), 309-319. https://doi.org/10.1016/j.ejca.2013.09.008

Rittmeyer, A., Barlesi, F., & Waterkamp, D. (2017, Apr 8). Atezolizumab versus docetaxel in patients with previously treated non-small-cell lung cancer (OAK): a phase 3, open-label, multicentre randomised controlled trial (vol 389, pg 255, 2016). *Lancet, 389*(10077), E5-E5. <Go to ISI>://WOS:000398345100002

Rizvi, N. A., Hellmann, M. D., Snyder, A., Kvistborg, P., Makarov, V., Havel, J. J., Lee, W., Yuan, J. D., Wong, P., Ho, T. S., Miller, M. L., Rekhtman, N., Moreira, A. L., Ibrahim, F., Bruggeman, C., Gasmi, B., Zappasodi, R., Maeda, Y., Sander, C., Garon, E. B., Merghoub, T., Wolchok, J. D., Schumacher, T. N., & Chan, T. A. (2015, Apr 3). Mutational landscape determines sensitivity to PD-1 blockade in non-small cell lung cancer. *Science, 348*(6230), 124-128. https://doi.org/10.1126/science.aaa1348

Rizzo, G., Bertotti, A., Leto, S. M., & Vetrano, S. (2021, Jun 1). Patient-derived tumor models: a more suitable tool for pre-clinical studies in colorectal cancer. *J Exp Clin Cancer Res, 40*(1), 178. https://doi.org/10.1186/s13046-021-01970-2

Robert, C., Schachter, J., Long, G. V., Arance, A., Grob, J. J., Mortier, L., Daud, A., Carlino, M. S., McNeil, C., Lotem, M., Larkin, J., Lorigan, P., Neyns, B., Blank, C. U., Hamid, O., Mateus, C., Shapira-Frommer, R., Kosh, M., Zhou, H., Ibrahim, N., Ebbinghaus, S., Ribas, A., & Investigators, K.-. (2015, Jun 25). Pembrolizumab versus Ipilimumab in Advanced Melanoma. *New England Journal of Medicine, 372*(26), 2521-2532. https://doi.org/10.1056/NEJMoa1503093

Rodriguez-Salas, N., Dominguez, G., Barderas, R., Mendiola, M., Garcia-Albeniz, X., Maurel, J., & Batlle, J. F. (2017, Jan). Clinical relevance of colorectal cancer molecular subtypes. *Crit Rev Oncol Hematol, 109*, 9-19. https://doi.org/10.1016/j.critrevonc.2016.11.007

Roepman, P., Schlicker, A., Tabernero, J., Majewski, I., Tian, S., Moreno, V., Snel, M. H., Chresta, C. M., Rosenberg, R., Nitsche, U., Macarulla, T., Capella, G., Salazar, R., Orphanides, G., Wessels, L. F., Bernards, R., & Simon, I. M. (2014, Feb 1). Colorectal cancer intrinsic

subtypes predict chemotherapy benefit, deficient mismatch repair and epithelial-to-mesenchymal transition. *Int J Cancer, 134*(3), 552-562. https://doi.org/10.1002/ijc.28387

Roseweir, A. K., Park, J. H., Hoorn, S. T., Powell, A. G., Aherne, S., Roxburgh, C. S., McMillan, D. C., Horgan, P. G., Ryan, E., Sheahan, K., Vermeulen, L., Paul, J., Harkin, A., Graham, J., Sansom, O., Church, D. N., Tomlinson, I., Saunders, M., Iveson, T. J., & Edwards, J. (2020, Oct). Histological phenotypic subtypes predict recurrence risk and response to adjuvant chemotherapy in patients with stage III colorectal cancer. *J Pathol Clin Res, 6*(4), 283-296. https://doi.org/10.1002/cjp2.171

Ryan, E., Sheahan, K., Creavin, B., Mohan, H. M., & Winter, D. C. (2017, Aug). The current value of determining the mismatch repair status of colorectal cancer: A rationale for routine testing. *Crit Rev Oncol Hematol, 116*, 38-57. https://doi.org/10.1016/j.critrevonc.2017.05.006

Sakaguchi, S., Yamaguchi, T., Nomura, T., & Ono, M. (2008, May 30). Regulatory T cells and immune tolerance. *Cell, 133*(5), 775-787. https://doi.org/10.1016/j.cell.2008.05.009

Salama, P., Phillips, M., Grieu, F., Morris, M., Zeps, N., Joseph, D., Platell, C., & Iacopetta, B. (2009, Jan 10). Tumor-Infiltrating FOXP3(+) T Regulatory Cells Show Strong Prognostic Significance in Colorectal Cancer. *Journal of Clinical Oncology, 27*(2), 186-+. https://doi.org/10.1200/Jco.2008.18.7229

Saleh, R., Sasidharan Nair, V., Toor, S. M., Taha, R. Z., Murshed, K., Al-Dhaheri, M., Khawar, M., Petkar, M. A., Abu Nada, M., Al-Ejeh, F., & Elkord, E. (2020, Sep). Differential gene expression of tumor-infiltrating CD8(+) T cells in advanced versus early-stage colorectal cancer and identification of a gene signature of poor prognosis. *J Immunother Cancer, 8*(2). https://doi.org/10.1136/jitc-2020-001294

Schaafsma, E., Fugle, C. M., Wang, X., & Cheng, C. (2021, Aug). Pan-cancer association of HLA gene expression with cancer prognosis and immunotherapy efficacy. *Br J Cancer, 125*(3), 422-432. https://doi.org/10.1038/s41416-021-01400-2

Schachter, J., Ribas, A., Long, G. V., Arance, A., Grob, J. J., Mortier, L., Daud, A., Carlino, M. S., McNeil, C., Lotem, M., Larkin, J., Lorigan, P., Neyns, B., Blank, C., Petrella, T. M., Hamid, O., Zhou, H. H., Ebbinghaus, S., Ibrahim, N., & Robert, C. (2017, Oct 21). Pembrolizumab versus ipilimumab for advanced melanoma: final overall survival results of a multicentre, randomised, open-label phase 3 study (KEYNOTE-006). *Lancet, 390*(10105), 1853-1862. https://doi.org/10.1016/S0140-6736(17)31601-X

Schreuders, E. H., Ruco, A., Rabeneck, L., Schoen, R. E., Sung, J. J., Young, G. P., & Kuipers, E. J. (2015, Oct). Colorectal cancer screening: a global overview of existing programmes. *Gut, 64*(10), 1637-1649. https://doi.org/10.1136/gutjnl-2014-309086

Scott J. Antonia, A. V., Davey Daniel, David Vicente, Shuji Murakami, Rina Hui, Takashi Yokoi, Alberto Chiappori, Ki H. Lee, M.D., Maike de Wit, Byoung C. Cho, Maryam Bourhaba, Xavier Quantin, Takaaki Tokito, Tarek Mekhail, David Planchard, Young-Chul Kim,

Christos S. Karapetis, Sandrine Hiret, Gyula Ostoros, Kaoru Kubota, Jhanelle E. Gray, Luis Paz-Ares, Javier de Castro Carpeño, Catherine Wadsworth, Giovanni Melillo, Haiyi Jiang, Yifan Huang, Phillip A. Dennis, and Mustafa Özgüroğlu. (2017). Durvalumab after Chemoradiotherapy in Stage III Non–Small-Cell Lung Cancer. *The New England Journal of Medicine, 377*(20), 11.

Seiwert, T. Y., Haddad, R. I., Gupta, S., Mehra, R., Tahara, M., Berger, R., Lee, S. H., Burtness, B., Le, D. T., Heath, K., Blum, A., Dolled-Filhart, M., Emancipator, K., Pathiraja, K., Cheng, J. D., & Chow, L. Q. (2015, Jun 20). Antitumor activity and safety of pembrolizumab in patients (pts) with advanced squamous cell carcinoma of the head and neck (SCCHN): Preliminary results from KEYNOTE-012 expansion cohort. *Journal of Clinical Oncology, 33*(18). <Go to ISI>://WOS:000378096500012

Shang, B., Liu, Y., Jiang, S. J., & Liu, Y. (2015, Oct 14). Prognostic value of tumor-infiltrating FoxP3(+) regulatory T cells in cancers: a systematic review and meta-analysis. *Scientific Reports, 5*. https://doi.org/ARTN 15179

10.1038/srep15179

Shanker, A., & Marincola, F. (2011, Aug). Cooperativity of adaptive and innate immunity: implications for cancer therapy. *Cancer Immunology Immunotherapy, 60*(8), 1061-1074. https://doi.org/10.1007/s00262-011-1053-z

Shaukat, A., Kahi, C. J., Burke, C. A., Rabeneck, L., Sauer, B. G., & Rex, D. K. (2021, Mar 1). ACG Clinical Guidelines: Colorectal Cancer Screening 2021. *Am J Gastroenterol, 116*(3), 458-479. https://doi.org/10.14309/ajg.0000000000001122

Shen, L., & Waterland, R. A. (2007, Sep). Methods of DNA methylation analysis. *Curr Opin Clin Nutr Metab Care, 10*(5), 576-581. https://doi.org/10.1097/MCO.0b013e3282bf6f43

Shen, R. F., Li, P., Li, B., Zhang, B. T., Feng, L., & Cheng, S. J. (2020, Jan 10). Identification of Distinct Immune Subtypes in Colorectal Cancer Based on the Stromal Compartment. *Frontiers in Oncology, 9*. https://doi.org/ARTN 1497

10.3389/fonc.2019.01497

Shiga, K., Hara, M., Nagasaki, T., Sato, T., Takahashi, H., & Takeyama, H. (2015, Dec). Cancer-Associated Fibroblasts: Their Characteristics and Their Roles in Tumor Growth. *Cancers, 7*(4), 2443-2458. https://doi.org/10.3390/cancers7040902

Shinozaki, E., Kawazoe, A., Kuboki, Y., Komatsu, Y., Nishina, T., & Hara, H. (2018, May 20). Multicenter phase I/II trial of BBI608 and pembrolizumab combination in patients with metastatic colorectal cancer (SCOOP Study): EPOC1503. *Journal of Clinical Oncology, 36*(15). https://doi.org/DOI 10.1200/JCO.2018.36.15_suppl.3530

Singh, M. P., Rai, S., Pandey, A., Singh, N. K., & Srivastava, S. (2021, Mar). Molecular subtypes of colorectal cancer: An emerging therapeutic opportunity for personalized medicine. *Genes Dis, 8*(2), 133-145. https://doi.org/10.1016/j.gendis.2019.10.013

Singh, P. P., Sharma, P. K., Krishnan, G., & Lockhart, A. C. (2015, Nov). Immune checkpoints and immunotherapy for colorectal cancer. *Gastroenterology Report, 3*(4), 289-297. https://doi.org/10.1093/gastro/gov053

Soldevilla, B., Carretero-Puche, C., Gomez-Lopez, G., Al-Shahrour, F., Riesco, M. C., Gil-Calderon, B., Alvarez-Vallina, L., Espinosa-Olarte, P., Gomez-Esteves, G., Rubio-Cuesta, B., Sarmentero, J., La Salvia, A., & Garcia-Carbonero, R. (2019, Dec). The correlation between immune subtypes and consensus molecular subtypes in colorectal cancer identifies novel tumour microenvironment profiles, with prognostic and therapeutic implications. *European Journal of Cancer, 123*, 118-129. https://doi.org/10.1016/j.ejca.2019.09.008

Stanley J. Oiseth, M. S. A. (2017a). Cancer immunotherapy: a brief review of the history, possibilities, and challenges ahead [Review Article]. *J Cancer Metastasis Treat, 3*, 12. https://doi.org/ 10.20517/2394-4722.2017.41

Stanley J. Oiseth, M. S. A. (2017b). Cancer immunotherapy: a brief review of the history, possibilities, and challenges ahead [Review Article]. *Journal of Cancer Metastasis and Treatment, 3*, 12. https://doi.org/ 10.20517/2394-4722.2017.41

Stratton, M. R., Campbell, P. J., & Futreal, P. A. (2009, Apr 9). The cancer genome. *Nature, 458*(7239), 719-724. https://doi.org/10.1038/nature07943

Sun, C., Wang, X., Hui, Y., Fukui, H., Wang, B., & Miwa, H. (2021, Jul 3). The Potential Role of REG Family Proteins in Inflammatory and Inflammation-Associated Diseases of the Gastrointestinal Tract. *Int J Mol Sci, 22*(13). https://doi.org/10.3390/ijms22137196

Sun, X. W., Feng, Z. J., Wang, Y. X., Qu, Y., & Gai, Y. Z. (2017, Jun). Expression of Foxp3 and its prognostic significance in colorectal cancer. *International Journal of Immunopathology and Pharmacology, 30*(2), 201-206. https://doi.org/10.1177/0394632017710415

Sung, H., Ferlay, J., Siegel, R. L., Laversanne, M., Soerjomataram, I., Jemal, A., & Bray, F. (2021, May). Global Cancer Statistics 2020: GLOBOCAN Estimates of Incidence and Mortality Worldwide for 36 Cancers in 185 Countries. *CA Cancer J Clin, 71*(3), 209-249. https://doi.org/10.3322/caac.21660

Tabuso, M., Homer-Vanniasinkam, S., Adya, R., & Arasaradnam, R. P. (2017, Aug). Role of tissue microenvironment resident adipocytes in colon cancer. *World Journal of Gastroenterology, 23*(32), 5829-5835. https://doi.org/10.3748/wjg.v23.i32.5829

Takimoto, C. H., Chao, M. P., Gibbs, C., McCamish, M. A., Liu, J., Chen, J. Y., Majeti, R., & Weissman, I. L. (2019, Mar 1). The Macrophage 'Do not eat me' signal, CD47, is a clinically

validated cancer immunotherapy target. *Ann Oncol, 30*(3), 486-489. https://doi.org/10.1093/annonc/mdz006

Tan, Z., Lei, Y., Zhang, B., Shi, S., Liu, J., Yu, X., Xu, J., & Liang, C. (2021). Analysis of Immune-Related Signatures Related to CD4+ T Cell Infiltration With Gene Co-Expression Network in Pancreatic Adenocarcinoma. *Front Oncol, 11*, 674897. https://doi.org/10.3389/fonc.2021.674897

Tao, L. L., Huang, G. C., Song, H. Z., Chen, Y. T., & Chen, L. B. (2017, Sep). Cancer associated fibroblasts: An essential role in the tumor microenvironment. *Oncology Letters, 14*(3), 2611-2620. https://doi.org/10.3892/ol.2017.6497

Tariq, K., & Ghias, K. (2016, Mar). Colorectal cancer carcinogenesis: a review of mechanisms. *Cancer Biol Med, 13*(1), 120-135. https://doi.org/10.28092/j.issn.2095-3941.2015.0103

Terzic, J., Grivennikov, S., Karin, E., & Karin, M. (2010, Jun). Inflammation and colon cancer. *Gastroenterology, 138*(6), 2101-2114 e2105. https://doi.org/10.1053/j.gastro.2010.01.058

Thomas Powles, P. H. O. D., Christophe Massard, Hendrik-Tobias Arkenau, Terence W. Friedlander, Christopher J. Hoimes, Jae Lyun Lee, Michael Ong, Srikala S. Sridhar, Nicholas J. Vogelzang, Mayer N. Fishman, Jingsong Zhang, Sandy Srinivas, Jigar Parikh, Joyce Antal, Xiaoping Jin, Ashok K. Gupta, Yong Ben, and Noah M. Hahn. (2017). Efficacy and safety of durvalumab in locally advanced or metastatic urothelial carcinoma updated results from a phase 1/2 open-label study. *Jama Oncology, 3*(19), e172411.

Toor, S. M., Syed Khaja, A. S., El Salhat, H., Bekdache, O., Kanbar, J., Jaloudi, M., & Elkord, E. (2016). Increased Levels of Circulating and Tumor-Infiltrating Granulocytic Myeloid Cells in Colorectal Cancer Patients. *Front Immunol, 7*, 560. https://doi.org/10.3389/fimmu.2016.00560

UICC. (2021, Monday 5 July 2021). *TNM*. Retrieved December 7 from https://www.uicc.org/resources/tnm

Urruticoechea, A., Alemany, R., Balart, J., Villanueva, A., Vinals, F., & Capella, G. (2010, Jan). Recent Advances in Cancer Therapy: An Overview. *Current Pharmaceutical Design, 16*(1), 3-10. https://doi.org/Doi 10.2174/138161210789941847

Van Allen, E. M., Miao, D., Schilling, B., Shukla, S. A., Blank, C., Zimmer, L., Sucker, A., Hillen, U., Foppen, M. H. G., Goldinger, S. M., Utikal, J., Hassel, J. C., Weide, B., Kaehler, K. C., Loquai, C., Mohr, P., Gutzmer, R., Dummer, R., Gabriel, S., Wu, C. J., Schadendorf, D., & Garraway, L. A. (2015, Oct 9). Genomic correlates of response to CTLA-4 blockade in metastatic melanoma. *Science, 350*(6257), 207-211. https://doi.org/10.1126/science.aad0095

Venter, C., & Niesler, C. (2018, Feb 1). A triple co-culture method to investigate the effect of macrophages and fibroblasts on myoblast proliferation and migration. *Biotechniques, 64*(2), 52-58. https://doi.org/10.2144/btn-2017-0100

Vis, M. A. M., Ito, K., & Hofmann, S. (2020). Impact of Culture Medium on Cellular Interactions in in vitro Co-culture Systems. *Front Bioeng Biotechnol, 8*, 911. https://doi.org/10.3389/fbioe.2020.00911

Vlad, C., Kubelac, P., Fetica, B., Vlad, D., Irimie, A., & Achimas-Cadariu, P. (2015, Jan-Feb). The prognostic value of FOXP3(+) T regulatory cells in colorectal cancer. *Journal of Buon, 20*(1), 114-119. <Go to ISI>://WOS:000351566500017

Vogelstein, B., Papadopoulos, N., Velculescu, V. E., Zhou, S., Diaz, L. A., Jr., & Kinzler, K. W. (2013, Mar 29). Cancer genome landscapes. *Science, 339*(6127), 1546-1558. https://doi.org/10.1126/science.1235122

Vuik, F. E., Nieuwenburg, S. A., Bardou, M., Lansdorp-Vogelaar, I., Dinis-Ribeiro, M., Bento, M. J., Zadnik, V., Pellise, M., Esteban, L., Kaminski, M. F., Suchanek, S., Ngo, O., Majek, O., Leja, M., Kuipers, E. J., & Spaander, M. C. (2019, Oct). Increasing incidence of colorectal cancer in young adults in Europe over the last 25 years. *Gut, 68*(10), 1820-1826. https://doi.org/10.1136/gutjnl-2018-317592

Wang, H., Tian, T., & Zhang, J. (2021, Aug 6). Tumor-Associated Macrophages (TAMs) in Colorectal Cancer (CRC): From Mechanism to Therapy and Prognosis. *Int J Mol Sci, 22*(16). https://doi.org/10.3390/ijms22168470

Wang, X., Duanmu, J., Fu, X., Li, T., & Jiang, Q. (2020, Aug 28). Analyzing and validating the prognostic value and mechanism of colon cancer immune microenvironment. *J Transl Med, 18*(1), 324. https://doi.org/10.1186/s12967-020-02491-w

Wang, X., & Sun, Q. (2017, Jan 3). TP53 mutations, expression and interaction networks in human cancers. *Oncotarget, 8*(1), 624-643. https://doi.org/10.18632/oncotarget.13483

Waniczek, D., Lorenc, Z., Snietura, M., Wesecki, M., Kopec, A., & Muc-Wierzgon, M. (2017, Oct). Tumor-Associated Macrophages and Regulatory T Cells Infiltration and the Clinical Outcome in Colorectal Cancer. *Archivum Immunologiae Et Therapiae Experimentalis, 65*(5), 445-454. https://doi.org/10.1007/s00005-017-0463-9

Wen, Y. A., Xing, X., Harris, J. W., Zaytseva, Y. Y., Mitov, M. I., Napier, D. L., Weiss, H. L., Mark Evers, B., & Gao, T. (2017, Feb 2). Adipocytes activate mitochondrial fatty acid oxidation and autophagy to promote tumor growth in colon cancer. *Cell Death & Disease, 8*(2), e2593. https://doi.org/10.1038/cddis.2017.21

Wikberg, M. L., Ling, A., Li, X. R., Oberg, A., Edin, S., & Palmqvist, R. (2017, Oct). Neutrophil infiltration is a favorable prognostic factor in early stages of colon cancer. *Human Pathology, 68*, 193-202. https://doi.org/10.1016/j.humpath.2017.08.028

Wong, J. J. L., Hawkins, N. J., & Ward, R. L. (2007, Jan). Colorectal cancer: a model for epigenetic tumorigenesis. *Gut, 56*(1), 140-148. https://doi.org/10.1136/gut.2005.088799

Worthley, D. L., & Leggett, B. A. (2010, May). Colorectal cancer: molecular features and clinical opportunities. *Clin Biochem Rev, 31*(2), 31-38. https://www.ncbi.nlm.nih.gov/pubmed/20498827

Worthley, D. L., Whitehall, V. L., Spring, K. J., & Leggett, B. A. (2007, Jul 28). Colorectal carcinogenesis: Road maps to cancer. *World Journal of Gastroenterology, 13*(28), 3784-3791. <Go to ISI>://WOS:000248382500002

Wu, D., Rice, C. M., & Wang, X. (2012, May 1). Cancer bioinformatics: a new approach to systems clinical medicine. *BMC Bioinformatics, 13*, 71. https://doi.org/10.1186/1471-2105-13-71

Yahaya, M. A. F., Lila, M. A. M., Ismail, S., Zainol, M., & Afizan, N. A. R. N. M. (2019). Tumour-Associated Macrophages (TAMs) in Colon Cancer and How to Reeducate Them. *Journal of Immunology Research, 2019*. https://doi.org/Artn 2368249

10.1155/2019/2368249

Yearley, J. H., Gibson, C., Yu, N., Moon, C., Murphy, E., Juco, J., Lunceford, J., Cheng, J., Chow, L. Q. M., Seiwert, T. Y., Handa, M., Tomassini, J. E., & McClanahan, T. (2017, Jun 15). PD-L2 Expression in Human Tumors: Relevance to Anti-PD-1 Therapy in Cancer. *Clinical Cancer Research, 23*(12), 3158-3167. https://doi.org/10.1158/1078-0432.Ccr-16-1761

Zahir, M. N., Azhar, E. M., Rafiq, S., Ghias, K., & Shabbir-Moosajee, M. (2014). Clinical features and outcome of sporadic colorectal carcinoma in young patients: a cross-sectional analysis from a developing country. *ISRN Oncol, 2014*, 461570. https://doi.org/10.1155/2014/461570

Zanoni, M., Piccinini, F., Arienti, C., Zamagni, A., Santi, S., Polico, R., Bevilacqua, A., & Tesei, A. (2016, Jan 11). 3D tumor spheroid models for in vitro therapeutic screening: a systematic approach to enhance the biological relevance of data obtained. *Sci Rep, 6*, 19103. https://doi.org/10.1038/srep19103

Zeestraten, E. C., Van Hoesel, A. Q., Speetjens, F. M., Menon, A. G., Putter, H., van de Velde, C. J., & Kuppen, P. J. (2013, Apr). FoxP3- and CD8-positive Infiltrating Immune Cells Together Determine Clinical Outcome in Colorectal Cancer. *Cancer Microenviron, 6*(1), 31-39. https://doi.org/10.1007/s12307-011-0071-x

Zhao, X., Hu, D., Li, J., Zhao, G., Tang, W., & Cheng, H. (2020). Database Mining of Genes of Prognostic Value for the Prostate Adenocarcinoma Microenvironment Using the Cancer Gene Atlas. *Biomed Res Int, 2020*, 5019793. https://doi.org/10.1155/2020/5019793

Zhao, X. T., Zhu, Y., Zhou, J. F., Gao, Y. J., & Liu, F. Z. (2021, Jan). Development of a novel 7 immune-related genes prognostic model for oral cancer: A study based on TCGA database. *Oral Oncol, 112*, 105088. https://doi.org/10.1016/j.oraloncology.2020.105088

Zhou, Y., Shao, N., Aierken, N., Xie, C., Ye, R., Qian, X., Hu, Z., Zhang, J., & Lin, Y. (2017). Prognostic value of tumor-infiltrating Foxp3+ regulatory T cells in patients with breast cancer: a meta-analysis. *J Cancer, 8*(19), 4098-4105. https://doi.org/10.7150/jca.21030

Zhou, Z., Xie, X., Wang, X., Zhang, X., Li, W., Sun, T., Cai, Y., Wu, J., Dang, C., & Zhang, H. (2021). Correlations Between Tumor Mutation Burden and Immunocyte Infiltration and Their Prognostic Value in Colon Cancer. *Front Genet, 12*, 623424. https://doi.org/10.3389/fgene.2021.623424

Appendix - R codes

1. R-codes for IHC cut off value

```
#CD3_cutoff = surv_cutpoint(CD3_2021, time = "Survival_Months", event =
"Other0_CD1",variables = c("Tumour_CD3"))
plot(CD3_cutoff, "Tumour_CD3")
```

2. R-codes for Mutational analysis

2.1 Plot summary

```
#plotmafSummary(maf = all.four.groups.tumour, rmOutlier = TRUE, addStat = 'median',
dashboard = TRUE, titvRaw = FALSE)
```

2.2 Co-bar plot

```
#coBarplot(m1 = all.four.groups.tumour, m2 = all.four.groups.stroma, m1Name = "All groups
tumour", m2Name = "All groups stroma", genes = genes)
```

3. R-codes for Transcriptomics analysis

3.1 DESEq2 normalisation

```
#dds = DESeqDataSetFromMatrix(countData = counts.t, colData = sample_data, design =
~sample_group_all)
#dds = DESeq(dds)
#norm_counts.t = counts(dds, normalized = TRUE)
#DE = results(dds, c("sample_group.all", "myeloid.high", "t.high"))
```

3.2 Volcano plot

```
#ggp1 = ggplot(master_bind, aes(x=log2FoldChange, y=mlog10pvalue, colour = direction)) +
geom_point() + geom_point(data=master_non_sig, colour = "gray") +
geom_point(data=master_sig_up, colour = "red") + geom_text(data = master_sig_up_top5,
aes(label=Gene_names), colour = "red", hjust=-0.1, vjust=0.1, size = 3) +
scale_colour_manual(values = c("gray","red")) + geom_vline(xintercept = -1, linetype="dashed") +
geom_vline(xintercept = 1, linetype="dashed") + geom_hline(yintercept = -log10(0.05),
linetype="dashed") + labs(title = "Volcano (myeloid.high vs t.high)", x="Log2 fold change",
y="log10 (p-value)") + xlim(c(-20,40)) + ylim(c(-0,25))
```

3.3 MA plot

#ggp2 = ggplot(master_bind, aes(x=log10(mean_expression), y=log2FoldChange, colour = direction)) + geom_point() + geom_point(data=master_non_sig, colour = "gray") + geom_point(data=master_sig_up, colour = "red") + geom_text(data = master_sig_up_top5, aes(label=Gene_names), colour = "red", hjust=-0.1, vjust=0.1, size = 3) + scale_colour_manual(values = c("gray","red")) + geom_hline(yintercept=1,linetype="dashed") + geom_hline(yintercept=-1,linetype="dashed") + xlim(c(-2,10)) + ylim(c(-10,25)) + labs(title = "MA (myeloid.high_vs_t.high)", x= "Mean expression (log10)", y= "Log2 fold change")

3.4 PCA plot

#ggp3 = ggplot(pca_coordinates, aes(x=PC1, y= PC2, colour = ss_all_four_t$tumour_group)) + geom_point() + labs(title = "PCA 4 groups", x= x_axis_label, y= y_axis_label) + stat_ellipse(geom = "polygon", aes(fill = ss_all_four_t$tumour_group), alpha = 0.1)

3.5 Multi-boxplot

#ggp4 = ggplot(gene_data.candidate_gene.1.melt, aes(x = variable, y = value, fill = sample_group)) + geom_boxplot() + labs(title = "23 Significant genes (myelod.high vs t.high)", x = "Significant genes", y = "Expression") + theme(axis.text.x = element_text(angle = 45, hjust = 1)) + ylim(c(0,300)) + facet_wrap(~sample_group, nrow = 2)

3.6 Heatmap plot

#cat_df = data.frame("immune_status" = c(rep("t.high", 3), rep("myeloid.high", 24), rep("both.high", 14), rep("both.low", 7)))
#row.names(cat_df) = colnames(em_scaled.11)
#pheatmap(em_scaled.11.top20, scale = "row", main = "pheatmap row scaling", annotation_col = cat_df)

3.7 Venn diagram plot

#grid.newpage()
#draw.triple.venn(area1 = 23, area2 = 1, area3 = 20,
n12 = 0, n13 = 0, n23 = 0, n123 = 0,
fill = c("pink", "green", "orange"),
lty = "blank", category = c("Group 1", "Group 2", "Group 3"))

3.8 Pathway analysis

```
#geneSymbols.mt = c("SLC51A","ORM1", "CPA2", "CFHR3", "SCL15A1", "MUC6", "ST18",
"TTC29", "CXCL5", "KRT34", "PEPD", "FAM3B", "SNTB1", "ZNF416", "NKX2-1",
"DHRS7B", "ADM5", "USP28", "ANKRD20A8P", "PDE11A", "DCAF4L1", "MAGEA11",
"BCL3")
#geneIDs2.mt = ensembldb::select(EnsDb.Hsapiens.v79, keys= geneSymbols.44, keytype =
"SYMBOL", columns = c("SYMBOL","GENEID"))
#geneIDs2.mt
#master_sig.a$ENSEMBL = c("ENSMUSG00000035699", "ENSG00000229314",
"ENSMUSG00000071553", "ENSG00000116785", "ENSMUSG00000035699",
"ENSG00000184956", "ENSMUSG00000033740", "ENSG00000137473", "ENSG00000163735",
"ENSG00000083817", "ENSG00000109016", "ENSG00000048028", "ENSG00000224420",
"ENSG00000182308", "ENSG00000128655", "ENSG00000151773", "ENSG00000152291")
#sig_genes_entrez.44 = bitr(sig_genes.44, fromType = "ENSEMBL", toType = c("ENTREZID"),
#OrgDb = org.Hs.eg.db)
#go_enrich.44 = enrichGO(gene = sig_genes_entrez.44$ENTREZID, OrgDb = org.Hs.eg.db,
readable = T, ont = "BP", pvalueCutoff = 0.05, qvalueCutoff = 0.10)
#ggp = cnetplot(go_enrich.44, showCategory = 15, categorySize = "padj")
```